A DOUBLE COMPETITION DIALYSIS ASSAY FOR THE ANALYSIS OF THE DISTRIBUTION OF OPTOELECTRONICALLY ACTIVE COMPONENTS OVER NUCLEIC ACID STRUCTURES

KARMA MARZOOQ S ALBALAWI

A thesis submitted for the Degree of Doctor of Philosophy

School of Chemistry

Cardiff University

November 2018

DECLARATION

This work has not been submitted in substance for any other degree or award at this or any other university or place of learning, nor is being submitted concurrently in candidature for any degree or other award.

Signed…….. (candidate) Date ...……..…

STATEMENT 1

This thesis is being submitted in partial fulfillment of the requirements for the degree of Doctor of philosophy.

Signed…….. (candidate) Date ...……..…

STATEMENT 2

This thesis is the result of my own independent work/investigation, except where otherwise stated, and the thesis has not been edited by a third party beyond what is permitted by Cardiff University's Policy on the Use of Third Party Editors by Research Degree Students. Other sources are acknowledged by explicit references. The views expressed are my own.

Signed…….. (candidate) Date ...……..…

STATEMENT 3

I hereby give consent for my thesis, if accepted, to be available online in the University's Open Access repository and for inter-library loan, and for the title and summary to be made available to outside organisations.

Signed…….. (candidate) Date ...……..…

STATEMENT 4: PREVIOUSLY APPROVED BAR ON ACCESS

I hereby give consent for my thesis, if accepted, to be available online in the University's Open Access repository and for inter-library loans **after expiry of a bar on access previously approved by the Academic Standards & Quality Committee.**

Signed…….. (candidate) Date ...……..…

Acknowledgements

Firstly, I thank the Almighty Allah for bestowing his infinite bounties and grace upon me that have given me the strength, patience and knowledge to continue and complete my research work even when the task was at times arduous.

The accomplishment of this work was made possible by the collaboration with several people and I now have the pleasure to express my gratefulness.

To my supervisor Dr. Niek Buurma, I am grateful for the trust you have placed in my work and for the motivation you have demonstrated along this arduous time. Your endless support was without a doubt crucial throughout my project.

I am very thankful to my Mentor Prof. Nigel Richards and my examiner Dr. James Redman for for their comments and question during my 21-monthly *viva voce* examinations.

A special thank you also goes to Dr Alison Paul, for choosing me and for giving me an opportunity to be a member of the Athena Swan committee. It has been a privilege to be a member in the Athena Swan committee and an absolute pleasure to have been part of this experience with all the staff.

In addition, I must to extend my deepest gratitude to Dr. Joseph Beames for his cooperation, support, encouragement and his wonderful words. I would also like to thank Dr Glenn Burley (Strathclyde) for the kind gift of compound GB01.

I appreciate the support received from Dr Hiwa Ahmad, Dr Ibrahim Saeed, Dr Andrea Taladriz Sender, Dr Helen Whitfield, Thomas Stonelake, Eman Alwattar and Nathan Watson for all the help, guidance, encouragement and kind words.

My sincere thanks to Cardiff University and Prof. Allemann's group, especially, Dr. Enas Behiry for allowing me to use the CD machine for the CD-titrations, and Alun Davies from the chemistry workshop for creating the competition dialysis device.

More importantly, I would also like to express my appreciation to my parents who have a very special place and are very dear to me. Thank you, my mother and father, sisters and brothers for all constant love and endless support which gave me the ability to complete this work.

My sincere gratitude to my husband Mr Eid Albalawi who was always there for me throughout this journey. His enthusiasm, support, encouragement and love were incredible. Also, to my heroes, my boys who were always around, filling my heart with love and motivation. Thank you very much for giving me the strength while the task was at times arduous.

And finally, I would like to thank with most gratitude, Saudi Arabia's Ministry of Higher Education for the scholarship and funding my Ph.D. studies. Last but not least, I thank everyone who provided me with the education needed to complete this task and helped me during my study.

Contents

Summary

This thesis presents DNA binding studies and our work to develop a double competition dialysis assay.

Chapter 1 describes DNA structure, including duplex, triplex and quadruplex structures, and functioning in storing the genetic code. This Chapter also presents an overview of the interactions of small molecules with nucleic acids structures. Moreover, the chapter describes the techniques that have been used for our DNA-binding studies, viz, UV - visible spectroscopy, circular dichroism spectroscopy and isothermal titration calorimetry. The chapter also describes potential applictions of small molecule DNA binders. Finally, we describe the competition dialysis in this chapter.

Chapter 2 describes the determination of extinction coefficients for selected optoelectronically active π-conjugated molecules in aqueous buffers. Furthermore, we established the light sensitivity of the compounds. In addition, the chapter describes the binding studies of nucleic acid binders from a library of available ligands using UV-visible, circular dichroism, and isothermal titration calorimetry.

Chapter 3 describes the development of a custom competition dialysis device. We test this device to determine affinity and selectivity of ligands for nucleic acids structures. We analysed the affinity and selectivity of a single ligand for FS-DNA, specific duplex sequences $(dAdT)_{12}$●$(dAdT)_{12}$ and $(dGdC)_{12}$●$(dGdC)_{12}$, and different quadruplex structures such as c-myc, 22AG and EAD2. The data agree with the results from UV-vis titrations.

In Chapter 4 we explore how double competition dialysis allows screening of two ligands against an array of nucleic acids structures. Several compounds were tested showing that our assay deals reasonably well with fading unless the latter progresses to the extent when absorbance is too low to measure reliably. Although we have identified compounds with promising affinity profiles, even in the presence of a second binder we are yet to identify binders with an orthogonal selectivity profile.

In Chapter 5 we present general conclusions and suggestions for future work.

List of abbreviations

UV	Ultra-violet
Vis	Visible
CD	Circular Dichroism Spectroscopy
ICD	Induced circular dichroism
ITC	Isothermal Titration Calorimetry
°C	Degree Celsius
V	Volume
Ml	Millilitre
T	Time
Min	Minutes
G	Gram
Cm	Centimetre
M	Molar
mM	Millimolar
Nm	Nanometer
A	Absorbance
a.u.	Arbitrary unit
Cal	Calorie
kcal	Kilocalore
k_{obs}	Observed rate constant
Θ	Ellipticity
λ_{max}	Lambda max
Λ	Wavelength
V	Wave number
E	Dielectric constant or extinction coefficient
FS-DNA	fish sperm DNA
DNA	Deoxyribonucleic acid
dsDNA	double-stranded deoxyribonucleic acid
MOPS	3-(N-morpholino) propanesulfonic acid
EDTA	Ethylenediaminetetraacetic acid
DMSO	Dimethyl sulfoxide
H33258	bisBenzimide H33258

TF1	2,4-bis(4-dimethylaminostyryl)-1-methylpyridinium
DAPI	4',6-diamidino-2-phenylindole
DODC	3,3′-Diethyloxadicarbocyanine iodide
MWCO	molecular weight cut-off
DT	dialysis tube
K_b	Binding constant
b.p.	Base pairs
N	Binding site size
K_{agg}	Aggregation constant
ΔH_{agg}	Change in enthalpy of aggregation
PNA	Peptide nucleic acids
PB	Pacific blue
YO	Oxazole yellow
Cy3	Cynine 3
ODNs	Oligodeoxyribonucleotides
SMFS	Single-molecule fluorescence spectroscopy
Betaine 30	Reichardt's dye
DHPs	Dervan’s hairpin polyamides

Chapter 1

Introduction

Abstract

DNA, the molecule of life, plays a key role in many important fields, for instance medical and pharmaceutical science. Moreover, DNA is also used as a building block in directed assembly. This chapter provides a brief overview of the importance of DNA in life. Furthermore, we present an overview of the binding of small molecules with nucleic acid structures such as duplex and quadruplex DNA. The Chapter also describes the typical binding modes with duplex DNA, which are electrostatic, intercalation and groove interactions. The second part of this chapter describes briefly selected established techniques that have been used for DNA-binding studies, viz UV-visible, circular dichroism spectroscopy (CD), isothermal titration calorimetry (ITC), fluorescence resonance energy transfer (FRET) and competition dialysis. The Chapter finishes with the aim of this project, which is the development of an assay that allows the identification of orthogonal recognition elements for the directed assembly of functional nanostructures.

1.1. DNA structure and functions

Nucleic acids are one of the most important biomacromolecules. They are vital to all known forms of life. All living cells contain both DNA and RNA, except some cells such as red blood cells, while viruses contain either DNA or RNA, but usually not both. The function of nucleic acids is to encode, store, transmit and express genetic information to the benefit of the cell itself and ultimately to pass the information onto the next generation of each organism.[1]

In 1869 Johann Friedrich Miescher reported discovering a weakly acidic substance in the nuclei of human white blood cells and named the substance "nuclein". He subsequently separated nuclein into protein and nucleic acid components. This is known to be the first isolation of what we now refer to as deoxyribonucleic acid (DNA).[2]

In the 1920's nucleic acids were reported to be major components of chromosomes, gene-carrying structures in the nuclei of most living cells. Further analysis of nucleic acids showed the presence of phosphorus, in addition to carbon, hydrogen, oxygen and nitrogen, but no sulphur, unlike proteins.[3]

Most scientists, however, remained convinced that the more complex proteins must be the carriers of genetic information as DNA is made up of only four different nucleotides – not enough, it was believed, to store the huge amount of genetic information. Extensive interest in nucleic acids was not rekindled until the 1940-1950s, when in classical experiments it was unequivocally demonstrated that DNA is the carrier of genetic information. This culminated in creation of the now iconic three-dimensional model of DNA, which was worked out by Watson and Crick using the X-ray diffraction photographs taken by Franklin and Wilkins.[3-5]

Nucleic acids are linear biopolymers. Their monomers are nucleotides, hence the other name of nucleic acids, polynucleotides.[6] Each nucleotide consists of three components: a nitrogenous base (also known as a nucleobase, or simply as a base), a pentose (5-carbon) sugar (ribose in RNA and deoxyribose in DNA) and a phosphate group, associated with the acidic nature of the nucleic acid (Figure 1.1).[7]

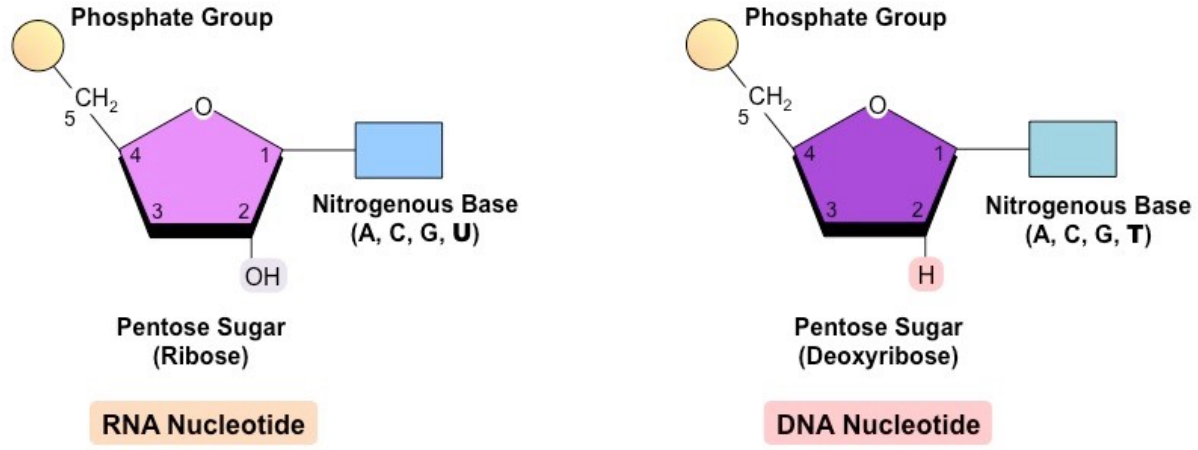

Figure 1.1 Comparison of DNA and RNA nucleotides.

Different genes have different sequences of these four nucleotides.[8] Since the deoxynucleotides differ only in the bases they carry, this sequence can be recorded simply as a base sequence. The substructure of a nucleotide, which consists of a nitrogenous base and a sugar, is known as nucleoside (Figure 1.2); we find ribonucleosides are found in RNA and deoxynucleosides in DNA. In chemical terms therefore, a nucleotide is a phosphate ester of a nucleoside.[9]

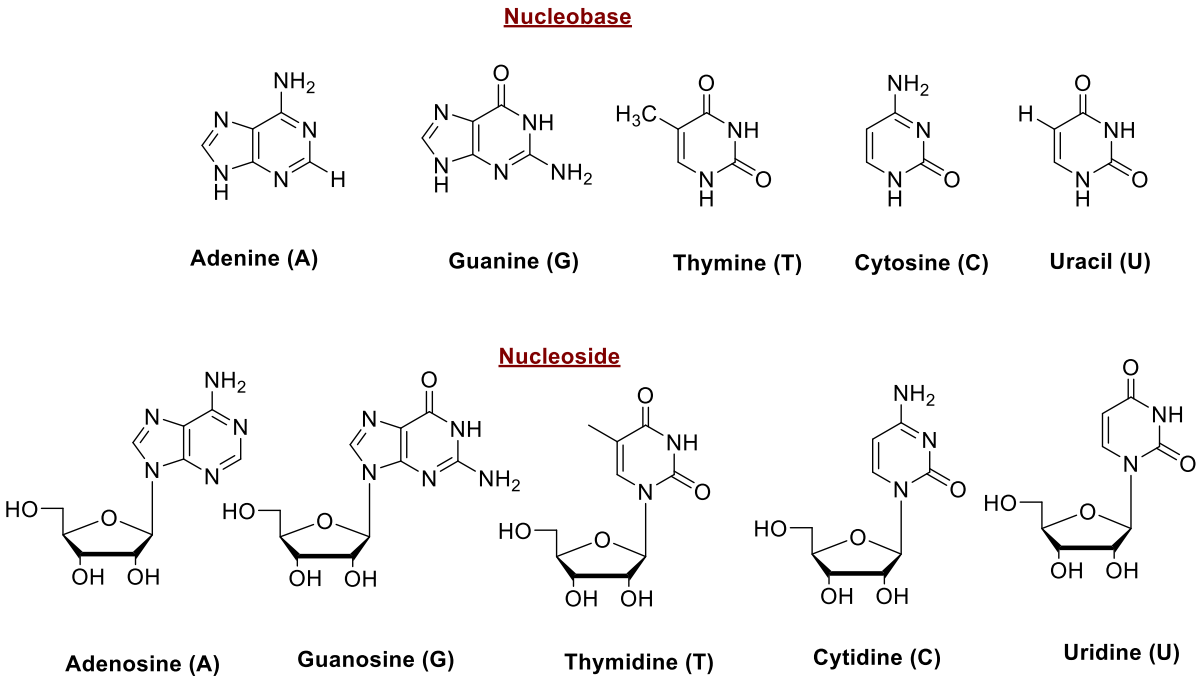

Figure 1.2 The structures of the nucleosides.

The five nitrogenous bases – Adenine (A), Guanine (G), Cytosine (C), Thymine (T) and Uracil (U) - are the fundamental units of the genetic code. The bases A, G, C, and T are characteristic for DNA while A, G, C, and U are found in RNA. These bases belong to two chemical classes: pyrimidines (C, T, U) are composed of a single carbon-nitrogen ring, while purines (A and G) are double-ring structures with two joined carbon-nitrogen rings, but with different side-chains (Figure 1.3).[6] Thymine and uracil have an identical structure except for a methyl group, which is present in T but not in U (Figure 1.3).[10]

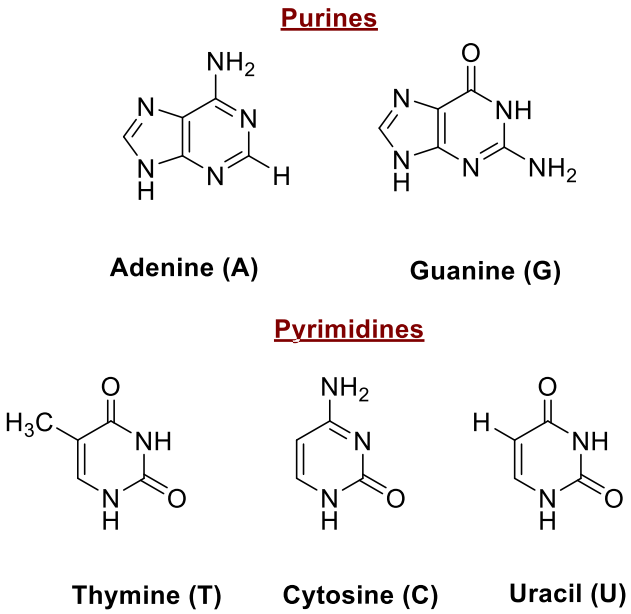

Figure 1.3 The purines and the pyrimidines.

Several structures can be distinguished for DNA and the structure is described on different levels viz. primary, tertiary and quaternary (Figure 1.4).[11]

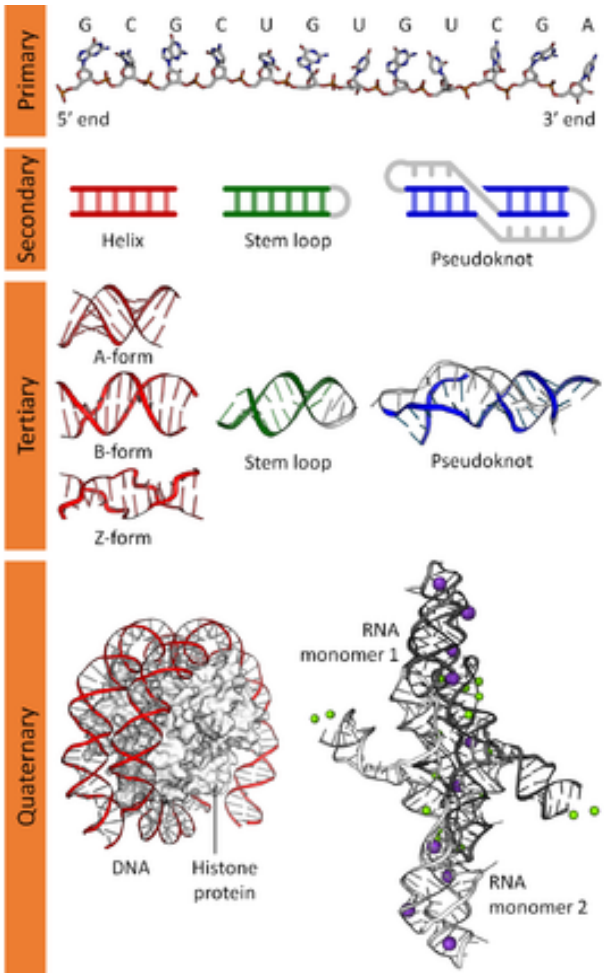

Figure 1.4 Nucleic acid structures (primary, secondary, tertiary, and quaternary) using DNA helices and examples from the VS ribozyme and telomerase and nucleosome.

1.2. Primary structure of DNA

The primary structure of DNA consists of the linear sequence of nucleotides that are linked together. The different nucleotides are covalently joined to form a long polymer chain by covalent bonding between the phosphates and sugars. For any one nucleotide, the phosphate attached to the -OH group at the 5' position of the sugar is in turn bonded to the -OH group on the 3' carbon of the sugar of the of the next nucleotide. As each phosphate-hydroxyl bond is an ester bond, the linkage between two deoxynucleotides is a 3'5' phosphodiester bond (Figure 1.5). Thus, in a DNA chain, all of the 3' and 5' hydroxyl groups are involved in phosphodiester bonds except for the first and the last nucleotide in the chain. The first nucleotide has a free 5' phosphate and the last nucleotide has a free 3' hydroxyl.[12] Therefore, each DNA chain has polarity; it has a 5' end and a 3' end. Traditionally the base sequence is written in the order from the 5' end of the DNA chain to the 3' end. [13-15]

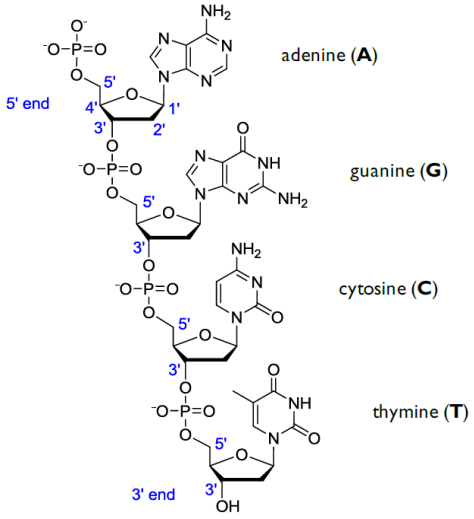

Figure 1.5 3'5' phosphodiester bonds formed between nucleotides in a DNA molecule.

1.3. Secondary and tertiary structure of duplex DNA

Secondary structure is determined by the set of interactions between bases which form the primary structure. These interactions are called base pairing and can occur within a single polynucleotide chain or between two polynucleotide chains.

Two nucleotides on opposite complementary DNA strands that are connected through hydrogen bonds are called a base pair (bp). In DNA adenine forms a base pair with thymine and guanine forms one with cytosine (Figure 1.6).

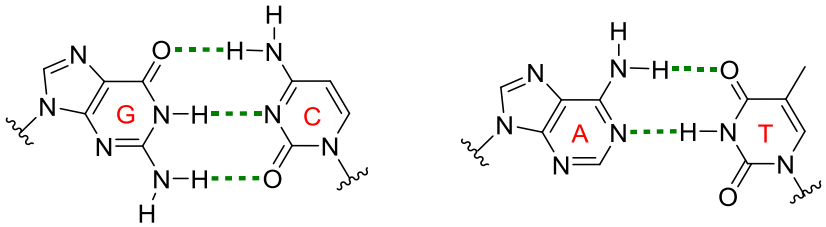

Figure 1.6 DNA complementary base pairs. (Left), a GC base pair demonstrating three intermolecular hydrogen bonds; (Right), an AT base pair demonstrating two intermolecular hydrogen bonds shown in green.

As a result of base pairing, DNA typically exists in the double-stranded helical form (a tertiary structure) proposed by James Watson and Francis Crick in 1953 on the basis of X-ray diffraction data by Rosalind Franklin and colleagues.[16, 17] The double helix is composed of two anti-parallel strands of DNA that contain a phosphate-linked deoxyribose sugar backbone with pendant nucleotide bases.[18] The two anti-parallel strands of DNA are held together by

hydrogen bonds between the adjacent nucleotide bases, where adenine pairs with thymine and guanine pairs with cytosine as shown above. Adenine and thymine form a double hydrogen bond, whereas between cytosine and guanine there is a triple hydrogen bond. The uniquely selective interactions between strands of DNA underpin both the storage of genetic information in biological systems and the use of DNA in the directed assembly. The hydrogen bonds formed between the two nucleotide bases in a base pair force π–π interaction (also called π stacking) between consecutive base pairs. A key driving force for the formation of the double helix is provided by the hydrophobic interaction between the stacked base pairs. The two anti-parallel strands form a helical structure in which the strands are closer at one side than on the other side. The region where the backbones are far apart is called the major groove and the region where they are close is called the minor groove.[19] The grooves are thus unequal in size, the major groove is 22 Ångstrom wide, and the minor groove is 12 Ångstrom wide.[20] The double helix of DNA is shown in Figure 1.7.

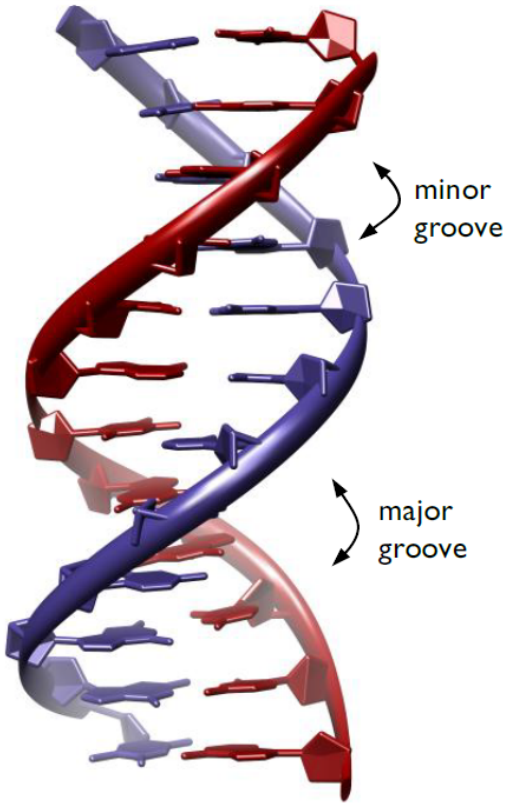

Figure 1.7 B-DNA double helix (Nucleic acid database (NDB) ID: BD0003).

Many double-helical forms are possible; for DNA the three biologically relevant forms are A-DNA, B-DNA, and Z-DNA (Figure 1.8 and Table 1.1). The Watson-Crick structure is B-DNA. The B form is the most stable structure for a random-sequence DNA molecule under

physiological conditions and is therefore the standard point of reference in any study of the properties of DNA. [21, 22, 23]

Figure 1.8 The main DNA conformations (left to right): **(A)** A-DNA (NDB ID: AD0003), **(B)** B-DNA (NDB ID: BD0003) and **(C)** Z-DNA (NDB ID: ZD0008). A-DNA, B-DNA, and Z-DNA conformations of DNA. [22, 24]

Table 1.1. Comparisons of B-form, A-form and Z-DNA.[22]

Property	A-DNA	B-DNA	Z-DNA
Helix handedness	Right-handed	Right-handed	Left-handed
Repeating helix unit	one base pair	one base pair	two base pair
Diameter	~23 Å	~20 Å	~ 18 Å
Rotation per base pair	33.6°	36°	30°
Base pairs per turn	10.7	10.0	12
Helix rise per base pair	2.3 Å	3.32 Å	3.8 Å
Sugar pucker	C3'-endo	C2'-endo	C2' -endo at C C3' -endo at G
Major groove	Narrow and deep	Wide and deep	Narrow and deep
Minor groove	Wide and shallow	Narrow and deep	Narrow and deep

1.4. Triplex DNA

Nucleic acids can also form triplex structures (Figure 1.9).

Figure 1.9 DNA triplex structure (NDB ID: BD0017).

The DNA triplex structure consists of three strands of DNA, one of which is wound around two other strands (which are in a B-form) through so-called Hoogsteen hydrogen bonds (Figure 1.10), hence allowing the formation of triplex DNA. The non-Watson-Crick pairing is called Hoogsteen pairing after Karst Hoogsteen, who in 1963 first recognized the potential for these unusual pairings.[25] The triplex shown is most stable at low pH because the C ≡ G * C^+ triplet requires a protonated cytosine.[26] In Hoogsteen hydrogen bonding, there is pairing between two homopyrimidines and one homopurine, where one homopurine in the third strand runs parallel to the second homopyrimidine.[27, 28]

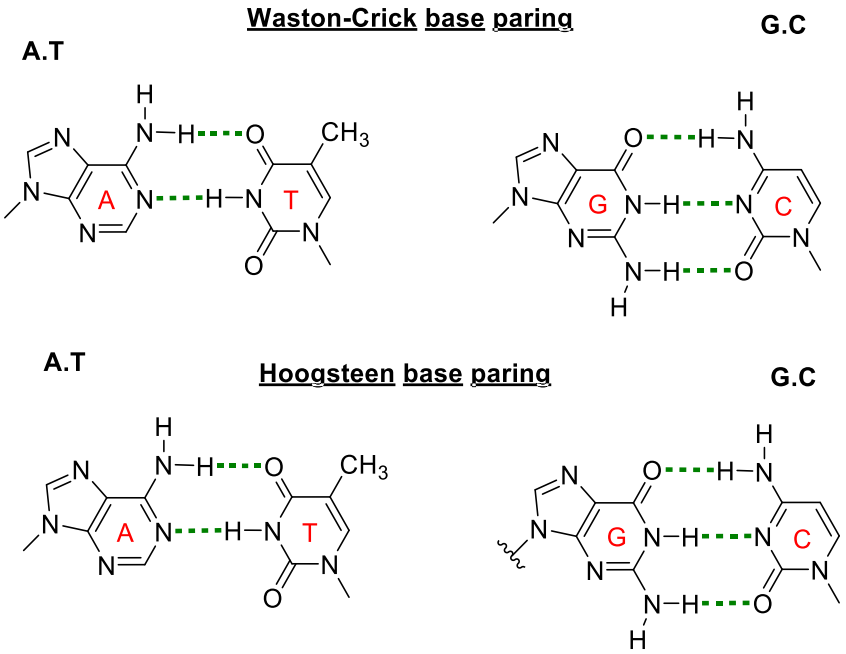

Figure 1.10. Schematic illustration of the A: T and G:C Watson-Crick and Hoogsteen base pairs. Hydrogen bonds are shown as dashed lines.

1.5. Quadruplex DNA

G-quadruplexes (G4s) are formed by DNA sequences that are rich in guanosine nucleotides and form four-stranded secondary structures of DNA. Guanosine bases are important for the formation of the quadruplex structure,[29] where four guanosine nucleotides group together through Hoogsteen hydrogen bonding to form a planar quad-structure known as the guanine tetrad (G-tetrad) (Figure 1.11). The quadruplex structure is further stabilized by the presence of a cation, especially potassium, which sits in a central channel between each pair of tetrads.[30]

While metal atoms plays largely a structural role in most G4 binders, there are also examples where they interact directly with G4s by electrostatic interactions or direct coordination with nucleobases (Figure 1.11).[31]

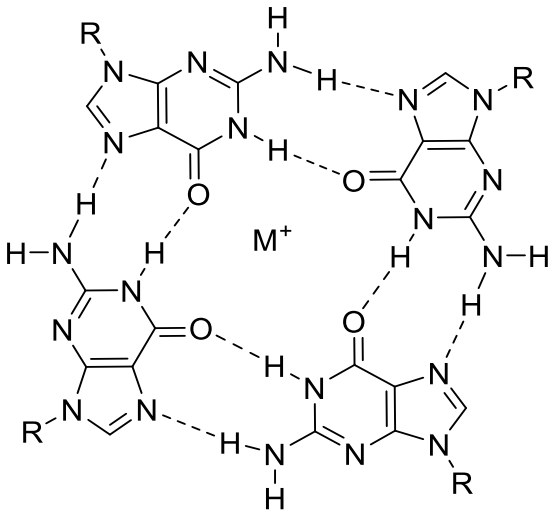

Figure 1.11 (G-tetrad) as the basis for quadruplex DNA formation.

The orientation of strands in the tetraplex can vary, as shown in Figure 1.12.

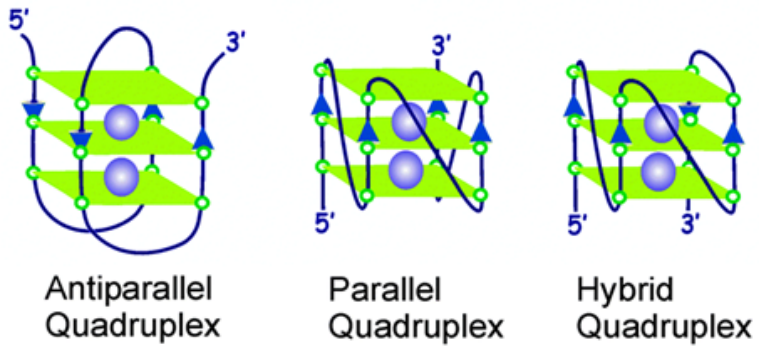

Figure 1.12 the several common topologies found in G-quadruplex.[32]

'If G-quadruplexes form so readily in vitro, Nature will have found a way of using them in vivo', said Aaron Klug, British chemist over thirty years ago.[33] The evidence emerges that their location is non-random, correlating with functionally important genomic regions and that they play an impotant role in various cellular pathways including DNA replication, gene expression and telomere maintenance.[34, 35]

Only a small part of the genome is responsible for coding proteins (for example, only 2% of the human genome encode protein sequences), but a rising percentage is being shown to have regulatory functions, including most sequences within introns. When there is much non-coding DNA, a large proportion appears to have no biological function, as predicted in the 1960s.[36, 37]

Telomeres [5′-(TTAGGG)n-3′] and associated proteins form a unique DNA–protein structure located at the ends of linear chromosomes.[38] These structures are required for capping the chromosome ends from being recognized as DNA double-strand breaks, and provide protection from chromosomal deterioration during DNA replication. Telomeres also regulate telomerase activity.[39] This enzyme is a reverse transcriptase that adds TTAGGG repeats to the ends of chromosomes and thus plays a vital role in telomere length homeostasis.[40] To ensure optimal telomerase activity, telomeric G-rich single strands must unfold. On the other hand, folding of the unfolded structures into a G-quadruplex structure is expected to hinder telomere elongation by telomerase.[41, 42]

Since telomerase is overexpressed in human cancer cells, it has emerged as a potential target in the development of anti-cancer drugs. One of the several different approaches to telomerase inhibition, the stabilization of G-quadruplexes by small molecules, has received much attention.[43]

A promoter is a region of DNA that initiates transcription of a gene. Promoters are located on the same strand and upstream on the DNA, i.e. towards the 5' region of the sense strand. Promoters can be about 100–1000 base pairs long.[44] It has been shown that promoter regions are significantly enriched in quadruplex motifs relative to the rest of the genome, with more than 40% of human gene promoters containing one or more quadruplex motif.[44] Furthermore, these promoter quadruplexes strongly associate with nuclease hypersensitive sites identified throughout the genome via biochemical measurement. Regions of the human genome that are both nuclease hypersensitive and within promoters show a remarkable enrichment of quadruplex elements, compared to the rest of the genome. These quadruplex motifs identified in promoter regions also show an interesting structural bias towards more stable forms.[44] These observations support the proposal that promoter G-quadruplexes are directly involved in the regulation of gene expression. It is established that G-quadruplex DNA motifs are embedded within the promoters of human oncogenes as well in several genes that encode transcription factors but are under-represented in the promoters of housekeeping genes and tumor suppressor genes.[45]

Two examples of the formation of G-tetrads in promoter regions include c-myc and EAD2 as a form of parallel conformation. Moreover, another form of G-quadruplexes formed in human telomeres is the mixed-hybrid conformation 22AG. The G-quadruplex structures 22AG, c-myc and EAD2 are demonstrated in Figure 1.13.[46]

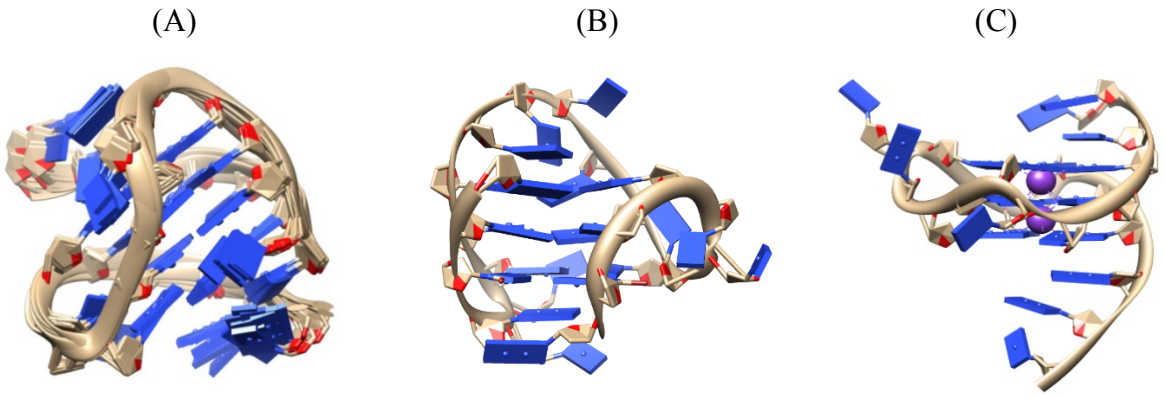

Figure 1.13 (A) G-quadruplex structures of DNA (PDB: ID 2HY9), **(B)** 22AG and **(C)** c-myc (PDB: ID 2HY9).

1.6. The genetic code

According to the central dogma of molecular biology (Figure 1.14), the genetic information present in DNA in the form of codons is transferred to messenger RNA (mRNA) by the process of transcription and then the information is "translated" into protein sequence by the process of translation.[47,48] A codon is a triplet of nucleotides that codes for a specific amino acid. Translation occurs in such a way that these nucleotide triplets are read in a successive, nonoverlapping fashion. A specific first codon in the sequence establishes the reading frame, in which a new codon begins every three nucleotide residues. There is no punctuation between codons for successive amino acid residues. The amino acid sequence of a protein is defined by a linear sequence of contiguous triplets.

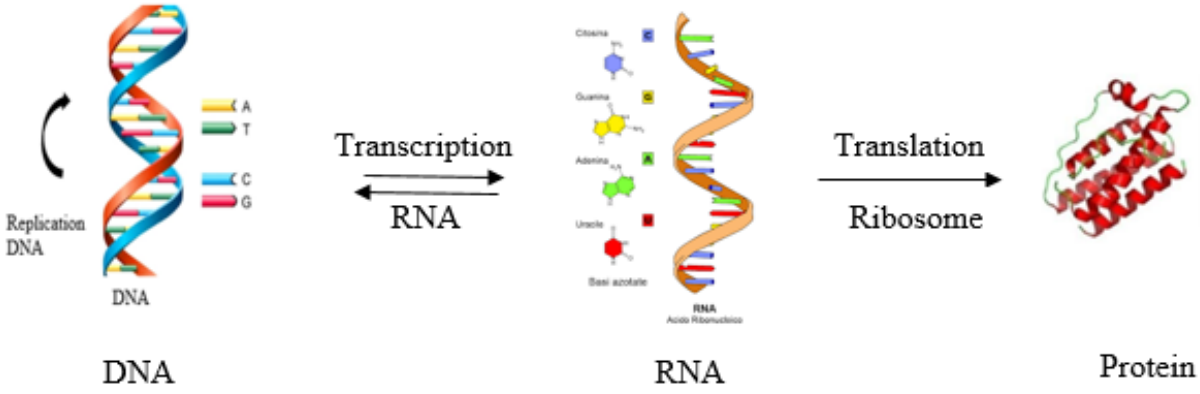

Figure 1.14 The central dogma of molecular biology.

Figure 1.14 shows the two-step process, transcription and translation, by which the information in genes flows into proteins: DNA ⇌ RNA ⟶ protein. Transcription is the synthesis of an RNA copy of a segment of DNA.

The cracking of the genetic code is regarded as one of the most important scientific discoveries of the twentieth century. A striking feature of the genetic code is that an amino acid may be specified by more than one codon, so the code is described as degenerate. This does not suggest that the code is flawed: although an amino acid may have two or more codons, each codon specifies only one amino acid. The genetic code is nearly universal. Human, tobacco plant, E. coli, cobra, and Human Immunodeficiency virus share the same genetic code. Thus, all life forms have a common evolutionary ancestor, whose genetic code has been preserved throughout biological evolution.

1.7. Interaction of small molecules with nucleic acids

The investigation of molecules that target DNA is an interesting field and could prompt applications by which it will be much easier to control numerous hereditary illnesses.

1.7.1. Interaction of small molecules with duplex DNA

Many molecules, including proteins interact with DNA via various modes of interaction. Furthermore, molecules can interact either reversible or irreversibly with DNA. Irreversible binding normally involves non-specific covalent bonding to the phosphate or sugar part of the DNA backbone. This typically means that the DNA breakage, for instance in the case of cisplatin, an anticancer drug, acts exactly in this manner when it binds to nitrogen atoms within DNA bases (Figure 1.15).

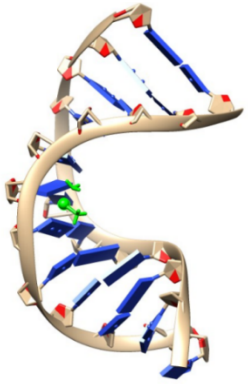

Figure 1.15 Cisplatin interactions with DNA (NDB ID: 1A84).

Molecules can bind to DNA reversibly via several binding modes. Reversible DNA binders interact with DNA via (a) electrostatic interactions (b) intercalation (c) groove binding (major and minor). Electrostatic interactions occur on the backbone of the DNA. Groove binding or intercalation between the base pairs are shown in Figure 1.16.

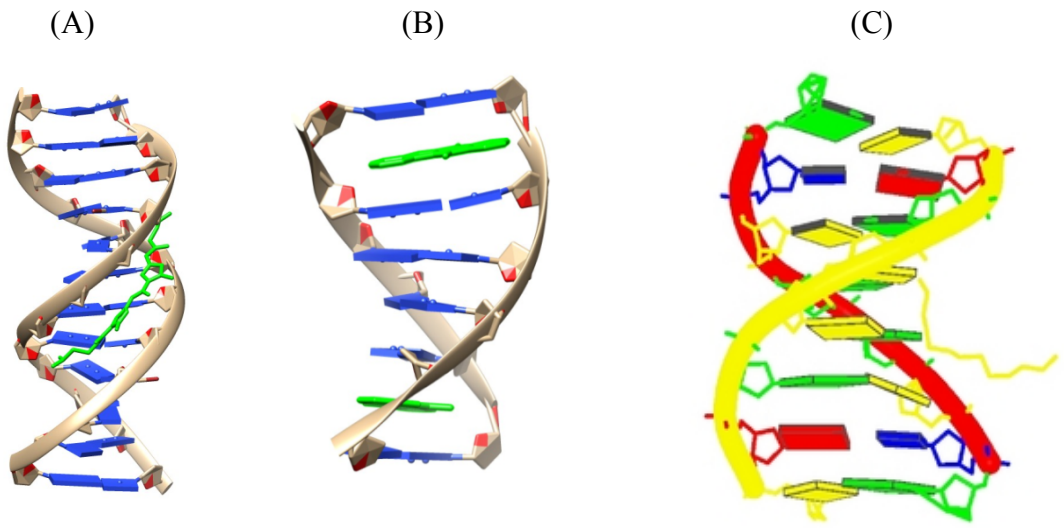

Figure 1.16 Examples of different reversible interactions between molecules and DNA, **(A)** minor groove binding (NDB ID: GDLB05), **(B)** intercalation (NDB ID: DD0070) and **(C)** electrostatic (NDB ID: 2MCJ).

A brief description of the three modes of interaction is provided further.

1.7.2. Electrostatic interaction

Electrostatic interactions are normally non-specific and occur along the outside surface of the double helix structure of DNA. Because the structural framework of nucleic acids is made by alternating phosphate and sugar groups, the DNA backbone is negative charged. This negative charge allows occurrence of electrostatic interactions between DNA and cationic molecules.[49] This specific mode of interaction can be affected by the size of the ligand, the charge on the ligand and ligand hydrophobicity. Electrostatic interactions normally play an important role for stability of the DNA. Nonetheless, non-specific interaction with, for instance, Na^+ or Mg^{2+} leads to partial neutralization of the phosphate backbone's charge. For that reason, the binding of small molecules to DNA is dependant on the ionic strength of the medium.

1.7.3. Intercalation and intercalators

The concept of intercalation was introduced by Lerman in 1961. In this mode of binding, planar (flat and rigid) molecules slide in between the base pairs. Typically, intercalators are not flexible and normally have an aromatic conjugated system. Intercalation occurs between base pairs of DNA.[50] The driving force in this event is π-π stacking interactions and Van der Waals interactions between the planar aromatic molecule and base pairs of DNA. Such

compounds as methylene blue, ethidium bromide and coralyne are intercalators (Figure 1.17). All these compounds are flat and rigid molecules. Metal complexes have several features that make them particularly suitable as G4 DNA binders and therefore as potential drugs.

As human telomeric single-stranded DNA can fold into several intramolecular G-quadruplex structures, the structural features that are considered during the development of ligands include the G-tetrad surface, discrete grooves resulting from combinations of syn- and anti-deoxyguanosine conformations, a central channel with a negative charge and motifs within the flexible loop regions.[32, 51] Several classes of small molecules that bind and stabilize telomeric G-quadruplex structures have been reported. Most of the reported ligands have a planar aromatic surface and interact with the external surface of the G-quartet by π-stacking interactions. Moreover, selectivity and affinity of a ligand can be enhanced by electrostatic as well as H-bonding interactions of the neutral/cationic side chain with the grooves/loops of the quadruplex structure.[44, 52]

Several techniques can be used to assess whether a compound binds to DNA via intercalation. For example, there have been many studies in the literature to investigate the mode of binding of ethidium bromide to duplex DNA. [53, 54] These studies have involved CD spectroscopy, UV-vis spectroscopy.[55]

Coralyne is another example of an intercalating molecule.[56] [57, 58] There are many studies on the interaction between coralyne and DNA.[57] The main binding forces are provided by the planar surface,[59] and the positive charge. In addition, many analytic techniques such as, UV-vis, CD spectroscopy, viscometry and fluorescence spectral study have been used to investigate the intercalation mode of binding.

Another noteworthy example is daunomycin, an anticancer drug. X-ray studies have been used to investigate the intercalation mode of binding of daunomycin to d (CGTACG) which involves insertion of the aromatic system between base pairs (Figure 1.18).

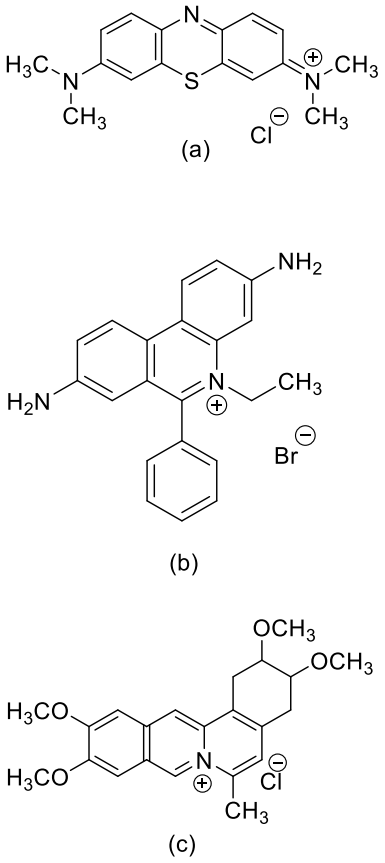

Figure 1.17 Chemical formulae of intercalators, (a) methylene blue, (b) ethidium bromide and (c) coralyne.

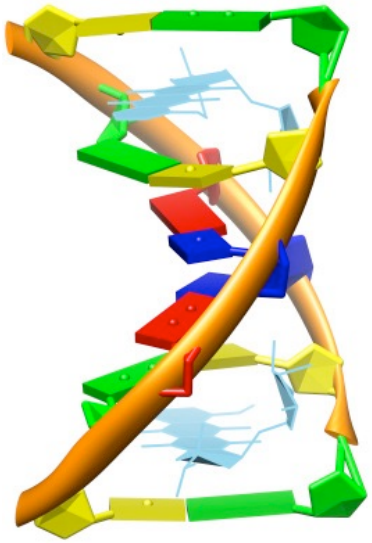

Figure 1.18 X‐ray structure of daunomycin bound to d (CGTACG) (NDB DDF018).

1.7.4 Major and Minor groove binding

Groove binding involves molecules interacting with DNA in the major or the minor groove. Groove binding has the advantage of allowing certain molecules to interact selectid with DNA. Major groove binding by proteins plays important roles in transcription and replication because the major groove provides a binding region allowing DNA-binding proteins to interact in a sequence-selective manner.[60] The major groove is wide, which allows large biomolecules such as proteins to bind to the major groove predominantly through recognition of hydrogen bond donating and accepting sites (Figure A1.19 & B1.20). On the other hand, small molecules are often minor groove binders. Minor groove binders have several characteristics, for instance they are typically long and flexible. Often, minor groove binders are positively charged, and interaction can therefore also occur between the DNA binder and the anionic phosphate backbone of the DNA. In addition, these molecules also interact with the hydrophobic interior in the minor groove as well as through hydrogen bonding with donors and acceptors at the bottomof the minor groove.[61]

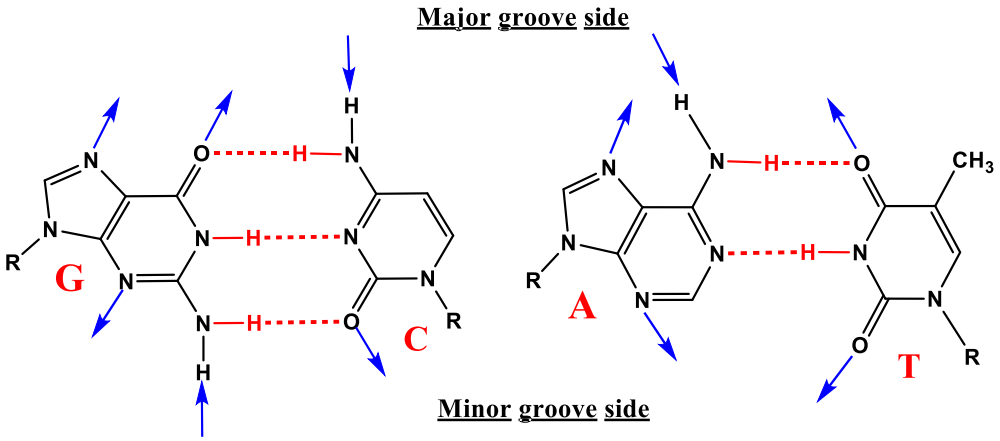

Figure A1.19 nucleic acid base adenine (A), thymidine (C) cytosine and (G) guanine linked by hydrogen bonds (dot lines).

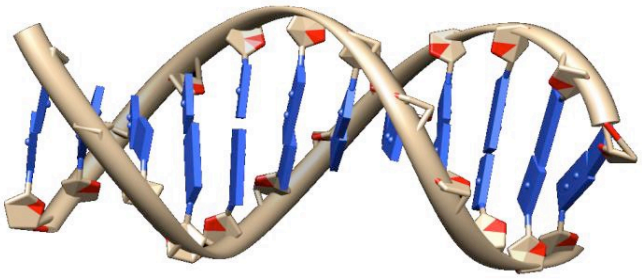

Figure B 1.20 Major and minor grooves of DNA structure (NDB ID: BD0002).

A well-known example of a minor groove binder is Hoechst 33258. Hoechst 33258 has a crescent shape similar to netropsin and distamycin. Hoechst 33258 also has a π-conjugated oligoheteroaromatic framework. Moreover, Hoechst 33258 has enough rotational flexibility around the bonds to fit into the minor groove (Figure 1.21).

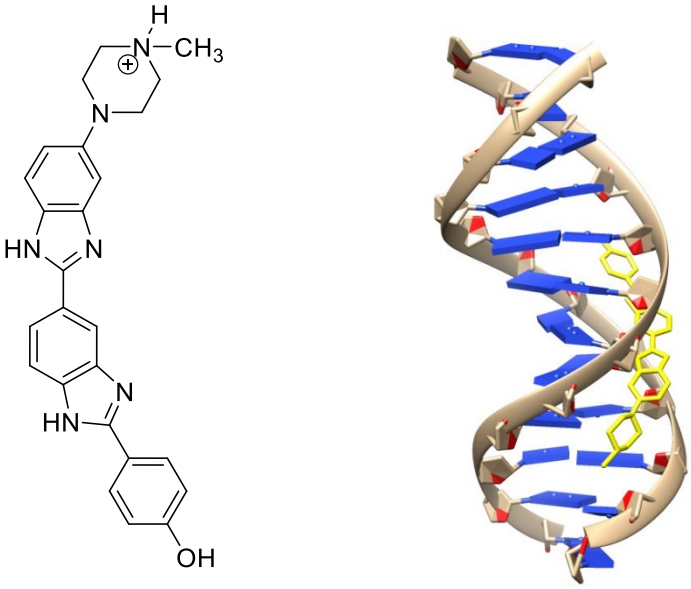

Figure 1.21 Structure of H33258 (left), binding of H33258 to the minor groove d(CGCAAATTTGCG)2 (NDB ID: GDL028) (right).

Studies of the interactions of H33258 to the minor groove show that H33258 interacts specifically with A●T-rich sequences, and has a binding site size of 4-5 base pairs. Nevertheless, H33258 also binds to G●C-rich sequences in the minor groove but with low affinity. Its binding has been studied through a variety of techniques, including Förster resonance energy transfer (FRET), UV-visible spectroscopy, isothermal titration calorimetry

(ITC), circular dichroism (CD) spectroscopy, fluorescence spectroscopy and pulsed gradient spin echo NMR.[62]

Similar to H33258, studies have confirmed the interaction between DAPI and DNA by several biophysical methods such as UV-vis, fluorescence spectroscopy, viscosity and circular dichroism (Figure 1.22).

Figure 1.22 Crystal structure of DAPI bound to DNA sequence D (CGTGAATTCACG) (NDB ID: 5T4W).

Further examples of DNA minor groove binders include distamycin and netropsin (Figures 1.23 and 1.24). Distamycin and netropsin are long, flexible and crescent-shaped. In 1974, Wartell et al showed minor groove binding for netropsin.[63, 64] The driving force for binding to netropsin to A•T rich regions of B-DNA (Figure 1.23) is displacement of water molecules that hydrate the minor groove of DNA. The binding selectivity of netropsinto A•T rich sequences was attributed to the formation of hydrogen bonds between the NH groups on netropsin and the nitrogen in adenine and oxygen of thymine on each adjacent base pair by electrostatic and Van der Waals interactions. The binding of netropsin to DNA always occurs in a 1:1 ratio along four consecutive A•T base pairs. Distamycin binds to DNA in the minor groove by two different modes, viz. 1:1 and 2:1 ratio along five base pairs (Figure 1.23).

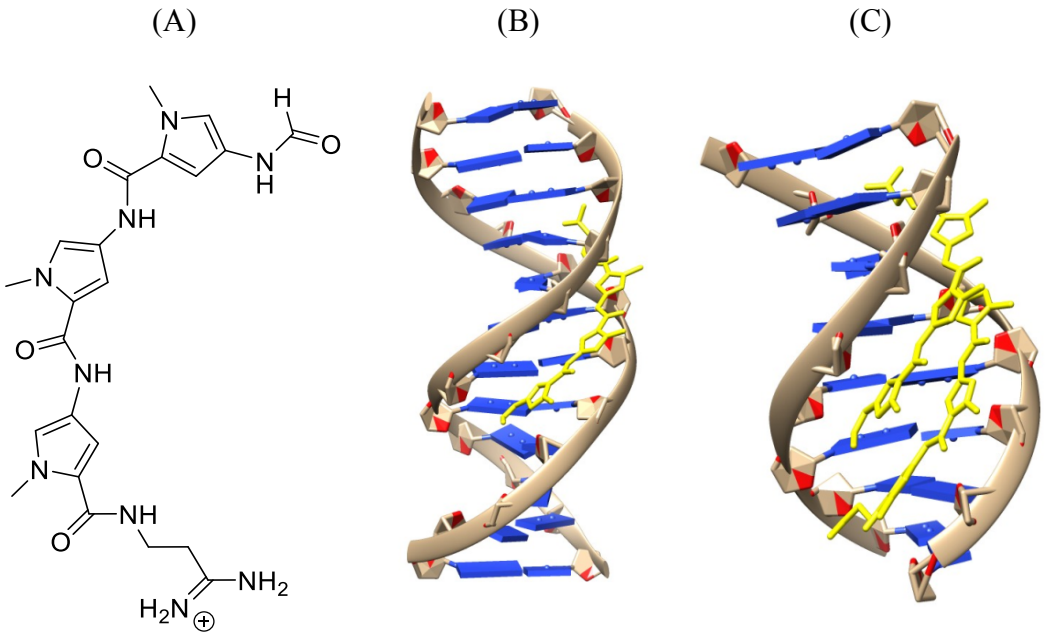

Figure 1.23 Structure of distamycin (A), the groove binding modes of distamycin with DNA duplexes, 1:1 binding of distamycin to DNA (NDB ID: GDL 003) (B); side-by-side binding of distamycin to DNA (NDB ID: GDH060) (C).

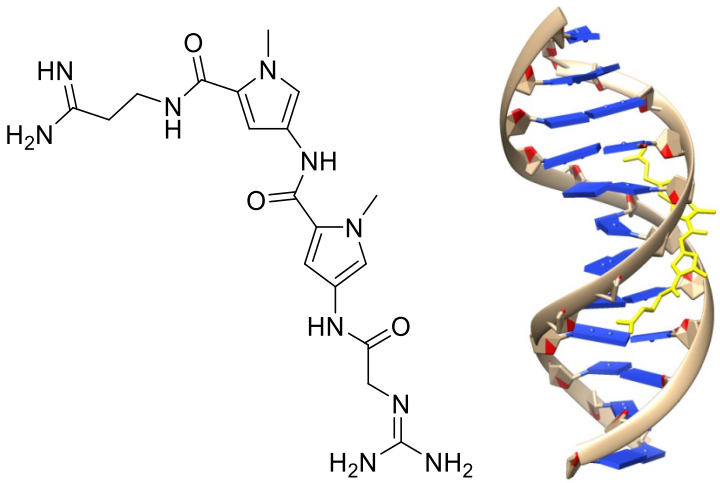

Figure 1.24 Structure of netrospin (left), 1:1 binding of netropsin in the minor groove (based on NDB ID: GDL B05) (right).

A partilarly well-known class of polyamide minor groove binders are known as Dervan's hairpin polyamides (DHP). Dervan et al, whose research was inspired by sequence-selective natural compounds such asnetropsin and distamycin, provided insight into the molecular forces that govern the affinity and specificity of pyrrole-imidazole polyamides. Hairpin

polyamides are synthetic ligands for sequence-specific recognition in the minor groove of double-helical DNA. DHPs are composed of amide-coupled heterocycles, which two polyamides binding to double-stranded DNA in the minor groove in a side-by-side manner forming 1:1 complexes with A•T base pairs. Furthermore, a 2:1 binding mode for this class of compounds was revealed for 1-methylimidazole-2-carboxamide netropsin (2-Im-N) which specifically binds to 5'-TGAT (Figure 1.25).

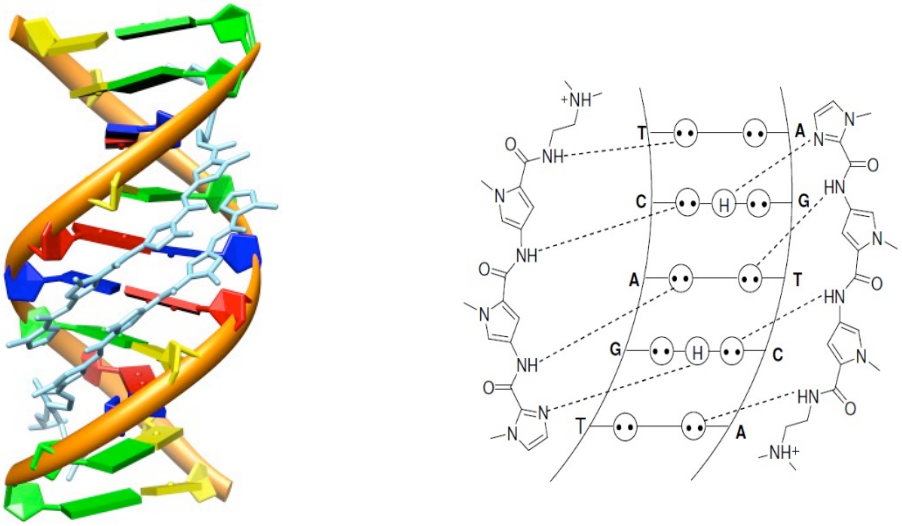

Figure 1.25 X-Ray structure (left) and hydrogen bonds view of side-by-side dimer of 2-Im-N bound to d(TGACT) (NDB ID: BDD003).

Recognition of double-stranded DNA by DHPS is limited to five base pairs. The reason for that is the curvature polyamide molecules no longer matches with the minor groove of DNA.[65] Hence, Dervan and co-workers synthesized polyamides to bypass this, and "turn to turn" or "turn to tail" tandems recognise longer DNA sequences extending the selectivity to 10 base pairs (Figure 1.26).[66]

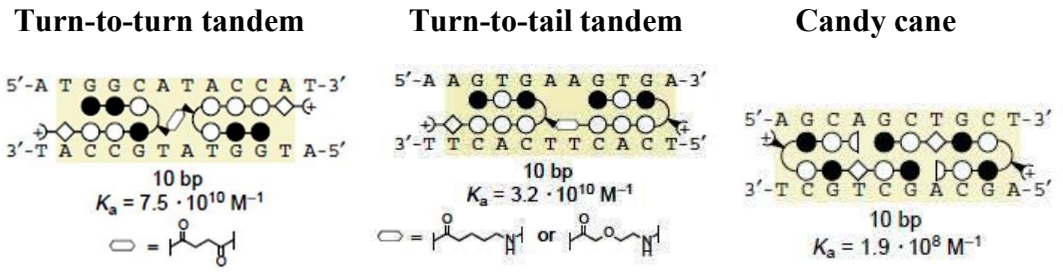

Figure 1.26 cartoon representations of polyamide models for binding to extended DNA sequences. [45]

Additionally, minor groove binders can form hydrogen bonds with nucleotide bases. Examples of such groove binders are H33258, GB01, DAPI and DODC (Figure 1.27).

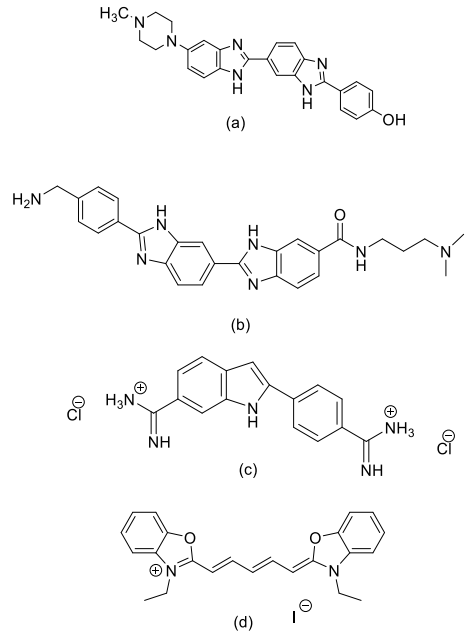

Figure 1.27 Chemical formulae of minor groove binders (a) H33258, (b) GB01 (c) DAPI and (d) DODC.

On the other hand, some compounds combine two modes of interaction because the typically higher flexibility and also flat polycyclic aromatic ring molecules such as basic yellow (thioflavin T) and thiazole orange (Figure 1.28).[67]

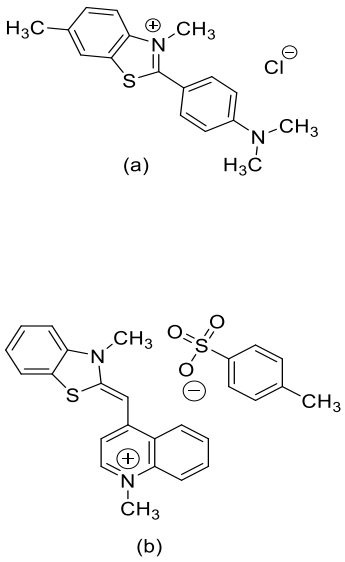

Figure 1.28 Chemical formulae of minor groove binders and intercalators, (a) basic yellow (thioflavin T) and (b) thiazole orange.

Basic yellow (thioflavin T) is a typical example of a fluorescent dye. The different binding modes of basic yellow have been investigated by spectrophotometric and spectrofluorometric methods. It has been reported that basic yellow (thioflavin T) displays several binding modes, including intercalating and minor groove binding.[68] Key intercalated interactions are hydrophobic between benzothiazole and dimethylaniline groups and base pairs. Moreover, basic yellow is cationic by its nature, also allowing electrostatic interactions.

1.8. Techniques for studying interactions between small molecules and nucleic acids

The interaction of DNA binding-small molecules can be studied through a variety of techniques, viz. UV-visible, circular dichroism spectroscopy (CD), isothermal titration calorimetry (ITC), fuorescence resonance energy transfer (FRET) and competition dialysis. These techniques are briefly described below.

1.8.1. UV-Visible Spectroscopy (UV-vis)

UV-visible spectroscopy measures the amount of radiation absorbed by a sample at each wavelength in the ultraviolet and visible regions of the spectrum. The absorption of ultraviolet (200-400 nm) and visible (400-800 nm) light by molecules is associated with the excitation of valency electrons from the electronic ground state to higher energy states. The absorption of UV-visible radiation by a molecule typically results in the electronic transition of an electron from the highest occupied molecular orbital (HOMO) to the lowest unoccupied molecular orbital (LUMO). The wavelength of the absorbed radiation depends on the energy difference between the orbital originally occupied by the electron and the orbital to which it

is promoted. Absorbance (A) often, but not always, increases linearly with the concentration (c) of the chromophore as described by the Beer Lambert law (equation 1.1):

$$A = \varepsilon \times c \times l \quad (1.1)$$

where c is the concentration of the sample in moles per litre of the solution, ε the molar extinction coefficient in M^{-1} cm^{-1}, and l the optical path length.[69]

Absorption spectroscopy is an important technique for studying ligand-DNA interactions since spectroscopic information can be deconvoluted to yield concentrations of free and bound species. Because of interactions of molecules with DNA, modification in structural conformations of ligands and changes in the properties of the medium surrounding the binder occur, resulting in changes in spectroscopic response. Titration of a ligand with DNA can show changes in the position of the wavelength of maximum absorbance (λ_{max}) and in extinction coefficient.

These changes may be an increase (hyperchromicity) or decrease (hypochromicity) in molar absorptivity of ligands or conceivably a movement of the wavelength of highest absorption to higher wavelength (red shift) or to lower wavelengths (blue shift).[70] Plotting these absorption spectra in one graph may reveal an isosbestic point which is the wavelength at which two species involved in the titration have the same molar absorptivity.[71, 72] An example of an isosbestic point is demonstrated in Figure 1.29.

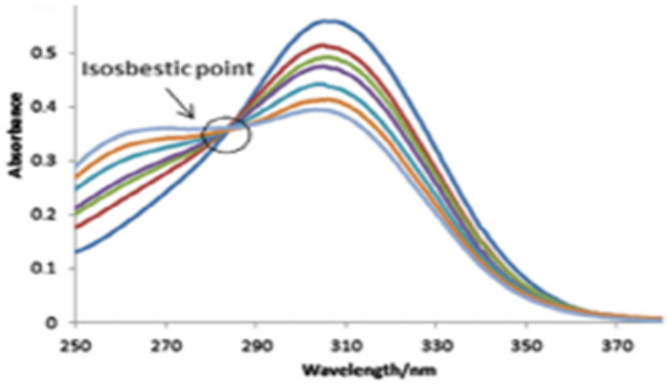

Figure 1.29 Spectrum showing an isosbestic point[73]

The observation of an isosbestic point suggests that an equilibrium is achieved between two species viz. free and bound ligand.[74]

When the spectra have been recorded, titration curves can be extracted from the UV-visible data by plotting the absorbance at one or more wavelengths against DNA concentration.[75]Absorbance data is then typically analysed in term of the multiple independent binding sites (MIS) model, which is used to determine the binding constant $K_{binding}$ and binding site size (n) or binding stoichimetries. The MIS model is derived from the complexation equilibrium (equation 1.2).

$$L_f + bs_f \longleftrightarrow L_b \qquad (1.2)$$

L_f and bs_f, and complex are the concentrations of free ligand, free binding site and bound ligand (complex) which are related through $K_{binding}$ (equation 1.3).

$$K_{binding} = [L]_b / [L]_f . [bs]_f \qquad (1.3)$$

Each binding site will cover a ligand-specific number of base pairs n for a single ligand molecule.

$$[bs] = [DNA] / n \qquad (1.4)$$

The concentration of binding sites is the concentration of DNA base pairs divided by the binding site size n. The concentration of free ligand $[L]_f$, free binding sites $[bs]_f$ and complex concentration [C] are related through the total ligand concentration $[L]_{tot}$ and total binding site concentration $[bs]_{tot}$ (1.5), (1.6).

$$[L]_t = [L]_f + [C] \quad \longleftrightarrow \quad [L]_f = [L]_t - [C] \qquad (1.5)$$

$$[bs]_t = [bs]_f + [C] \quad \longleftrightarrow \quad [bs]_f = [L]_t - [C] \qquad (1.6)$$

Consequently, it is possible to establish an overall equation describing the equilibrium (1.7)

$$[C] = K_{bind} [bs]_t.[L]_t - K_{bind}. [C]. [bs]t - K_{bind}. [C].[L]_t - K_{bind}.[C]^2 \qquad (1.7)$$

which is rearranged to give quadratic equation (1.8).

$$K_{bind} [C]^2 - (1 + K_{bind}. [bs]_t + K_{bind}. [L]_t). [C] + K_{bind}. [bs]_t.[L]_t = 0 \qquad (1.8)$$

The quadratic equation (1.8) is solved using the classic Equation 1.9 to provide an expression for the concentration of complex [C] as a function of total ligand and binding site concentrations (1.10).

$$[C] = \frac{-b \pm \sqrt{b^2 - 4ac}}{2a} \quad (1.9)$$

$$[C] = \frac{1 + K[bs]_t + K[L]_t \pm \sqrt{(1 + K[bs]_t + K[L]_t)^2 - 4K^2[bs]_t\,[L]_t}}{2K} \quad (1.10)$$

By inserting the concentrations into the Beer-Lambert Law (Equation 1.1), modified for background absorbance, the observed absorbance is given by Equation 1.11. This equation can be fit to a plot of absorption against total DNA concentration to find the best approximation for binding constant and binding site size.

$$\text{signal}_{obsd} = \text{background} + \text{signal}_{free,\,m}.[L]_t + \Delta_{binding}\,\text{signal}_m \frac{1 + K.\frac{DNA}{N} + K.[L]_t - \sqrt{\left(1 + K.\frac{DNA}{N} + K.[L]_t\right)^2 - 4K^2.\frac{DNA}{N}.[L]_t}}{2K}$$

Equation 1.11

The terms in equation 1.11 are defined as follows.[76] The term signal_{obsd} is the observed absorbance at the selected wavelength; $\text{signal}_{background}$ is the background signal (baseline or buffer absorbance); $\text{signal}_{free,m}$ is the molar signal of the free ligand (the molar extinction coefficient when UV-visible spectroscopy is used); $[L]_{tot}$ is the total ligand concentration; $\Delta_{binding}\,\text{signal}_m$ is the change in the molar extinction coefficient signal upon binding; *K* is the binding constant or equilibrium constant; $[DNA]_{tot}$ is the total DNA concentration in base pairs: *n* is the binding site size in base pairs.

1.8.2. Circular Dichroism Spectroscopy (CDS)

Circular dichroism (CD) spectroscopy is a technique that is widely used[77] to study chiral molecules and for non-chiral molecules interacting with chiral compounds such as biomacromolecules.[78, 79] Circular dichroism spectroscopy uses the difference in the absorption of left–handed circularly polarised light (L-CPL) and right–handed circularly polarised light (R-CPL) by chiral chromophores.[78, 80, 81] If the molecules contains chiral chromophores, or if an achiral chromophore is placed in a chiral environment, then the chromophore will absorb one form of circularly polarised light to a higher extent than the other. For instance, if right-circularly polarised light (R-CPL) is absorbed to a smaller amount extent than left-circularly polarised light (L-CPL), a CD signal will appear at the corresponding wavelength.[82, 83] Thus, CD spectroscopy has been used to study a wide range of biological molecules and processes such as DNA–ligand binding, and protein-ligand binding.[83] CD spectroscopy can show how the DNA binds with the ligand by varying the

environment that a binder experiences.[82] The effect where a chiral environment (such as DNA) causes a non-chiral molecule to display a circular dichroism signal is called induced circular dichroism (ICD). Previous studies have reported that large ICD signals and small ICD signals are indicative of groove binding and intercalation, respectively. For intercalation, small ICD signals are common (< 10 M^{-1} cm^{-1}) and the ICD signals (ellipticities) are usually negative. However, for groove binders, the ICD signal is typically strong and positive.[84] Examples of no change in CD spectrum (sulforhodamine in the presence of DNA) and negative ICD (basic fuchsin **(4)** in the presence of DNA) are shown in Figure 1.30.

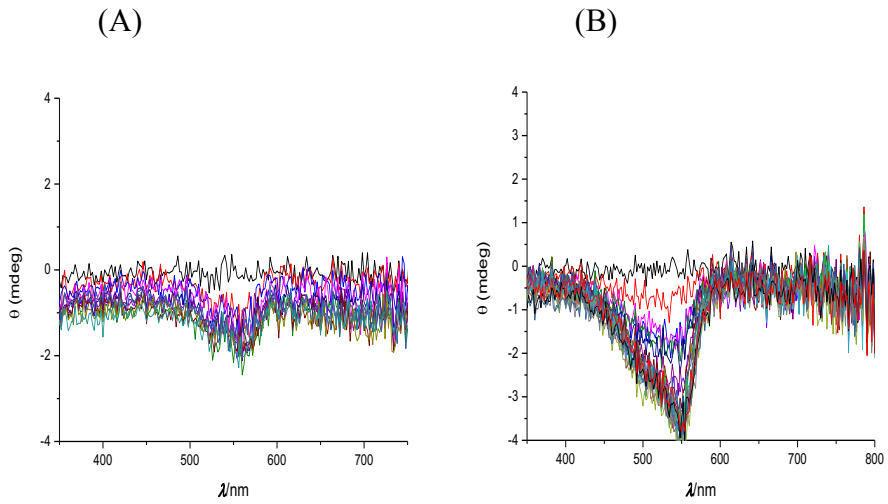

Figure 1.30 Circular dichroism spectra for (A) no change for sulforhodamine, and (B) negative ICD for basic fuchsin.

1.8.3. Isothermal Titration Calorimetry (ITC)

Isothermal titration calorimetry (ITC) is a technique that can be used to study biomolecular interactions.[85] ITC measures the heat generated or absorbed as a result of molecular interactions.[86] A microcalorimeter contains two identical cells (Figure 1.31), one reference cell (filled with water or buffer), and one sample cell which contains the macromolecule. These two cells are kept at the same temperature by the microcalorimeter. When a ligand is titrated into the sample cell, there are two possible heat effects. If the reaction or interaction is exothermic, the temperature in the sample cell will increase relative to the reference cell. When this occurs the feedback power to the sample cell decreases. If the reaction is endothermic, the temperature in the sample cell decreases and the feedback power to the sample cell is increased.[87]

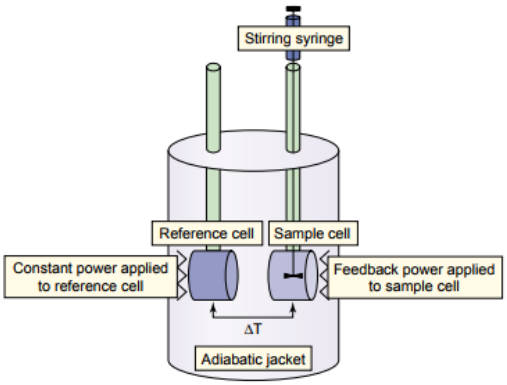

Figure 1.31 Schematic representation of a power compensation ITC[88]

1.8.4. Isothermal Titration Calorimetry data analysis through IC-ITC

In the case of isothermal titration calorimetry experiments, self-aggregation can happen because of the high concentration of ligand in the injection syringe.[89] This is why the self-aggregation of the ligand needs to be taken into account during the data analysis in conjunction with the consideration of DNA-binding parameters. The group has previously developed software called IC-ITC to analyse numerically calorimetric data for combined self-aggregation and DNA binding.[89] Using IC-ITC we can determine thermodynamic parameters for the various equilibria involved (Figure 1.32).

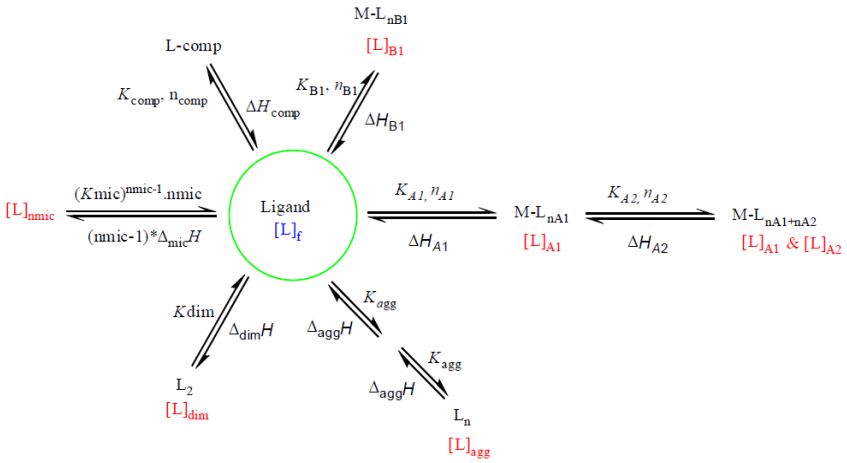

Figure 1.32 [90]

The software first calculates the concentrations of ligand and biomolecule after each addition of the ligand into the sample cell.[62]

The mass balance equation is expressed in terms of Equation 2.

$-[L]_{total} + \sum_x [L]_x = 0$ Equation 2

The terms in equation 2 are as follows,

The term $[L]_{total}$ is the total ligand concentration; $[L]_x$ is the concentration of ligand in all various forms X, for instance free, ligand, DNA-bound ligand, aggregated ligand, etc.

Equation 3 shows the formal link between the ligand concentrations taken up in the complexes and in the aggregates, $[L]_x$, and the free ligand concentration $[L]_f$, which also depends on the total macromolecule concentrations $[M]_t$ and the interaction parameters $\mathbf{a}_x$ for the complexation events for instance, equilibrium constants and the stoichiometry.

$[L]_x = f([L]_t, [M]_t, \mathbf{a}_x)$ Equation 3

Using a set of interaction parameters $\mathbf{a}_x$, the equilibrium concentrations are determined numerically by solving the mass balance equation using the Newton-Raphson algorithm.[91]

IC-ITC provides the optimised values for the binding parameters $\mathbf{a}_x$, as identified by the lowest sum over square deviations. Furthermore, IC-ITC allows the determination of the error margins and covariance for various variables.

1.8.5. Fluorescence resonance energy transfer (FRET)

Fluorescence resonance energy transfer **(**FRET) is a physical mechanism of radiationless transfer of energy between two dye molecules called chromophores. FRET depends on the distance between donor and acceptor molecules. It is most suitable when the donor-acceptor distance is within 10 nm range.[92] The donor molecule initially absorbs the energy which is subsequently transferred to the acceptor molecule.[93] The donor fluorophore in a FRET experiment can be excited by using light.[81] An excited electron can either return to the ground state by emitting light (fluorescence) or go through a non-radiative process, which requires an acceptor molecule in proximity. This interaction occurs over greater than interatomic distances without any molecular collision or any conversion to thermal energy. The energy transfer depletes the donor's fluorescence intensity and its excited state lifetime and increases the emission intensity of the acceptor.

A pair of molecules that interacts in such a manner that FRET occurs is often referred to as a donor/acceptor pair. FRET involves the energy transfer between excited states in donor molecules to acceptor molecules as a result of non-radiative dipole–dipole coupling.[94]

The process can be described with the following scheme [D-Donor, A-Acceptor]:[95]

$D + hv \rightarrow D^*$

$D^* + A \rightarrow D + A^*$

$A^* \rightarrow A + hv'$

While there are many factors that influence FRET, the primary conditions that need to be met for FRET to occur are relatively few. These include the following:

- proximity between donor and acceptor molecules,
- overlap of absorption and excitation spectra of donor and acceptor, respectively.
- dipole orientations must be approximately parallel to each other,
- sufficient lifetime of the fluorescence of the fluorophores. [96]

The required spectral overlap integral between the excited states in the donor molecules and the absorbance of the acceptor molecules is illustrated in Figure 1.33.

FRET is actively used in biomedical research and drug discovery.[97] For example, FRET is used to study structure and conformation of proteins and nucleic acids, spatial distribution and assembly of proteins, distribution and transport of lipids, interactions between receptor/ligand

interactions, nucleic acid hybridization, membrane potential sensing, also to detect SNPs, to perform imunoassays and real-time PCR etc.[98]

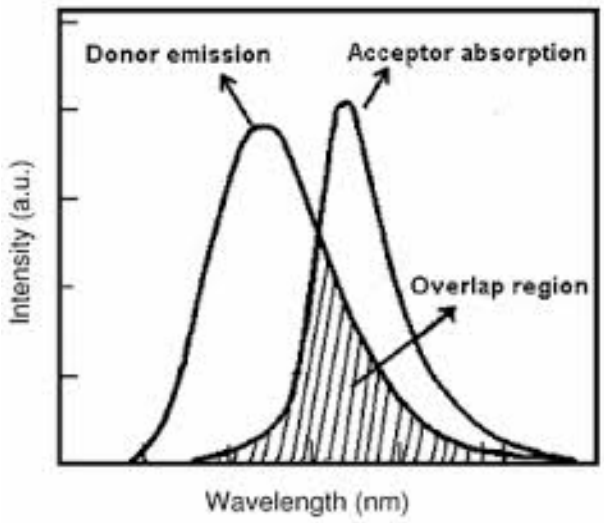

Figure 1.33 The FRET spectral overlap integral.

Induced Fluorescence Resonance Energy transfer (iFRET) is used for the detection of DNA hybridization. This method is perfectly suited for melting curve analysis and entails using a double-strand DNA-specific intercalating dye (e.g., SYBR Green I) as the FRET donor, with

a conventional FRET acceptor affixed to one of the DNA molecules. Three strategies for detecting DNA hybridization with fluorescence are illustrated in Figure 1.34.[99]

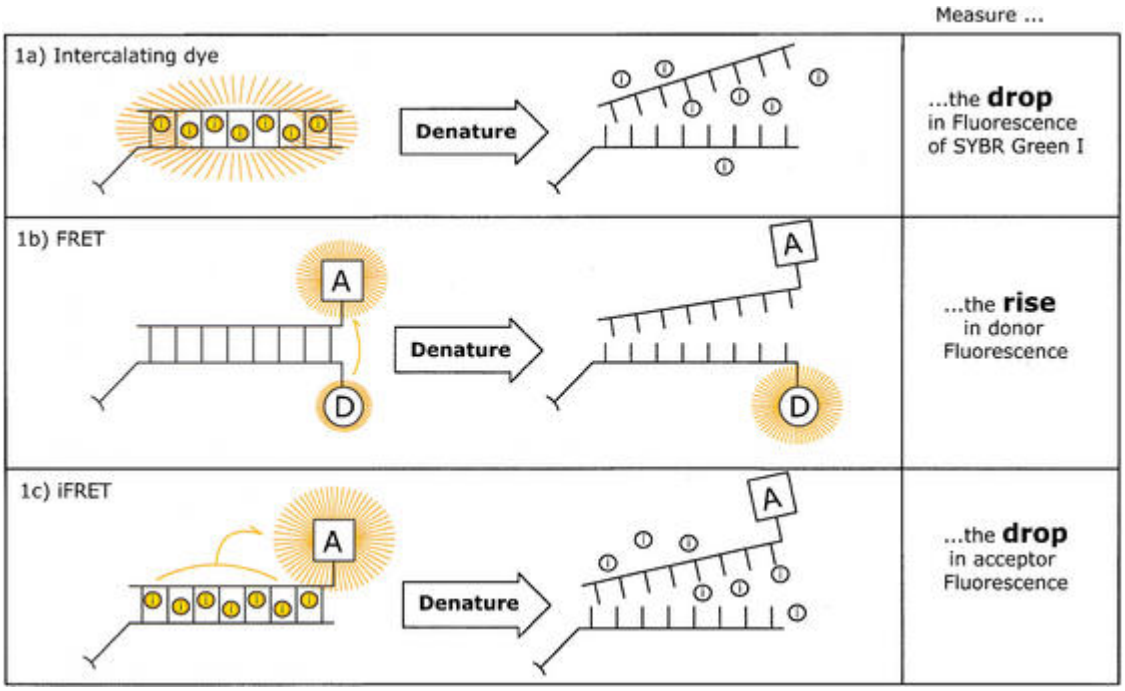

Figure 1.34 Three strategies for detecting DNA hybridization with fluorescence. Fluorescent outputs are indicated by radiating lines. (i) Intercalating dye, (D) donor moiety, and (A) acceptor moiety.

iFRET provides fluorescence signals of enhanced magnitude, implying many advantages. For example, smaller volume or weaker PCR reactions will be possible to assay, and less sophisticated imaging equipment is used for signal detection. iFRET also reduces cost by removing the necessity for a physically attached donor on one of the interacting DNA molecules, yet it preserves the spectral-multiplexing potential afforded by FRET. Essentially all forms of florenscence background allow for very clean assays with all the benefits that naturally follow from this, such as allowing throughputs to increase and automation to replace human intervention.

1.9. Application of small molecule DNA binders.

1.9.1. Biosensors

The enormous amount of genetic information brought by extensive genome sequencing allowed understanding how life is sustained, how diseases develop or how we can cure them.[100, 101] Biosensor also has raised the need for simple, cheap and high-throughput

analytical devices to attend the growing market of molecular diagnostics for decentralized DNA testing.

Such analytical devices, known as biosensors, convert a biochemical reaction or interaction into an analytical signal that can be further amplified, processed and recorded. Among them, DNA biosensors consist of an immobilized DNA strand to detect the complementary sequence by DNA–DNA hybridization. Biosensors have become extremely popular over last 20 years.[102]

Today biosensors are vitally important and are being used in many applications including industrial, clinical, chemical and environmental.[103, 104] Some of the significant benefits for using biosensors include the high sensitivity and fast response. The most important reasons for using a biosensor in medicine are to establish the presence of pathogens or to estimate the chances of diseases to occur in the future.

A typical biosensor includes a bioelement and a transducer. The bioelement is a biological molecule, which recognizes the target analyte while the transducer has capacity to convert that recognition event into a measurable signal. Transduction could be generated through several different mechanisms, or even through a combination of any of these mechanisms (Figure 1.35).

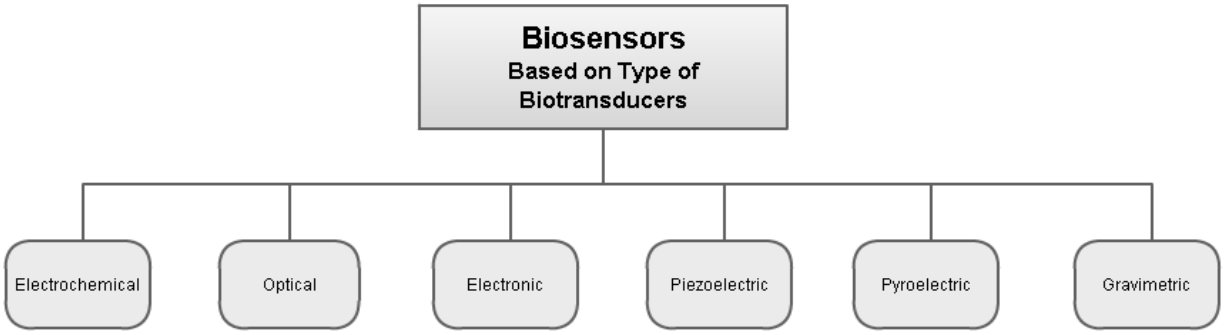

Figure 1.35 Classification of biosensors based on type of biotransducer.

Nucleic acid-based biosensors, also called genosensors, are considered one of the best biosensors in medicine due to the high sensitivity of detection.[105] The recognition process in genosensors is based on the principle of complementary base pairing in DNA. If the target sequence is known, complementary sequences can be synthesized, labelled, and then immobilized on the sensor. The hybridization probes can then base pair with the target sequences, generating an optical signal.[106] The favoured transduction principle employed in

this type of sensor has been optical detection (Figure 1.36). Genosensors are widely used not only in medicine but also in food industry and environmental monitoring.[107]

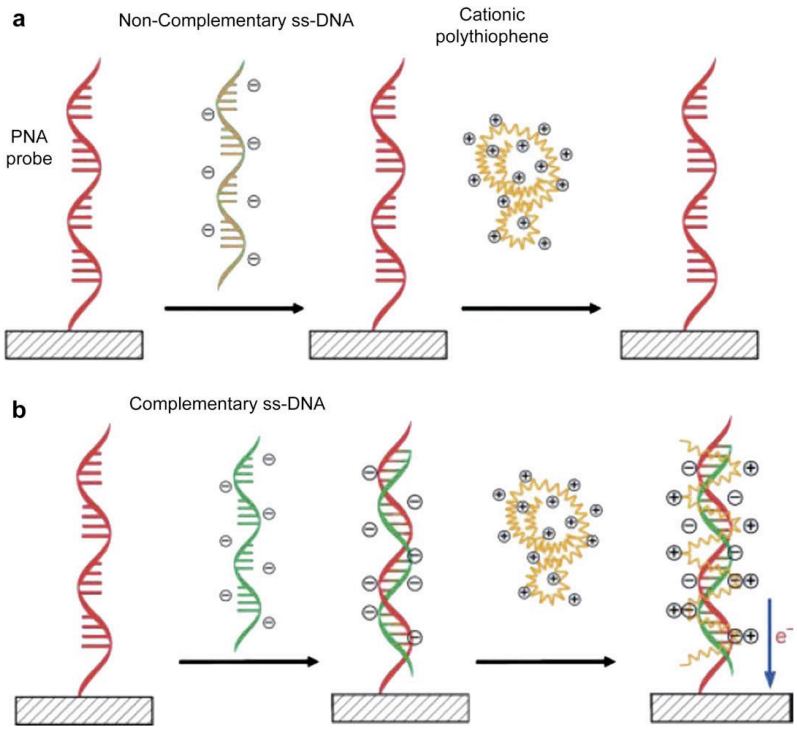

Figure 1.36 description of the electrochemical detection of DNA targets, (a) without and (b) with non-complementary ss-DNA.[108]

The initial efforts that have been carried out to detect the hybridization of DNA through electrochemical means were put forth by Garnier and his team, who covalently connected the probe of ssDNA to the backbone of polypyrrole.[109] The most frequently used approach for detection of nucleic acids uses a single-stranded capture strand (ssDNA or ssPNA) which is typically immobilised on a transducing element such as an electrode. The capture strand is exposed to the sample solution where it finds its complementary target strand if it is present.[110] The intrinsic sequence selectivity of DNA base pair formation assures the sequence specificity. Figure 1.37 illustrates a genosensor design where (a) denotes a surface-immobilised capture strand and (b) denotes the duplex formed as a result of hybridisation with the target strand. The design then uses the fluorescence or redox property of the π-conjugated DNA binders as a sensitizer. The detection procedure can be either labelled or label-free. In labelled detection, the target strands are covalently labelled with the sensitiser.[111] In case of label-free detection, the nucleic acids are not required to be labelled

covalently, rather the sensitizer non-covalently binds to the target strand, as seen in Figure 1.37 (c).

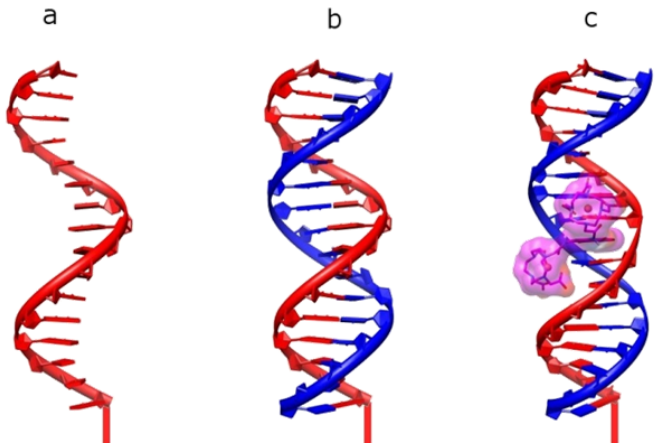

Figure 1.37 schematic design of a genosensor for the sequence selectivity of the DNA detection including a duplex- DNA binding sensitizer.

A transformation to a more positive potential of oxidation can be seen for the construct of the polypyrrole-oligonucleotide in a cyclic voltammogram. Such alterations in the electronic characteristics of polypyrrole were linked to the modifications in the conformation of polymer that takes place during the formation of duplex resulting from the attachment of a strand to the conjugate of polymer-oligonucleotide. Subsequently, several modified polythiophenes were used to detect the hybridization of DNA electrochemically. For instance, it has been reported by Lee et al.[108] that terthiophene can be electropolymerised on the glassy carbon electrode surface due to the presence of the electroactive carboxylic acid groups (Figure 1. 38). The incorporation of functional groups like carboxylic group onto the polymer backbone in covalently bound by an oligonucleotide may serve as a biosensor for DNA recognition involved the studying of genetic disease.[112]

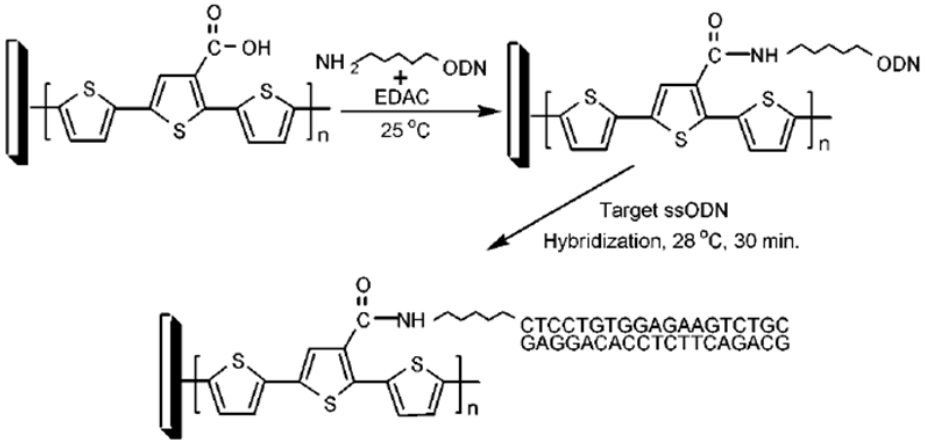

Figure 1.38 Hybridization of terthiophene.

Another example is provided by peptide nucleic acids (PNA), synthesized synthetic polymer similar to nucleic acid but replacing phosphate ester linkages with peptide linkages. Peptide nucleic acids are DNA mimics in which the sugar-phosphate backbone is replaced by 2-aminoethyl-glycine linkages and the nucleotide bases are attached to the peptide nucleic acid's backbone by a methylene bridge and also by a carbonyl group.[113] The advantages of using PNAs as an example of capture probes in biosensing include elimination of repulsion forces between two hybridized strands because of the neutral backbone of PNAs.[114] As a result, PNA can bind to complementary strands with a higher affinity and selectivity than DNA.[115-117]

The thermodynamic stability of peptide nucleic acids (PNA) is greater than DNA. This is because the lack of electrostatic repulsion forces between the uncharged PNA backbone and negatively charged DNA or RNA backbone.[118]

Leclerc and his colleagues have developed a ferrocene-functionalised cationic polythiophene that was used as a biosensor for free DNA detection paving the way to a new family of biosensors potentially useful for monitoring drinking water distribution systems.[119, 120] The design of a genosensor for the sequence selectivity of the DNA detection is shown in Figure 1.37.

1.9.2. DNA in directed assembly

DNA applications are also useful outside biology and medicine. The development of DNA origami and DNA nanotechnology uses the uniquely selective interactions between DNA strands for the directed assembly of functional nanostructures.[121]

The challenge in DNA-based self-assembly is the integration of different molecular constituents like fluorophores into the groups. DNA-based photonic wire systems have been designed, however, they have substantial energy losses during the energy transfer.[122] Inefficient communication between the components during the self-assembling of the structure suggests that tools which would help to control the location and spatial arrangements of the fluorophores are required. It has been shown, that DHPs can act as a controller ligand binding to the DNA duplex with high precision. The resulting DHP-appended fluorophores are able to exhibit high-energy transfer over distancesof over 27 nm. In addition, when tested through FRET, DHP-appended fluorophores were shown to be efficient in controlling energy loss during energy transfers (Figure 1.39).

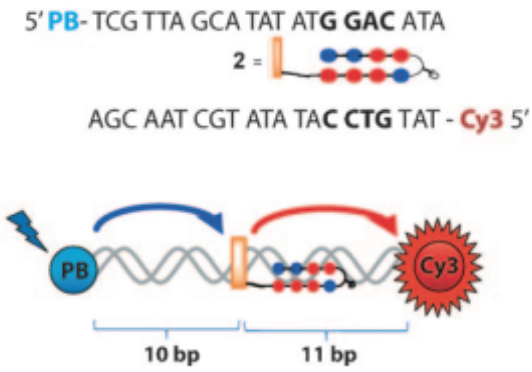

Figure 1.39 schematic of the exemplar DNA-based photonic.[122]

Three fluorophores used in a recent study are pacific blue (PB), oxazole yellow (YO) and cyanine 3 (Cy3). Pacific blue (PB) is the initial donor chromophore and oxazole yellow (YO) the terminal energy acceptor.[122] The stepping-stones are the oxazole yellow dyes which are central to the design through the processes of homo-FRET. A significant amount of remaining energy exist in the YO dyes rather than being transported to the final acceptor dye. This results in the dropping off of the efficiencies of ET sharply by increasing the numbers of steps of YO-YO ET, as the ET process among the YO dyes is considered to be bi-directional.

The length of the photonic wires is increased due to the modularity of perfect fluorophore, which helps to optimize the interfluorophores distances and increase the photonic lengths. Most importantly, the DHPs can target virtually all DNA sequences and thus can be used within high throughput multi-dimensional arrays and circuits.

For nanophotonic applications, DNA is programmed to compose special scaffolds in order to organize and manipulate fluorescence resonance energy transfer (FRET). Moreover, the ability to self-assemble into different arrays over small surface areas and with high precision makes DNA unique. DNA self-assembly leads to formation of programmable nanostructures with wide applications. DNA nanostructures are assembled with different materials through different methods. Solid phase chemical synthesis is the most common method, which is used to produce modified oligodeoxyribonucleotides (ODNs), where DNA nanostructure is assembled with non-natural functionality.[123] Furthermore, DHPs are also used to organize the non-natural functionality together with DNA nanostructures. The DHPs have high selectivity and affinity for the DNA structures and are thus able to construct a DNA-based photonic wire. It is clear that "PA-programming" is able to programme a uni-directional FRET process. In addition, in order to complete the photonic wire in to the surface, single-molecule fluorescence spectroscopy (SMFS) is used and this ensures that 100% FRET is observed. DHPs are thus effective in the construction of fluorophore sequences templated by duplex DNA so that the FRET process is effectively controlled by the DNA duplex.

1.9.3. Competition dialysis

This study focuses on the development of a custom competition dialysis device to determine affinity and selectivity of ligands for nucleic acids structures. According to Muller and Crothers, who first described competition dialysis, it was intended to revise the first choice of ligand for the base pairs of the G•C or A•T.[124] The competition dialysis experiment is illustrated through a typical device in Figure 1.40.

Figure 1.40 the competition dialysis assay. [125]

The principle of competition dialysis is based on the laws of thermodynamics and is very straightforward to put into practice.

Ligands that bind to nucleic acids, having structural or sequence selectivity, can be identified using a powerful tool called competition dialysis.[125] This process is used as a simple and common test for affinity and selectivity of ligands and comprises of the dialysis of a ligand against an array of nucleic acids with different structures or sequences.[124] For example, duplex DNA, triplex DNA and quadruplex DNA in dialysis tubing can be placed in a beaker with a ligand solution, illustrated in Figure 1.41.

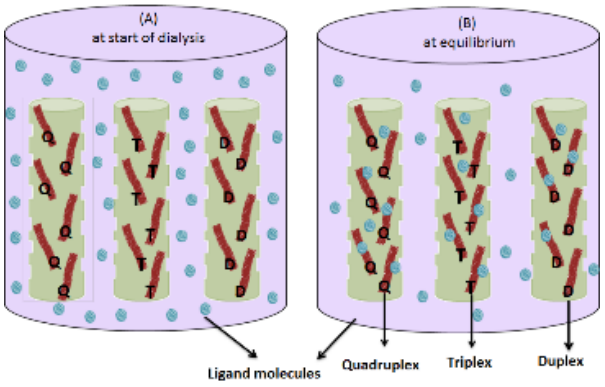

Figure 1.41 Schematic illustration of the competition dialysis process involving three nucleic acid structures, viz. quadruplex (Q), duplex (D) and triplex (T), and a ligand.

Allowing adequate time for the diffusion to take place allows the ligand to diffuse across the dialysis tubing. The uniformly sized pores of the dialysis tubing will allow the ligand molecules to diffuse in and out of the dialysis tubing to achieve the equilibrium concentrations while the large nucleic acids are retained within the dialysis tubing. The equilibrium concentrations are defined by the affinity between the duplex DNA, triplex DNA and quadruplex and the ligand.[126]

If the ligand binds to duplex DNA, triplex DNA and/or quadruplex DNA,[127] when equilibrium is reached the ligand molecules are retained within the dialysis tubing. For instance, if a molecule has high affinity for triplex DNA, it will accumulate in the dialysis tubing with triplex DNA. Analysis of the ligand concentration in the different dialysis tubing then gives the affinity of the ligand for the different nucleic acid structures.

1.10. Project Aims

This work aims to establish and identify couples of compounds displaying orthogonal selectivity for nucleic acid structures such as duplex, triplex and quadruplex DNA. The mutually orthogonal interaction pairs are required for the construction of self-assembled functional nanostructures, directing fluorescent molecules into a pre-designed sequence so that energy transfer by FRET takes place (illustrated in Figure 1.42). To achieve this, we develop and validate the double competition dialysis assay for the identification of mutually orthogonal interaction pairs as required for this process. Double competition dialysis can be used as a test for affinity and selectivity of ligands and comprises of the dialysis of a two (or more) ligands against an array of nucleic acids with different structures or sequences.

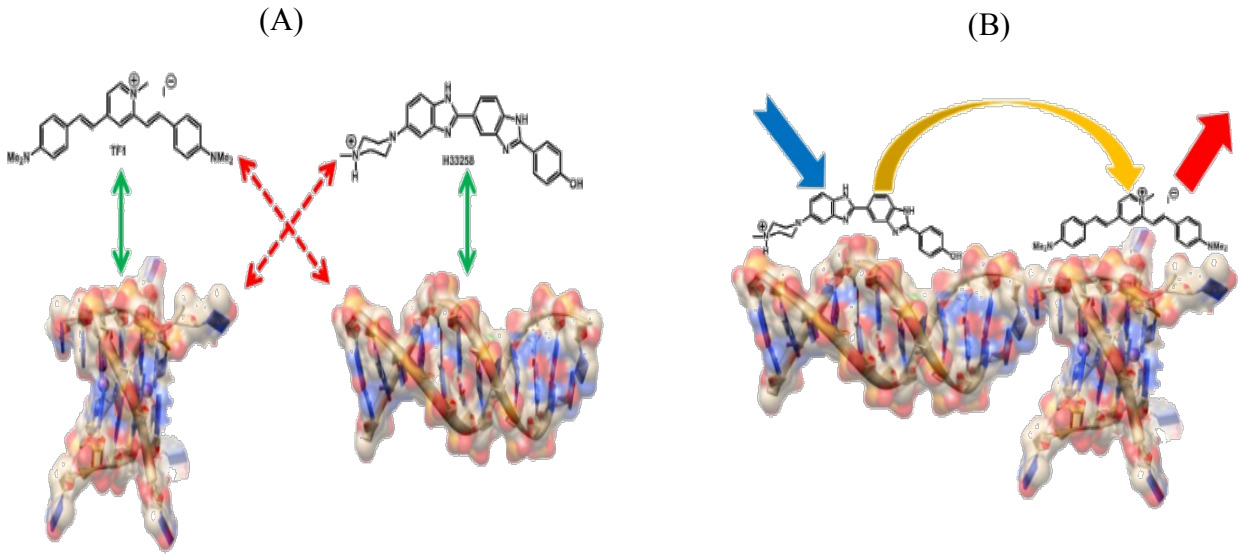

Figure 1.42. (A) quadruplex DNA has a high affinity to bind selectively with TF1; duplex DNA has a high affinity for H33258; (B) FRET measures the energy which is transferred from H33258 on the duplex DNA to TF1 on the quadruplex DNA and will show whether the functional nanostructure is formed or not.

Chapter 2

Selection of optoelectronically active π-conjugated compounds

Abstract

This chapter provides an overview of our attempts to determine extinction coefficients for selected optoelectronically active π-conjugated molecules in our aqueous buffers. Compounds eosin b, ponceau s, sulforhodamine, basic fuchsin, basic yellow (thioflavin T), ethidium bromide, DAPI, H33258, GB01 and coralyne were found to have extinction coefficients of (57063 ± 457), (36355 ± 581), (84469 ± 563), (79644 ± 192), (24073 ± 135), (6645 ± 65.27), (23570 ± 786), 42000, 33000 and 14500 M^{-1} cm^{-1}, respectively. These compounds were found to be stable and not sensitive to light. On the other hand, TF1, methylene blue, thiazole orange and DODC were found to fade upon exposure of light. Moreover, this chapter describes binding studies of a series of potential nucleic acid binders from a library of available (commercial and in-house synthesised) ligands. Binding of potential ligands to double-stranded FS-DNA and to different quadruplex-forming sequences (c-myc, 22AG and EAD2) is studied using UV-visible, circular dichroism spectroscopy (CD), and isothermal titration calorimetry (ITC). As anticipated, negatively charged compounds were found not to bind to DNA, whereas positively charged compounds all showed binding with varying affinities.

2.1 Introduction

2.1.1 Solubility and stability

Solubility is the property which describes the ability of a substance, the solute, to dissolve in a solvent. Solubility is defined as the amount of substance that passes into solution to achieve a saturated solution at constant temperature and pressure. Solubility is expressed in terms of maximum volume, mass or number of moles of the solute that dissolve in a given volume or mass of a solvent at equilibrium.[128]

Absorbance is a measure of the capacity of a solution to absorb light of a specified wavelength. It is equal to the logarithm of the reciprocal of the transmittance and therefore is dimensionless.

Absorbance is not an adequate measure for making comparisons between substances and solutions as both concentration and path length have an impact on the absorbance in a similar way. If the concentration of solution is increased, then there are more molecules for the light to hit when it passes through. As the concentration increases, there are more molecules in the solution, and more light is blocked. Both concentration and pathlength of light passing through a solution are allowed for in the Beer-Lambert law.

The Beer–Lambert law relates the attenuation of light to the properties of the material through which the light is travelling. This relationship links concentration to absorbance in the following equation (Equation 1):

$$A = \varepsilon \times c \times l \quad (1)$$

Where A is the measured absorbance, c the concentration of the sample in moles per liter of the solution, ε is the molar extinction coefficient in $M^{-1}\,cm^{-1}$, and l is the path length.[69]

Equation (1), leads to the equation to determine the extinction coefficient if absorbance and concentration are known and the compound is sufficiently stable and soluble (Equation 2):

$$\varepsilon = A / c \times l \quad (2)$$

Therefore, the extinction coefficient is determined from the absorbance of the ligand divided by the concentration in moles per liter of the ligand and multiplied by the typical 1.0 cm path length of cuvette. In practice, extinction coefficients are determined as the slope of a plot of absorbance as a function of concentration of the dye of interest. Any deviations from linearity of such plots indicate that solutions may not involve individually solvated and/or stable molecules.

The Beer-Lambert law maintains linearity under specific conditions only. The law will lead to inaccurate measurements at high concentrations because at very high concentrations the molecules of the analyte exhibit stronger intermolecular and electrostatics interactions which is due to the lesser amount of space between molecules. This can change the molar absorptivity of the analyte. Not only do high concentrations change molar absorptivity, but it also changes the refractive index of the solution causing departures from the Beer-Lambert law.

Aggregation is the process where assemblages are formed in a solution or suspension leading to altered stability of colloidal systems. During aggregation, particles that are dispersed in the liquid phase agglomerate leading to a spontaneous formation of irregular particles called aggregates, flocs or clusters. Aggregation is usually an irreversible process if covalent (chemical) bond formation occurs between the aggregates. However, aggregation is typically reversible when weak (physical) bonds are formed between particles that can be broken by the change in temperature. The intrinsic rate of the process of bonding is dependent on the bond formation kinetics which is controlled by the chemical composition of the system, and cluster diffusion that controls the encounter rate of the clusters. These two factors are said to be vital limiters of the aggregation process leading to the aspects of chemically-controlled and physically-controlled limits.[129-131]

Extinction coefficient values depend not only on the chemical structure of a compound, but also on its environment. It is well established that many dyes can be strongly solvatochromic. Solvatochromism is the ability of a chemical compound to change colour due to a change in solvent polarity. For example, Reichardt's dye (Betaine 30) changes colour in response to polarity and gives a scale of ET (30) values. The ET (30) value corresponds to the transition energy between the ground state and the lowest excited state, in kcal/mol, of Reichardt’s ET (30) dye (Betaine 30). Extinction coefficients should therefore be determined in the solvent and at the temperature of interest.

2.1.2 The dye chemical structure

Typical dyes display a pi-conjugated system. A conjugated system is a system of connected p-orbitals with delocalized electrons in compounds with alternating single and multiple bonds, which in general may lower the overall energy of the molecule and therefore increase stability. Lone pairs, radicals or carbonium ions may be part of the system. The compound may be cyclic, acyclic, linear or mixed. Conjugation is the overlap of one p-orbital with

another across an intervening sigma bond (in larger atoms d-orbitals can be involved). A conjugated system has a region of overlapping p-orbitals, bridging the interjacent single bonds. They allow a delocalization of pi electrons across all the adjacent aligned p-orbitals. The pi electrons do not belong to a single bond or atom, but rather to a group of atoms.

The chemical structure of a dye molecule can be shown as the main skeleton and the substituent group. Each type of dyes has a specific skeleton. Generally, the skeleton determines lightfastness properties of a dye, and the substituent groups such as -OH and R-SO_3- groups change the photostability of a dye within a class to a lesser degree.[132]

There are over 25 essential classes of dyes, with natural dyes falling within the following eight groups: anthraquinones, hydroxyketones, carotenoids, naphthoquinones, indigoids, flavonones, flavonols and flavones.[133]

One of the most important tools in modern biology are “fluorescent probes” which are often based on particles and small molecules that are organic in nature.[134] Molecules that particularly react with biological molecular particles in order to produce an output in the concomitant change, in their photochemical nature are known as fluorescent probes, which are characterised by parameters such as fluorescent intensity, excitation and emission wavelength.

Tsien and his colleagues did their research on the Ca^{2+} probes over 20 years ago. The Journal of Biological Chemistry reported on a new generation of calcium probes that Tsien designed to replace quin2.[135] Since then phenomenal development and increase in the production of fluorescent probes across the world took place.[135] Today, several strategies for designing fluorescent probes, such as photo induced electron transfer (PET) intramolecular charge transfer (ICT), spirocyclization as well as fluorescence resonance energy transfer (FRET) are used in the producing different kinds of probes.[136]

Cyanine dyes are the most common examples used oligonucleotide labelling, which are fluorogenic and unsymmetrical in nature.[137-140] Upon interaction with certain kinds of proteins and nucleic acids, cyanine dyes become fluorescent and result in the formation of photochromic compounds.[141] Illumination also causes change in their optical properties. Fluorescent dyes are available in huge varieties also including the Acridine5 as well as Cyanine dye (Cy)4 families. Fluorescent dyes are used widely as oligonucleotide labels and/or probes. Cyanine dyes are even capable of non-covalent interactions with DNA either by base pair intercalation (acridines, cyanine dyes and monomethine) or through the

aggregation into the minor grooves within double stranded DNA (cyanine dyes of trimethine and pentamethine groups). Thiazole orange (TO) is a popular cyanine dye which is fluorogenic monomethine in nature that is also non-fluorescent when left free within the solution (caused by fast deactivation towards the ground state which is nonradiative in nature). Thiazole orange (TO) becomes extremely fluorescent where the polymethine chain motions are kept under control (e.g., when in viscous solvents or upon DNA intercalation).[142] Therefore, the different interactions between fluorescent dye thiazole orange and the DNA (see chapter 1).[142, 143] many of fluorescent dyes have negligible fluorescence in solution, and on mixing with nucleic acids produce immense fluorescence. The increased fluorescence arises when the bond rotations between these aromatic systems is controlled, thereby preventing non-radiative decay.[67, 144] Supramolecular chemical research of cyanine dyes shows that the working of the local environment on TO aggregation has restricted to nucleic acids.[145]

2.1.3 Fading

TF1, methylene blue, thiazole orange and 3,3′-diethylthiacyanine iodide (DODC) were found to fade upon exposure of light as discussed in Chapter 2. Most natural dyes have poor lightfastness, while synthetic dyes show the full range from poor to excellent lighfastness. These differences are due to their different chemical and physical characteristics. The change in colour of dyes due to light exposure is a complex reaction affected by both the chemical and physical state of the dye. This phenomenon is called photofading.[146-149]

The main factors influencing the photostability of dyes are:

- the wavelength of initial radiation
- the dye aggregation
- the presence of metal ions (bound in dyes or bound in impurities)

Furthermore, the composition and the concentration of buffer, temperature and pH can also influence the rate of fading.

It has been reported in the literature that the centralized methane hydrogen of TO can be substituted with an electron-withdrawing cyano group. This group is reported to decrease the sensitivity of the dye to singlet oxygen-mediated deviation.[150]

The existence of a low singlet excited state of a long duration can result in a degradation reaction. At this point intersystem crossing of molecules takes place where molecules are

allowed to cross to their matching triplet state. Triplet states can exist for more duration which may further result to production of more photo-degradation.

The Jablonski diagram shown in Scheme 2.1 is used to clearly demonstrate and analyse the effects of photochemistry on dyes, the diagram is used in demonstrating the fundamental alterations that exists on the electronic states. In the diagram, the lowest vibration energy levels on every electronic state are demonstrated by using thick lines, while other light lines shows higher vibrational energy levels that are related to every electronic state. The light that is absorbed by the molecule raises it from its ground electronic state (S_0) to excited states (S_1 or S_2 for next level). Due to the short lifetime of excited state, the molecule will return back to the original ground states. The process of transitioning back from the excited electronic state to ground electronic state is a result of loss of the energy that was absorbed, due to one of the following processes.

- Intersystem crossing which results to lack of radiative transition
- Release of the radiation energy
- photochemical reactions
- Energy transfer

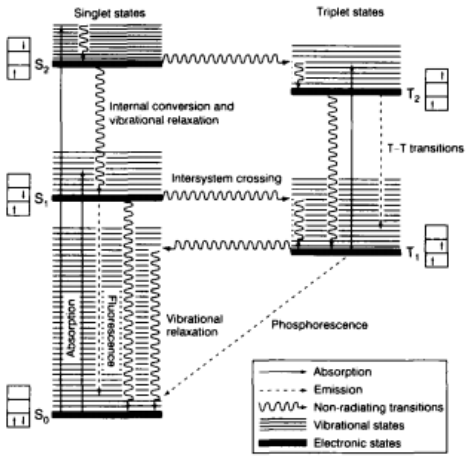

Scheme 2.1. Jablonski scheme

Scheme 2.1. demonstrates that the singlet excited state has a higher energy level which means that it has higher content of energy as compared to triplet state; this makes it more reactive. In contrast there exist a long lifetime with the triplet state, which means that it has more time to react.[151] The existence of reactive groups on dyes enables them to react even in the singlet excited state even though it may have a lifetime that is short. Furthermore, the

chances of the dye reacting with oxygen molecule are high in the triplet state, because oxygen is able to undergo diffusion on the neighboring molecules of the dye.

In the process of the dye being in the triplet state, chances are that in presence of oxygen it will experience a triplet – triplet annihilation, which results in the formation of singlet oxygen as shown in Scheme 2.2. The subsequent initiation of destruction of dye is shown in Scheme 2.3.

$$^3HD^* + {}^3O_2 \rightarrow HD + {}^1O_2$$

Scheme 2.2

$$^1O_2 + HD \rightarrow Decomposition$$

Scheme 2.3

Analysis of photosensitization principles through photo-oxidation has been done by Griffiths and Hawkins who explained the pathway of the azo dyes photo – oxidation.[152] The singlet oxygen sensitiser under the condition of the presence of the methylene blue in the solvent of alcohol. The pathway of the photochemical proceeded through the attack of the signet oxygen on the dye, by the intermediate unsaturated azo hydro-peroxide as shown in scheme 2.4. The signet oxygen attack on the hydrazine dye is presented as a process called type 2 photo – oxidation, because radicals are not involved in the primary reaction. The degradation will be observed to occur even in the absence of methylene blue.

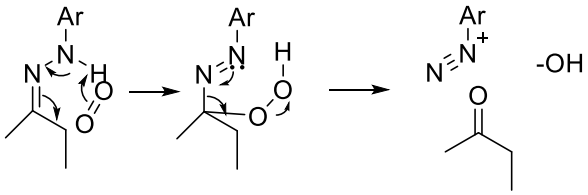

Scheme 2.4. Mechanism of oxidation of azo dyes by singlet oxygen

The degradation of dyes is predominantly through singlet oxygen where singlet oxygen sensitisers are present in combination with oxygen. Examples of singlet oxygen generator are methylene blue, copper (II) and phthalocyanine Their efficiency will depend on the type of the solvent that is used because this affects the singlet oxygen lifetime.[153, 154] The senstitiser are in a position to transfer their own energy from a lowest excited triplet state to an acceptor state. In doing so, the donorsmolecules return from their excited state to their ground state whereas the acceptor molecules are raised to the excited state.

2.1.4 Nucleic acid binding

In order to compare affinities and selectivities, the interaction of some optoelectronically active π-conjugated molecules (described in Chapter 1), with a double-stranded fish sperm DNA (FS-DNA) and three well-known quadruplex-forming sequences, specifically, c-myc, 22AG and EAD2 is studied.

Depending on the orientation of the strands in a G-quadruplex, oligonucleotides can either form parallel conformations (e.g, c-myc and EAD2) and antiparallel conformation or mixed/hybrid conformation (22AG) (see chapter 1).

Noncovalent binding of different compounds with DNA is an object of numerous studies, since these substances possess high biological activity and influence on many vitally important processes occurring in the cells. Some ligands are mutagens (ethidium bromide (EtBr)) and transcription inhibitors (EtBr, some antibiotics) which is determined by the ability of these compounds to form stable complexes and hence to obstruct DNA uncoiling. Binding can be studied through a range of techniques, including UV-visible and circular dichroism spectroscopy and isothermal titration calorimetry (ITC). A brief description these methods is provided in Chapter1.

Photophysical data obtained for methylene blue in complexes with DNA indicate different binding modes of the dye depending on base sequences. In addition, electrostatic interactions play an important role during DNA binding.[53] Previous studies have found a binding affinity of methylene blue to duplex DNA ($K_{binding}$) of ~ 2.2 $\times 10^5$ M^{-1}.[155]

Moreover, some ligands are multimodal in the nature of their binding to DNA. For example, EtBr (**10**) has three modes of binding to double-stranded DNA. EtBr also binds very well to triplex DNA and quadruplex DNA. Ethidium bromide (EtBr) is commonly used to detect nucleic acids from polymerase chain reaction experiments and restriction digests etc. in molecular biology laboratories. Previous studies have found a binding affinity ($K_{binding}$) of (1.23 ± 0.07) $\times 10^5$ M $(bp)^{-1}$ and a ($K_{binding}$) of 1.5 $\times 10^5$ M^{-1} for binding site size (n) of (1.0 ± 0.1) for the duplex and G-quadruplexes DNA, respectively.[156, 157]

Coralyne (**14**) is slightly soluble in water. The structure of coralyne contains four fused aromatic rings. It can bind with DNA triplexes poly(dT)●poly(dA)●poly(dT) and poly [d(TC)] ●poly-[d(GA)] ●poly[d(C+T)]. Studies have found binding affinitys ($K_{binding}$) of 3.5 $\times 10^6$ M^{-1} and 1.5 $\times 10^6$ M^{-1} for these two triplexes, respectively.[158]

Bisbenzimide H33258 (**6**) is a water-soluble groove binder with selectivity for A●T-rich sequences.[159, 160] GB01 (**7**) is related to the aforementioned minor groove binder H33258.[5]

Hoechst dyes are normally less toxic than DAPI, which ensures a higher viability of stained cells. 4′,6-Diamidino-2-phenylindole (DAPI) also is a water soluble fluorescent dye that binds strongly to adenine●thymine rich regions in DNA. This simple-to-use fluorescent stain visualizes nuclear DNA in both living and fixed cells. Cells stained with DAPI showed no ultrastructural changes compared to the appearance of cells not stained with DAPI. Previous studies have suggested that DAPI (**11**) binds by several modes to duplex DNA.[29, 161] DAPI staining allows multiple use of cells eliminating the need for duplicate samples. The binding affinity of DAPI to oligonucleotides containing three A●T base pairs is about 7×10^6 M^{-1} (bp).[162]

Another ligand, TF1 (**8**), has poor aqueous solubility. It is a groove binder with duplex DNA perhaps because of its length. Previous studies have found a binding affinity ($K_{binding}$) of 0.12 $\times10^6$ M^{-1} for a binding site size (n) of 2 base pairs. However, TF1 bind strongly to G-quadruplexes such as 22AG and c-myc with affinity 0.47 and 0.55 $\times10^6$ M^{-1}, respectively for a binding site size (n) of 2.[163]

DODC (**13**) is water-soluble. Previous studies have found that DODC binds to a quadruplex groove, with affinity (K_a) of ~$1–2\times10^5$ M^{-1}.[164]

Some ligands combine two modes of interaction (e.g. Thioflavin T and thiazole orange). Thioflavin T (also known as basic yellow (**5**)) is a cationic benzothiazole dye, which is water-soluble.[165] For over fifty years, Thioflavin T has been an extremely popular dye in biomedical research. This compound has a very high affinity for human telomeric G-quadruplexes. In addition, it becomes fluorescent upon interaction with such structures as duplex DNA, and therefore is often utilized as a light-up probe. Previous studies have found a binding affinity ($K_{binding}$) of ~10^4 M^{-1}. [166]

Thiazole orange (**12**) is water-soluble and is an example of the oldest synthetic cyanine dyes and commonly used in reticulocyte analysis.[167] TO binds strongly to triplex- and quadruplex DNA. Previous studies have found a binding affinity of TO for G4 structures of ~ 1-2×10^6 M^{-1}. The fluorescence efficiency increases approximately 1000-fold due to the binding of TO to DNA. [168]

2.1.5 Aims

My aims for this chapter are to determine the extinction coefficients for optoelectronically active compounds in our buffer solutions. It is anticipated that these studies will also highlight any lack of stability of these dyes. In addition, this chapter also describes the binding studies to screen binding between available fluorescent ligands and nucleic acids. Binding affinities will be determined using UV-visible spectroscopy, circular dichroism spectroscopy and isothermal titration calorimetry (ITC). The resulting data will allow validation of the results from our dialysis experiments in Chapter 3.

Chemical structures of the ligands chosen for this study are shown in Scheme 2.1. Ligands **4-14** were chosen through the literature review based on their ability to interact with different selectivity and affinity with various DNA sequences. Compounds **1-3**, namely eosin b (**1**), ponceau s (**2**), and sulforhodamine (**3**) are dyes that do not bind significantly with FS-DNA. Therefore, these compounds were chosen as reference controls for this study.

Most small molecules that bind to DNA are largely planar aromatic compounds of considerable hydrophobicity. Almost perversely, it is precisely this set of properties that makes compounds good intercalators and/or minor groove binders, which also favors self-aggregation in aqueous solution. The phosphodiester backbone of DNA is negatively charged at every nucleotide unit in aqueous conditions. The resulting water solubility is extended to many modified oligonucleotides, conferring solubility to hydrophobic molecules conjugated to DNA.

Methylene blue (**9**) is a water-soluble compound with redox features. There is a large volume of published studies describing that methylene blue binds strongly to DNA through several binding modes.[159, 169] It binds to DNA and induces photosensitized reactions which can be used for sequence-specific cleavage of the DNA backbone.

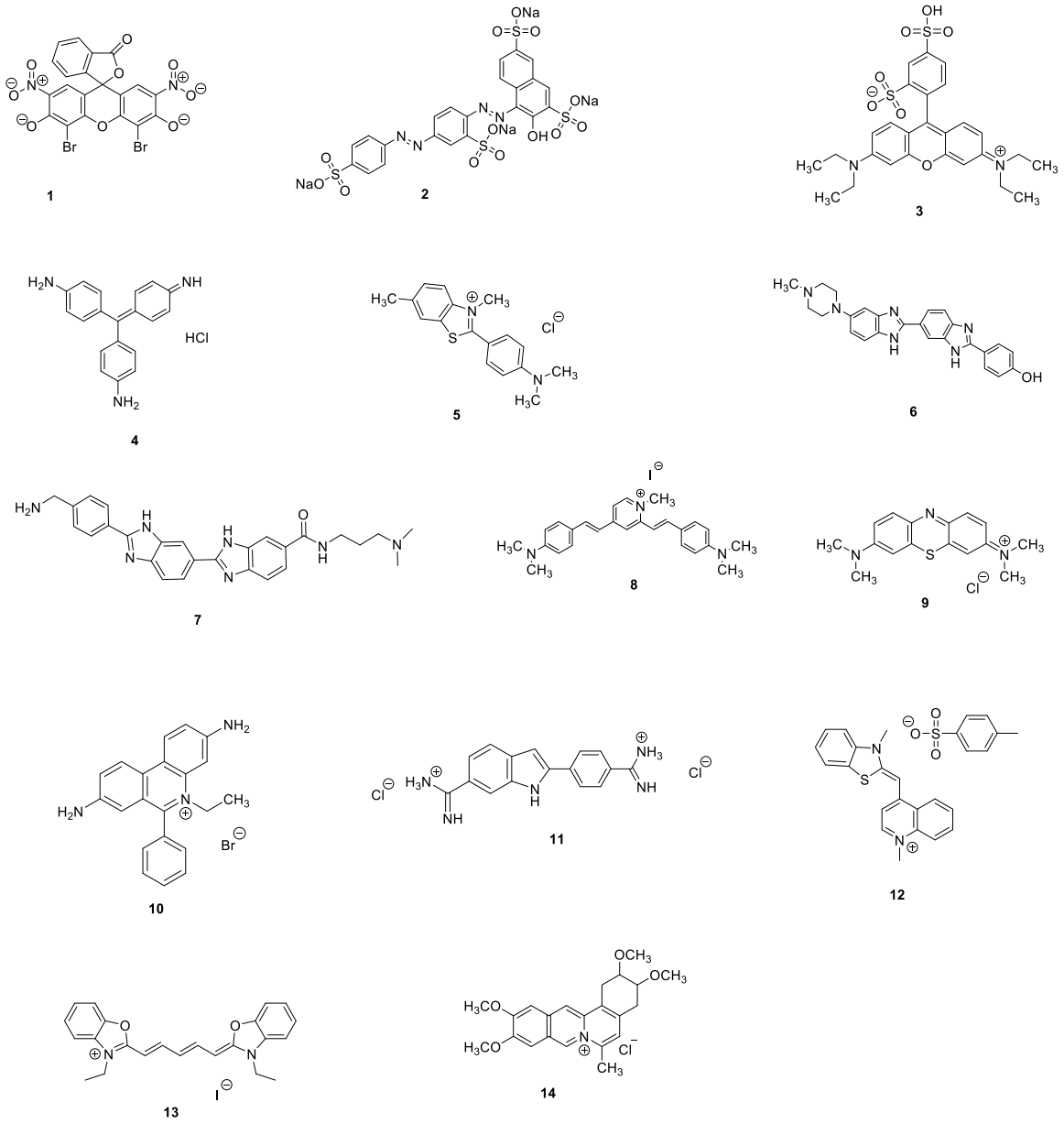

Scheme 2.5 Chemical formulae, **(1)** eosin b, **(2)** ponceau s, **(3)** sulforhodamine **(4)** basic fuchsin, **(5)** basic yellow (thioflavin T), **(6)** H33258, **(7)** GB01, **(8)** TF1, **(9)** methylene blue, **(10)** ethidium bromide, **(11)** DAPI, **(12)** thiazole orange, **(13)** DODC and **(14)** coralyne.

2.2 Results and Discussion

The results of the determination of the extinction coefficients for optoelectronically active compounds **1-14** are presented and discussed for each individual compound.

2.2.1 Extinction coefficient, stability and DNA binding of Eosin B

We wanted to determine the extinction coefficient of Eosin B (**1**). A stock solution of **1** (1.2 mM) in buffer (25 mM MOPS, pH 7.0, 50 mM NaCl) was prepared. A series of solutions of 0.0025, 0.0076, 0.012 and 0.017 mM was prepared from the stock solution and UV-visible spectra were recorded for these solutions in a 1.0 cm path length cuvette at 25 °C. Absorbances at the λ_{max} of 520 nm were plotted against ligand concentrations (Figure 2.1).

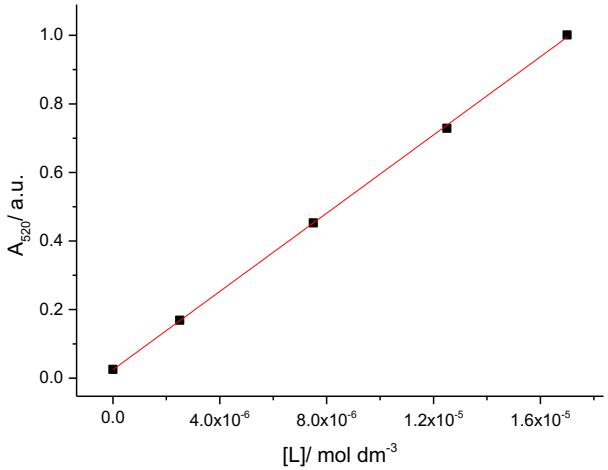

Figure 2.1 Absorbance for **1** as a function of concentration in buffer (25 mM MOPS, pH 7.0, 50 mM NaCl), at 25 °C.

Figure **2.1** shows a linear correlation between absorbance and concentration. A linear fit to the dtata (red line) yields an extinction coefficient of (57063 ± 457) M^{-1} cm^{-1}. The error margin as a percentage of the extinction coefficient is 0.8 %, which is acceptable. With the extinction coefficient established, we explored the stability of **1**, and in particular the photochemical stability.

To study the photochemical stability, we measured the absorbance of **1**, exposed to ambient light, in buffer (25 mM MOPS, pH 7.0, 50 mM NaCl and 1 mM EDTA), at 25 °C as a function of time (Figure 2.2).

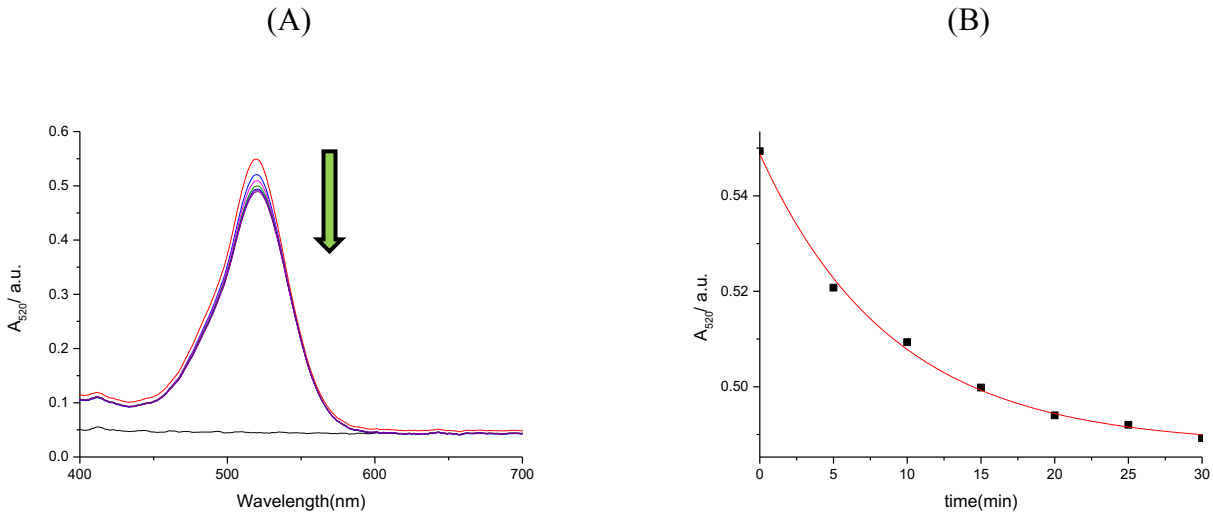

Figure 2.2 (A) Spectra for the solution of 0.5 mM **1** exposed to light, in buffer (25 mM MOPS, pH 7.0, 50 mM NaCl and 1 mM EDTA), at 25 °C. (B) The absorbance of **1** at 520 nm plotted as a function of time.

Figure 2.2 (A) shows a slight decrease in the spectra, which suggests that **1** has some sensitivity to light. Figure (B) confirms the decrease in the absorbance for **1**, but the decrease appears to stop after approximately 30 minutes with an overall loss of absorbance of around 10%. The loss of absorbance does not lead to a change in the shape of the spectrum, making it unlikely that the decrease corresponds to photochemical fading of **1**.

Binding of **1** to FS-DNA was studied using UV-visible spectroscopy. The changes in absorption of **1** upon addition of FS-DNA were recorded in buffer (25 mM MOPS, pH 7.0, 50 mM NaCl, 1 mM EDTA), at 25 °C (Figure 2.3).

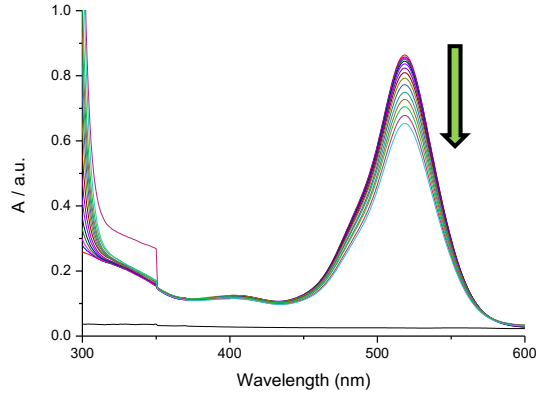

Figure 2.3 UV-visible spectra for a 0.015 mM solution of **1** upon addition of 0 – 4.17 mM FS-DNA in buffer (25 mM MOPS, pH 7.0, 50 mM NaCl, 1 mM EDTA), at 25 °C.

Figure 2.3 shows that the absorbance at λ_{max} (520 nm) of **1** decreases slightly upon addition of FS-DNA. We further note that the shape of the spectrum does not change significantly. This decrease in UV-visible absorption may have occurred as a result of **1** interacting weakly with DNA, but it is likely as a result of dilution.

To quantify the affinity of **1** for DNA, the absorbance at 520 nm was plotted as a function of concentration of FS-DNA (Figure 2.4, for numerical data, see Appendix Table A1).

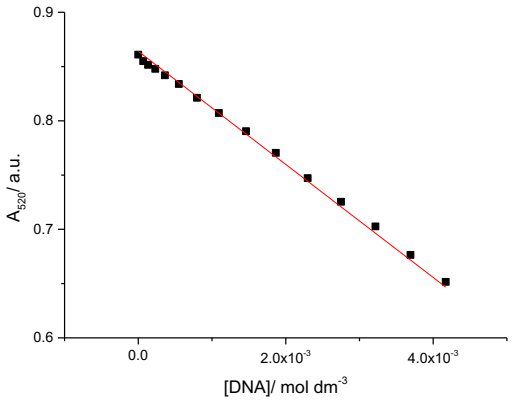

Figure 2.4 Absorbance at 520 nm for a 0.015 mM solution of **1** as a function of DNA concentration in buffer (25 mM MOPS, pH 7.0, 50 mM NaCl, 1 mM EDTA), at 25 °C. The line represents the best fit of a multiple independent binding sites model to the data.

Figure 2.4 shows that the multiple independent binding sites model generates a straight-line fit to the data, suggesting negligible interaction of **1** with the DNA and the decrease therefore merely represents the effect of dilution of the ligand that occurs when the DNA solution is added.

The fit of the multiple independent binding sites model to the data gives a binding affinity ($K_{binding}$) of ~0 M^{-1} for a binding site size restricted to 3 base pairs. This $K_{binding}$ confirms that **1** does not interact with FS-DNA, as expected considering **1** carries a negative charge. In addition, the spiro centre also leads to significant non-planarity of the molecule which likely hinders binding as well.

2.2.2 Extinction coefficient, stability and DNA binding of the Ponceau S

We set out to determine the extinction coefficient of Ponceau S (**2**). A stock solution of **2** (0.99 mM) in buffer (25 mM MOPS, pH 7.0, 50 mM NaCl) was prepared. A series of solutions of 0.0021, 0.0062, 0.010 and 0.014 mM was prepared from the stock solution. UV-visible spectra were recorded for these solutions in a 1.0 cm pathlength cuvette at 25 °C. Absorbances at the λ_{max} of 520 nm were plotted against ligand concentrations (Figure 2.5).

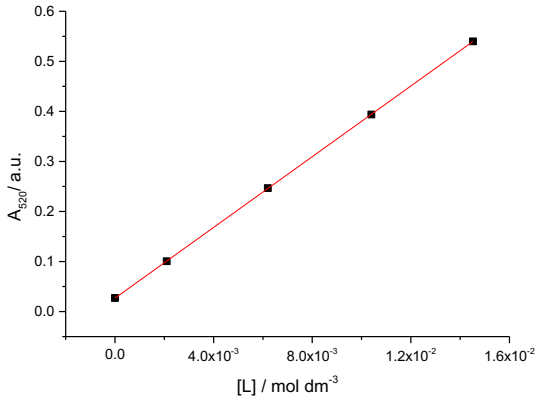

Figure 2.5 Absorbance at 520 nm as a function of concentration of **2** in buffer (25 mM MOPS, pH 7.0, 50 mM NaCl and 1 mM EDTA), at 25 °C.

The data follow a linear trend, suggesting no solubility problems over the range of concentrations studied. A linear fit (red line) was applied to the data in Figure 2.5 to obtain the extinction coefficient of (36355 ± 581) M^{-1} cm^{-1}. The error margin as a percentage of the extinction coefficient is 1.5 %, which is an acceptable margin of error. The good fit also suggests that **2** is stable in the buffer, at least on the timescale of the experiment.

Binding of **2** to FS-DNA was studied using UV-visible spectroscopy. The changes in absorption of **2** upon addition of FS-DNA were measured in buffer (25 mM MOPS, pH 7.0, 50 mM NaCl, 1 mM EDTA), at 25 °C (Figure 2.6).

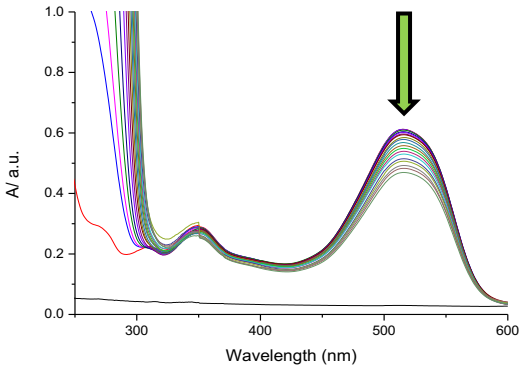

Figure 2.6 UV-visible spectra for a 0.016 mM solution of **2** upon addition of 0 – 4.26 mM FS-DNA in buffer (25 mM MOPS, pH 7.0, 50 mM NaCl, 1 mM EDTA), at 25 °C.

Figure 2.6 shows that the absorbance at λ_{max} (520 nm) of **2** decreases upon addition of FS-DNA. This change in UV-visible absorption might occur as a result of **2** interacting weakly with DNA, but it is more likely the result of simple dilution.

To quantify any affinity of **2** for DNA, the absorbance at 520 nm was plotted as a function of concentration of FS-DNA (Figure 2.7, see Appendix Table A2 for data in tabular format).

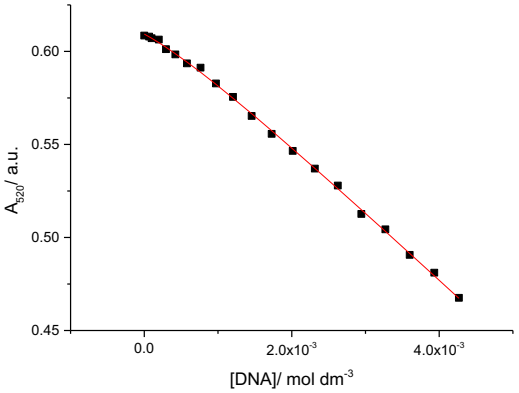

Figure 2.7 Absorbance at 520 nm for a 0.016 mM solution of **2** as a function of DNA concentration in buffer (25 mM MOPS, pH 7.0, 50 mM NaCl, 1 mM EDTA), at 25 °C. The solid line represents the best fit of the multiple independent binding sites model to the data.

Figure 2.7 shows that the fit to the data is mostly a straight-line with only a small apparent deviation from linearity at low DNA concentrations. The fit thus suggests that **2** interacts weakly with the DNA or not at all, in which case the decrease in absorbance is the result of dilution.

The fit of the multiple independent binding sites model to the data gives a binding affinity ($K_{binding}$) of (2.14 ± 0.73) $\times 10^3$ M^{-1} for a binding site size restricted to 3 base pairs. This equilibrium constant again confirms negligible binding of **2** to FS-DNA, as expected for a negatively charged compound.

To confirm limited binding, we calculate the fraction bound ligand at the end of the titration Assuming

$$[\text{ligand}]_{free} \approx [\text{ligand}]_{total}$$

$$\frac{\text{ligand bound}}{\text{ligand total}} \approx K \times \frac{[\text{DNA}]\ \text{total}}{n}$$

Therefore, fraction bound $\approx K \times \frac{[\text{DNA}]\text{total}}{n} = 2.14\times10^3 \times 0.00426/3 = 3.03$

The calculation thus shows that 75% of the ligand is bound, even in the presence of a high DNA concentration of 4.26 mM. The low binding affinity is reasonable in light of the fact that **2** is negatively charged.

2.2.3 Extinction coefficient, stability and DNA binding of Sulforhodamine

We wanted to determine the extinction coefficient of Sulforhodamine (**3**). A stock solution of **3** (0.5 mM) in buffer (25 mM MOPS, pH 7.0, 50 mM NaCl) was prepared. A series of solutions of 0.001 mM, 0.003 mM, 0.005 mM and 0.008 mM was prepared by dilution of the stock solution. UV-visible spectra were recorded for these solutions in a 1.0 cm pathlength cuvette at 25 °C. The absorbance at the λ_{max} of 563 nm was plotted against ligand concentration (Figure 2.8).

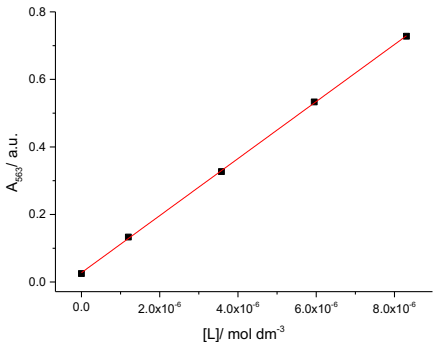

Figure 2.8 Absorbance for **3** as a function of concentration of **3** in buffer (25 mM MOPS, pH 7.0, 50 mM NaCl), at 25 °C.

Figure 2.8 shows a linear increase in absorbance with concentration. A linear fit (red line) was applied to obtain the extinction coefficient of (84.5 ± 0.6) $\times 10^3$ M^{-1} cm^{-1}. The error margin as a percentage of the extinction coefficient is 0.6 %, which is acceptable. The good fit also suggests that **3** is stable in the buffer, at least on the timescale of the experiment.

Binding of **3** to FS-DNA was evaluated using UV-visible spectroscopy. Absorption spectra for **3** upon addition of FS-DNA were recorded in buffer (25 mM MOPS, pH 7.0, 50 mM NaCl, 1 mM EDTA), at 25 °C (Figure 2.9).

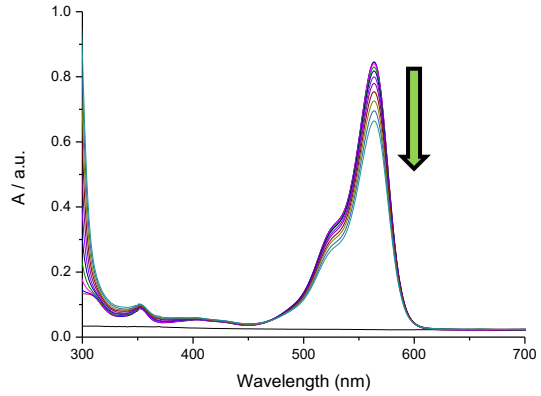

Figure 2.9 UV-visible spectra for a 0.0097 mM solution of **3** upon addition of 0 – 3.70 mM FS-DNA in buffer (25 mM MOPS, pH 7.0, 50 mM NaCl, 1 mM EDTA), at 25 °C.

Figure 2.9 shows that the absorbance at 563 nm decreases slightly upon the addition of DNA with no increases between 300 and 700 nm. The shape of the peak remains the same. Although this change in absorbance might still occur because **3** interacts very weakly with DNA, the decrease in absorbance is likely the result of simple dilution. To distinguish between the two possibilities, the absorbance at 563 nm was plotted as a function of concentration of FS-DNA (Figure 2.10, see Appendix Table A3 for numerical data).

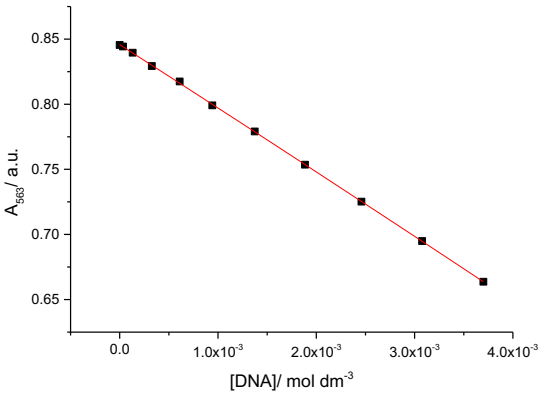

Figure 2.10 Absorbance at 563 nm for a solution of 0.0097 mM **3** as a function of DNA concentration in buffer (25 mM MOPS, pH 7.0, 50 mM NaCl, 1 mM EDTA), at 25 °C. The line represents the best fit of a multiple independent binding sites model to the data.

The MIS model fitted to the data in Figure 4.6 is once more a straight line, suggesting very weak or no binding between **3** and FS-DNA. In the absence of binding, the decrease merely represents the effect of dilution of the ligand. The fit of the multiple independent binding sites model to the data gives an equilibrium constant ($K_{binding}$) of (0.66 ± 2.34) $\times 10^2$ M^{-1} for the binding site size restricted to 3 base pairs. The binding constant for **3** is small, suggesting no binding.

To confirm limited binding, we calculate the fraction bound ligand at the end of the titration. This calculation uses the equation.

$$K = \frac{[\text{complex}]}{[\text{binding sites}] \times [\text{ligand}]_{\text{free}}}$$

therefore $\frac{\text{ligand bound}}{\text{ligand total}} \approx K \times \frac{[\text{DNA}]\,\text{total}}{n}$ if we assume $[\text{ligand}]_{\text{free}} \approx [\text{ligand}]_{\text{total}}$

Therefore, fraction bound $\approx K \times \frac{[\text{DNA}]\text{total}}{n} = 0.66 \times 10^2 \times 0.0037/3 = 0.08$

The calculation thus shows that less than 10% of the ligand is bound.

In order to further assess the interaction of **3** with FS-DNA, binding was studied using circular dichroism spectroscopy. Circular dichroism spectra for **3** were recorded in the presence of different concentrations (0 mM to 2.45 mM) of FS-DNA in 25 mM MOPS, pH 7.0, 50 mM NaCl, 1 mM EDTA, at 25 °C (Figure 2.11).

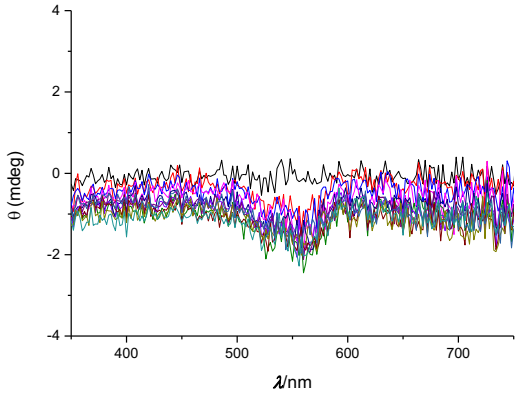

Figure 2.11 Circular dichroism spectra for 0.0097 mM **3** in the presence of different concentrations of FS-DNA (0 mM to 2.45 mM) in 25 mM MOPS, pH 7.0, 50 mM NaCl, 1 mM EDTA at 25 °C.

The circular dichroism spectra in Figure 2.11 show no change or appearance of an induced circular dichroism peak around the wavelength of interest (563 nm) where compound **3** absorbs upon addition of DNA. This suggests that **3** does not interact with the DNA. (Note: the small peak around 563 nm is an artefact that already appears for the ligand only) Therefore, the result is in agreement with the result from the UV-visible titration which showed no binding.

2.2.4 Extinction coefficient, stability and DNA binding of basic fuchsin

We set out to determine the extinction coefficient of basic fuchsin (**4**). A series of solutions of 0.0006 mM, 0.002 mM, 0.003 and 0.004 mM was prepared by dilution of a stock solution. UV-visible spectra were recorded for these solutions in a 1.0 cm path length cuvette at 25 °C. Absorbance at the λ_{max} of 539 nm was plotted against ligand concentration (Figure 2.12).

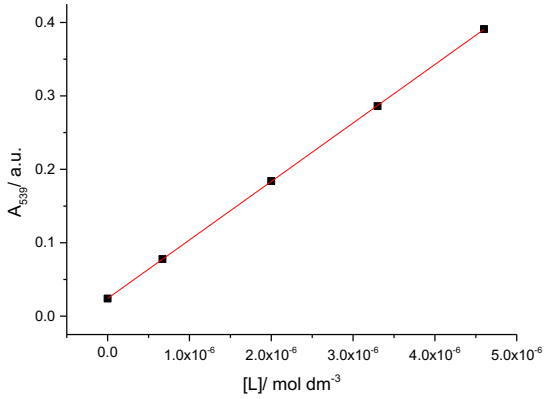

Figure 2.12 Absorbance at 539 nm as a function of concentration of **4** in buffer (25 mM MOPS, pH 7.0, 50 mM NaCl), at 25 °C.

Figure 2.12 shows that the absorbance at 539 nm increases linearly with concentration of **4**. A linear fit (red line) was applied to obtain the extinction coefficient of (79644 ± 192) M^{-1} cm^{-1}. The error margin as a percentage of the extinction coefficient is 0.2 %, which is a small margin of error. The extinction coefficient of (79644 ± 192) M^{-1} cm^{-1} is lower than the previous reported value of 116000 M^{-1} cm^{-1} at 544 nm in a different buffer (20 mM Tris-HCl, pH 7).[170]

2.2.4a Light sensitivity of basic fuchsin

There is a possibility that the difference in extinction coefficient for **4** is the result of exposure to light. To study whether **4** is sensitive to light, we plot the absorbance of **4** as a function of time exposed to ambient light, with **4** dissolved in buffer (25 mM MOPS, pH 7.0, 50 mM NaCl and 1 mM EDTA), at 25 °C (Figure 2.13).

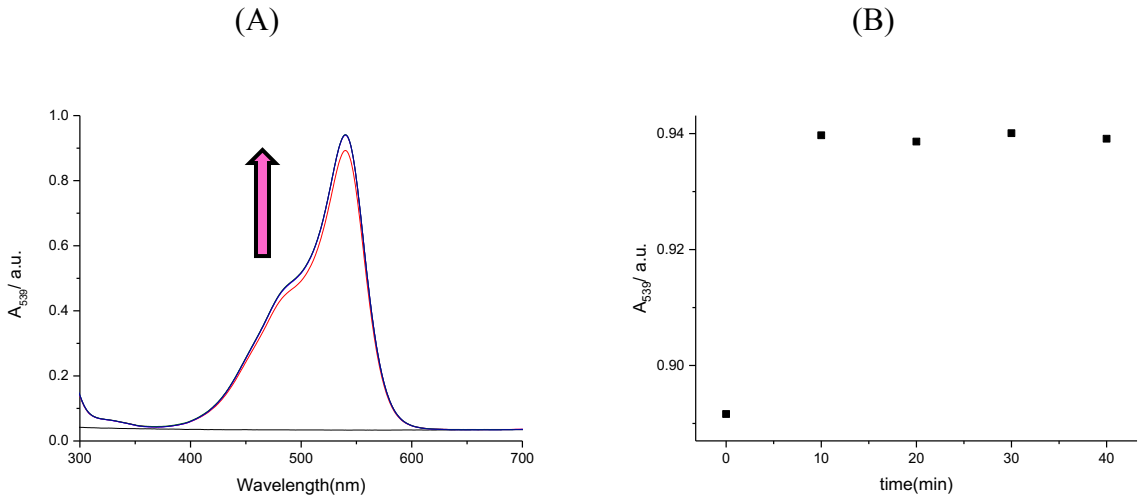

Figure 2.13 (A) Spectra of solutions of 0.013 mM **4** exposed to light, in buffer (25 mM MOPS, pH 7.0, 50 mM NaCl and 1 mM EDTA), at 25 °C. (B) The absorbance at 539 nm for **4** upon exposure to light plotted as a function of time.

Figure 2.13 (A) shows a very slight increase, which suggests that **4** has limited or no sensitivity to light. Figure 2.13 (B) confirms the data. This experiment therefore suggests that **4** is stable and not sensitive to light. It is therefore clear that the difference in extinction coefficients for **4** is not related to light sensitivity of the compound. In this instance, maybe the purity of **4** affected the extinction coefficient.

Binding of **4** to FS-DNA was studied using UV-visible spectroscopy. The changes in absorption of **4** upon addition of FS-DNA were measured in buffer (25 mM MOPS, pH 7.0, 50 mM NaCl, 1 mM EDTA), at 25 °C (Figure 2.14).

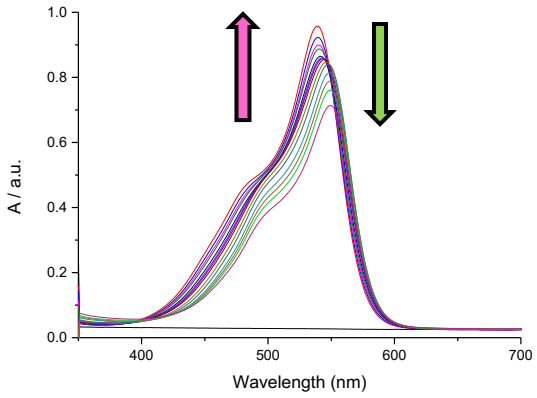

Figure 2.14 UV-visible spectra for a 0.0080 mM solution of **4** upon addition of 0 – 4.25 mM FS-DNA in buffer (25 mM MOPS, pH 7.0, 50 mM NaCl, 1 mM EDTA), at 25 °C.

Figure 2.14 shows a hypochromic and bathochromic shift upon addition of FS-DNA. This change in absorption maximum suggests that the conformation of **4** and/or it is surrounding medium changes upon the addition of DNA, suggesting that **4** binds to DNA.

To quantify the affinity of **4** for FS-DNA, the absorbance at 539 nm was plotted as a function of concentration of FS-DNA (Figure 2.15, see Appendix Table A4 for data in tabular format).

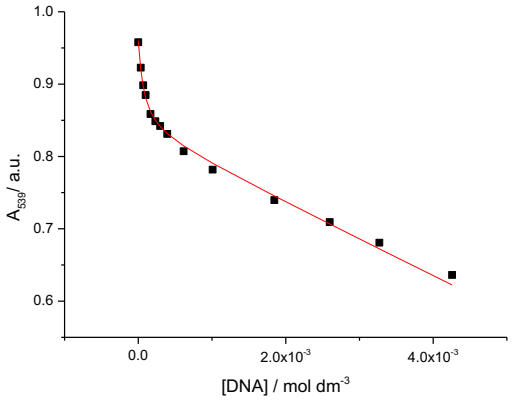

Figure 2.15 Absorbance at 539 nm of a solution of 0.0080 mM **4** as a function of DNA concentration in buffer (25 mM MOPS, pH 7.0, 50 mM NaCl, 1 mM EDTA), at 25 °C. The line represents the best fit of a multiple independent binding sites model to the data.

The titration curve in Figure 2.15 shows a decrease in absorbance at 539 nm upon the addition of FS-DNA. These changes in the UV-visible spectra occurred because **4** interacts with DNA. The titration data obtained for **4** was reproduced satisfactorily by the multiple independent binding sites model. Because the original binding site size of **4** was big (10.38 ± 4.94 basepairs) it was considered unreasonable. Therefore, we decided to restrict the binding site size to 3.0 base pairs. This fit of the multiple independent binding sites model to the data gives a binding affinity ($K_{binding}$) of (4.93 ± 0.94) $\times 10^4$ M^{-1} .

To investigate the binding mode of **4** with FS-DNA, we used circular dichroism spectroscopy. Induced circular dichroism spectra for **4** were recorded at different concentrations of FS-DNA (0 mM – 3.392 mM) in buffer (25 mM MOPS, pH 7.0, 50 mM NaCl, 1 mM EDTA), at 25 °C (Figure 2.16).

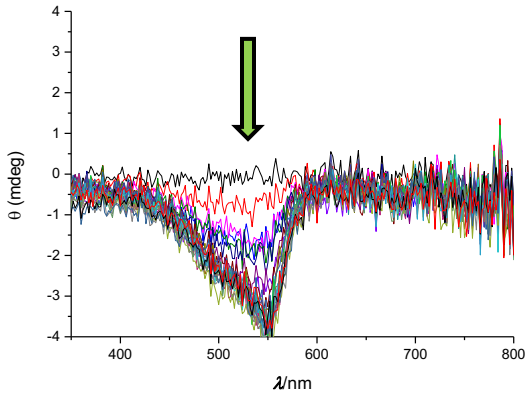

Figure 2.16 Circular dichroism spectra for 0.0120 mM **4** in the presence of different concentrations of FS-DNA (0 mM – 3.392 mM) in 25 mM MOPS, pH 7.0, 50 mM NaCl, 1 mM EDTA at 25 °C.

The circular dichroism spectra in Figure 2.16 show a negative induced circular dichroism signal at 550 nm, which increases upon addition of DNA. This weak negative ellipticity suggests an intercalative binding mode for **4** binding to FS-DNA. To quantify the affinity of **4** for FS-DNA, the ellipticities at 550 nm were plotted as a function of concentration of FS-DNA (Figure 2.17).

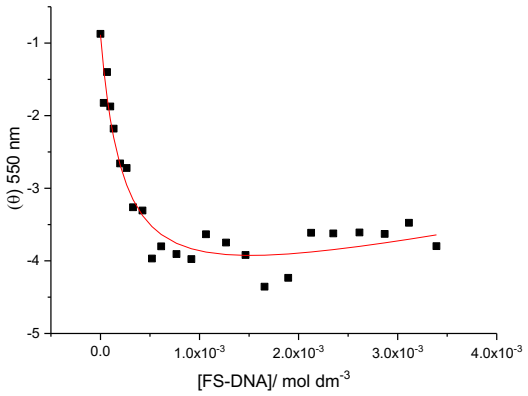

Figure 2.17 Ellipticity at 550 nm plotted against FS-DNA concentrations for 0.0120 mM of **4**, in buffer (25 mM MOPS, pH 7.0, 50 mM NaCl, 1 mM EDTA), at 25 °C. The solid line represents the best fit of a multiple independent sites model to the data.

The titration curve in Figure 2.17 was analysed by fitting a multiple independent binding sites model, which also takes ligand dilution into account, to the data. The fit gives an equilibrium constant ($K_{binding}$) of (1.44 ± 0.30) $\times 10^4$ M^{-1} for a binding site size of 3 base pairs. A negative ICD signal suggests that **4** intercalates between the base pairs.

2.2.5 Extinction coefficient, stability and DNA binding of thioflavin T

To determine the extinction coefficient for thioflavin T **(5)** in our buffer, three stock solutions of **5** were made up in buffer (25 mM MOPS, pH 7.0, 50 mM NaCl, and 1 mM EDTA). The first and second stock solutions were 0.06 mM (by weight) and a series of dilutions of the first stock solution was prepared (0.0099 mM, 0.010 mM, 0.011 mM and 0.012 mM). A second series of solution (0.0032 mM, 0.0061 mM, 0.0088 mM and 0.011 mM) was prepared from the second stock solution. The third stock solution was 0.47 mM (by weight). A series of solutions of 0.0092 mM, 0.018 mM, 0.026 mM and 0.034 mM was prepared from this stock solution. UV-visible spectra were recorded for all solutions in a 1.0 cm path length cuvette at 25 °C. Absorbance at the λ_{max} of 412 nm for all three dilution series were plotted against ligand concentration (Figure 2.18).

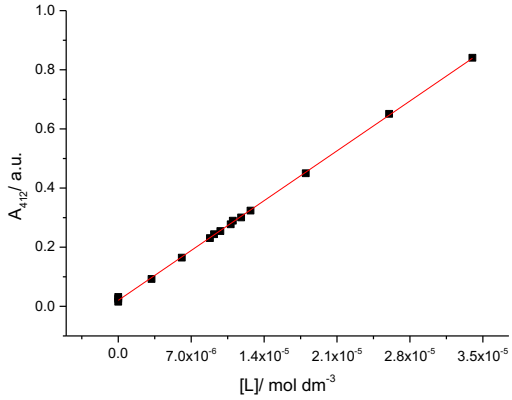

Figure 2.18 Absorbance at 412 nm as a function of concentration of **5** in buffer (25 mM MOPS, pH 7.0, 50 mM NaCl), at 25 °C.

Figure 2.18 shows that the absorbance at 412 nm increases linearly with concentration of **5**. A linear fit (red line) was applied to obtain the extinction coefficient of (24073 ± 135) M^{-1} cm^{-1}. The error margin as a percentage of the extinction coefficient is 0.5 % which is a sufficiently small error.

2.2.5a Light sensitivity of thioflavin T

To study whether **5** is sensitive to light, we plot the absorbance of **5** as a function of time exposed to ambient light, with **5** dissolved in buffer (25 mM MOPS, 50 mM NaCl. pH 7.0), at 25 °C (Figure 2.19).

(A) (B)

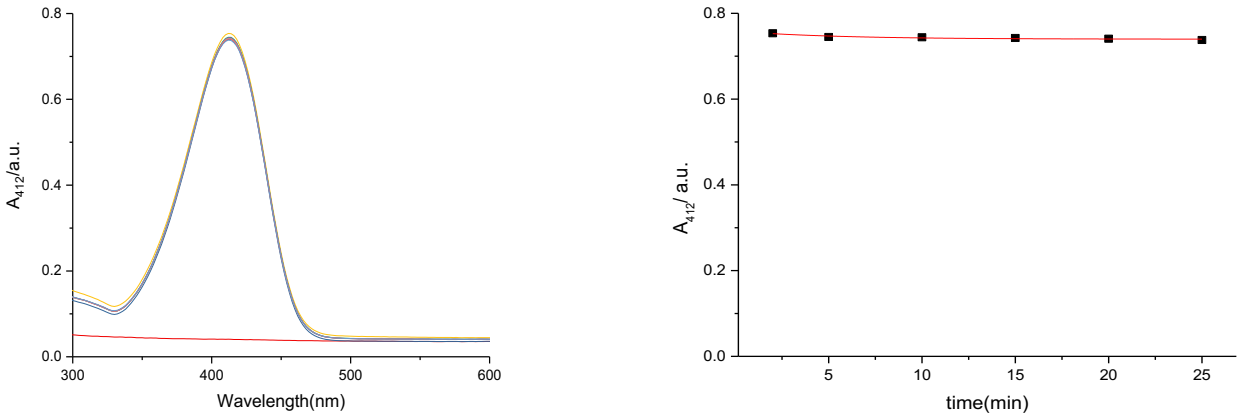

Figure 2.19 (A) Spectra of a 0.029 mM solution of **5** as a sample exposed to light, in buffer (25 mM MOPS, 50 mM NaCl. pH 7.0), at 25 °C. (B) The absorbance at 412 nm for **5** upon exposure to light plotted as a function of time.

Figure 2.19 (A) shows sufficient stability, which suggests that **5** has no sensitivity to light. Figure 2.19 (B) confirms the data. This experiment therefore suggests that **5** is stable and not sensitive to light.

We desired to know the affinity of **5** for DNA in our buffers.[171] UV-visible spectroscopy has been used. The changes in absorption of **5** upon addition of FS-DNA in buffer (25 mM MOPS, pH 7.0, 50 mM NaCl, and 1 mM EDTA), at 25 °C are reported in Figure 2.20.

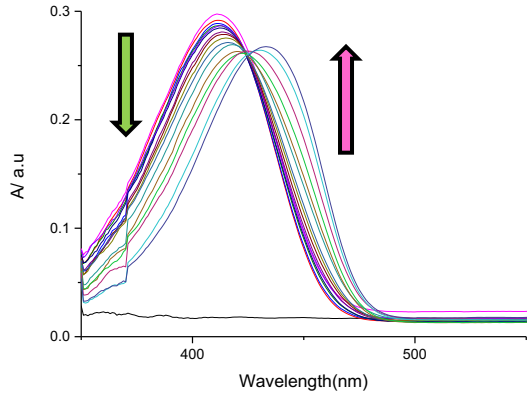

Figure 2.20 UV-visible spectra for a 0.011 mM solution of **5** upon addition of 0 – 0.74 mM FS-DNA in buffer (25 mM MOPS, pH 7.0, 50 mM NaCl, and 1 mM EDTA), at 25 °C.

Figure 2.20 shows hypochromic and bathochromic shifts for **5** upon addition of DNA. This change in UV-visible absorption indicates interaction of **5** with DNA and the change in spectrum may indicate a conformational change of **5** upon binding but it may also be a result of a local medium effect.

To quantify the affinity of **5** for FS-DNA, the absorbance at 412 nm was plotted as a function of concentration of FS-DNA (Figure 2.21, see Appendix Table A5 for numerical data).

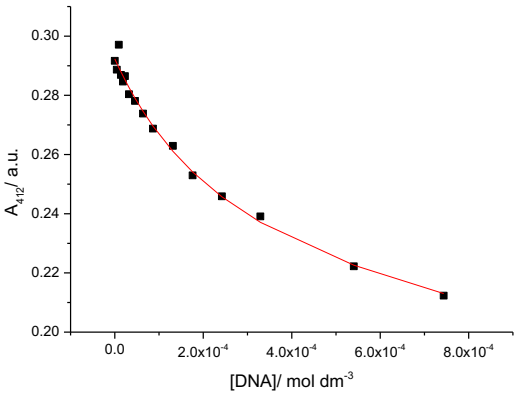

Figure 2.21 Absorbance at 412 nm of a solution of 0.011 mM **5** as a function of DNA concentration in buffer (25 mM MOPS, pH 7.0, 50 mM NaCl, and 1 mM EDTA), at 25 °C. The solid line represents the best fit of a multiple independent binding sites model to the data.

The titration data obtained for **5** were reproduced satisfactorily by the multiple independent binding sites model. This fit of the multiple independent binding sites model to the data gives an equilibrium constant ($K_{binding}$) of (1.18 ± 0.21) $\times 10^4$ M^{-1} for the binding site size restricted to 3 base pairs. This binding constant is in a good agreement with the reported equilibrium constant of ($K_{binding}$) of ~10^4 M^{-1}. [166]

2.2.6 Extinction coefficient, stability and DNA binding of H33258

There have been relatively recent studies on the molar extinction coefficient for H33258 **(6)** in SSC buffer containing 20 mM sodium citrate at pH 6.8. The extinction coefficient was found to be 42000 M^{-1} cm^{-1} at 343 nm.[172] In light of these studies, we opted not to determine the extinction coefficient for **6**. Compound 6 is also known to be sensitive to precipitation, but normally solutions can be prepared that are sufficiently stable to allow UV-visible totrations.[62]

We know from the literature that **6** binds to DNA, and most strongly with A●T sequences.[159] However, we desired to know if the presence of a co-solvent in our chosen buffers affects the affinity of **6** for FS-DNA. In order to study the affinity of **6** for DNA UV-visible spectroscopy was used as before. The changes in absorption of **6** upon addition of FS-DNA were measured in buffer (25 mM MOPS, pH 7.0, 100 mM KCl, 9 vol -% DMSO and 1 mM EDTA), at 25 °C and are shown in Figure 2.22.

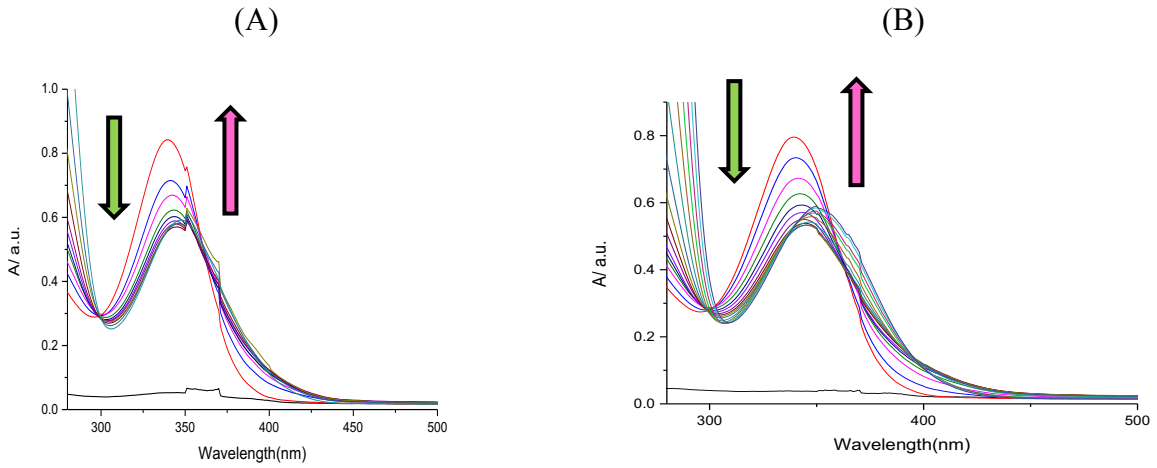

Figure 2.22 UV-visible spectra for (A) 0.018 mM **6** upon addition of 0 – 0.17 mM FS-DNA and, (B) 0.017 mM **6** upon addition of 0 – 0.65 mM FS-DNA, both in buffer (25 mM MOPS, pH 7.0, 100 mM KCl, 9 vol-% DMSO and 1 mM EDTA), at 25 °C.

Figure 2.22 shows that **6** displays a hypochromic and bathochromic shift in absorbance upon addition of DNA with a maximum change in absorbance at 338 nm. This decrease in UV-visible absorption occurs as a result of **6** interacting with DNA. To quantify the affinity of **6** for FS-DNA in our buffer, the absorbances at 338 nm for both titrations were plotted as a function of concentration of FS-DNA (Figure 2.23 and appendix Tables A6&A6.1).

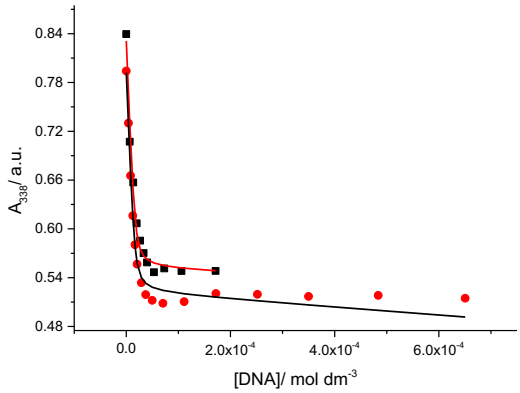

Figure 2.23 Absorbance at 338 nm (■) for a solution of 0.018 mM **6** and (●) for a solution of 0.017 mM **6**, both as a function of DNA concentration, in buffer (25 mM MOPS, pH 7.0, 100 mM KCl, 9 vol % DMSO and 1 mM EDTA) at 25 °C. The solid line represents the global fit of a multiple independent binding sites model to the data.

The titration curves in Figure 2.23 were analysed globally using the multiple independent binding sites model, which also takes ligand dilution into account. This fit produces an

apparent binding affinity ($K_{binding}$) of (8.5 ± 4.5) $\times 10^5$ M^{-1} and a binding site size of (0.9 ± 0.09) base pairs is a reasonable value. Therefore, the binding site size was not restricted to 3.0 base pairs.

2.2.7 Extinction coefficient of, stability and DNA binding of GB01

The molar extinction coefficient of GB01 **(7)** has been reported to be 33000 M^{-1} cm^{-1} at 332 nm, in water containing NaCl (0.1 M), KH_2PO_4 (10 mM), and EDTA (0.1 mM), (pH not reported). This extinction coefficient was used as reported.[173]

Compound **7** (Scheme 2.1) is related to the well-known minor groove binder H33258 **(6)**.[5] The binding of **7** to FS-DNA was studied using UV-visible spectroscopy; the changes in absorption of **7** upon addition of FS-DNA were measured in buffer (25 mM MOPS, pH 7.0, 50 mM NaCl, 1 mM EDTA), at 25 °C (Figure 2.24).

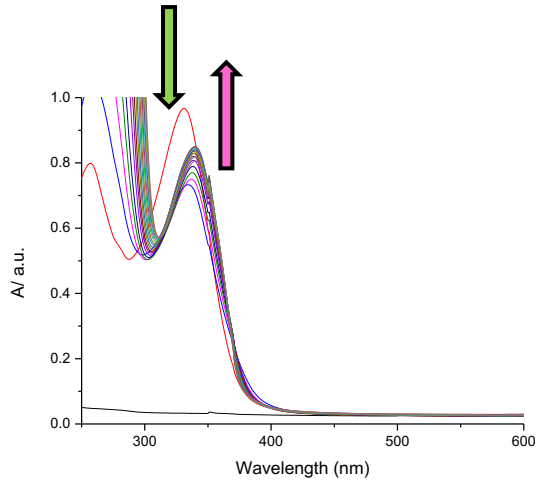

Figure 2.24 UV-visible spectra for a 0.028 mM solution of **7** upon addition of 0 – 2.90 mM FS-DNA in buffer (25 mM MOPS, pH 7.0, 50 mM NaCl, 1 mM EDTA), at 25 °C.

Figure 2.24 shows that the absorbance of **7** changed and the wavelength of maximum absorption has shifted upon addition of FS- DNA. This change in absorption spectrum suggests that the conformation of **7** and/or the surrounding medium of **7** has changed upon addition of DNA and thus suggests binding. The absorbance of **7** at 331 nm was plotted as a function of the concentration of FS- DNA (Figure 2.25, see Appendix Table A7 for data intabular ormat).

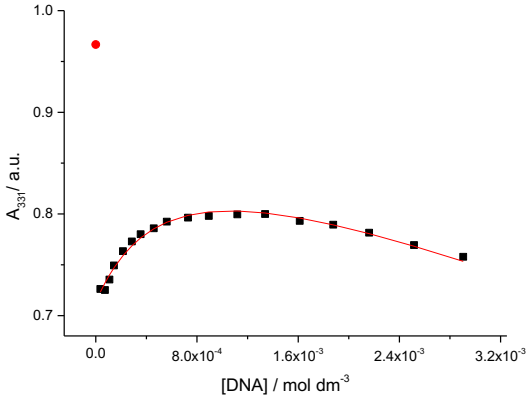

Figure 2.25 Absorbance at 331 nm for a solution of 0.028 mM **7** as a function of FS- DNA concentration in buffer (25 mM MOPS, pH 7.0, 50 mM NaCl, 1 mM EDTA), at 25 °C.

Figure 2.25 shows two events. The first event is a rapid decrease in absorbance upon the addition of a small amount of DNA. We attribute this decrease in absorbance to strong interactions of **7** with DNA in multiple types of binding sites, leading to precipitation of ligand-DNA complexes as a result of charge neutralization. When the DNA concentration is increased further, a second event occurs. The second event leads to a clear increase in the absorbance of **7**. We attribute this increase in absorbance to ligands binding to the actual preferred binding sites of **7** on DNA. A fit of the multiple independent binding sites model to the second part of data gives an apparent binding affinity ($K_{binding}$) of (5.15 ± 0.43) $\times 10^3$ M^{-1} for a binding site size restricted to 3 base pairs. This is an apparent affinity because of the competition between specific and non-specific binding sites.

We investigated the binding of **7** with FS-DNA further using isothermal titration calorimetry (ITC).

First, the self-aggregation of **7** in buffer was studied using an ITC dilution experiment. The differential heat flow and derived integrated heat effects were measured for dilution of a 0.95 mM solution of **7** into 25 mM MOPS, pH 7.0, 50 mM NaCl, 1 mM EDTA at 25 °C (Figure 2.26, Appendix Tables A7.1& A7.2 for numerical data).

(A) (B)

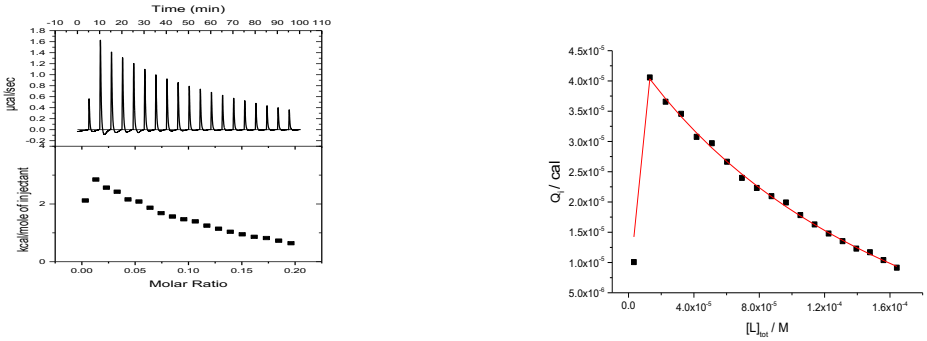

Figure 2.26 (A) Dilution of a 0.95 mM solution of **7** (25 mM MOPS, pH 7.0, 50 mM NaCl, 1 mM EDTA), at 25 °C (B) Integrated heat effects for dilution of a 0.95 mM solution of **4.7** into 25 mM MOPS, 50 mM NaCl, 1 mM EDTA, pH 7.0, at 25 °C, experimental heat effect per injection (■), calculated heat effect per injection (-).

According to Figure 2.26, the dilution of **7** is endothermic with non-constant heat effects. Non-constant heat effects are indicative of self-aggregation of **7**. We analysed this data using our ITC data analysis software IC-ITC.[62] The reason for using ICITC is that the complexity of the data, once dilution will be combined with DNA binding, will require a complex data analysis model.

We analysed the data in terms of a stepwise self-aggregation model, illustrated by model eqn.1 (Table 2.1).

$$n\ \text{ligand}_1 \rightleftharpoons \text{ligand}_2 + (n-2)\ \text{ligand}_1 \rightleftharpoons \text{ligand}_3 + (n-3)\ \text{ligand}_1 \rightleftharpoons \text{etc.} \quad \text{Eqn. 1}$$

Table 2.1: Thermodynamic parameters for aggregation of **7** in 25 mM MOPS, pH 7.0, 50 mM NaCl, 1 mM EDTA at 25 °C

ΔH dilution / kcal mol^{-1}	$K_{aggregation}$ / M^{-1}	$\Delta H_{aggregation}$ / kcal mol^{-1}
-0.9	1.48×10^3 (900-2200)	-9.0 (-12.8 - -7.2)
Note: values in brackets indicate confidence intervals.		

The affinity of **7** for duplex DNA was studied using ITC. The differential heat flow and derived integrated heat effects for titration of a 0.95 mM solution of **7** into a 0.2 mM FS-

DNA solution were measured in 25 mM MOPS, 50 mM NaCl, 1 mM EDTA, and pH 7.0, at 25 °C (Figure 2.27).

(A) (B)

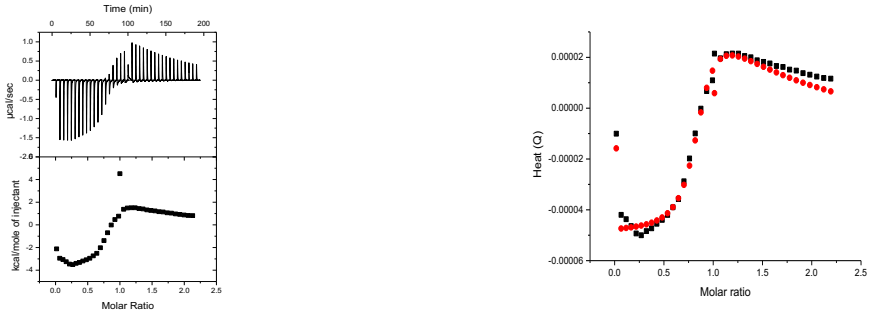

Figure 2.27 (A) Titration of a 0.95 mM solution of **7** into a 0.2 mM FS-DNA in 25 mM MOPS, 50 mM NaCl, 1 mM EDTA, and pH 7.0, at 25 °C. (B) Integrated calorimetric data for titration of a 0.95 mM solution of 7 into a 0.2 mM fish sperm DNA in 25 mM MOPS, 50 mM NaCl, 1 mM EDTA, pH 7.0, at 25 °C, experimental heat (■), calculated heat (●).

Figure 2.27A shows the enthalpogram for binding of **7** to FS-DNA. The enthalpogram for binding of **7** to DNA suggests at least one binding event which is followed by ligand dilution. There may be a second, high affinity and low stoichiometry, binding event as well but based on previous experience we did not attempt to fit this because it appears poorly defined by the data.

The fit of the model (Figure 2.27B) indicates that a binding model involving one type of binding event in combination with stepwise aggregation reproduces the data reasonably well. The binding constant *K* and binding site size *n* for binding of **7** to DNA in 25 mM MOPS, 50 mM NaCl, pH 7.0, at 25 °C are summarised in Table 2.2.

Table 2.2 Binding constant *K*, binding site sizes n, and interaction enthalpy Δ*H* for binding of **7** to DNA in 25 mM MOPS, 50 mM NaCl, pH 7.0, at 25 °C.

ΔH_{A1} / kcal mol^{-1}	K_{A1} / M^{-1}	n=1/n_{A1}
-6.9 (-7.3 - 6.4)	4.48×10^5 (1.8×10^5 - 5.8×10^5)	1.14 (1.10-1.18)
a) Aggregation parameters restricted to 1.48×10^3 M^{-1} and 9.02×10^3 cal mol^{-1}		

It is interesting to compare DNA binding of **6** and **7** because they are structurally related and both of them bind to DNA as groove binders (Table 2.3) and previous ITC studies for **6** binding to DNA are available.[62] The enthalpogram for binding of **7** to DNA suggests at least one binding event. Enthalpograms for binding of **6** to specific sequences of DNA suggests two binding modes of which the non-selective electrostatic binding mode has a similar binding site size of 1 base pair.

Table 2.3 Thermodynamic parameter for interaction of 6 to specific sequences of DNA in 0 mM MOPS, 100 mM NaCl, pH 7.0, at 25 °C, and 7 to FS-DNA in 25 mM MOPS, 50 mM NaCl, pH 7.0, at 25 °C.

Ligand	$K_{aggregation}$/ x10^3 M^{-1}	$\Delta H_{aggregation}$/ kcal mol^{-1}	K_{A1} / M^{-1}	ΔH_{A1} / kcal mol^{-1}
6	2.70	-10.79	8.2×10^6	-3.17
7	1.48	-9.02	4.48×10^5	-6.9

Table 2.3 demonstrates that $K_{aggregation}$ and $\Delta H_{aggregation}$, for **6** and **7** are similar. This observation suggests that both compounds aggregate in a similar manner. The binding affinity of the compound **6** is ten-fold higher than that of the compound **7**. However, the value of enthalpy change for the compound **7** is almost twice of the value of the compound **6**.

2.2.8 Extinction coefficient, stability and DNA binding of TF1

We wanted to determine the extinction coefficient of TF1 **(8)** in aqueous solutions. We attempted to dissolve **8** in buffer without added co-solvents but we found limited solubility in buffer. Therefore, we added 9 vol-% of DMSO to the buffer (25 mM MOPS pH 7.0, 100 mM KCl and 1 mM EDTA).

A stock mixture of **8** (0.048 mM) in buffer (25 mM MOPS pH 7.0, 100 mM KCl, 1 mM EDTA and 9 vol-% DMSO) was prepared. In this mixture, **8** was not fully dissolved. Three dilution series were made (0.005 mM, 0.006 mM, 0.008 mM and 0.009 mM; 0.006 mM, 0.007 mM, 0.008 mM and 0.009 mM; 0.0069 mM, 0.0076 mM and 0.009 mM). UV-visible spectra were recorded for those dilution series in a 1.0 cm pathlength cuvette at 25 °C. Absorbance at the λ_{max} of 476 nm was plotted against ligand concentration (Figure 2.28).

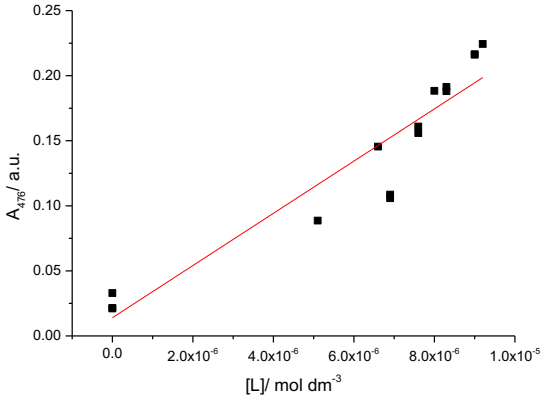

Figure 2.28 Absorbance as a function of concentration of **8** in buffer (25 mM MOPS pH 7.0, 100 mM KCl, 1 mM EDTA and 9 vol-% DMSO), at 25 °C (■).

Figure 2.28 shows an increase in absorbance at 476 nm with increasing concentration. This increase does not appear to be linear with concentration. A linear fit (red line) was applied to obtain the extinction coefficient of (20059 ± 1902) M^{-1} cm^{-1}. The error margin as a percentage of the extinction coefficient is 9 %. That is a very large margin of error. This large error may be because of limited solubility, and resulting precipitation, of **8** in 25 mM MOPS pH 7.0, 100 mM KCl, 1 mM EDTA and 9 vol-% DMSO.

The error on the extinction coefficient in this work suggests that 9 vol-% of DMSO as a co-solvent is not enough to keep **8** in solution. Alternatively, the poor correlation may result from fading of the colour of **8** during experiments (see below).

To avoid the challenge of limited solubility, we determined the extinction coefficient of **8** in pure DMSO and pure acetonitrile.

A stock solution of **8** (0.046 mM) (by weight) in DMSO was prepared and a dilution series was made (0.006 mM, 0.007 mM, 0.008 mM and 0.0086 mM). A second stock solution of the same concentration as the first stock solution was similarly used to prepare a second dilution series (0.002 mM, 0.004 mM, 0.006 mM, 0.007 mM and 0.009 mM). UV-visible spectra were recorded for the combined dilution series in a 1.0 cm pathlength cuvette at 25 °C. The UV-visible spectra show that the λ_{max} has shifted from 476 nm in aqueous buffer to 500 nm in DMSO. Absorbance at the λ_{max} of 500 nm was plotted against ligand concentration (Figure 2.29).

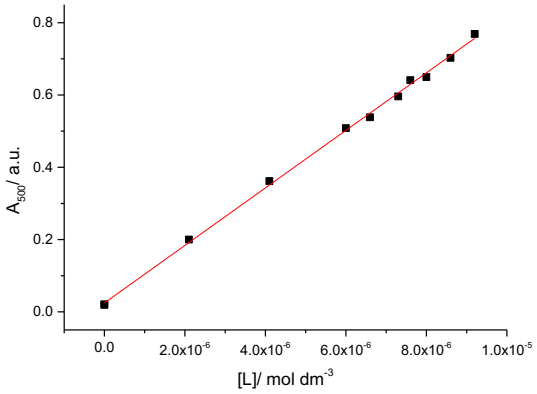

Figure 2.29 Absorbance at 500 nm as a function of concentration of **8** in DMSO at 25 °C

Figure 2.29 shows an increase in absorbance at 500 nm with increasing concentration. A linear fit (red line) was applied to obtain the extinction coefficient. The extinction coefficient is (79579 ± 967) M^{-1} cm^{-1}. The error margin as a percentage of the extinction coefficient is 1.2 %, which is acceptable.

We similarly examined the extinction coefficient for **8** in pure acetonitrile to explore potential solvent effects on the extinction coefficient of **8**.

A stock solution of **8** (0.050 mM) (by weight) in acetonitrile was prepared and a dilution series was made (0.0072 mM, 0.0079 mM, 0.008 mM and 0.009 mM). A second stock solution of the same concentration as the first stock solution led to a second dilution series (0.002 mM, 0.004 mM, 0.006 mM, 0.008 mM and 0.01 mM). UV-visible spectra were recorded for the combined dilution series in a 1.0 cm pathlength cuvette at 25 °C. Absorbance at the λ_{max} of 500 nm was plotted against ligand concentration (Figure 2.30).

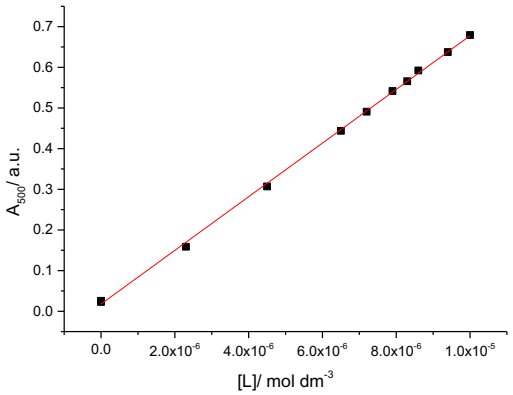

Figure 2.30 Absorbance as a function of concentration of **8** in acetonitrile at 25 °C.

Figure 2.30 shows an increase in absorbance at 500 nm with increasing concentration. A linear fit (red line) was applied to obtain the extinction coefficient. The extinction coefficient in acetonitrile is (65962 ± 531) M^{-1} cm^{-1}. The error margin as a percentage of the extinction coefficient is 0.7 %, which is a small margin of error.

The extinction coefficient in DMSO is bigger than that in acetonitrile; we do not currently have an interpretation for this observation.

We want to know how much co-solvent we need to create a stable solution. we therefore determined absorbances of **8** in 10 and 20 vol-% DMSO / buffer (25 mM MOPS pH 7.0, 50 mM NaCl and 1 mM EDTA), at 25 °C. A stock solution of **8** in DMSO was diluted in buffer (25 mM MOPS pH 7.0, 50 mM NaCl and 1 mM EDTA) and DMSO added as required to keep the fraction of DMSO constant.

The absorbances for **8** in both the buffer containing 10 vol-% DMSO and 20 vol-% DMSO were plotted together as a function of concentration of **8** (Figure 2.31).

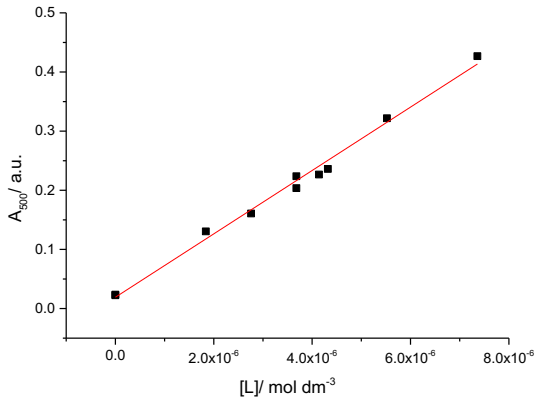

Figure 2.31 Absorbance as a function of concentration in 10 and 20 vol-% DMSO/ buffer (25 mM MOPS pH 7.0, 50 mM NaCl and 1 mM EDTA), at 25 °C.

Figure 2.31 shows that the absorbance increases linearly with concentration of **8** and there is no significant difference between the systems involving 10 and 20 vol-% DMSO. A linear fit (red line) was applied to obtain the extinction coefficient. The extinction coefficient is (53580 ± 1690) M^{-1} cm^{-1}. The error margin as a percentage of the extinction coefficient is 3.1 %, which is an acceptable margin of error. Compound **8** has sufficient solubility in both 10 and 20 vol-% DMSO/ buffer (25 mM MOPS pH 7.0, 50 mM NaCl and 1 mM EDTA), at 25 °C. The results of this investigation show that aqueous solutions containing 10 and 20 vol-%

DMSO work well as a solvent for **8**. These experiments also suggest that the scatter in Figure 2.31 is the result of in solubility of **8** at the concentration of the stock solution.

We next examine the effect of acetonitrile on the extinction coefficient in aqueous solution and compare the extinction coefficient with DMSO-containing aqueous solutions.

A stock solution of **8** in acetonitrile was diluted in buffer (25 mM MOPS pH 7.0, 50 mM NaCl and 1 mM EDTA) and acetonitrile added as required to keep the fraction of acetonitrile constant. The absorbance of **8** in 10 and 20 vol-% acetonitrile / buffer (25 mM MOPS pH 7.0, 50 mM NaCl and 1 mM EDTA) was measured at 25 °C. (Figure 2.32).

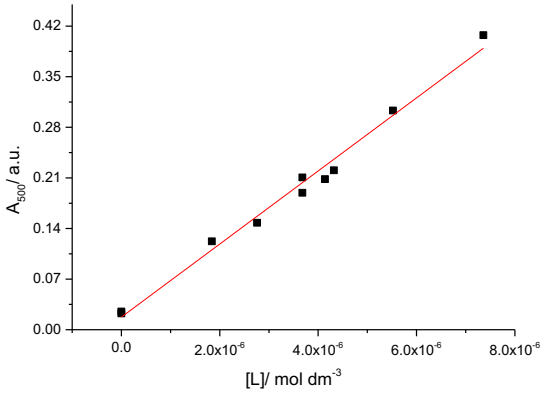

Figure 2.32 Absorbance as a function of concentration of **8** in 10 and 20 vol-% acetonitrile / buffer (25 mM MOPS pH 7.0, 50 mM NaCl and 1 mM EDTA), at 25 °C.

Figure 2.32 shows that the absorbance increases linearly with concentration of **8** and that there is no significant difference between the systems involving 10 and 20 vol-% acetonitrile. A linear fit (red line) was applied to obtain the extinction coefficient. The resulting extinction coefficient is (50539 ± 1984) M^{-1} cm^{-1}. The error margin as a percentage of the extinction coefficient is 3.9 %, which is an acceptable margin of error. This work suggests that the extinction coefficients for **8** in aqueous acetonitrile and aqueous DMSO are similar. Therefore, co-solvent[174] does not affect the extinction coefficient much.

Another factor that can affect the extinction coefficient is the sensitivity of a compound to light. We suspected that **8** is light sensitive. In order to study whether **8** is sensitive to light we recorded the absorbance spectra for **8** as a function of time exposed to ambient light and we compared this with data for a sample shielded from light. Compound **8** was dissolved in pure acetonitrile and diluted in buffer (25 mM MOPS pH 7.0, 50 mM NaCl and 1 mM

EDTA) and we recorded spectra with one sample exposed to light and the second sample shielded from light (Figure 2.33).

(A) (B)

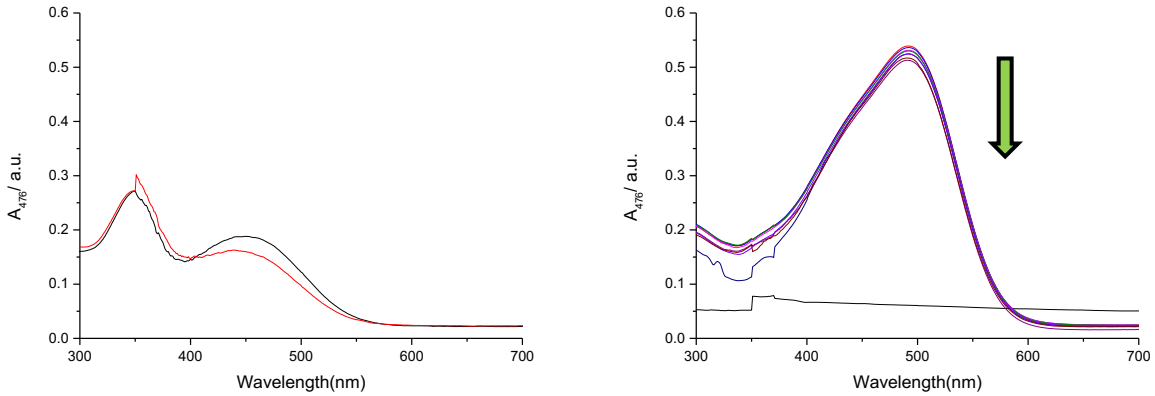

Figure 2.33 UV-visible spectra for **8** dissolved in pure acetonitrile and diluted in buffer (25 mM MOPS pH 7.0, 50 mM NaCl and 1 mM EDTA) to give the same concentration for A and B, (A) exposed to ambient light for 216 hours and (B) stored in a dark place for 260 hours (initial spectra are not shown).

Figure 2.33 (A**)** shows a clear decrease in the absorbance of 0.046 mM **8** at the λ_{max} of 476 nm for the sample exposed to light and shows that a new peak appears around 350 nm. Figure (B) shows that a solution of **8** which was stored in a dark place does not fade.

Moreover, it is clear that light affects **8** from visual observation as well because the solution becomes colourless with time, while the solution of **8** that was stored in a dark place does not show any visual change.

We repeated the experiment but this time we dissolved **8** in pure DMSO and diluted in buffer (25 mM MOPS pH 7.0, 100 mM KCl, 9 vol-% of DMSO and 1 mM EDTA). We plot the absorbance spectrum of **8** as a function of wavelength after storing the sample exposed to light or protected from light (Figure 2.34).

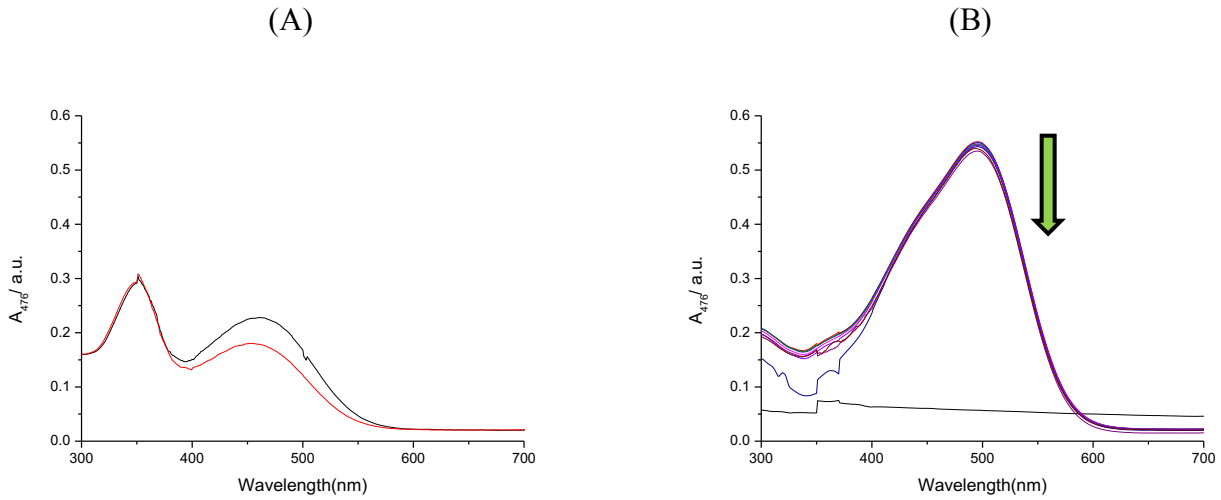

Figure 2.34 UV-visible spectra for **8** dissolved in DMSO and diluted in DMSO-containing buffer (25 mM MOPS pH 7.0, 100 mM KCl, 9 vol-% of DMSO and 1 mM EDTA); final concentration for A and B is identical. (A) exposed to light for 216 hours and (B) stored in a dark place for 260 hours. Note: initial spectra are not shown.

Figure 2.34 (A) shows the appearance of a new peak around 350 nm when the sample is exposed to light. Figure (B) shows a solution of 0.046 mM **8** which was stored in a dark place. No significant changes in the absorbance spectrum are apparent. We conclude that **8** is sensitive to the light. To avoid fading it should be stored in a dark place.

Based on our results, **8** is sparingly soluble in water but it is soluble in some organic solvents such as acetonitrile and DMSO. On the basis of it is structure, we suppose that **8** is a groove binder with duplex DNA because of it is length.[163] In order to study the binding of **8** with duplex DNA in the presence of acetonitrile and DMSO, we prepared aqueous solutions starting from stock solutions of **8** in acetonitrile and DMSO. We then did two types titrations. In the first titration, a stock solution of 0.28 mM **8** in acetonitrile was prepared. A volume of this stock solution was added to 2375 µl buffer (25 mM MOPS, pH 7.0, 50 mM NaCl, 1 mM EDTA), in a 1.00 cm pathlength cuvette. In the second and third titrations, stock solutions of

0.006 mM **8** and 0.0031 mM **8** were prepared directly in DMSO-containing buffer (25 mM MOPS, pH 7.0, 100 mM KCl, 9 vol-% DMSO and 1 mM EDTA).

In the first titration, binding of **8** to FS-DNA in 25 mM MOPS, pH 7.0, 50 mM NaCl, 1 mM EDTA in presence of 1.04 % of acetonitrile was studied using UV-visible spectroscopy. The changes in absorption of **8** upon addition of FS-DNA in buffer (25 mM MOPS, pH 7.0, 50 mM NaCl, 1 mM EDTA), at 25 °C are as shown in Figure 2.35.

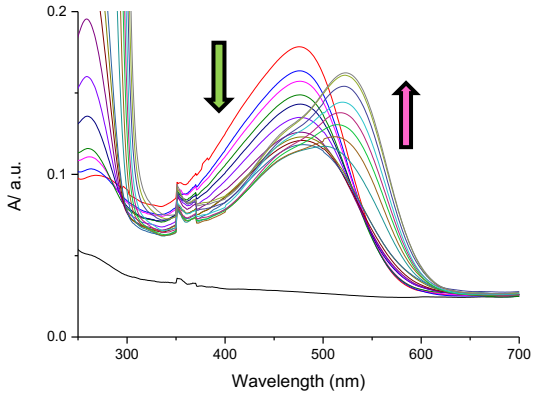

Figure 2.35 UV-visible spectra for a 0.0029 mM solution of **8** upon addition of 0 – 1.04 mM FS-DNA in buffer (25 mM MOPS, pH 7.0, 50 mM NaCl, 1 mM EDTA), at 25 °C.

Figure 2.35 shows that the absorbance of **8** changed and shifted upon addition of DNA. This change in absorption suggests that the conformation of **8** and/or the surrounding medium of **8** has changed upon addition of DNA.

The absorbance of **8** at 476 nm as well as the average absorbance in the range 670-700 nm was plotted as a function of the concentration of DNA (Figure 2.36 A, see Appendix Table A8 for numerical data).

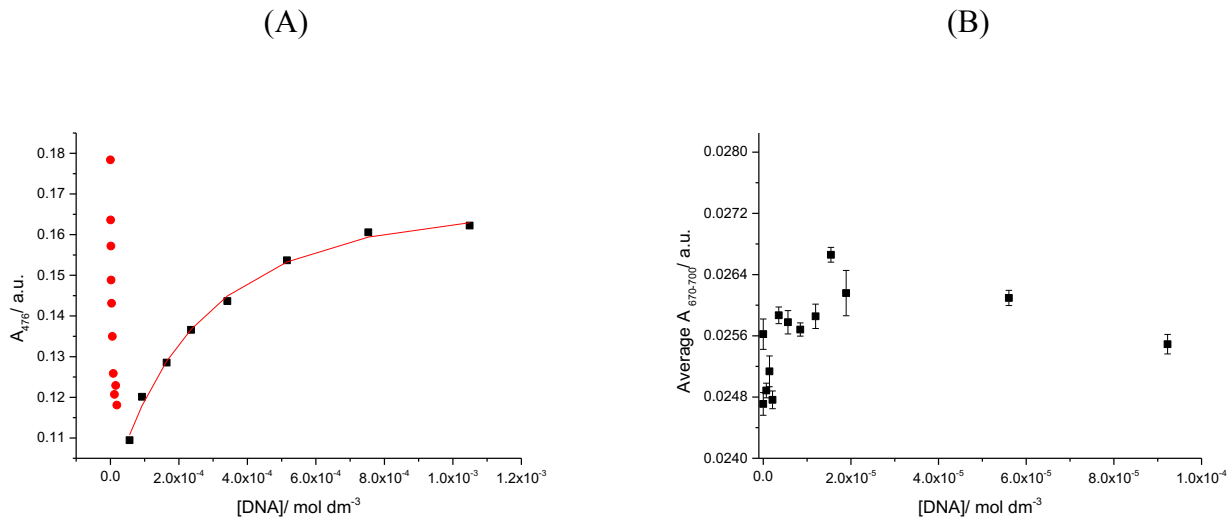

Figure 2.36 (A) Absorbance at 476 nm of a 0.0029 mM solution of **8** in the presence of 1.04 % of acetonitrile as a function of FS-DNA concentration in buffer (25 mM MOPS, pH 7.0, 50 mM NaCl, 1 mM EDTA), at 25 °C. (B) The average absorbance in the range 670-700 nm as a function of FS-DNA concentration in the same experiment.

Figure 2.36 (A) shows two events. The first event is accompanied by a rapid decrease in the absorbance upon addition of DNA. We attribute this decrease in absorbance to strong interactions of **8** with DNA in the regime where the ligand is present in large excess over the DNA. In this regime, the ligand binds to all available binding sites, leading to precipitation of ligand-DNA complexes as a result of charge neutralization.

Figure 2.36 (B) shows the average absorbance in the range 670-700 nm and there are indications of scattering effects as a results of poor solubility and precipitation of the complex formed when DNA is saturated with bound **8**. When the DNA concentration is increased, a second event occurs (figure 2.36A), leading to an increase in the absorbance of **8**. This event corresponds to binding of the ligand bound in secondary binding sites (together with any remaining free ligand) to the principal binding sites on the DNA. A fit of the multiple independent binding sites model to the second part of the data gives an apparent binding affinity ($K_{binding}$) of (9.7 ± 1.44) $\times 10^3$ M^{-1} for a binding site size restricted to 3 base pairs. The first and second binding events as described above are illustrated in Figure 2.36.

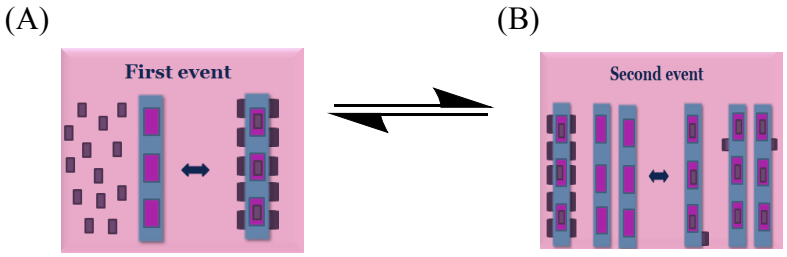

Figure 2.37 Cartoon representation of the DNA (blue rod) interacting with the ligands (pink oblong).

Figure 2.37 (A) shows that the first event happens when many ligand molecules bind strongly to the backbone and the base pairs of the DNA at low concentration of DNA. Figure 4.17 (B) shows the second event, which happens when the concentration of DNA increases.

In the second titration, the binding of **8** to FS-DNA in 25 mM MOPS, pH 7.0, 100 mM KCl, 9 vol-% DMSO and 1 mM EDTA was studied using UV-visible spectroscopy. The changes in absorption of **8** upon addition of FS-DNA at 25 °C are shown in Figure 2.38.

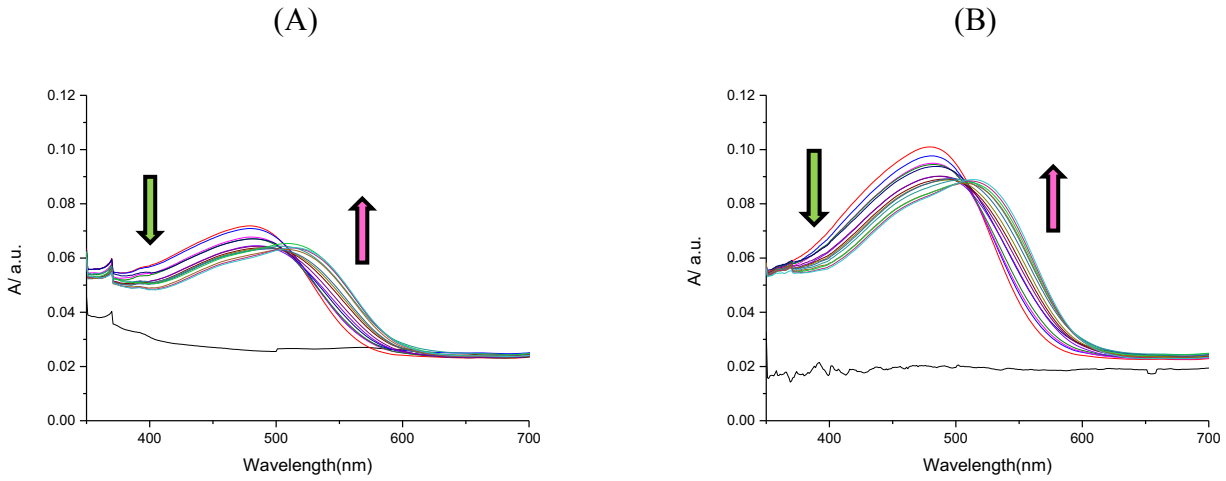

Figure 2.38 UV-visible spectra for **(A)** a 0.0008 mM solution of **8** upon addition of 0 – 0.44 mM, FS-DNA and **(B)** 0.0015 mM solution of **8** upon addition of 0 – 0.45 mM FS-DNA, both in buffer (25 mM MOPS, pH 7.0, 100 mM KCl, 9 vol-% DMSO and 1 mM EDTA), at 25 °C.

Figure 2.38 shows a hypochromic and a bathochromic shift in absorbance of **8** upon addition of DNA. This change in UV-visible absorption may occur as a result of distortion upon interaction between **8** and DNA. It also may be a local medium effect. The absorbances of **8**

at 476 nm for both titrations were plotted as a function of the concentration of DNA (Figure 2.39, see Appendix Tables A8.1& A8.2 for numerical data).

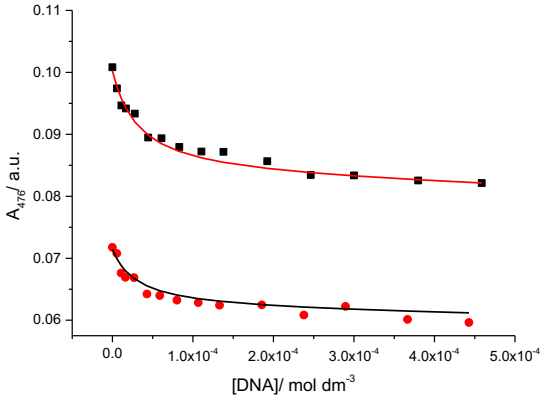

Figure 2.39 Absorbance at 476 nm (■) for a solution of 0.0015 mM of **8** and (●) for a solution of 0.0008 mM **8**, as a function of DNA concentration in buffer (25 mM MOPS, pH 7.0, 100 mM KCl, 9 vol-% DMSO and 1 mM EDTA), at 25 °C. The solid lines represent a global fit of a multiple independent sites model to the data.

In this titration experiment, we did not observe the initial drop in absorbance. This observation suggests the absence of the initial precipitation observed in the absence of DMSO. The titration curves in Figure 2.39 were therefore analysed by fitting a multiple independent binding sites model to the data. The obtained binding stoichiometry was small hence the data were reanalysed at fixed binding site size of 3.0 base pairs, giving an equilibrium constant ($K_{binding}$) for **8** binding to FS-DNA of (1.04 ± 0.84) ×10^5 M^{-1}. Previous studies reported a binding affinity ($K_{binding}$) of 0.12 ×10^6 M^{-1} for a binding site size (n) of 2, in excellent agreement with our data.[163]

2.2.9 Extinction coefficient, stability and DNA binding of methylene blue

Most previous studies have determined the extinction coefficient of **9** in different buffers such as phosphate buffer in which the extinction coefficient at 665 nm was found to be 81600 M^{-I} cm^{-1}. [175] In distilled deionized water containing 5 mM sodium sulfate, 1 mM phosphate buffer at pH 7 the extinction coefficient was found to be 82600 M^{-1} cm^{-1} at 665 nm.[169]

We wanted to know if a co-solvent affects the extinction coefficient of methylene blue (**9**). We therefore determined the extinction coefficient of **9** in the presence of DMSO as a co-solvent.[176]

A stock solution of **9** (0.15 mM) in buffer (25 mM MOPS, pH 7.0, 100 mM KCl, 9 vol-% DMSO and 1 mM EDTA) was prepared. A series of solutions (0.0011 mM, 0.0018 mM, 0.0025 mM and 0.0033 mM) was prepared from the stock solution. UV-visible spectra were recorded for these solutions in a 1.0 cm pathlength cuvette at 25 °C. Absorbance at the λ_{max} of 663 nm was plotted against ligand concentration (Figure 2.40).

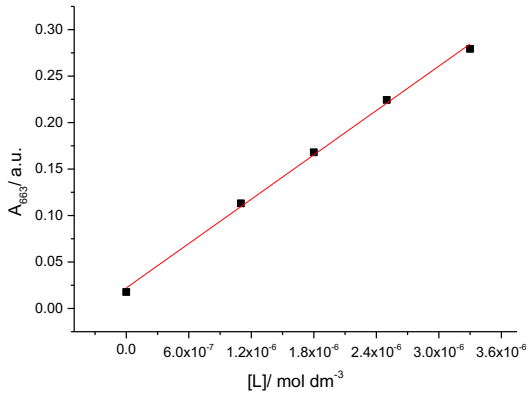

Figure 2.40 Absorbance at 663 nm as a function of concentration of **9** in buffer (25 mM MOPS, pH 7.0, 100 mM KCl, 9 % DMSO and 1 mM EDTA), at 25 °C.

Figure 2.40 shows an increase in absorbance at 663 nm with increasing concentration. A linear fit (red line) was applied to obtain the extinction coefficient of (79533 ± 2018) M^{-1} cm^{-1}. The error margin as a percentage of the extinction coefficient is 2.5 % which is an acceptable margin of error.

We also examine the extinction coefficient of **9** in the buffer without co-solvent. A stock solution of **9** (0.081 mM) in buffer (25 mM MOPS, pH 7.0, 50 mM NaCl, and 1 mM EDTA) was prepared. A series of solutions of 0.0015, 0.0023 0.0031 and 0.0038 mM was prepared by dilution. A second stock solution of 0.13 mM **9** in buffer (25 mM MOPS, pH 7.0, 50 mM NaCl, and 1 mM EDTA) was prepared. A second series of solutions (0.0015, 0.0040 0.0064 and 0.0087 mM) was prepared from the second stock solution. UV-visible spectra were recorded for all diluted solutions in a 1.0 cm pathlength cuvette at 25 °C. Absorbance at the λ_{max} of 663 nm for both dilution series were plotted against ligand concentrations (Figure 2.41).

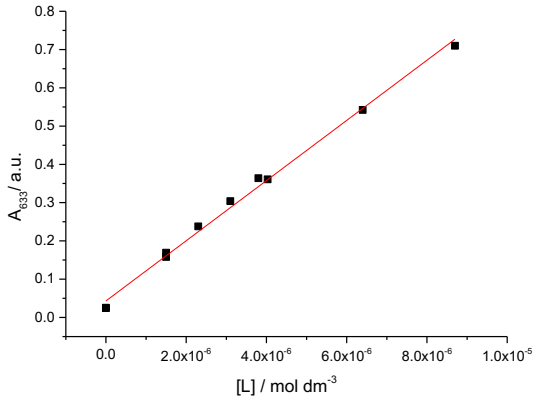

Figure 2.41 Absorbance at 663 nm as a function of concentration of **9** in buffer (25 mM MOPS, pH 7.0, 50 mM NaCl, and 1 mM EDTA), at 25 °C.

Figure 2.41 shows an increase in absorbance at 663 nm with increasing concentration. A linear fit (red line) was applied to obtain the extinction coefficient of (78618 ± 1922) M^{-1} cm^{-1}. The error margin as a percentage of the extinction coefficient is 2.4 %. That is an acceptable margin of error. The extinction coefficient for **9** in the presence and absence of co-solvent is the same, which suggests again that co-solvent does not affect the extinction coefficient.

These extinction coefficients are both roughly within the error margin of our extinction coefficient and are therefore in good agreement.

Based on previous reports we assumed that **9** is light sensitive.[177, 178] To study this light sensitivity, we plotted the absorbance of **9** as a function of time under exposure to light in buffer (25 mM MOPS pH 7.0, 50 mM 50 mM NaCl and 1 mM EDTA) (Figure 2.42).

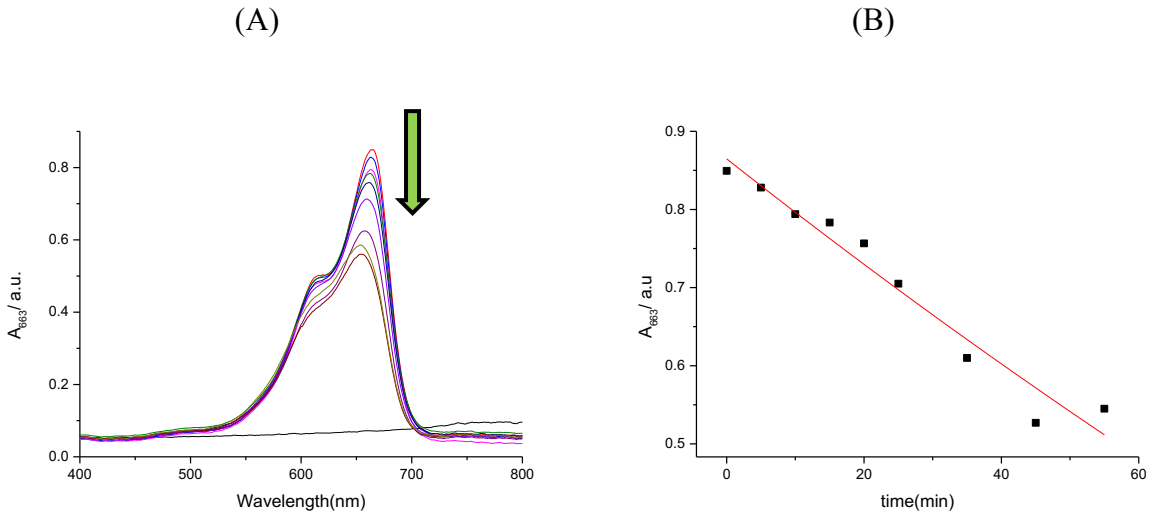

Figure 2.42 (A) UV-visible spectra for **9** dissolved in buffer (25 mM MOPS pH 7.0, 50 mM NaCl and 1 mM EDTA) and exposed to light at 25 °C (B) The absorbance of **9** at 663 nm as a function of time.

Figure 2.42 (A) shows that the spectra for a solution of **9** show a decrease upon exposure to light. This decrease suggests that **9** is sensitive to light. Figure 2.42 (B) shows the decrease of absorbance of **9** as a function of time.

We wanted to know whether different buffers affect the fading of **9**. To study the effect of buffer choice, we prepared an analogous stock solution of **9** but instead of MOPS buffer **we** made the stock solution in phosphate buffer and left out EDTA. The reason for this is that MOPS and EDTA contain an amine functional group. This amine could act as an electron donor to the excited state of **9** similar to the action of sacrificial amines as electron donors as used in development of photovoltaic systems.

To study whether MOPS caused the light-driven fading, we plotted the absorbance of **9** as a function of time exposed to light in phosphate buffer (25 mM Na_2HPO_4, pH 7.0, and 50 mM NaCl) (Figure 2.43).

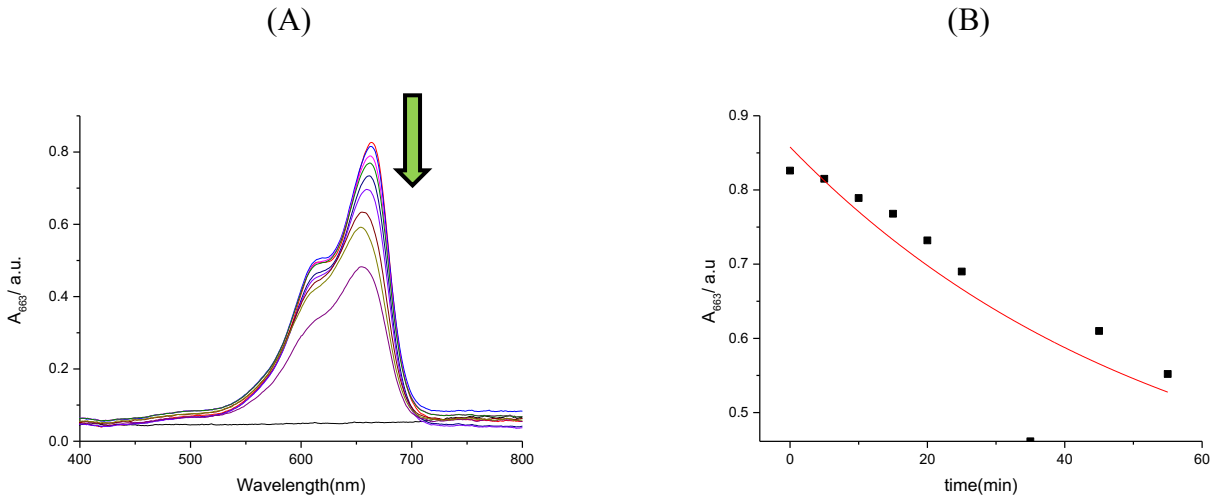

Figure 2.43 (A) UV-visible spectra for **9** dissolved in phosphate buffer (25 mM Na_2HPO_4, pH 7.0, and 50 mM NaCl), at 25 °C and under exposure to ambient light. Figure (B) the absorbance of **9** at 663 nm plotted as a function of time of exposure to light.

Figure 2.43 (A) again shows a decrease. The time trace in Figure 2.43 (B) shows the extent of the decrease in absorbance of **9** as a function of time. These results indicate that the buffer does not affect significantly the sensitivity of **9** to light, and this indicates that MOPS and EDTA do not act as sacrificial electron donors in this particular reaction.

In order to evaluate the binding of **9** with DNA in our buffers, UV-visible titrations were carried out. Binding of **9** to FS-DNA was studied using UV-visible spectroscopy. The changes in absorption of **9** upon addition of FS-DNA were measured in buffer (25 mM MOPS, pH 7.0, 50 mM NaCl, and 1 mM EDTA), at 25 °C and are shown in Figure 2.44.

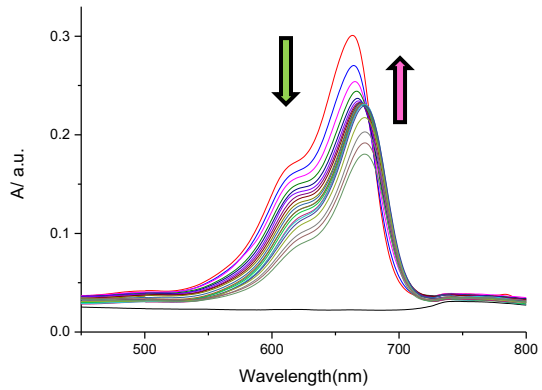

Figure 2.44 UV-visible spectra for a 0.0035 mM solution of **9** upon addition of 0 – 4.6 mM FS-DNA in buffer (25 mM MOPS, pH 7.0, 50 mM NaCl, and 1 mM EDTA), at 25 °C.

Figure 2.44 shows a hypochromic shift in absorbance (at the λ_{max} of 664 nm) of **9** upon addition of DNA. This change in absorption suggest that the conformation of **9** or the surrounding medium of **9** has changed upon the addition of DNA. Either way, of these changes would be the result of binding of **9** to DNA. The absorbance of **9** at 664 nm was plotted as a function of concentration of FS-DNA (Figure 2.45, see Appendix, Table A9 for data in tabular format).

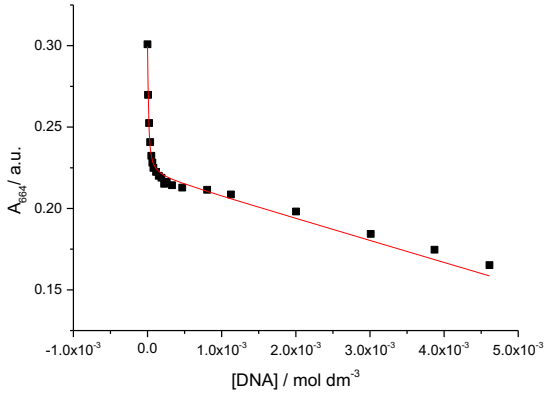

Figure 2.45 Absorbance at 664 nm for a solution of 0.0035 mM **9** as a function of DNA concentration in buffer (25 mM MOPS, pH 7.0, 50 mM NaCl, and 1 mM EDTA), at 25 °C. The line represents the best fit of a multiple independent binding sites model to the data.

The titration curve in Figure 2.45 shows a decrease in absorbance of **9** upon the addition of FS-DNA. This change in absorbance indicates that **9** interacts with DNA. The titration data obtained for **9** was reproduced satisfactorily by the multiple independent binding sites model. This fit of the multiple independent binding sites model to the data gives a binding affinity

($K_{binding}$) of (3.8 ± 0.78) $\times 10^5$ M^{-1} for the binding site size restricted to 3 base pairs. This binding constant is in agreement with the reported equilibrium constant of ($K_{binding}$) of ~ 2.2 $\times 10^5$ M^{-1}.[155]

We wanted to know if added co-solvent affects the affinity of **9** for FS-DNA, because co-solvent may be required in the double competition dialysis assay. Therefore, we did the same titration as above but in the presence of DMSO.

Binding of **9** to FS-DNA was studied using UV-visible spectroscopy. The changes in absorption of **9** upon addition of FS-DNA in buffer (25 mM MOPS, pH 7.0, 100 mM KCl, 9 vol-% DMSO and 1 mM EDTA), at 25 °C are shown in Figure 2.46.

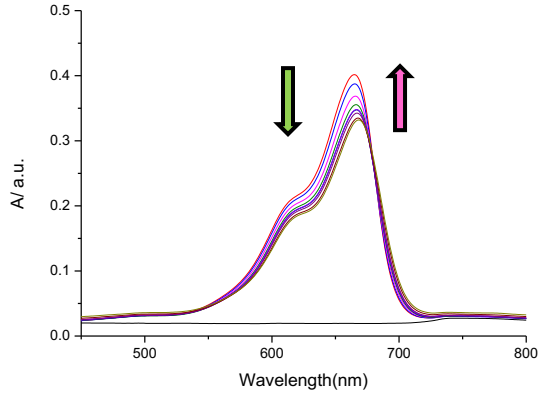

Figure 2.46 UV-visible spectra for a 0.004 mM solution of **9** upon addition of 0 – 0.19 mM FS-DNA in buffer (25 mM MOPS, pH 7.0, 100 mM KCl, 9 vol-% DMSO and 1 mM EDTA), at 25 °C.

Figure 2.46 shows a hypochromic shift and a bathochromic shift in absorbance (at the λ_{max} of 664 nm) of **9** upon addition of DNA. This change in UV-visible absorption suggests that the conformation or the surrounding medium of **9** changes upon the addition of DNA. To quantify the affinity of **9** for FS-DNA, the absorbance at 664 nm was plotted as a function of concentration of FS-DNA (Figure 2.47, Appendix, Table A9.1 for data in tabular format).

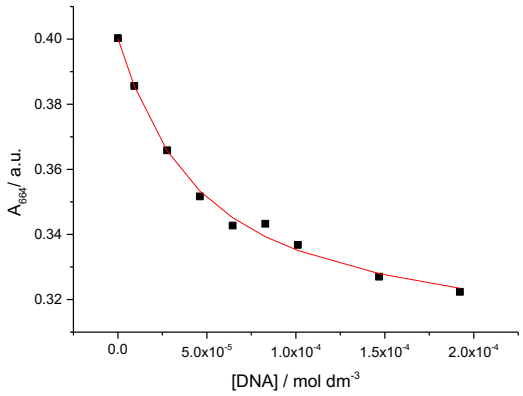

Figure 2.47 Absorbance at 664 nm of a solution of 0.004 mM **9** as a function of DNA concentration in buffer (25 mM MOPS, pH 7.0, 100 mM KCl, 9 vol-% DMSO and 1 mM EDTA), at 25 °C. The line represents the best fit of a multiple independent binding sites model to the data.

The titration data obtained for **9** were reproduced satisfactorily by the multiple independent binding sites model. This fit of the multiple independent binding sites model to the data gives a binding affinity ($K_{binding}$) of (8.5 ± 1.35) $\times 10^4$ M^{-1} for the binding site size restricted to 3 base pairs.

Based on the results from Figures 2.45 and 2.46, DMSO affects the interaction between **9** and DNA. The affinity is roughly five-fold weaker in the presence of DMSO then in the absence of DMSO.[179]

Compound **9** is known to have affinity for a range of quadruplex sequences as well. Binding of **9** to c-myc[180] was studied using UV-visible spectroscopy. The changes in absorption of **9** upon addition of c-myc were measured in a buffer solution (25 mM MOPS, pH 7.0, 50 mM NaCl, and 1 mM EDTA), at 25 °C (Figure 2.48).

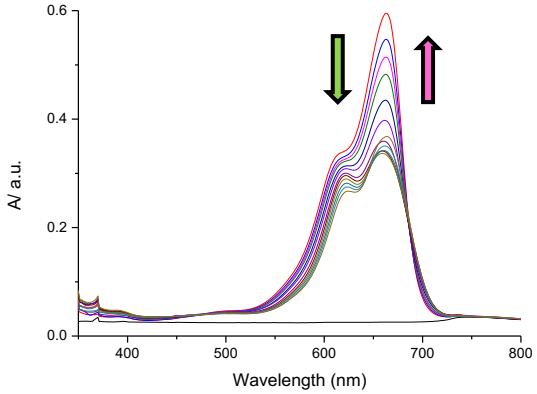

Figure 2.48 UV-visible spectra for a 0.007 mM solution of **9** upon addition of 0 – 0.006 mM c-myc in buffer (25 mM MOPS, pH 7.0, 50 mM NaCl, and 1 mM EDTA), at 25 °C.

Figure 2.48 shows a hypochromic shift in absorbance (at the λ_{max} of 663 nm) which is accompanied by a bathochromic shift of **9** upon addition of c-myc. This change in UV-visible absorption may occur as a result of conformational changes when **9** interacts with c-myc, but it may also be a result of a local medium effect. To quantify the affinity of **9** for c-myc, the absorbance at 663 nm was plotted as a function of concentration of c-myc (Figure 2.49, Appendix Table A9.2 for data in tabular format).

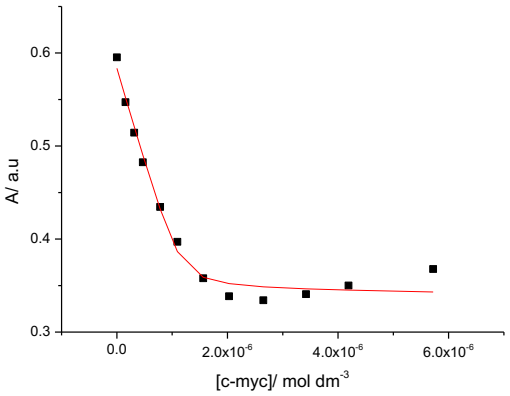

Figure 2.49 Absorbance at 663 nm for a solution of 0.0073 mM of **9** as a function of c-myc concentration in buffer (25 mM MOPS, pH 7.0, 50 mM NaCl, and 1 mM EDTA), at 25 °C. The line represents the best fit of a multiple independent binding sites model to the data.

The titration data obtained for **9** were analysed satisfactorily by fitting the multiple independent binding sites model to the data. This fit of the multiple independent binding sites model to the data gives a binding affinity ($K_{binding}$) of (5.25 ± 7.79) $\times 10^6$ M^{-1} for a binding site

size (n) of (0.17 ± 0.02), i.e 0.17 quadruplexes per ligand. This suggests that 6 ligands bind per quadruplex.

Binding of **9** to 22AG was studied using UV-visible spectroscopy. The changes in absorption of **9** upon addition of 22AG were measured in a buffer solution (25 mM MOPS, pH 7.0, 50 mM NaCl, and 1 mM EDTA), at 25 °C (Figure 2.50).

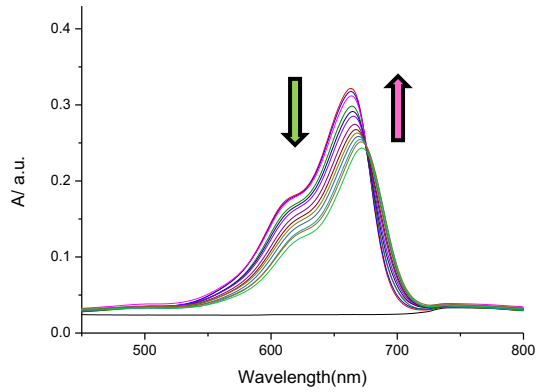

Figure 2.50 UV-visible spectra for a 0.0038 mM of a solution of **9** upon addition of 0 – 0.035 mM 22AG concentration in buffer (25 mM MOPS, pH 7.0, 50 mM NaCl, and 1 mM EDTA), at 25 °C.

Figure 2.50 shows a hypochromic and bathochromic shift of **9** upon addition of 22AG. This change in absorption suggests that the conformation of **9** or the surrounding medium of **9** has changed upon the addition of DNA. The change in absorption therefore indicates an interaction between **9** and 22AG. To quantify the affinity of **9** for 22AG, the absorbance at 663 nm was plotted as a function of concentration of 22AG (Figure 2.51, Appendix Table A9.3 for numerical data).

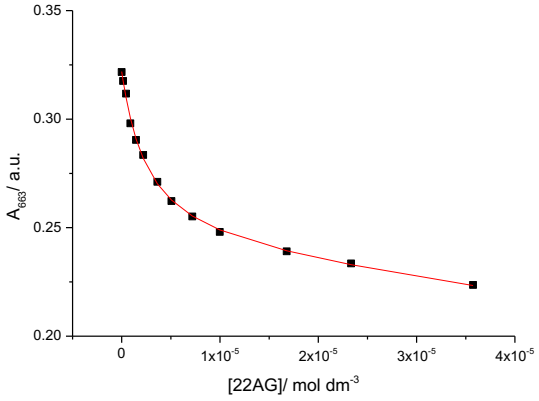

Figure 2.51 Absorbance at 663 nm for a solution of 0.0038 mM **9** as a function of 22AG concentration in buffer (25 mM MOPS, pH 7.0, 50 mM NaCl, and 1 mM EDTA), at 25 °C. The line represents the best fit of a multiple independent binding sites model to the data.

The titration data obtained for **9** were analysed by fitting the multiple independent binding sites model to the data. This fit of the multiple independent binding sites model to the data gives an equilibrium constant ($K_{binding}$) of (5.95 ± 7.64) $\times 10^4$ M^{-1} for a binding site size (n) of (0.13 ± 0.15). This suggests that 7 ligands bind per quadruplex.

EAD2 was recently identified as a good target for **9**.[181] Binding of **9** to EAD2 was studied using UV-visible spectroscopy. The changes in absorption of **9** upon addition of EAD2 were measured in a buffer solution (25 mM MOPS, pH 7.0, 100 mM KCl, and 1 mM EDTA), at 25°C (Figure 2.52).

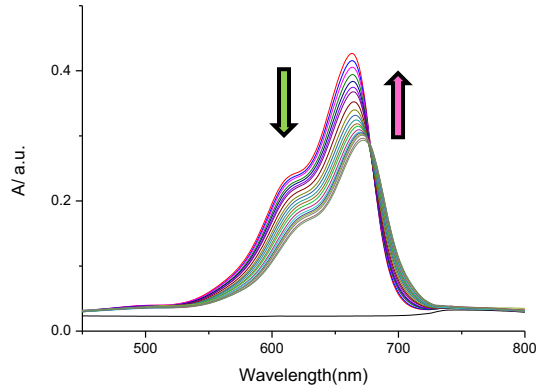

Figure 2.52 UV-visible spectra for a 0.0051 mM solution of **9** upon addition of 0 – 0.0069 mM EAD2 in buffer (25 mM MOPS, pH 7.0, 100 mM KCl, and 1 mM EDTA), at 25 °C.

Figure 2.52 shows a hypochromic and bathochromic shift of **9** upon addition of EAD2. This change in absorption suggests that the conformation of **9** or the surrounding medium of MB has changed upon the addition of DNA. To quantify the affinity of **9** for EAD2, the absorbance at 663 nm was plotted as a function of concentration of EAD2 (Figure, 2.53 Appendix Table A9.4 for data in tabular format).

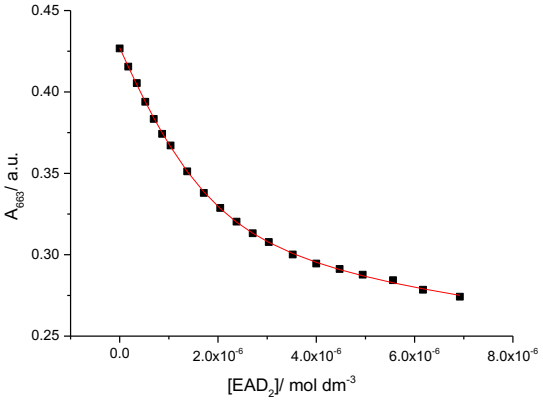

Figure 2.53 Absorbance at 663 nm for a solution of 0.0051 mM **9** as a function of EAD2 concentration in buffer (25 mM MOPS, pH 7.0, 100 mM KCl, and 1 mM EDTA), at 25 °C. The line represents the best fit of a multiple independent binding sites model to the data.

The titration data obtained for **9** were reproduced satisfactorily by the multiple independent binding sites model. This fit of the multiple independent binding sites model to the data gives a binding affinity ($K_{binding}$) of (5.86 ± 0.61) $\times 10^5$ M^{-1} for a binding site size (n) of (0.3 ± 0.01) which means 3 ligands bind per quadruplex. Previous studies have found a binding affinity (K_{binding}) of ~ 1.3 $\times 10^6$ M^{-1} for a binding site size (n) of 1.0, in reasonable agreement with our data.[155]

The binding parameters for compound **9** interacting with FS-DNA and quadruplex structures are summarised in Table 2.4.

Table 2.4 Binding parameters from UV-visible spectroscopy of 9 interacting with FS-DNA, c-myc 22AG and EAD2, in buffer.

	FS-DNA		c-myc		22AG		EAD2	
Compound	*Binding constant* K / M^{-1}	*Binding site size* N	*Binding constant* $10^6 K / M^{-1}$	*Binding site size* n	*Binding constant* K / M^{-1}	*Binding site size* n	*Binding constant* $10^6 K / M^{-1}$	*Binding site size* n
9 [(a)]	$(3.83 \pm 0.78) \times 10^5$	3*	/	/	/	/	/	/
9 [(b)]	$(8.5 \pm 1.35) \times 10^4$	3*	/	/	/	/	/	/
9 [(c)]	/	/	(5.25 ± 7.79)	(0.17 ± 0.02)	(5.95 ± 7.64) $\times 10^4$	(0.13 ± 0.15)	/	/
9 [(d)]	/	/	/	/	/	/	(0.586 ± 0.061)	(0. 3 ± 0.01)

(25 mM MOPS, pH 7.0, 50 mM NaCl, and 1 mM EDTA) in the presence of 1.04 % of acetonitrile [(a)], in buffer (25 mM MOPS, pH 7.0, 100 mM KCl, 9 vol-% DMSO and 1 mM EDTA) [(b)], in buffer (25 mM MOPS, pH 7.0, 50 mM NaCl, and 1 mM EDTA) [(c)] and in buffer (25 mM MOPS, pH 7.0, 100 mM KCl, and 1 mM EDTA), at 25 °C.

Table 2.4 shows that compound **9** has a higher affinity for c-myc than for 22AG and EAD2. The binding stoichiometry for **9** interacting with c-myc was found to be 6 ligands per quadruplex. We attribute this high affinity of **9** for quadruplex structures to the presence of more aromatic rings, which leads to an increase in hydrophobic interactions between **9** and DNA. The weakest binding for **9** is to duplex FS-DNA with a binding constant ~ 10^4. The affinity is roughly five-fold weaker in the presence of DMSO than in the absence of DMSO. DMSO thus affects the interaction between **9** and DNA. The binding site size for **9** to duplex FS-DNA is restricted to 3.0 base pairs in order to obtain a good fit to the titration curve.

2.2.10 Extinction coefficient and DNA binding of ethidium bromide

Two stock solutions of ethidium bromide **(10)**, both of 0.12 mM, were made up in buffer (25 mM MOPS, pH 7.0, 50 mM NaCl, and 1 mM EDTA) and two dilution series (0.014 mM, 0.018 mM, 0.022 mM and 0.025 mM and 0.004 mM, 0.016 mM, and 0.026 mM) were prepared. UV-visible spectra were recorded for these solutions in a 1.0 cm pathlength cuvette at 25 °C. Absorbances at the λ_{max} of 481 nm were plotted against ligand concentrations (Figure 2.54).

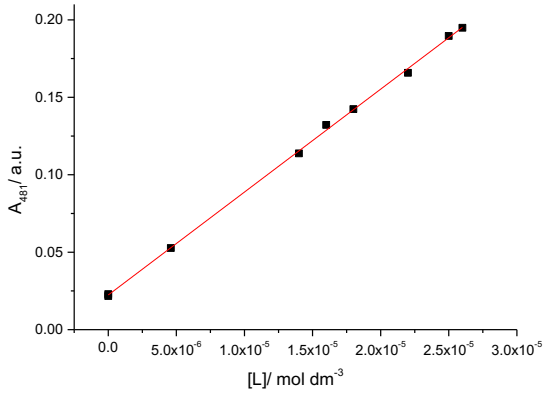

Figure 2.54 Absorbance at 481 nm as a function of concentration of **10** in buffer (25 mM MOPS, pH 7.0, 50 mM NaCl, and 1 mM EDTA), at 25 °C.

Figure 2.54 shows an increase in absorbance at 481 nm with increasing concentration of **10**. A linear fit (red line) was applied to obtain the extinction coefficient of (6645 ± 65.27) M^{-1} cm^{-1}. The error margin as a percentage of the extinction coefficient is 0.9 %, which is a small margin of error.

There have been several studies of the extinction coefficient for **10** in BPES buffer (6 mM Na_2HPO_4, 4 mM NaH_2PO_4, 1 mM Na_2EDTA, and 100 mM NaCl), at pH 7.00, and this was found to be 5680 M^{-1} cm^{-1} at 478 nm, and 5860 M^{-1} cm^{-1} at 480 nm in aqueous solution.[156] Our extinction coefficient is therefore remarkably higher for currently unknown reasons.

Compound **10** is well known to bind to duplex DNA.[182] We set out to determine whether **10** binds to quadruplex DNA such as c-myc in our buffer. Binding of **10** to c-myc was studied using UV-visible spectroscopy. The changes in absorption of **10** upon addition of c-myc were measured in a buffer (25 mM MOPS, pH 7.0, 100 mM KCl, and 1 mM EDTA), at 25 °C (Figure 2.55).

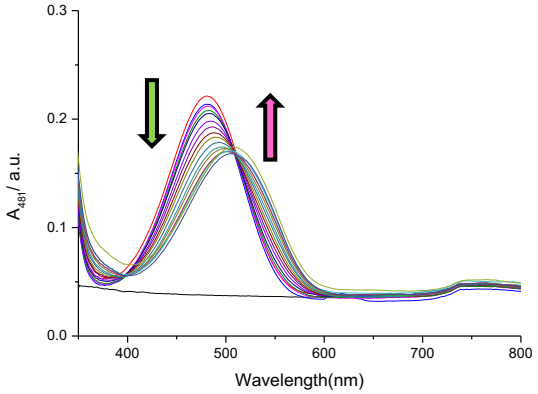

Figure 2.55 UV-visible spectra for a 0.027 mM solution of **10** upon addition of 0 – 0.023 mM c-myc concentration in buffer (25 mM MOPS, pH 7.0, 100 mM KCl, and 1 mM EDTA), at 25 °C.

Figure 2.55 shows a decrease in absorbance (at λ_{max} of 481 nm) and a bathochromic shift with an isosbestic point at 510 nm upon addition of c-myc.

To quantify the affinity of **10** for c-myc, the absorbance at 481 nm was plotted as a function of concentration of c-myc (Figure 2.56, Appendix Table A10 for numerical data).

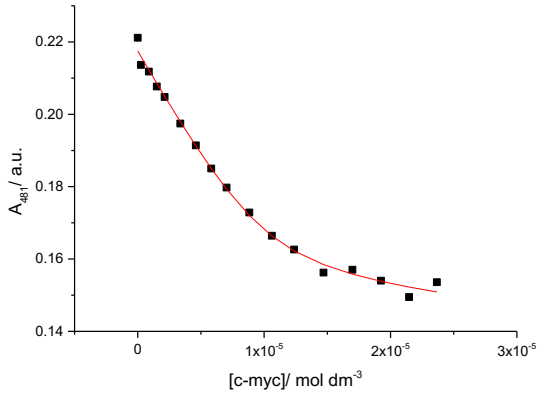

Figure 2.56 Absorbance at 481 nm of a solution of 0.027 mM **10** as a function of c-myc concentration in buffer (25 mM MOPS, pH 7.0, 100 mM KCl, and 1 mM EDTA), at 25 °C. The line represents the best fit of a multiple independent binding sites model to the data.

The data in Figure 2.56 were analysed in terms of a multiple independent binding sites model, given an equilibrium constant ($K_{binding}$) of (4.01 ± 2.60) $\times 10^5$ M^{-1} for a binding site size (n) of (0.37 ± 0.03) quadruplexes per ligand. This suggests that 3 ligands bind per

quadruplex. This binding constant is in agreement with the previously reported equilibrium constant of ($K_{binding}$) of 1.5 ×10^5 M^{-1} for a binding site size (n) of (1.0 ± 0.1).[157]

2.2.11 Extinction coefficient and DNA binding of DAPI

We made two stock solutions of DAPI **(11)** (3.5 mM) and used these to prepare two dilution series (0.012 mM, 0.025 mM, 0.037 mM, 0.05 mM and 0.006 mM, 0.012 mM, 0.019 mM, 0.025 mM). A third stock solution of **11** (1.3 mM) was used to prepare a third dilution series (0.007 mM, 0.014 mM, 0.02 mM, 0.028 mM). Finally, a fourth stock solution of **11** (2.3 mM) was used to create one further dilution series (0.016 mM, 0.024 mM, 0.03 mM, 0.041 mM). All solutions were prepared in buffer (25 mM MOPS, pH 7.0, 50 mM NaCl). UV-visible spectra were recorded for these solutions in a 1.0 cm path length cuvette at 25 °C. Absorbance at λ_{max} of 342 nm for all dilution series were plotted together against ligand concentrations (Figure 2.57).

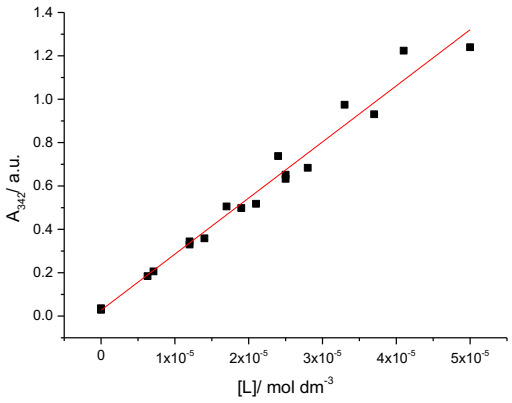

Figure 2.57 Absorbance as a function of concentration of **11** in buffer (25 mM MOPS, pH 7.0, 50 mM NaCl), at 25 °C.

Figure 2.57 shows an increase in absorbance at 342 nm with increasing concentration. A linear fit (red line) was applied to obtain the extinction coefficient of (23570 ± 786) M^{-1} cm^{-1}. The error margin as a percentage of the extinction coefficient is 3.3 %, which is acceptable. Previous studies have reported that the extinction coefficient of **11** in water is slightly higher at 27000 M^{-1} cm^{-1}, more or less in agreement with our extinction coefficient.[161]

DAPI is known to bind to duplex DNA.[183] The binding of **11** to 22AG was studied using UV-visible spectroscopy; the changes in absorption of **11** upon addition of 22AG were measured in a buffer solution (25 mM MOPS, pH 7.0, 50 mM NaCl, and 1 mM EDTA), at 25 °C (Figure 3.58).

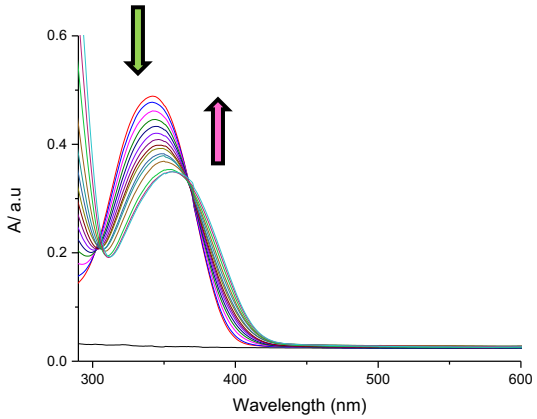

Figure 2.58 UV-visible spectra for a 0.019 mM solution of **11** upon addition of 0 – 0.007 mM 22AG in buffer (25 mM MOPS, pH 7.0, 50 mM NaCl, and 1 mM EDTA), at 25 °C.

Figure 2.58 shows a decrease in absorbance (at the λ_{max} of 342 nm) and a bathochromic shift with isosbestic point at 367 nm upon addition of 22AG to **11**. This change in UV-visible absorption suggests that **11** interacts with 22AG, and it may represent a local medium effect exerted by 22AG or a conformational change of **11** caused by the binding event. The affinity of **11** for 22AG was quantified by plotting the absorbance at 342 nm as a function of concentration of (22AG) (Figure 2.59, Appendix Table A11 for data in tabular format).

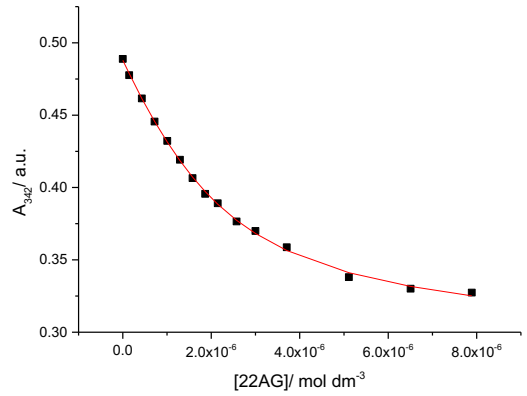

Figure 2.59 Absorbance at 342 nm for a solution of 0.019 mM **11** as a function of 22AG concentration in buffer (25 mM MOPS, pH 7.0, 50 mM NaCl, and 1 mM EDTA), at 25 °C. The line represents the best fit of a multiple independent binding sites model to the data.

The titration data obtained for **11** were reproduced satisfactorily by the multiple independent binding sites model. This fit of the multiple independent binding sites model to the data gives an equilibrium constant ($K_{binding}$) of (9.62 ± 2.88) $\times 10^4$ M^{-1} for a binding site size (n) of (0.09 ± 0.01). This suggests that 11 molecules of DAPI ligand bind per 22AG quadruplex. This corresponds to one molecule of DAPI for every two bases in the quadruplex structure. This ratio is remarkably like the ratio required for full charge cancellation, so the interaction may be purely electrostatic.

Binding of **11** to c-myc was also studied using UV-visible spectroscopy. The changes in absorption of **11** upon addition of c-myc were measured in a buffer (25 mM MOPS, pH 7.0, 100 mM KCl, and 1 mM EDTA), at 25 °C (Figure 2.60).

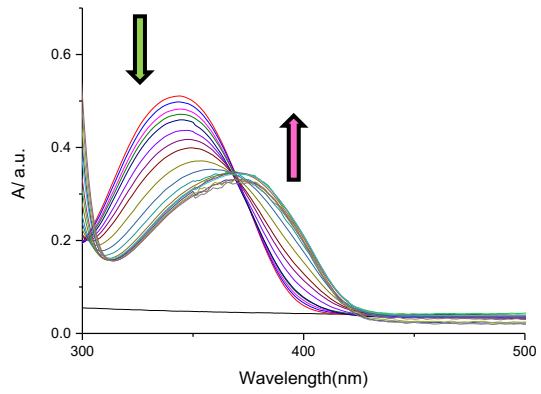

Figure 2.60 UV-visible spectra for a 0.019 mM solution of **11** upon addition of 0 – 0.025 mM c-myc concentration in buffer (25 mM MOPS, pH 7.0, 100 mM KCl, and 1 mM EDTA), at 25 °C.

Figure 2.60 shows hypochromic and bathochromic shifts in absorbance at the λ_{max} of 342 nm, leading to an isosbestic point at 370 nm, upon addition c-myc. This change in UV-visible absorption shows that **11** interacts with c-myc.

The affinity of **11** for c-myc was quantified by plotting the absorbance at 342 nm as a function of concentration of c-myc (Figure 2.61, Appendix Table A11.1 for numerical data).

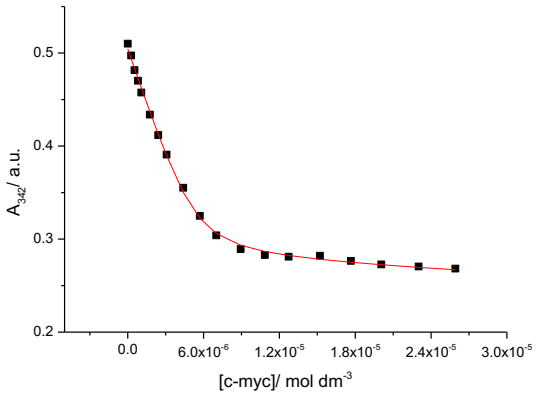

Figure 2.61 Absorbance at 342 nm of a solution of 0.019 mM **11** as a function of the concentration of c-myc in buffer (25 mM MOPS, pH 7.0, 100 mM KCl, and 1 mM EDTA), at 25 °C. The line represents the best fit of a multiple independent binding sites model to the data.

The titration data obtained for **11** were analysed in terms of the multiple independent binding sites model. This fit of the multiple independent binding sites model to the data gives a binding affinity ($K_{binding}$) of (7.4 ± 1.9) $\times 10^5$ M^{-1} for a binding site size (n) of (0.27 ± 0.012). This suggests that 4 ligands bind per quadruplex.

2.2.12 Extinction coefficient, stability and DNA binding of thiazole orange

Four stock solutions of thiazole orange **(12)** were made up in buffer (25 mM MOPS, pH 7.0, 50 mM NaCl, and 1 mM EDTA). The first stock solution of **12** was 0.62 mM and a dilution series of the first stock solution was prepared (0.0036 mM, 0.0073 mM, 0.010 mM and 0.014 mM). The second stock solution of **12** (0.67 mM) was used to prepare a second series of solutions (0.0053 mM, 0.0092 mM, 0.01 mM and 0.016 mM). The third stock solution of **12** (0.83 mM) was used to generate a third series (0.0098 mM, 0.013 mM, 0.016 mM and 0.019 mM). The final stock solution of **12** (0.69 mM) was used for a final series of solutions (0.0054 mM, 0.0095 mM, 0.013mM and 0.017 mM). UV-visible spectra were recorded for all solutions in a 1.0 cm path length cuvette at 25 °C. Absorbances at the λ_{max} of 500 nm for all solutions were plotted against ligand concentrations (Figure 2.62).

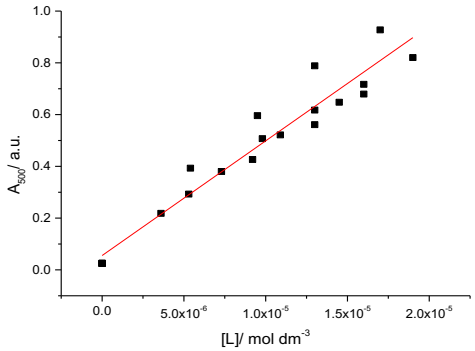

Figure 2.62 Absorbance at 500 nm as a function of concentration of **12** in buffer (25 mM MOPS, pH 7.0, 50 mM NaCl, and 1 mM EDTA), at 25 °C.

A linear fit (red line) was applied to the data in Figure 2.62 to obtain the extinction coefficient of (44309 ± 2642) M^{-1} cm^{-1}. This extinction coefficient is different from values reported in the literature. For example, in 20 mM Tris-HCl (pH 7.4), 140 mM NaCl, 5 mM KCl and 5 mM $MgCl_2$ the extinction coefficient for **12** has been reported to be 63000 M^{-1} cm^{-1} at 501 nm.[184] The extinction coefficient for **12** in methanol was found to be > 70000 M^{-1} cm^{-1}. [185]

Beased on the scatter in Figure 2.61 and the differences with reported extinction coefficients, we assumed that **12** is light sensitive.[184] To study the light sensitivity, we recorded the absorbance of **12** as a function of time exposed to ambient light in buffer (25 mM MOPS pH 7.0, 50 mM 50 mM NaCl and 1 mM EDTA) (Figure 2.63).

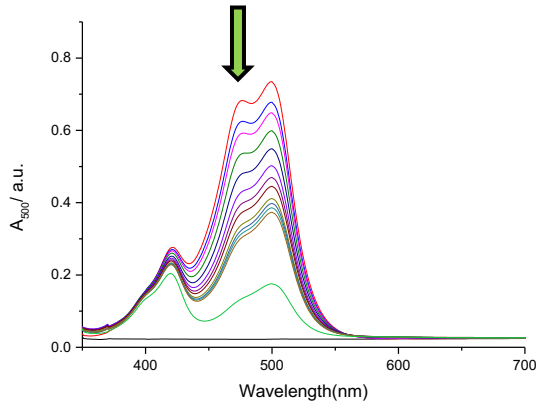

Figure 2.63 UV-visible spectra for **12** dissolved in buffer (25 mM MOPS pH 7.0, 50 mM NaCl and 1 mM EDTA) and exposed to ambient light.

Figure 2.63 shows a decrease in absorbance without an increase between 600 and 700 nm, which suggests that **12** does not precipitate but is sensitive to light.

To study the sensitivity to light further we repeated the experiment with **12** dissolved in two different buffers because we wanted to check whether the buffers affect fading or not.[141] We plot the absorbance of **12** as a function of time exposed to light in MOPS-based buffer (25 mM MOPS pH 7.0, 50 mM 50 mM NaCl and 1 mM EDTA) (Figure 2.62) and in phosphate-based buffer with no EDTA (see below, Figure 2.64).

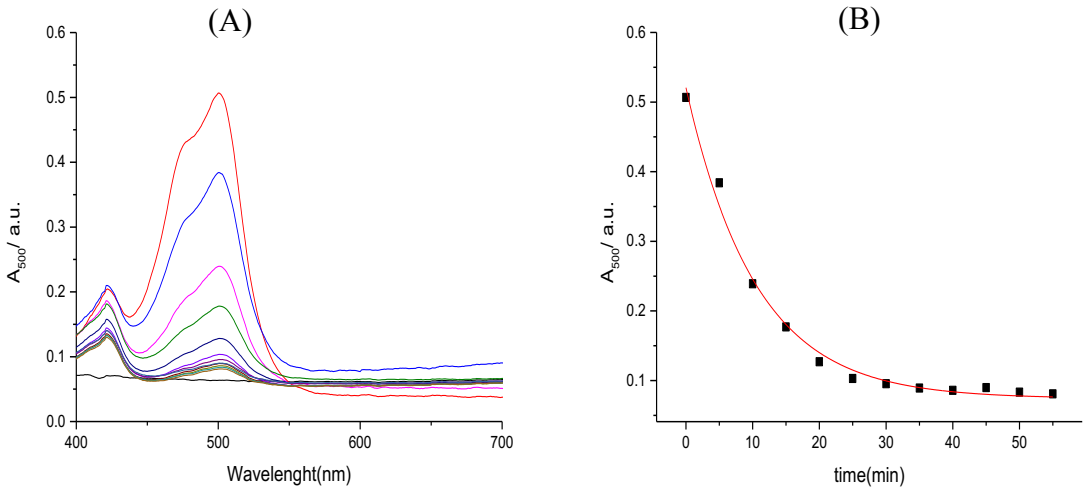

Figure 2.64 (A) UV-visible spectra for **12** dissolved in buffer (25 mM MOPS pH 7.0, 50 mM NaCl and 1 mM EDTA) exposed to light. (B) Absorbance for **12** as a function of time upon exposure to light.

The spectra in Figure 2.64 show a rapid decrease, in agreement with figure 2.62 **12** is sensitive to light.

A solution of **12** of the same concentration as above, but in phosphate buffer, was prepared. The absorbance of **12** as a function of time exposed to light in phosphate buffer (25 mM Na_2HPO_4, pH 7.0, and 50 mM NaCl) was recorded (Figure 2.65).

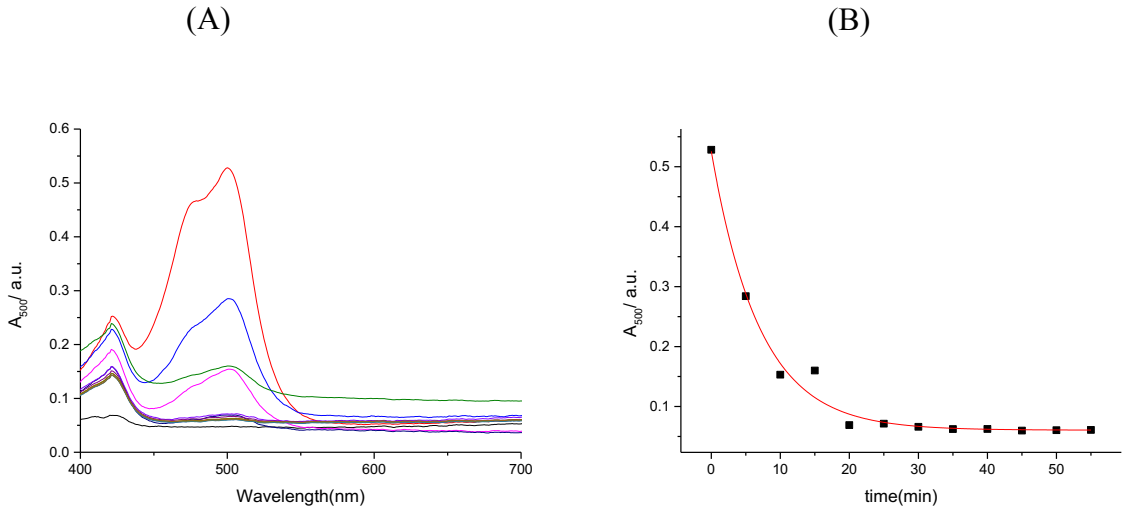

Figure 2.65 (A) UV-visible spectra for **12** dissolved in phosphate buffer (25 mM Na_2HPO_4, pH 7.0, and 50 mM NaCl), at 25 °C upon exposure to light (B) The absorbance of **12** at 500 nm plotted as a function of time.

Figure 2.65 (A) shows that the spectra display a rapid decrease upon exposure to light. This decrease suggests that **12** is sensitive to light in the absence of MOPS and EDTA as well.

We combined the two time traces to confirm that the buffer does not affect the fading of **12**. In other words, we checked whether phosphate buffer and MOPS and EDTA buffer influence the sensitivity of **12** (Figure 2.66).

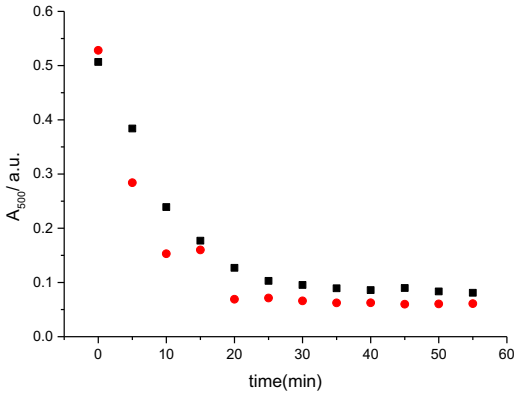

Figure 2.66 The absorbance of **12** at 500 nm in buffer (25 mM MOPS pH 7.0, 50 mM NaCl and 1 mM EDTA) (black squares) and in phosphate buffer (25 mM Na_2HPO_4, pH 7.0, and 50 mM 50), at 25 °C (red dots) as a function of time.

Figure 2.66 (A) shows that the decrease in absorbance in MOPS-based buffer and in phosphate-based buffer are very similar. This shows that the buffer does not affect the fading.

Visual inspection also clearly shows the effect of light on the colour of solutions of **12** as shown in Figure 2.67.

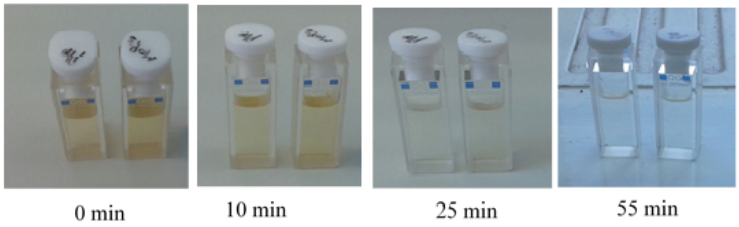

Figure 2.67 Solutions of **12**, as afunction of time exposed to ambient light.

From Figure 2.67 it is clear the colour of the solution fades in 55 min.

It has been reported in the literature that thiazole orange **(12)** has a higher affinity for quadruplex and triplex DNA compared with double-stranded DNA.[168] This study set out to confirm the affinity of **12** for different sequences of quadruplex DNA, namely c-myc and 22AG, in our buffer.

Binding of **12** to c-myc was studied using UV-visible spectroscopy. The changes in absorption of **12** upon addition of c-myc were measured in buffer (25 mM MOPS, pH 7.0, 50 mM NaCl, and 1 mM EDTA), at 25 °C (Figure 2.68).

(A) (B)

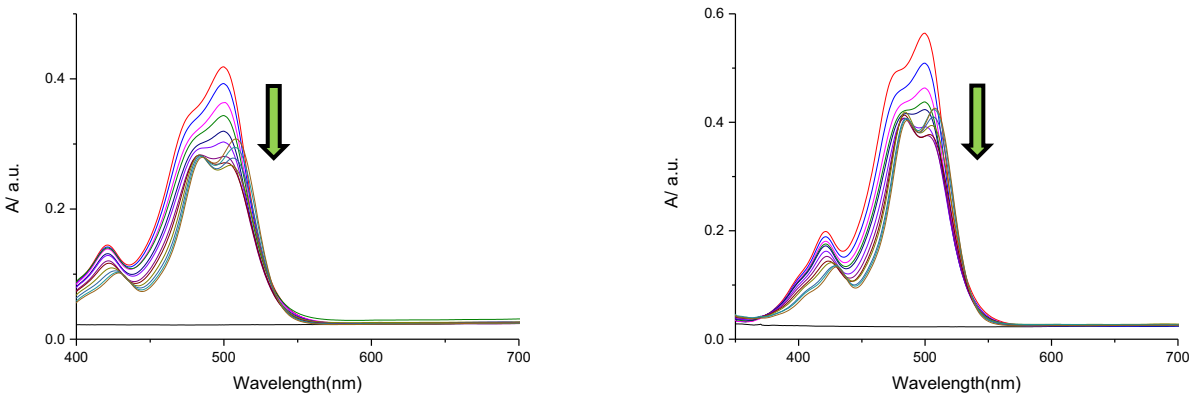

Figure 2.68 UV-visible spectra for (A) a 0.0061 mM solution of **12** upon addition of 0 – 0.0027 mM c-myc and (B) a 0.0083 mM solution of **12** upon addition of 0 – 0.0066 mM c-myc, in buffer (25 mM MOPS, pH 7.0, 50 mM NaCl, and 1 mM EDTA), at 25 °C.

Figure 2.68 shows a decrease in absorbance (at the λ_{max} of 500 nm) and a bathochromic shift upon addition c-myc. This change in UV-visible absorption shows that **12** interacts with c-myc.

To establish the affinity of **12** for c-myc, the absorbance at 500 nm was plotted as a function of concentration of c-myc (Figure 2.69, Appendix Tables A12& A12.1 for data in tabular format).

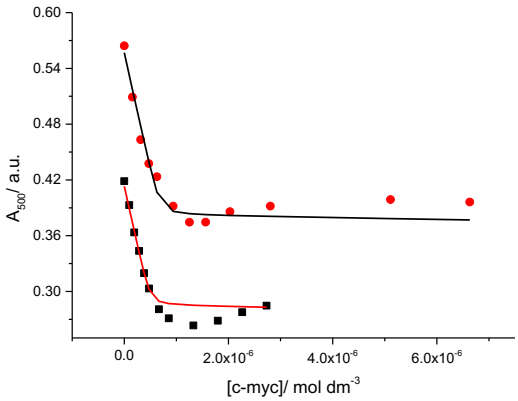

Figure 2.69 Absorbance at 500 nm for (●) a solution of 0.0061 mM of **12** and (■) a solution of 0.00083 mM, as a function of c-myc concentration in buffer (25 mM MOPS, pH 7.0, 50 mM NaCl, and 1 mM EDTA), at 25 °C. Solid lines represent a global fit of a multiple independent sites model to the titration data.

The titration data obtained for **12** were analysed by globally fitting the multiple independent binding sites model to the two titrations. The binding constant ($K_{binding}$) was found to be (1.19 ± 2.38) $\times 10^7$ M^{-1} for a binding site size (n) of (0.081 ± 0.008). This suggests that 12 molecules of ligand bind per quadruplex. However, considering the shape of the titration curves in Figure 2.66, these parameters are interpreted as apparent parameters. The reason for this is the dip in absorbance followed by a small gradual increase, suggesting multiple binding events.

Binding of **12** to 22AG was similarly studied using UV-visible spectroscopy. The absorption spectra for **12** upon addition of 22AG were recorded in buffer (25 mM MOPS, pH 7.0, 50 mM NaCl, and 1 mM EDTA) at 25 °C (Figure 2.70).

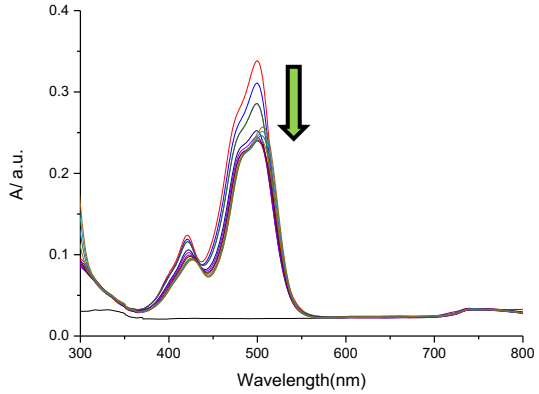

Figure 2.70 UV-visible spectra for a 0.0048 mM solution of **12** upon addition of 0 – 0.003 mM 22AG in buffer (25 mM MOPS, pH 7.0, 50 mM NaCl, and 1 mM EDTA), at 25 °C.

Figure 2.70 shows a decrease in absorbance at the λ_{max} of 500 nm of **12** upon addition of 22AG. This change in UV-visible absorption is likely a result of **12** interacting with 22AG.

The affinity of **12** for 22AG was quantified by plotting the absorbance at 500 nm as a function of concentration of 22AG (Figure 2.71, Appendix Table A12.2 for numerical data).

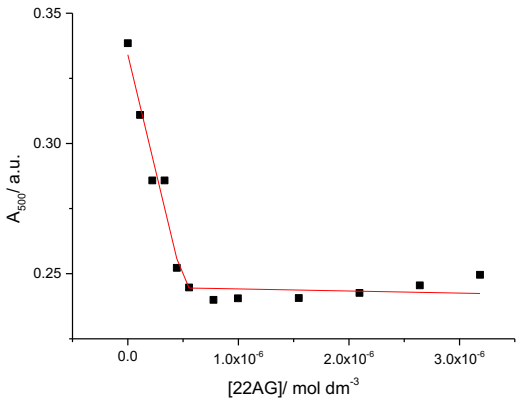

Figure 2.71 Absorbance at 500 nm (■) for a solution of 0.0048 mM **12** as a function of 22AG concentration, in buffer (25 mM MOPS, pH 7.0, 50 mM NaCl, and 1 mM EDTA), at 25 °C. The line represents the best fit of a multiple independent binding sites model to the data.

The titration data obtained for **12** were analysed by fitting the multiple independent binding sites mode to the data. The binding constant ($K_{binding}$) was found to be $2.29 \times 10^{18} \pm 3.63 \times 10^{29}$ M^{-1}. The value of the affinity constant should not be taken literally but indicates that the affinity is too high to accurately quantify from these data. The binding site size (n) was found to be (0.10 ± 0.009). This indicates that 10 ligands bind per quadruplex.

2.2.13 Extinction coefficient, stability and DNA binding of DODC

A stock solution of 0.16 mM **13** in buffer (25 mM MOPS, pH 7.0, 50 mM NaCl and 1 mM EDTA) was prepared. A series of solutions (0.0018 mM, 0.0025 mM, 0.0031 mM and 0.0037 mM) was prepared from the stock solution and UV-visible spectra were recorded for these solutions in a 1.0 cm path length cuvette at 25 °C. Absorbance at the λ_{max} of 576 nm were plotted against ligand concentrations (Figure 2.72).

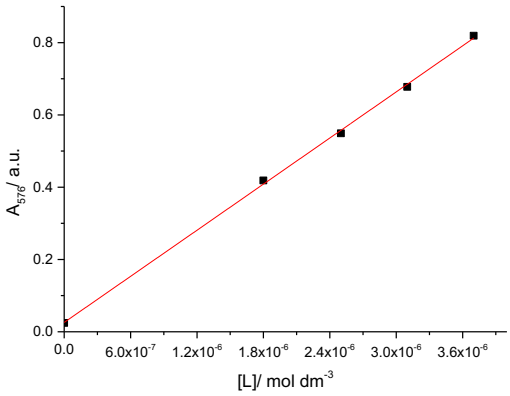

Figure 2.72 Absorbance as a function of concentration of **13** in buffer (25 mM MOPS, pH 7.0, 50 mM NaCl and 1 mM EDTA), at 25 °C.

Figure 2.72 shows an increase in absorbance at 576 nm with increasing concentration. A linear fit (red line) was applied to obtain the extinction coefficient of (212590 ± 3306) M^{-1} cm^{-1}. The error margin as a percentage of the extinction coefficient is 1.5 % which is an acceptable margin of error.

We set out to establish whether **13** is light sensitive. To study the light sensitivity of **13** we recorded the absorbance of **13** as a function of time exposed to light [186] in buffer (25 mM MOPS pH 7. 0, 50 mM 50 mM NaCl and 1 mM EDTA) (Figure 2.73).

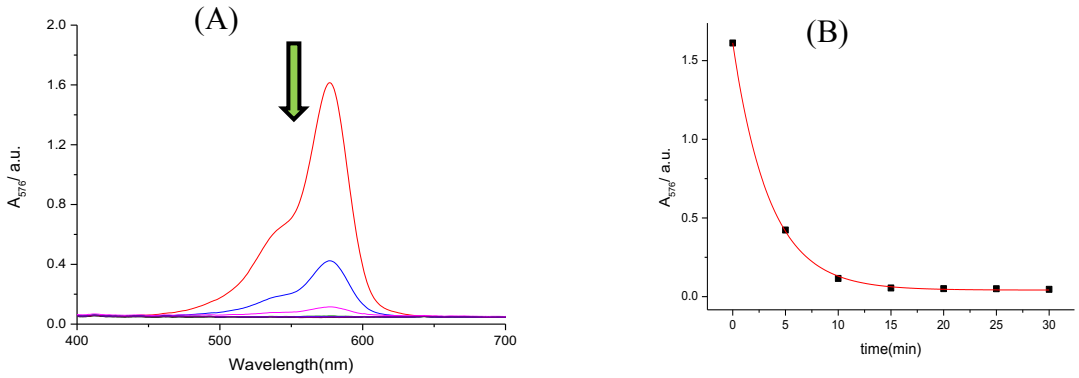

Figure 2.73 (A) UV-visible spectra for **13** dissolved in buffer (25 mM MOPS pH 7.0, 50 mM 50 mM NaCl and 1 mM EDTA) upon exposure to light. (B) The absorbance of **13** at 576 nm plotted as a function of time.

Figure 2.73 shows that when **13** is exposed to light, the UV-visible spectra show a decrease. This observation suggests that **13** is indeed sensitive to light.

In order to find out whether the fading of **13** is dependent on the buffer [187] we repeated the experiment using a phosphate buffer. We measured again the absorbance of **13** as a function of time exposed to light in phosphate buffer (25 mM Na_2HPO_4, pH 7.0, and 50 mM NaCl) (Figure 2.74).

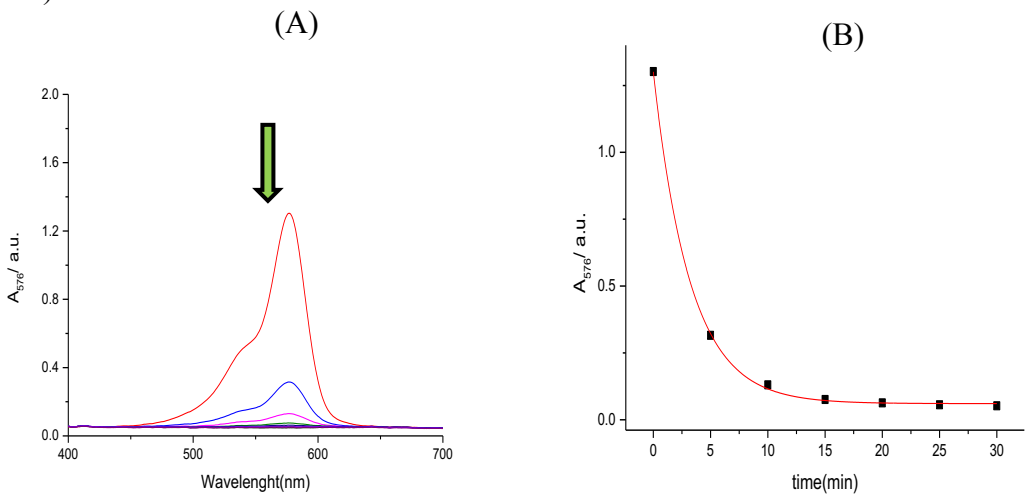

Figure 2.74 (A) UV-visible spectra for **13** in phosphate buffer (25 mM Na_2HPO_4, pH 7.0, and 50 mM NaCl) upon exposure to light. (B) The absorbance of **13** at 576 nm plotted as a function of time.

The spectra in Figure 2.74 show a decrease, which suggests that **13** is sensitive to light in a phosphate buffer as well. As before, this indicates that the amine functional group in MOPS and EDTA is not acting as an electron donor in the fading process.

The sensitivity of compounds to light may be affected by the presence of oxygen. To study the potential effect of oxygen on the fading, we carried out four experiments. The first experiment involves exposure of **13** to light and oxygen, the second experiment involves exposing **13** to light in the absence of oxygen, while the third experiment involves keeping **13** in the dark in the absence of oxygen. The fourth experiment involves **13** exposed to oxygen, but not to light.

For the first experiment, we recorded the absorbance of **13** as a function of time exposed to light and oxygen, in buffer (25 mM MOPS pH 7.0, 50 mM 50 mM NaCl and 1 mM EDTA) (Figure 2.75, see Appendix Table A13).

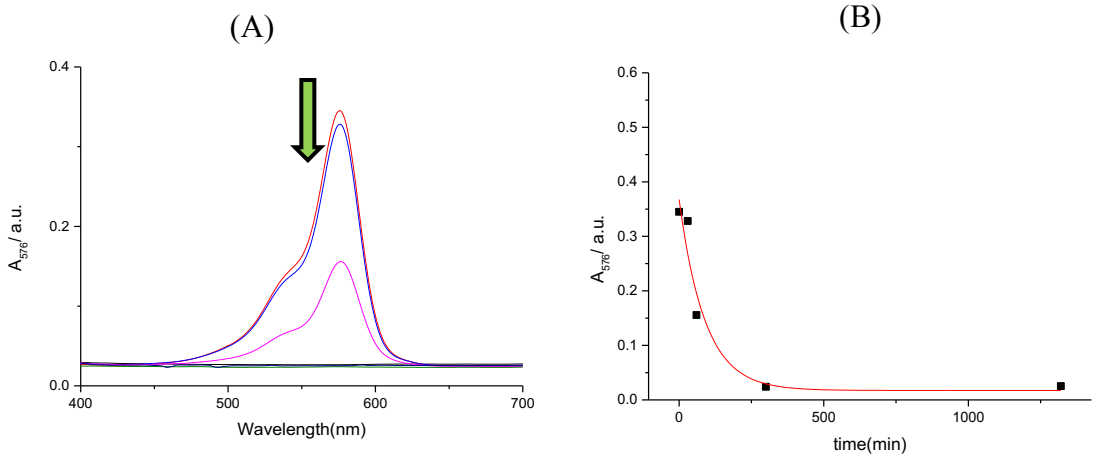

Figure 2.75 (A) UV-visible spectra for **13** in buffer (25 mM MOPS pH 7.0, 50 mM 50 mM NaCl and 1 mM EDTA) (B) The absorbance of **13** at 576 nm as a function of time.

Figure 2.75 shows that the absorbance decreases over time.

In the second experiment, the solution of **13** was degassed by using the freeze-pump-thaw method and placed under a nitrogen atmosphere. Therefore, we can see if the significant reduction in oxygen concentration causes any change to the fading.

We recorded the absorbance of **13** as a function of time exposed to light in the absence of oxygen in buffer (25 mM MOPS pH 7.0, 50 mM 50 mM NaCl and 1 mM EDTA) (Figure 2.76).

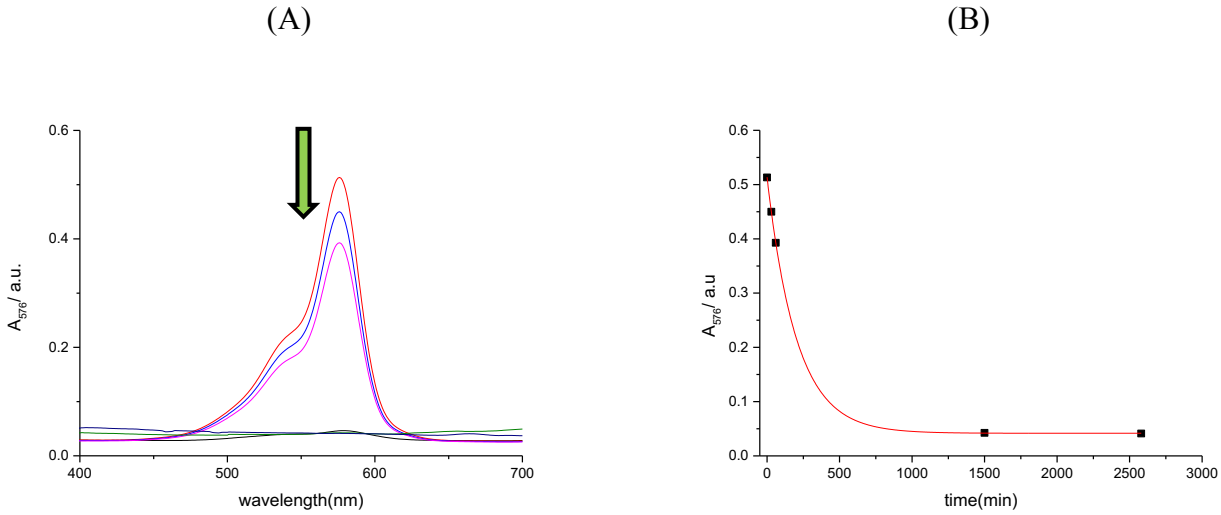

Figure 2.76 (A) UV-visible spectra for **13** in buffer (25 mM MOPS pH 7.0, 50 mM 50 mM NaCl and 1 mM EDTA) exposed to light in the absence of oxygen. (B) The absorbance of **13** at 576 nm plotted as a function of time.

Similar to Figure 2.75, Figure 2.76 shows a decrease in absorbance but now in the absence of oxygen. This observation suggests that the absence and presence of oxygen do not affect the fading kinetics of **13**.

The third experiment examined **13** in the absence of both light and oxygen. The absorbance spectra for **13** were again recorded as a function of time in buffer (25 mM MOPS pH 7.0, 50 mM 50 mM NaCl and 1 mM EDTA) (Figure 2.77).

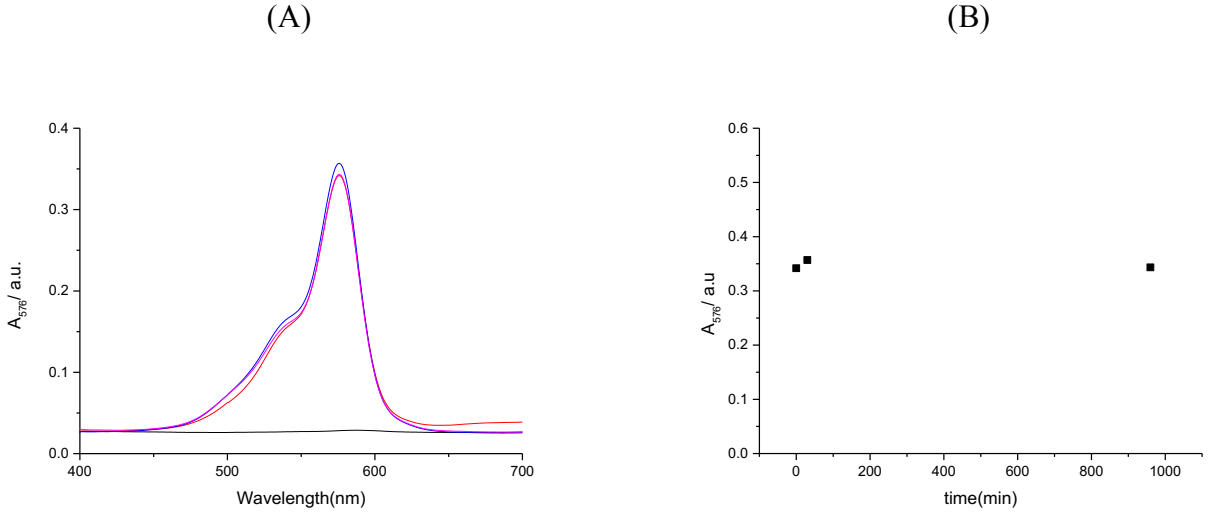

Figure 2.77 (A) UV-visible spectra for **13** in the absence of light and oxygen in buffer (25 mM MOPS pH 7.0, 50 mM 50 mM NaCl and 1 mM EDTA). (B) The absorbance of **13** at 576 nm plotted as a function of time.

The spectra in Figure 2.77 show no significant change in the absorbance of **13** in the absence of light and oxygen.

In the final experiment **13** was exposed to oxygen in the absence of light. As before, we recorded the absorbance of **13** as a function of time (Figure 2.78).

(A) (B)

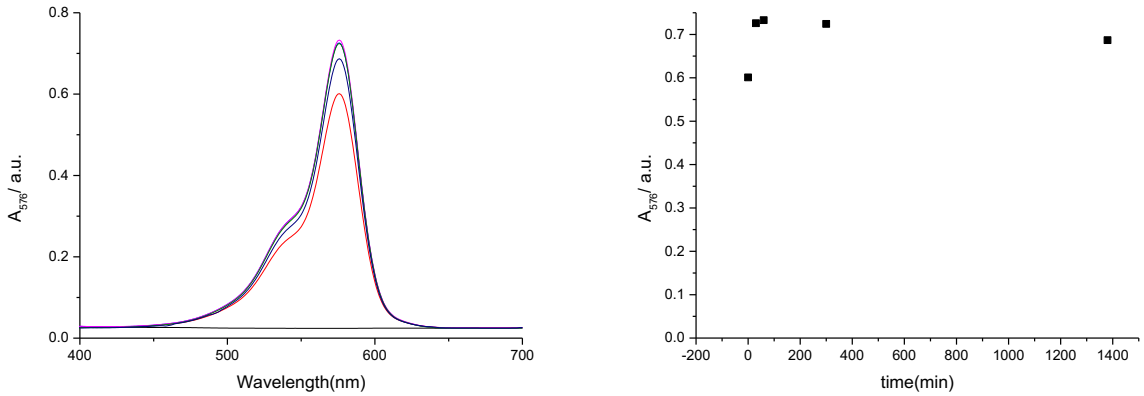

Figure 2.78 (A) UV-visible spectra for **13** in the absence of light and presence of oxygen in buffer (25 mM MOPS pH 7.0, 50 mM 50 mM NaCl and 1 mM EDTA). (B) The absorbance of **13** at 576 nm plotted as a function of time.

The spectra in Figure 2.78 show no significant change in the absorbance of **13** in the absence of light but in the presence of oxygen. Overall, these experiments suggest that fading of **13** is caused by light, but does not involve oxygen, at least not in the rate-determining step.

Visual inspection also clearly shows the effect of light on the colour of solutions of **13** as shown in Figure 2.79.

0 min 2 min 5 min 10 min 15 min 20 min 60 min

Figure 2.79 Solutions of **13**, as afunction of time rxposed to ambient light.

From Figure 2.79 it is clear the colour of the solution fades in 60 min.

2.2.14 Extinction coefficient of coralyne

Recent studies on the molar extinction coefficient for **14** in aqueous buffers (128 mM sodium cacodylate buffer pH 7) reported it to be 14500 M^{-1} cm^{-1} at 420 nm.[58, 59] Other research has shown the molar extinction coefficient for **14** in 30% ethanolic medium to be 17500 M^{-1} cm^{-1} at 424 nm.[188]

Because of the poor solubility of coralyne (**14**) in buffer (25 mM MOPS, pH 7.0, 100 mM KCl, and 1 mM EDTA). We filtered the coralyne solution to remove any particulate matter. However, the absorption was low (0.1a.u). This is why we was unable to record the UV-visible titration.[58, 59, 188]

2.2.15 Summary

The UV-visible titrations have shown that ligands **1-3** do not bind significantly with FS-DNA. However, ligands **4-9** show affinity for FS-DNA. The affinities of these compounds for FS-DNA are summarised in Table 2.5.

Table 2.5 Binding affinities and binding site sizes for binding of 1-9 to FS-DNA in buffer

Ligand	Binding constant K / M^{-1}	Binding site size n / bp
1	negligible	n.a.
2	negligible	n.a.
3	negligible	n.a.
4	$(4.93 \pm 0.94) \times 10^4$	3*
5	$(1.18 \pm 0.21) \times 10^4$	3*
6 [(a)]	$(8.5 \pm 4.5) \times 10^5$	0.9 ± 0.09
7	$(5.15 \pm 0.43) \times 10^3$	3*
8 [(a)]	$(9.79 \pm 1.44) \times 10^3$	3*
8 [(b)]	$(1.0 \pm 0.84) \times 10^5$	3*
9 [(a)]	$(3.83 \pm 0.78) \times 10^5$	3*
9 [(b)]	$(8.5 \pm 1.35) \times 10^4$	3*

(25 mM MOPS, pH 7.0, 50 mM NaCl, 1 mM EDTA) In the presence of 1.04 % of acetonitrile [(a)] and in DMSO-containing buffer (25 mM MOPS, pH 7.0, 100 mM KCl, 9 vol-% DMSO and 1 mM EDTA), [(b)] at 25 °C.

* restricted.

Ligands **1** - **3** are negatively charged and the lack of binding is because the negative charge leads to electrostatic repulsion between ligand and DNA. The interaction of **3** with FS-DNA does not result in an important induced circular dichroism signal, which suggests that **3** does not interact strongly with DNA.

At the same time, **4** and **5** have a high affinity (~ 10^4 M^{-1}) for DNA. When we explored the binding mode for **4** with FS-DNA, ICD suggests that **4** binds with FS-DNA through intercalation. [84] On the other hand, the high affinity of **9** for DNA is clear from it is binding constant of ~ 10^5 M^{-1}. We attribute the strong binding to the presence of a positive charge on **9**. Moreover, **9** is a planar aromatic compound. The planarity leads to increase in hydrophobic interactions between ligand and DNA, stabilising the interaction between **9** and DNA.[159]

Table 2.5 shows that organic co-solvents play an important role during the interaction process decreasing the affinity between the ligands and DNA. However, DMSO is a useful co-solvent to help avoid precipitation of ligands and of ligand-DNA complexes.[176]

It is obvious that **6** has a higher affinity for DNA with a binding constant of ~ 10^5 M^{-1} in DMSO-containing buffer (25 mM MOPS, pH 7.0, 50 mM NaCl, 1 mM EDTA) than in the presence of 1.04 % of acetonitrile at 25 °C.

The data in Tables 2.5 shows that binding is weaker in the presence of acetonitrile. DMSO can affect DNA structure and may also improve ligand solubility, thus decreasing binding affinity.[179] Interestingly, **8** in the presence of DMSO has a higher affinity (~ 10^5 M^{-1}) compared to the apparent affinity of **8** for DNA in presence of acetonitrile (~ 10^3 M^{-1}). This is because the poor solubility and precipitation of the complex formed between **8** and DMSO in the presence of acetonitrile.

All the binding site sizes for **1-9** were restricted to 3.0 base pairs in order to obtain a good fit to the titration curve with reasonable binding parameters. However, the binding site size for **6** was reanalysed at 1.0 base pair per binding site, in order to obtain reasonable binding parameters.

The interactions of **9-12** with specific quadruplex-forming sequences such as c-myc, 22AG and EAD2, were quantified using UV-visible spectroscopy titrations. The binding parameters for **9-12** compounds interacting with quadruplex structures are summarised in Table 2.6.

Table 2.6 Binding parameters from UV-visible spectroscopy of 9-12 to c-myc, 22AG, and EAD2.

	c-myc		22AG		EAD2	
Compound	*Binding constant* 10^6 *K / M*$^{-1}$	*Binding site size* *n*	*Binding constant* *K / M*$^{-1}$	*Binding site size* *n*	*Binding constant* 10^6 *K / M*$^{-1}$	*Binding site size* *N*
9 [a]	(5.25 ± 7.79)	(0.17 ± 0.02)	(5.95 ± 7.64) ×10^4	(0.13 ± 0.15)	/	/
9 [b]	/	/	/	/	(0.586 ± 0.061)	(0. 3 ± 0.01)
10[b]	(0.401 ± 0.260)	(0.37 ± 0.03)	/	/	/	/
11[a]	/	/	(9.62 ± 2.88) ×10^4	(0.09 ± 0.01)	/	/
11[b]	(0.74 ± 0.19)	(0.27 ± 0.012)	/	/	/	/
12	(11.9 ± 23.8)	(0.081 ± 0.008)	2.29 × 10^{18} ± 3.63 ×10^{29}	(0.10 ± 0.009)	/	/

in buffer (25 mM MOPS, pH 7.0, 50 mM NaCl, and 1 mM EDTA) [a] and in buffer (25 mM MOPS, pH 7.0, 100 mM KCl, and 1 mM EDTA) [b], at 25 °C.

In general, **9** has a high affinity for c-myc with a binding constant of ~ 10^6 M^{-1} which is stronger than $K_{binding}$ for EAD2 and 22AG. The binding stoichiometry for **9** with c-myc was found to be 6 ligands per quadruplex.

Several studies have revealed that **10** binds very strongly to duplex DNA.[125] The interaction between **10** and c-myc has a binding constant of ~ 10^5 M^{-1} and a stoichiometry of 3 ligands per quadruplex.

Compound **11** also binds more strongly to c-myc than to 22AG with a binding constant of ~ 10^5 M^{-1} and a stoichiometry which suggests that 4 ligands bind per quadruplex of c-myc. The

binding stoichiometry for 22AG was found to be 11 ligands per quadruplex. Interestingly, **12** has a very strong affinity for 22AG comparing to c-myc with a binding constant that is too high to quantify from the current data.

2.3 Conclusion

Compounds **1-7** and **9-13** are highly soluble in our aqueous buffers. Compound **8** is sparingly soluble in water, but it is soluble in some organic solvents such as acetonitrile and DMSO. To avoid the challenge of limited solubility, we determined the extinction coefficient of **8** in pure DMSO and pure acetonitrile but also in aqueous solutions containing DMSO and acetonitrile. The results show that the extinction coefficients for **8** in aqueous acetonitrile and aqueous DMSO are similar. Therefore, co-solvent does not affect the extinction coefficient of **8** much. Furthermore, all our compounds are stable except **8**, **9** **12** and **13**; these compounds are found to fade upon exposure to light.

Compounds **4-9** bind to duplex FS-DNA, with a high affinity of **9** for FS-DNA as quantified by a binding constant of ~ 10^5 M^{-1}. However, anionic compounds **1-3** show no significant binding to duplex FS-DNA. Moreover, compounds **6**, **8** and **9** bind to duplex FS-DNA in the presence of co-solvents such as DMSO and acetonitrile. All DNA binding site sizes for **1-9** are restricted to 3.0 base pairs in order to obtain a good fit to the titration curve corresponding to reasonable binding parameters. The binding site size for **6** was reanalysed at 1.0 base pair per binding site, in order to obtain reasonable binding parameters. Moreover, compounds **9-12** bind to specific quadruplex-forming sequences such as c-myc, 22AG and EAD2. Compound **9** has a higher affinity for c-myc than for 22AG and EAD2. The binding stoichiometry for **9** with c-myc was found to be 6 ligands per quadruplex. Compound **11** also binds more strongly to c-myc than to 22AG. The binding stoichiometry for **11** with c-myc was found to be 4 ligands bind per quadruplex. Compound **12** has a strong affinity for 22AG than for c-myc. Therefore, its binding to 22AG was not possible to determine.

2.4 Materials and Methods

2.4.1 Buffer preparation

All experiments were carried out in one of 4 buffers. Buffer A contained 25 mM MOPS, 50 mM NaCl and 1 mM EDTA, pH 7.0; buffer B contained 25 mM MOPS, 50 mM NaCl, 1 mM EDTA and 9 vol-% DMSO, pH 7.0; buffer C contained 25 mM MOPS, 100 mM KCl and 1 mM EDTA, pH 7.0; phosphate buffer D contained 25 mM Na_2HPO_4, pH 7.0, and 50 mM NaCl. The buffer components were purchased from Melford (CAS 1132-61-2), NaCl was purchased from Fisher Scientific (CAS 7647-14-5), KCl was purchased from Sigma Aldrich (CAS 7447-40-7), Na_2HPO_4 was purchased from Melford (CAS 7558-79-4), EDTA was purchased from VWR (CAS 60-00-4) and DMSO from Fisher Scientific (CAS 67-68-5). Buffers were titrated with aqueous NaOH or KOH to the required pH. The pH of aqueous solutions was determined using a Hanna microprocessor pH 113 pH-meter equipped with a VWR 662-1382 glass electrode. Materials were weighed out on a Fisherbrand 4-decimal balance. De-ionised water was produced using an ELGA water purifier for all solutions.

Buffer A, containing 25 mM MOPS (3-(N-morpholino) propanesulfonic acid), 50 mM sodium chloride (NaCl) and 1 mM EDTA was prepared by dissolving MOPS, sodium chloride (NaCl) and EDTA in distilled water and stirring at room temperature until the solid dissolved. A solution of sodium hydroxide (NaOH) was used for adjusting the pH to 7.0 and the buffer was made up to 2 liters in a volumetric flask.

Buffer B, containing 25 mM MOPS (3-(N-morpholino) propanesulfonic acid), 50 mM sodium chloride (NaCl) and 1 mM EDTA was prepared by dissolving MOPS, sodium chloride (NaCl) and EDTA in distilled water and stirring at room temperature until the solid dissolved. 9 vol-% of DMSO was add to the buffer solution. Sodium hydroxide (NaOH) was used for adjusting the pH to 7.0 and the buffer was made up to 2 liters in a volumetric flask.

Buffer C, containing 25 mM MOPS (3-(N-morpholino) propanesulfonic acid), 100 mM potassium chloride (KCl) and 1 mM EDTA was prepared by dissolving MOPS, potassium chloride (KCl) and EDTA in distilled water and stirring at room temperature until the solid dissolved. Potassium hydroxide (KOH) was used for adjusting the pH to 7.0 and the buffer was made up to 2 liters in a volumetric flask.

Phosphate buffer D contained 25 mM Na_2HPO_4 (sodium phosphate) and 50 mM NaCl, and was prepared by dissolving Na_2HPO_4 and NaCl in distilled water and stirring at room

temperature until the solid dissolved. Sodium hydroxide (NaOH) solution was used for adjusting the pH to 7.0 and the buffer was made up to 2 liters.

2.4.2 DNA preparation

Fish sperm DNA was purchased from Acros Organics (CAS 68938-01-2). The stock solution of fish sperm DNA was prepared by dissolving approximately 0.1217grams DNA in 10 ml of buffer and sonicating the solution of FS-DNA for about 10 minutes. All DNA solutions were dialysed against buffer. The dialysis process for the DNA solution was carried out by taking the DNA solution and placing it into the dialysis tube of sufficient pore size (3.5 kDa MWCO).[189] The dialysis tube was suspended for 24 hours inside a beaker that contains the MOPS buffer to allow impurities to diffuse out. The DNA concentrations were determined using the extinction coefficient for FS-DNA of 12800 M^{-1} cm^{-1} (bp) at 260 nm.[190]

The concentration of c-myc (dTdGdA dGdGdG dTdGdG dGdTdT dGdGdG dTdGdG dGdTdAdA) was determined using UV-visible spectroscopy using the extinction coefficient of 228700 M^{-1} cm^{-1} at 260 nm.[76] The concentration of 22AG (dAdGdG dGdTdT dAdGdG dGdTdT dAdGdG dGdTdT dAdGdGdG) was determined using UV-visible spectroscopy using the extinction coefficient of 228500 M^{-1} cm^{-1} at 260 nm.[76]

For double-stranded synthetic DNA, i.e poly (dAdT) and poly (dGdC), we dissolve each sequence in 1 ml of buffer. Then, the dialysis process for the DNA solution was carried out by taking the DNA solution and placing it into the dialysis tube of sufficient pore size (3.5 kDa MWCO). The dialysis tube was suspended for 24 hours inside a beaker that contains the MOPS buffer until the impurities were completely diffused out. The DNA concentration was determined using UV-visible spectroscopy using the extension coefficient of 14800 M^{-1} cm^{-1} at 254 nm for poly (dGdC) and of 12000 M^{-1} cm^{-1} at 260 nm for poly (dAdT).[127] Then, the DNA solutions were annealed by placing each DNA solution into an Eppendorf and placing the Eppendorf in a beaker that contains a water at 95 °C, allowing to cool down and finally determine the concentration of each solution.

For single-stranded DNA such as poly (dA) and poly (dT), we dissolve each sequence in 1 ml of buffer in (25 mM MOPS, 50 mM NaCl and 1 mM EDTA, pH 7.0, at 25 °C). The dialysis process for the DNA solution was carried out by taking the DNA solution and placing it into the dialysis tube of sufficient pore size (3.5 kDa MWCO). The dialysis tube was suspended for 24 hours inside a beaker that contains the MOPS buffer until the impurities were completely diffused out. The DNA concentration was determined using UV-visible

spectroscopy and the extinction coefficient of 8600 M^{-1} cm^{-1} at 257 nm for single-strand purine poly (dA) and 8520 M^{-1} cm^{-1} at 264 nm for single-stranded primidine poly (dT). We then mixed both sequences to have a 1:1 mixture of strands in an Eppendorf. The duplex was annealed by placing the Eppendorf in a beaker that contains water at 95 °C and allowing to cool to room temperature.[124] Finally, the concentration of each solution was determined using UV-visible spectroscopy using the extinction coefficient of 12000 M^{-1} cm^{-1} at 260 nm for poly (dA)-poly (dT). [127]

2.4.3 Dialysis units

The dialysis tubing was purchased from (Medicell Membranes Ltd, MWCO 12-14000 and 3500 Daltons).

2.5 Equipment

2.5.1 Spectroscopic studies

UV-visible spectra were recorded using a Jasco V-630BIO spectrophotometer with a Peltier temperature controller at 25 °C. All UV-visible titrations were carried out in a 1.0 cm path length cuvette starting with the volume of the buffer (2000-2500 µl). After that an aliquot from the ligand solution was added and the absorbance was measured. UV-visible titrations were carried out by adding the stock solution of DNA into the 1.0 cm cuvette which contains the ligand solution. UV-visible spectra in the range 200 - 600 nm were recorded after each addition of DNA. The absorption of the ligand was kept in the range of 0.1-0.8 a.u. The absorptions at selected wavelength were plotted against DNA concentrations. The multiple independent binding sites model was used to analyse the data of UV-visible spectra using Origin 9. Circular dichroism spectra CD were recorded using a Chirascan CD spectrometer. [84]

2.5.2 Isothermal titration calorimetry

ITC experiments were conducted using a Microcal VP-ITC microcalorimeter at 25 °C. Concentrations for **7** were determined using UV-visible spectroscopy based on the extinction coefficient of **7** of 33000 M^{-1} cm^{-1} at 332 nm[173] in 25 mM MOPS, 50 mM NaCl, 1 mM EDTA, and pH 7.0 at 25 °C.

First of all we cleaned both cells and the syringe with ethanol and after that with distilled water.[89] The sample cell was filled with a FS-DNA solution (approximately 1.9 ml) and the

syringe was filled with the ligand solution (approximately 300 µl). The concentration of the ligand solution is higher than the DNA solution (usually 12-fold higher than DNA solution). The ligand solution was added in 1 injection of 5 µl and 19 injections of 15 µl each to the sample cell and injecting every 300 second automatically with a stirring speed of 307 rpm. Origin (Microcal, Inc) was used to calculate the heat effects per injection (dh). We analysed integrated heat effects using our ITC data analysis software IC-ITC.

Chapter 3

Development and validation of a custom device for competition dialysis assays

Abstract

This chapter describes the development of a custom competition dialysis device. We test the use of this device to determine affinity and selectivity of ligands for nucleic acids structures. We studied the affinity and selectivity of single ligands for FS-DNA, specific duplex sequences $(dA)_{24} \bullet (dT)_{24}$ *and* $(dG)_{24} \bullet (dC)_{24}$*, and different quadruplex structures such as, c-myc, 22AG and EAD2. We compare the results with the results from UV-vis titrations (as shown in Chapter 2) and conclude that both results are in agreement.*

Part A

3.1 Introduction

3.1.1 Competition dialysis

Ligands that bind to nucleic acids, having structural or sequence selectivity, can be identified using a powerful tool called "competition dialysis".[125] This process is used as a test for affinity and selectivity of ligands for nucleic acids and comprises of the dialysis of a ligand against an array of nucleic acids with different structures or sequences.[124] In this method, separate nucleic acid structures are exposed to a solution of a potential nucleci acid binder through a dialysis membrane. As dialysis progresses, equilibration of the system is achieved with the binder accumulating where its highest affinity target is. Absorbance or fluorescence measurements are then used to determine the amount of ligand bound to each structure. The competition dialysis process is amenable to the study of soluble and stable ligands.

In the traditional setup, dialysis tubing is filled with samples of different nucleic acids. The dialysis tubing is placed in a beaker with a ligand solution, allowing enough time for the diffusion of the ligand across the dialysis tubing to take place (Figure 3.2).

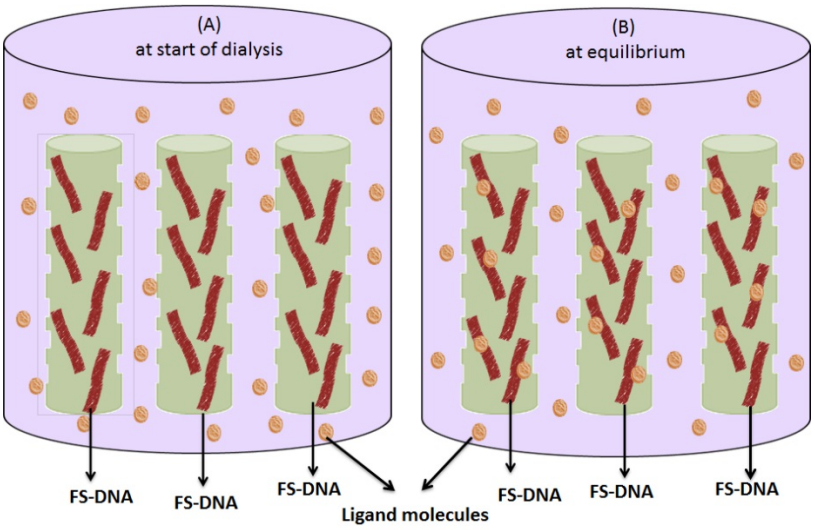

Figure 3.2 Schematic illustration of the dialysis process involving three different concentrations of FS-DNA, and a ligand (orange dots).

The uniformly sized pores of the dialysis tubing (e.g. 3.5 kDa MWCO) allow the ligand molecules to diffuse in and out of the multiple dialysis tubing to achieve the equilibrium concentration, while the large nucleic acids are retained within the dialysis tubing.[124] The

equilibrium concentrations are defined by the affinity between the FS-DNA and the ligand (Equation 1).

$$K = [\text{ligand}]_{\text{bound}} / ([\text{ligand}]_{\text{free}} \times [\text{binding sites}]_{\text{free}}) \qquad \text{Equation 1}$$

It has been previously reported by Brad Chaires[127] that the first generation of the competition dialysis enabled the determination of the selectivity and affinity for 13 different samples of the nucleic acid structure as shown in Scheme 3.1. In this study, MMQ1, a dibenzophenthroline, adriamycin, an anthracycline antibiotic and DODC, a cyanine dye were chosen and their selectivities studied (Scheme 3.1).

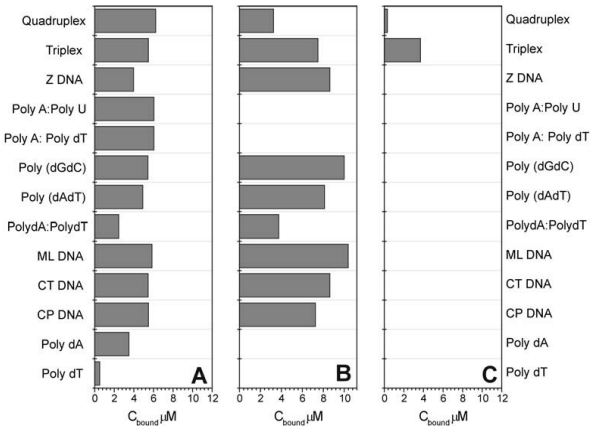

Scheme 3.1. First generation of the competition dialysis results for the amount of bound for each of the 13 different structure of DNA. A) MMQ1, a dibenzophenthroline. B) Adriamycin, an anthracycline antibiotic and c) DODC, a cyanine dye.

The data show that MMQ1 has different selectivity for different structures of DNA. Adriamycin has a selectivity for triplex and quadruplex DNA structure, while DODC has a higher affinity toward triplex DNA rather than toward any other structures.

The second generation of the competition dialysis method enabled evaluation of 14 to 19 nucleic acid samples. Both methods of the competition dialysis utilized 200 ml of 1 uM ligand solution and 0.5 mL of 75 uM of the nucleic acid structures placed in the dialysis units.

A quantitative analysis was applied to the competition dialysis data (Scheme 3.2).

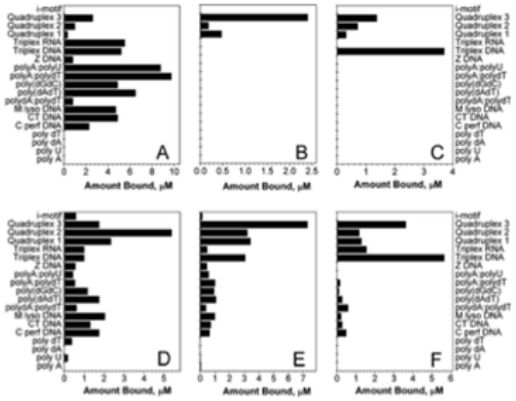

Scheme 3.2. The second generation of the competition dialysis assay for different ligands such as A) Ethidium bromide has selectivity for the DNA:RNA hybrid polyrAdT and for the RNA sequence polyrArU. B) NMM has selectivity for quadruplex structures especially on (50G10T4G10) 4. C) DODC has a high selectivity for the triplex DNA polydAdT-dT. D) PIPER is selective for the human telomere. E) Methylene blue is also selective for the telomere. F) Berberine has a selectivity for the triplex DNA polydAdT-dT and also for quadruplex (50G10T4G10)4, Quadruplex 1, (50T2G20T2)4, Quadruplex 2, human telomere.

The third generation of competition dialysis utilises a 96-well format in Sceme 3.3. The volume for each well is around 150-200 uL of 75 um samples of the nucleic acid structure, 250 mL was the volume of the ligand solution. Examples of data analysis conducted in this experiment include competition dialysis assay involving extensive ranges of DNA sequences and structures (Scheme 3.4).

Scheme 3.3. The competition dialysis assay.[124]

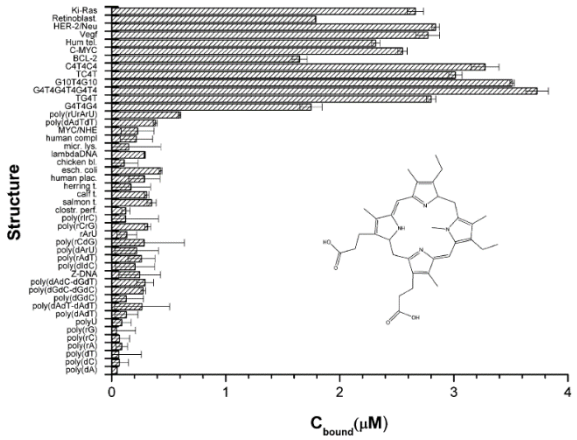

Scheme 3.4. The third generation of competition dialysis result for NMM. NMM is found to be selective for the G-quadruplex (50G4T4)3, however NMM has similar affinities for the quadruplex (50G10T4G10) and i-motif quadruplex (50C4T4C4).[124]

To improve the wetting property of the solution, surfactants were added. Surfactants lower the surface tension while improving the wetting and ultimately binding characteristics. The ligand solution was added at the end as a surfactant solution to the dialysate solution to introduce lower surface tension between the dialysate solutions and to act as an emulsifier in the nucleic acid. Hence, the presence of a surfactant results in free flow of the molecules across the dialysis unit.

Scheme 3.5 shows all three generations of the competition dialysis assay for the ethidium bromide with 13, 19 and 46 nucleic acids structures.

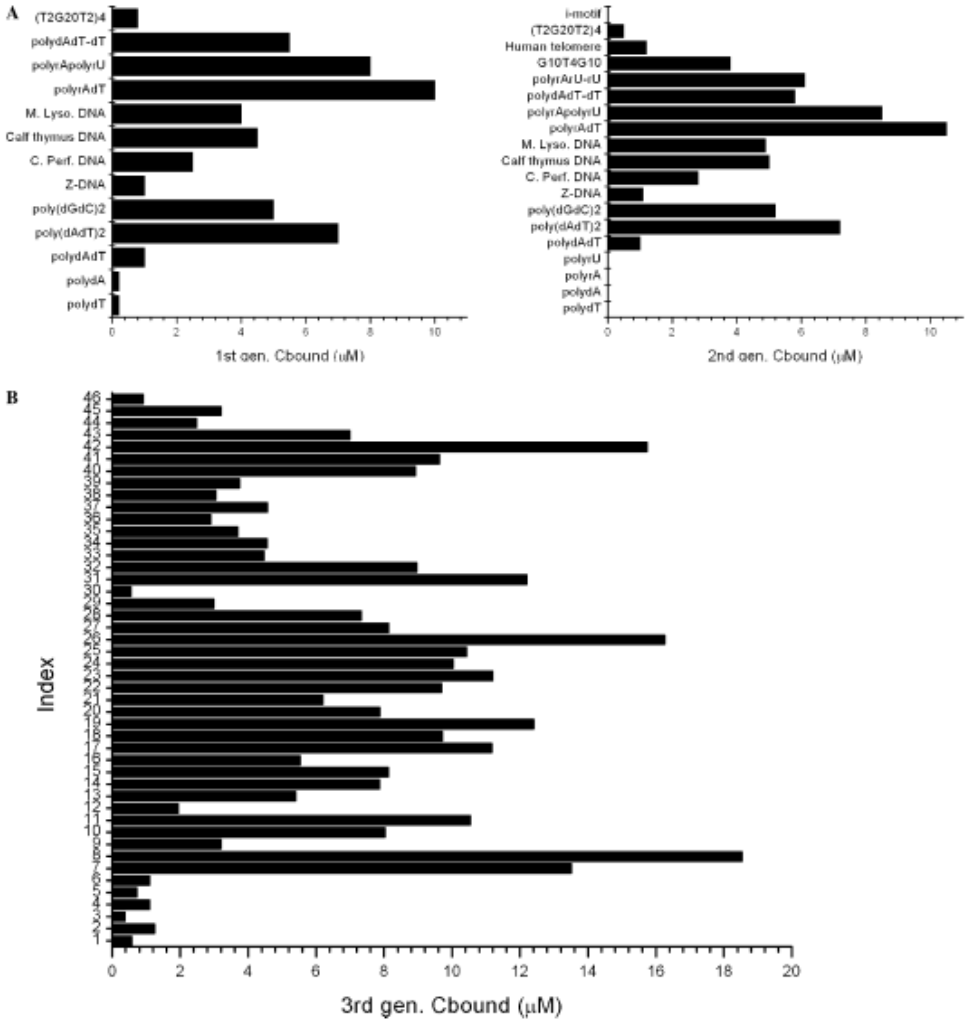

Scheme 3.5. Development of the competition dialysis results for ethidium bromide. A) The first and second generation assays for ethidium bromide with 13 and 19 nucleic acid structures. Ethidium bromide appears to be selective for duplex RNA and DNA–RNA hybrid, poly (rAdT), and binding strongly to duplex and triplex DNA. B) The third generation assay involves 46 structures and ethidium bromide prefers the quadruplex VEGF, also to DNA and RNA triplexes, DNA–RNA hybrid forms and finally to duplex DNA with alternating purine-pyrimidine sequences.[125]

A further quantitative analysis was performed for DAPI, this includes the first and third generations of the competition dialysis assay (Scheme 3.6).

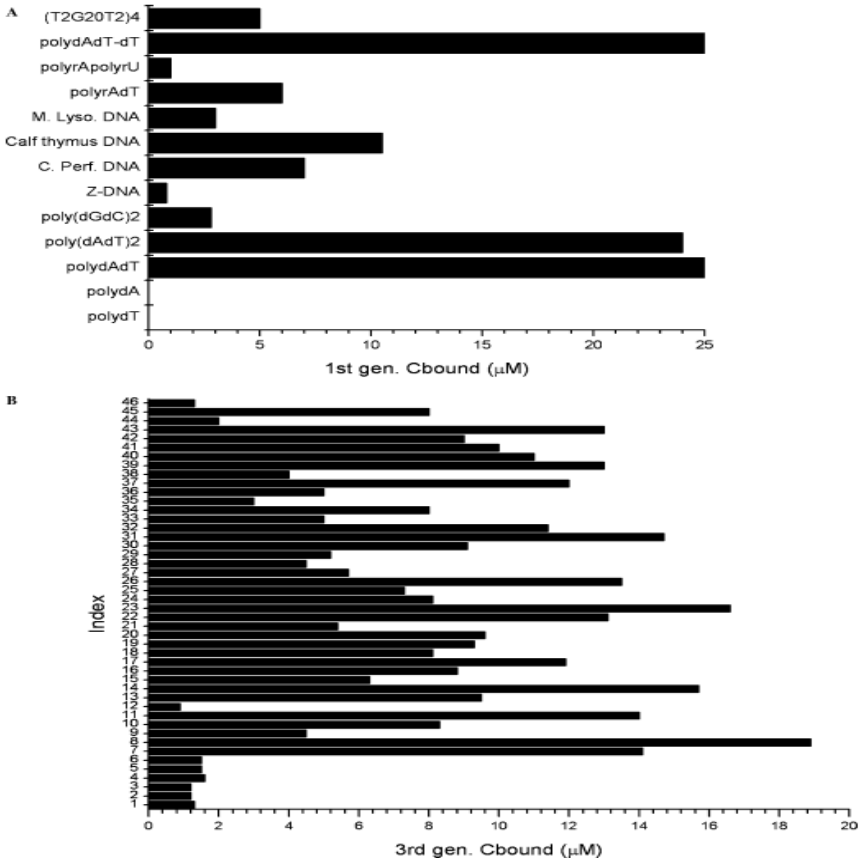

Scheme 3.6. Development of the competition dialysis results for DAPI. A) The first generation assay which representing DAPI bound to ATrich duplex DNA, also DAPI has a moderate binding to the DNA–RNA hybrid poly(rA)–poly(dT) and the quadruplex (T2G20T2)4. B) The third generation assay confirmed that DAPI is still preference to AT-rich duplex DNA.[125]

Selectivity graphs were plotted using difference plots in order to obtain a set of bindings of test compounds that fits the structure of the DNA and to offer a selection of compounds that have the most preferred target (Scheme 3.7).

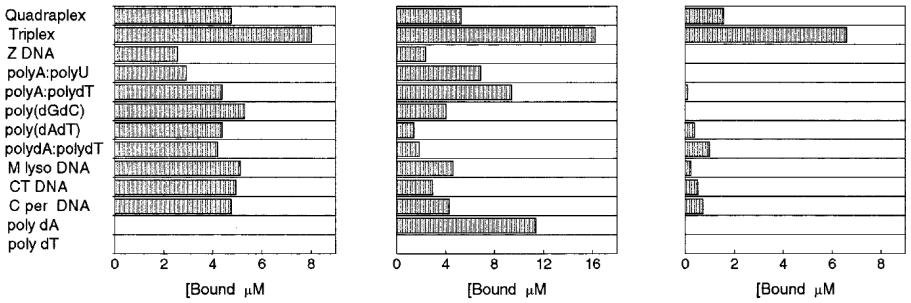

Scheme 3.7. The competition dialysis results for the selectivity of BePI (left), coralyne (middle), and berberine (right) for different nucleic acid structures.[126]

Scheme 3.7 shows difference plots to discover the selectivity of three compounds for triplex DNA structures. The graph on the right is for berberine and shows weaker biding to triplex DNA compared with coralyne to triplex DNA. Utilizing difference plots is effective in selective compounds having a particular affinity and aimed at a specific target.

Typically, (UV)-visible spectroscopy, circular dichroism spectroscopy and thermal denaturation studies are being used to control all the experiments to determine the concentrations and the extinction coefficient of the DNA/ ligand samples.

3.1.2 An overview of selected nucleic acid binders with structural selectivity

Table 3.1 shows the properties of ligands chosen for this study and their nucleic acid targets like optical emission, absorption, and structural selectivity.

Table 3.1: Optical emission, absorption and nucleic acid targets for optoelectronically active nucleic acid binders.

Ligand	*Solubility*	*Nucleic acid target*	λ_{ex} */nm*	λ_{em} */nm*	*Ref.*
basic yellow (thioflavin)	Soluble	Quadruplex 22AG	330	450	191
methylene blue	Soluble	Telomere G-quadruplex DNA	663	/	124
ethidium bromide	Soluble	polyA • polyT Triplex	481	616	125,126

Table 3.1 lists the properties of selected combinations of ligands and nucleic acid structures like optical emission, absorption and selectivity. Basic yellow and methylene blue target G-quadruplex DNA. Ethidium bromide has affinity toward triplex but also to polyA • polyT. Optical emission and absorption for the basic yellow, methylene blue and ethidium bromide are very important for selection of the second ligand for double competition dialysis. The importance of the optical emission spectrum of the donor and the absorption spectrum of the acceptor relative to each other is critical for FRET.

3.1.3 Aims

There are several aims to discuss in this chapter.

Firstly, in part A, we will validate the traditional approach to competition dialysis for the quantification of affinities for FS-DNA using dialysis tubing. We will develop a device which allowed me to carry out competition dialysis in a simpler manner, which is compatible with UV-vis spectroscopy and which allows us to follow equilibration as a function of time. Finally, in part B, we will studiy the affinity of selected ligands for FS-DNA, $(dA)_{24}$ $(dT)_{24}$, and different quadruplex structures such as c-myc, 22AG and EAD2. For these studies, we pre-identified some compounds potentially displaying orthogonal selectivity for nucleic acid structures.

We will compare the selectivity and affinity obtained using both the traditional assay and our approach to competition dialysis. We will studiy the affinity and selectivity of a single ligand for FS-DNA, specific duplex sequences $(dAdT)_{12}$ and $(dGdC)_{12}$, and different quadruplex structures, viz c-myc, 22AG and EAD2. Fish sperm DNA, deoxyribonucleic acid sodium salt were used to study DNA binding.

Finally, this chapter will also present the results from our competition dialysis assay for the compounds, which were selected based on their previously reported properties such as optical emission, absorption and selectivity toward to nucleic acid.

3.2 Results and discussion

Part A

3.2.1 Development and optimisation of a device for competition dialysis

3.2.1a Validation of the traditional approach to competition dialysis methods for the quantification of affinities of small molecules for FS-DNA.

We wanted to test the validity of affinities determined using the traditional approach to competition dialysis to this end, 500 ml of a solution of known concentration (1.2×10^{-5} M) of methylene blue (**9**) in buffer (25 mM MOPS, 50 mM NaCl, 1 mM EDTA and pH 7) is placed in a beaker. We placed 10 ml of solutions of three different concentrations of FS-DNA (27 µM, 63 µM, and 248 µM) in dialysis tubing (DT) and placed the dialysis tubing in the beaker. We assumed that equilibrium had been achieved after around 48 hours and analysed the contents of the dialysis tubing using UV-visible spectroscopy (Table 3.2).

Table 3.2: Equilibrium constant *K* for 9 [a] intreacting with FS-DNA[b]

dialysis tubing	DT1	DT2	DT3
$[DNA]_{total}$ / M	2.7×10^{-5}	6.3×10^{-5}	2.48×10^{-4}
unit conc	bp	bp	Bp
bind. sites / unit conc.[d]	3.33×10^{-1}	3.33×10^{-1}	3.33×10^{-1}
$[binding\ sites]_{total}$ / M	9.00×10^{-6}	2.10×10^{-5}	8.27×10^{-5}
$A_{663\ nm}$	0.1382	0.1795	0.354
$A_{663\ nm,\ bound}$ [c]	0.0200	0.0613	0.2358
C_{bound} / M [c]	3.66×10^{-6}	1.12×10^{-5}	4.31×10^{-5}
$[ligand]_{free}$ / M	1.13×10^{-5}	1.13×10^{-5}	1.13×10^{-5}
$[binding\ sites]_{free}$ / M	5.34×10^{-6}	9.78×10^{-6}	3.95×10^{-5}
K / M^{-1}	6.03×10^{4}	1.01×10^{5}	9.61×10^{4}

a) Concentration of **9** in the beginning was 12 µM.

b) In buffer (25 mM MOPS, 50 mM NaCl, 1 mM EDTA and pH=7), at 25 °C.

c) $A663_{bg} = 0.0295$, $A663_{free} = 0.0887$, $\varepsilon_{free} = 78000\ M^{-1}\ cm^{-1}$ and $\varepsilon_{bound} = 54618\ M^{-1}\ cm^{-1}$.

d) We assume the binding site size in base pairs is 3.0.

Table 3.2 shows a higher absorbance of **9** with a higher concentration of FS-DNA in the dialysis tubing. The average value for the equilibrium constant ($K_{binding}$) is (8.5 ± 2.22) × 10^4 M^{-1}. The result is in reasonable agreement with the results from the UV-visible titrations as shown in Chapter 2 which gave $K_{binding}$ of (3.83 ± 0.78) ×10^5 M^{-1}. The slightly lower apparent affinity may be the result of incomplete equilibration.

We realised that it it is probably a better idea to repeat the same experiment but for a longer time in order to check whether we achieve equilibration. We therefore, carried out the same experiment of **9** (12 μM) in 25 mM MOPS, 50 mM NaCl, 1 mM EDTA and pH 7. The concentrations and apparent affinities of the ligand were determined after 72 hours, i.e. after more time than the previous experiment (Table 3.3).

Table 3.3: Equilibrium constants *K* for 9 [a] interacting with DNA[b]

dialysis tubing	DT1	DT2	DT3
$[DNA]_{total}$ / M	2.7×10^{-5}	7.4×10^{-5}	2.4×10^{-4}
unit conc.	bp	bp	Bp
bind. sites / unit conc.[d]	3.33×10^{-1}	3.33×10^{-1}	3.33×10^{-1}
$[binding\ sites]_{total}$ / M	9.00×10^{-6}	2.47×10^{-5}	8.00×10^{-5}
A663 $_{nm}$	0.1436	0.2255	0.5321
A663, $_{bound}$ [c]	0.0517	0.1336	0.4402
C $_{bound}$ / M [c]	9.46×10^{-7}	2.44×10^{-6}	8.05×10^{-6}
$[ligand]_{free}$ / M	8.84×10^{-7}	8.84×10^{-7}	8.84×10^{-7}
$[binding\ sites]_{free}$ / M	8.05×10^{-6}	2.22×10^{-5}	7.19×10^{-5}
K / M^{-1}	1.33×10^{5}	1.24×10^{5}	1.27×10^{5}

a) Concentration of **9** in the beginning was 12 μM.

b) In buffer (25 mM MOPS, 50 mM NaCl, 1 mM EDTA and pH=7), at 25 °C.

c) A663 $_{bg}$= 0.0229, A663 $_{free}$ = 0.069, ε $_{free}$ 78000 M^{-1} cm^{-1} = and ε $_{bound}$ = 54618 M^{-1} cm^{-1}.

d) We assume the binding site size in base pairs is 3.0.

Table 3.3, shows the higher absorbance of **9** with the higher DNA concentration in DT3. The equilibrium constant for the three different FS-DNA concentrations are almost the same with an average equilibrium constant ($K_{binding}$) of (12.8 ± 0.4) × 10^4 M^{-1}. Comparison with the data in Table 3.2 shows that the equilibrium has been not achieved after around 48 hours. This means that we cannot be sure that the solutions are fully equilibrated by only looking at the end point of the experiments. The result is in agreement with the results from the UV-visible titrations as shown in Chapter 2 which gave $K_{binding}$ of (3.8 ± 0.78) ×10^5 M^{-1}.

We wanted to know whether the equilibrium constant was affected by the presence of 9 vol-% DMSO because DMSO is a useful cosolvent to help avoid ligand precipitation.[176] We carried out the same experiment, but with MOPS buffer containing 9 vol-% DMSO. The concentrations and apparent affinities of the ligand are reported in Table 3.4.

Table 3.4: Equilibrium constants *K* for 9 [a] interacting with DNA[b]

dialysis tubing	DT1	DT2	DT3
$[DNA]_{total}$ / M	2.3×10^{-5}	5.8×10^{-5}	2.49×10^{-4}
unit conc.	bp	bp	Bp
bind. sites / unit conc.[d]	3.33×10^{-1}	3.33×10^{-1}	3.33×10^{-1}
$[binding\ sites]_{total}$ / M	7.67×10^{-6}	1.93×10^{-5}	8.30×10^{-5}
$A_{663\ nm}$	0.1533	0.1804	0.2835
$A_{663\ nm,\ bound}$ [c]	0.0160	0.0431	0.1462
C_{bound} / M [c]	2.92×10^{-6}	7.89×10^{-6}	2.67×10^{-5}
$[ligand]_{free}$ / M	1.34×10^{-5}	1.34×10^{-5}	1.34×10^{-5}
$[binding\ sites]_{free}$ / M	4.74×10^{-6}	1.14×10^{-5}	5.62×10^{-5}
K / M^{-1}	4.60×10^{4}	5.13×10^{4}	3.54×10^{4}

a) Concentration of **9** in the beginning was 14 µM.

b) In buffer (25 mM MOPS, pH 7.0, 100 mM KCl, 9 vol-% DMSO and 1 mM EDTA), at 25 °C.

c) $A663_{bg}$ = 0.0324, $A663_{free}$ = 0.1049, ε_{free} = 78000 M^{-1} cm^{-1} and ε_{bound} = 54618 M^{-1} cm^{-1}.

d) We assume the binding site size in base pairs is 3.0.

As Table 3.4 shows, there is no significant difference between the equilibrium constants ($K_{binding}$) for the different concentrations of FS-DNA. The average equilibrium constant ($K_{binding}$) is (4.42 ± 0.80) × 10^4 M^{-1}. The result is in reasonable agreement with the results from the UV-visible titrations in the presence of DMSO as shown in Chapter 2 which gave $K_{binding}$ of (8.5 ± 1.35) ×10^4 M^{-1}. The data clearly confirm that binding is weaker compared with the result in the absence of DMSO.

DMSO can affect DNA structure and may also improve ligand solubility, thus decreasing binding affinity. Just like in the absence of DMSO, the apparent affinity according to competition dialysis may be lower than the affinity according to UV-visible titrations because of incomplete equilibration.

3.2.1b Some problems of the traditional approach to competition dialysis

Competition dialysis relies on solubility and chemical stability of the ligand in the buffer over the duration of the experiment. One of the more significant findings to emerge from our first experiments is that precipitation occurred when using TF1 (**8**) (Figure 3.3).

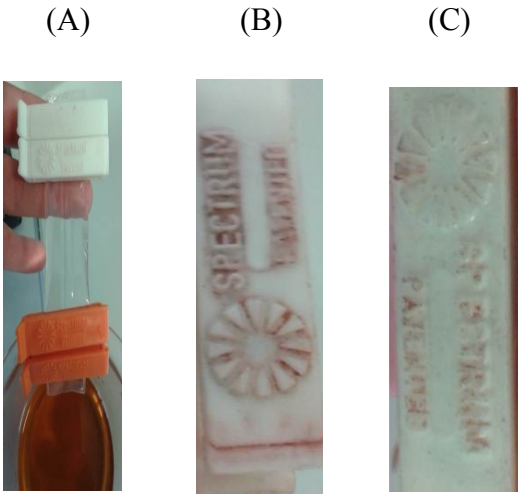

Figure 3.3 (A) Precipitation of ligand **8** on the dialysis tubing and (B) on the clip but (C) less precipitation of **8** in the presence of 9 vol-% DMSO.

Figure 3.3 Shows that the precipitation can occur during the competition dialysis study. To address this challenge, we have to study ligands that have very good solubility in the buffer, if necessary in the presence of added DMSO, to avoid precipitation of the ligand.

In addition, the lack of access to the nucleic acid solutions during the experiment means that we cannot follow the equilibration process. This means that we cannot be sure that the solutions are fully equilibrated.

3.2.1c A new competition dialysis device

To facilitate our competition dialysis studies, we decided to design a new device, based on previously available commercial devices.

The design criteria were as follows:

- Holes containing nucleic acids compatible with typical volumes required for 1 cm pathlength cuvettes.
- Reservoir containing initial ligand solution compatible with volumetric glassware, and the volume must correspond to a large excess over the volume of the initial nucleic acid solutions in the top of the device.
- Easy access to solutions during competition dialysis so that equilibration can be followed.
- Material easy to clean.

The basic device we designed was made out of Teflon and encompasses three major components as shown in Figure 3.4 (B). The bottom of the device contains the ligand solution, and has a capacity of just below 100 mL.

The middle part of the device provides support for the dialysis membrane. Dialysis membrane will allow the ligand molecules to diffuse in and out of the holes containing the nucleic acid structures to achieve the equilibrium concentration.

The top of the device has five holes for different concentrations of DNA or for different sequences of DNA such as duplex DNA, triplex DNA and quadruplex.[192] The maximum capacity of each hole is 10 mL. However, in practice, 3 ml was used which is enough volume to fill a quartz cuvette. The actual device is shown in Figure 3.4B.

A) (B)

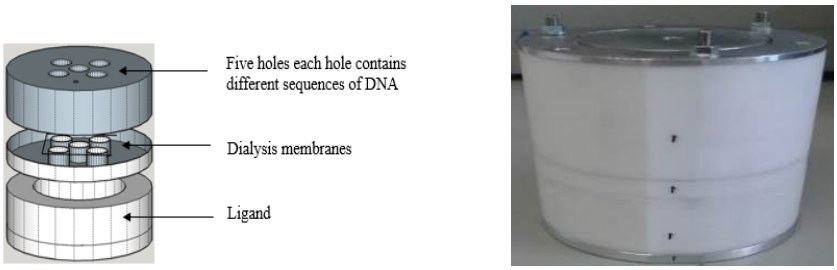

Figure 3.4 (A) the design of a new competition dialysis device, (B) a photo of the new competition dialysis device.

To check if there is any leak in any part of the dialysis device, we filled the complete device with water. Unfortunately, the device failed this test. Then, we tried to test it part by part and it leaked again. We noted that the leaking occurred from the second part of device. Therefore, to stop the leaking, we added a rubber O-ring between parts 1 and 2. This modification stopped the leaking.

To test the middle part of the device, we checked the diffusion between the bottom part of the device and the top of the device by placing a dye solution of methylene blue **(9)** in the bottom of the device and recording the UV-visible absorbance of the solutions in the holes above as a function of time (Table 3.5).

Table 3.5: Testing the diffusion of a solution of methylene blue (9) in our device [a]

time / hours	hole 1	hole 2	hole 3	hole 4	hole 5	Buffer
5	0.0248	0.0233	0.0239	0.0249	0.0243	0.0213
23	0.0403	0.0303	0.2229	0.074	0.1275	0.0268
41	0.0359	0.0459	0.2282	0.0838	0.1264	0.032
48	0.0416	0.0454	0.2217	0.0924	0.1288	0.0323
72	0.0428	0.0484	0.2217	0.1008	0.124	0.0274
96	0.0421	0.0462	0.2131	0.109	0.1268	0.0274

a) In buffer (25 mM MOPS, 50 mM NaCl, 1 mM EDTA and pH=7), at 25 °C.

b) Concentration of **9** in the beginning was 0.0088 µM.

Table 3.5 shows that the absorbances for some of the holes in the top of the device are close to the absorbance for the buffer. Nevertheless, some other holes, in particular hole 3, show a

higher absorbance at 663 nm. We explored several solutions to the failure of the dye to reach the top of the device, such as washing the dialysis membrane and the placement of the dialysis membrance.

The success of our method is contingent on the solution in the bottom of the device being in contact with the solution in the top part through the dialysis membrane. This means that the solution in the device must show a convex surface when the middle part of the device is in place as clearly shown in Figure 5.5. If this is the case, no bubbles will form below the dialysis membrane. Bubbles break the contact between the liquids. In addition, it is important to clean the dialysis membrane before use by placing it in a beaker of hot water for 10 min, to remove any impurities.

Figure 3.5 a convex meniscus on the solution on the top of the middle part of the device

To investigate that the device works well if good contact between the solutions was created, we carried out the same experiment involving a solution of **9** in the bottom of the device and MOPS buffer in the top of the device. UV-visible spectroscopy was used to determine the concentration of **9** at 663 nm as a function of time (Table 3.5).

Table 3.6: for testing the diffusion of solution of methylene blue (9) [a]

time/ hours	hole 1	hole 2	hole 3	hole 4	hole 5	Buffer
5	0.594	0.6371	0.8731	0.7035	0.7334	0.0231
24	1.9726	1.9193	2.1191	2.0445	2.1411	0.0219
72	2.4015	2.4012	2.4376	2.4296	2.4865	0.0208
95	2.4148	2.4255	2.4473	2.4452	2.5181	0.022

a) In buffer (25 mM MOPS, 50 mM NaCl, 1 mM EDTA and pH=7), at 25 °C.

b) The concentration of 9 in the beginning of this experiment was 0.055 μM.

c) The concentration of **9** in the end of this experiment was 1.9×10^{-3} μM.

d) $A663_{bg} = 0.0274$, $A663_{free} = 0.1542$, $A_{reservoir} = 0.1816$.

Table 3.6, shows that the absorbance of **9** at 663 nm is similar for all holes. This absorbance result suggests that diffusion is now satisfactory. In general, the top and middle part of device are working well.

In order to test the device further, we determined the affinity of **9** for FS-DNA at different concentrations of FS-DNA (26 μM, 69 μM, and 230 μM) at a concentration of **9** of 1.4×10^{-6} M. The concentrations and apparent affinities of the ligand for DNA in 25 mM MOPS, 50 mM NaCl, 1 mM EDTA and pH 7 were determined (Table 3.7).

Table 3.7: Equilibrium constants *K* for 9 [a] interacting with FS-DNA[b]

DNA	FS-DNA	FS-DNA	FS-DNA	FS-DNA	buffer
$[DNA]_{total}$ / M	2.6×10^{-5}	6.9×10^{-5}	2.3×10^{-4}	2.3×10^{-4}	0
unit conc.	bp	bp	bp	Bp	/
bind. sites / unit conc. [d]	3.33×10^{-1}	3.33×10^{-1}	3.33×10^{-1}	3.33×10^{-1}	/
$[binding\ sites]_{total}$	8.67×10^{-6}	2.30×10^{-5}	7.67×10^{-5}	7.67×10^{-5}	/
$A_{663\ nm}$	0.0815	0.1001	0.1564	0.1566	0.0924
$A_{663\ nm,\ bound}$ [c]	0.0165	0.0351	0.0914	0.0916	0.0274
C_{bound} / M [c]	6.04×10^{-7}	1.28×10^{-6}	3.35×10^{-6}	3.35×10^{-6}	/
$[ligand]_{free}$ / M	1.09×10^{-6}	1.09×10^{-6}	1.09×10^{-6}	1.09×10^{-6}	1.09×10^{-6}
$[binding\ sites]_{free}$ / M	8.06×10^{-6}	2.17×10^{-5}	7.33×10^{-5}	7.33×10^{-5}	/
K / M^{-1}	6.84×10^{4}	5.41×10^{4}	4.17×10^{4}	4.18×10^{4}	/

a) Concentration of **9** was 1.4 μM.

b) In buffer (25 mM MOPS, 50 mM NaCl, 1 mM EDTA and pH 7), at 25 °C.

c) $A_{bg,}$ = 0.0223, $A_{free,}$ = 0.0427, $A663_{\ reservoir}$ = 0.0650, $\varepsilon_{\ free}$ = 78000 M^{-1} cm^{-1} and $\varepsilon_{\ bound}$ = 54618 M^{-1} cm^{-1}.

d) We assume the binding site size in base pairs is 3.0.

Table 3.7 presents a higher absorbance of **9** with a higher concentration of FS-DNA. The two holes with 2.3×10^{-4} M^{-1} FS-DNA give the same absorbance. What is promising in this data is that the equilibrium constant *K* for the three different concentrations of DNA are almost the same. The average equilibrium constant ($K_{binding}$) is (5.1 ± 1.2) × 10^4 M^{-1}. Accordingly, the result is in agreement with the results from the UV-visible titrations as shown in Chapter 2. However, we also note that the absorbance of the buffer is much higher than the absorbance of the ligand solution in the bottom of the device. Unfortunately, our control therefore shows us that there is a problem with **9**. This problem was later attributed to fading of **9**.

We set to determine if the position of the holes in the top of the device can affect the apparent affinity. For example, data from the hole in the middle of the device always suggested a higher affinity compared with other holes. To investigate this, the experiment is repeated. This experiment focused on the positions of the holes as shown in Figure 3.6.

Figure 3.6 the top of the device with five holes.

A solution of 1.3×10^{-6} M **9** was exposed to different concentrations of FS-DNA (25 μM, 69 μM, and 208 μM) in 25 mM MOPS, 50 mM NaCl, 1 mM EDTA and pH 7 in the top of the device. The fifth hole was filled with buffer as a control experiment. After equilibration for 72h, the concentrations and apparent affinities of the ligand and DNA were determined (Table 3.8).

Table 3.8: Equilibrium constants *K* for 9 interacting with FS-DNA[a]

DNA	FS-DNA	FS-DNA	FS-DNA	FS-DNA	Buffer
$[DNA]_{total}$ / M	2.5×10^{-5}	6.9×10^{-5}	2.08×10^{-4}	2.08×10^{-4}	0
unit conc.	bp	bp	bp	Bp	/
bind. sites / unit conc. [d]	3.33×10^{-1}	3.33×10^{-1}	3.33×10^{-1}	3.33×10^{-1}	/
$[binding\ sites]_{total}$ / M	8.33×10^{-6}	2.30×10^{-5}	6.93×10^{-5}	6.93×10^{-5}	/
$A663_{nm}$	0.1203	0.1644	0.2502	0.3219	0.1106
$A663nm,_{bound}$ [c]	0.0284	0.0725	0.1583	0.23	0.0187
C_{bound} / M [c]	5.199×10^{-7}	1.32×10^{-6}	2.89×10^{-6}	4.21×10^{-6}	/
$[ligand]_{free}$ / M	9.00×10^{-7}	9.00×10^{-7}	9.00×10^{-7}	9.00×10^{-7}	9.00×10^{-7}
$[binding\ sites]_{free}$ / M	7.81×10^{-6}	2.17×10^{-5}	6.64×10^{-5}	6.51×10^{-5}	/
K / M^{-1}	7.39×10^{4}	6.81×10^{4}	4.85×10^{4}	7.18×10^{4}	/

a) Concentration of **9** in the beginning was 1.3 µM.

b) In buffer (25 mM MOPS, 50 mM NaCl, 1 mM EDTA and pH=7), at 25 °C.

c) A_{bg}, 0.0217, A_{free}, 0.0702, $A663_{reservoir}$ was 0.0919, ε_{free} = 78000 M^{-1} cm^{-1} and ε_{bound} = 54618 M^{-1} cm^{-1}.

d) We assume the binding site size in base pairs is 3.0.

Table 3.8 demonstrates that the device is not working well and that the results are not independent of the hole used in the experiment. The problem appears from the results that show a different absorbance of **9** at 663 nm with the same concentration of DNA (2.08×10^{-4} M). The cause is probably evaporation because the lid of the device has a small hole above the center hole of the top part of the device as shown that in table 3.13.

Furthermore, the data presented a similar equilibrium constant of $(6.5 \pm 1.17) \times 10^4$ M^{-1}. However, we observe another problem that appears from the control for this experiment. The absorbance of free ligand in the reservoir was 0.0702 and in the control hole it was 0.1106. That is a big difference. Unfortunately, our control therefore again shows us there is a problem with **9**. This problem was later attributed to the fading.

3.2.1c DMSO affects the observed affinities in competition dialysis

As we have shown in Chapter 2, DMSO affects the interaction between **8** and FS-DNA. Here, we want to test this effect again in our competition dialysis assay and compare the results to those from UV-visible spectroscopic titrations. The experiment involved different concentrations of FS-DNA (25 µM, 60 µM, and 227 µM) and a concentration of **8** of 1.16×10^{-6} M in a DMSO-containing buffer (25 mM MOPS, pH 7.0, 100 mM KCl, 9 vol-% DMSO and 1 mM EDTA). The concentrations and apparent affinities of the ligand after equilibration were determined and are shown in Table 3.9.

Table 3.9: for testing the concentration of 8[a] exposed to different concentrations of FS-DNA [b]

Time / hours	buffer	FS-DNA	FS-DNA	FS-DNA	FS-DNA
24	0.0346	0.0354	0.0352	0.0337	0.0345
48	0.0444	0.0458	0.0435	0.0429	0.0456
72	0.048	0.0557	0.0469	0.0482	0.0494
96	0.0516	0.0595	0.0489	0.0503	0.0516
120	0.052	0.0607	0.0522	0.0516	0.0526
144	0.0494	0.0648	0.0513	0.0534	0.053
168	0.0529	0.0664	0.0523	0.0521	0.0516

a) Concentration of **8** was 1.1 µM.

b) In buffer (25 mM MOPS, pH 7.0, 100 mM KCl, 9 vol-% DMSO and 1 mM EDTA), at 25 °C.

c) The **8** concentration in the end of this experiment was 0.6 µM.

d) A_{bg}, 0.0207, A_{free}, 0.0324 and A476 $_{reservoir}$ was 0.0531.

Table 3.9 shows all the absorbance data for **8** at 476 nm are close to absorbance of the buffer. This absorbance result suggests that diffusion is not satisfactory, which may be due to a low solubility of **8** and resulting precipitation which can affect our data. To avoid that error, the experiment was repeated using both a magnetic stirrer in the bottom part of the device and placing the device inside a Heidolph incubator at 25 °C for all experiments from now on.

Table 3.10: Equilibrium constants *K* for 8 [a] interacting with FS-DNA[b]

DNA	FS-DNA	FS-DNA	FS-DNA	FS-DNA	buffer
$[DNA]_{total}$ / M	2.23×10^{-4}	2.6×10^{-5}	6.8×10^{-5}	2.6×10^{-5}	0
unit conc.	bp	bp	bp	Bp	/
bind. sites / unit conc. [d]	3.33×10^{-1}	3.33×10^{-1}	3.33×10^{-1}	3.33×10^{-1}	/
$[binding\ sites]_{total}$ / M	7.43×10^{-5}	8.67×10^{-6}	2.27×10^{-5}	8.67×10^{-6}	/
$A476_{nm}$	0.5669	0.3969	0.3853	0.4581	0.3838
$A476,_{bound}$ [c]	0.2037	0.0337	0.0221	0.0949	0.0206
C_{bound} / M [c]	5.53×10^{-6}	9.15×10^{-7}	6×10^{-7}	2.58×10^{-6}	/
$[ligand]_{free}$ / M	6.57×10^{-6}	6.57×10^{-6}	6.57×10^{-6}	6.57×10^{-6}	6.57×10^{-6}
$[binding\ sites]_{free}$ / M	6.88×10^{-5}	7.75×10^{-6}	2.21×10^{-5}	6.09×10^{-6}	/
K / M^{-1}	1.22×10^{4}	1.80×10^{4}	4.14×10^{3}	6.44×10^{4}	/

a) Concentration of **8** was 6.2 µM.

b) In buffer (25 mM MOPS, pH 7.0, 100 mM KCl, 9 vol-% DMSO and 1 mM EDTA), at 25 °C.

c) A_{bg}, 0.0254, A_{free}, 0.3378, $A476_{reservoir}$ was 0.3632, $\varepsilon_{free} = 51398\ M^{-1}\ cm^{-1}$ and $\varepsilon_{bound} = 36828\ M^{-1}\ cm^{-1}$.

d) We assume the binding site size in base pairs is 3.0.

To check if we can solve the solubility problem shown above by adding DMSO, two experiments were carried out. The first experiment involved different concentrations of FS-DNA (26 µM, 68 µM, and 223 µM) and 6.2×10^{-6} M **8**, while the The second experiment involved FS-DNA (24 µM, 67 µM, and 176 µM) and 7.7×10^{-6} M **8**.

Both experiments were in buffer (25 mM MOPS, pH 7.0, 100 mM KCl, 9 vol-% DMSO and 1 mM EDTA) at 25 °C. The concentrations and apparent affinities of the ligand after equilibrium were determined in Tables 3.10 and 3.11.

Table 3.11: Equilibrium constants *K* for 8 [a] interacting with FS-DNA[b]

DNA	FS-DNA	FS-DNA	FS-DNA	FS-DNA	buffer
$[DNA]_{total}$ / M	1.76×10^{-4}	2.4×10^{-5}	1.76×10^{-4}	6.7×10^{-5}	/
unit conc.	bp	bp	Bp	bp	/
bind. sites / unit conc. [d]	3.33×10^{-1}	3.33×10^{-1}	3.33×10^{-1}	3.33×10^{-1}	/
$[binding\ sites]_{total}$ / M	5.87×10^{-5}	8.00×10^{-6}	5.87×10^{-5}	2.23×10^{-5}	/
$A476_{nm}$	0.4935	0.3966	0.4948	0.4547	0.4798
$A476_{bound}$ [c]	0.1672	0.0703	0.1685	0.1284	0.1535
C bound / M [c]	4.53×10^{-6}	1.91×10^{-6}	4.58×10^{-6}	3.48×10^{-6}	/
$[ligand]_{free}$ / M	5.84×10^{-6}	5.84×10^{-6}	5.84×10^{-6}	5.84×10^{-6}	5.84×10^{-6}
$[binding\ sites]_{free}$ / M	5.41×10^{-5}	6.09×10^{-6}	5.41×10^{-5}	1.88×10^{-5}	/
K / M^{-1}	1.44×10^{4}	5.36×10^{4}	1.45×10^{4}	3.17×10^{4}	/

a) Concentration of **8** was 7.7 µM.

b) In buffer (25 mM MOPS, pH 7.0, 100 mM KCl, 9 vol-% DMSO and 1 mM EDTA), at 25 °C.

c) A_{bg}, 0.0259, A_{free}, 0.3004, $A476_{reservoir}$ was 0.3263, ε_{free} = 51398 M^{-1} cm^{-1} and ε_{bound} = 36828 M^{-1} cm^{-1}.

d) We assume the binding site size in base pairs is 3.0.

Tables 3.10 and 3.11 present the affinities of **8** for FS-DNA as determined at different concentrations of FS-DNA. The data in Tables 3.10 and 3.11 give the same affinities of **8** for FS-DNA. These absorbance results suggest that the diffusion is satisfactory. The average equilibrium constants ($K_{binding}$) are (2.4 ± 2.7) × 10^4 M^{-1} and (2.8 ± 1.8) × 10^4 M^{-1}, respectively. These results are in agreement with the results from the UV-visible titrations as shown in Chapter 2 which gave $(K_{bindin)g}$ of (1.04 ± 0.84) × 10^5 M^{-1}.

We further tested whether a magnetic stirrer can be added in the bottom reservoir of the device (Tables 3.10 and 3.11). The data show that a magnetic stirrer enhances the experiment. The reason to store the device at 25 °C is to keep all the conditions the same to compare this data with Chapter 2. The device was stored at 25 °C during equilibration. Despite the precautions, however, the low solubility of **8** causes precipitation, which affects our data as shown in Figure 3.7.

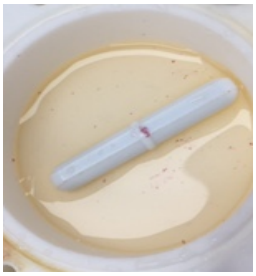

Figure 3.7 Precipitate of **8** in the bottom reservoir of the device and on the magnetic stirrer in buffer containing 9 vol-% DMSO.

It is obvious that 9 vol % DMSO was not enough to keep **8** in solution. We avoided using more than 10 vol % of any of organic solvents, such as DMSO and acetonitrile, as we have shown in Chapter 2 that this can affect the affinities and the literature indicates that higher fractions of DMSO may destabilise nucleic acid structures.

To further explore the validity of affinities determined using dialysis, we employed ligand **6** together with 23 μM, 64 μM, and 152 μM of FS-DNA at a concentration of **6** of 5.9×10^{-5} M, in 25 mM MOPS, pH 7.0, 100 mM KCl, 9 vol-% DMSO and 1 mM EDTA. The concentrations and apparent affinities of the ligand at equilibrium were determined in Table 3.12.

Table 3.12: Equilibrium constants *K* for 6 [a] interacting with FS-DNA[b]

DNA	FS-DNA	FS-DNA	FS-DNA	FS-DNA	buffer
$[DNA]_{total}$ / M	2.3×10^{-5}	6.4×10^{-5}	1.52×10^{-4}	6.4×10^{-5}	/
unit conc.	bp	bp	bp	Bp	/
bind. sites / unit conc.	3.33×10^{-1}	3.33×10^{-1}	3.33×10^{-1}	3.33×10^{-1}	/
$[binding\ sites]_{total}$ / M	7.67×10^{-6}	2.13×10^{-5}	5.07×10^{-5}	2.13×10^{-5}	/
$A_{338\ nm}$	1.1712	0.944	0.5059	0.8043	1.211
$A_{338\ nm,\ bound}$	-0.2093	-0.4365	-0.8746	-0.5762	-0.1695
C_{bound} / M	/	/	/	/	/
$[ligand]_{free}$ / M	3.19×10^{-5}	3.19×10^{-5}	3.19×10^{-5}	3.19×10^{-5}	3.19×10^{-5}
$[binding\ sites]_{free}$ / M	1.57×10^{-5}	3.81×10^{-5}	8.43×10^{-5}	4.35×10^{-5}	/
K / M^{-1}	/	/	/	/	/

a) Concentration of **6** was 59 µM.

b) In buffer (25 mM MOPS, pH 7.0, 100 mM KCl, 9 vol-% DMSO and 1 mM EDTA), at 25 °C.

c) A_{bg}, 0.0405, A_{free}, 1.3406, $A338_{\ reservoir}$ was 1.381, $\varepsilon_{\ free}$ = 42000 M^{-1} cm^{-1} and $\varepsilon_{\ bound}$ = 26030 M^{-1} cm^{-1}.

d) we assume the binding site size in base pairs is 3.0.

The table 3.12 shows very strange data. For all DNA concentrations, the absorbance is lower than the absorbance of the solution in the hole containing only buffer and lower than the solution in the bottom reservoir of the device.

In this experiment, a very high concentration of ligand **6** was used. Precipitation of ligand was observed and this can affect the diffusion. Furthermore, we found some bubbles in the middle part of the device that could also have affected our data as shown in Figure 3.8 (C).

(A) (B) (C)

Figure 3.8 (A) precipitate of **6** on the bottom of the device and on the magnetic stirrer with 9 vol-% DMSO, (B) the dialysis membrane with clear precipitation of **6** and (C) bubbles in the middle part of the device.

In the next experiment, a more dilute solution of 3.2×10^{-6} M **6** was used to avoid precipitation. In addition different concentrations of synthetic nucleic acids $(dA)_{24}$ $(dT)_{24}$ were used (25 µM, 72 µM, and 176 µM) in 25 mM MOPS, pH 7.0, 50 mM NaCl, and 1 mM EDTA. The absorbance of **6** at 338 nm was plotted as a function of time (Figure 3.9).

(A) (B)

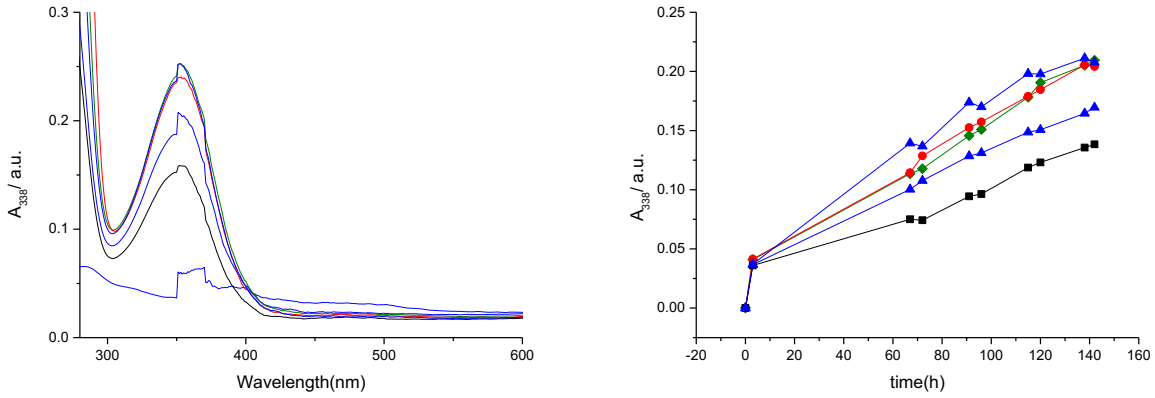

Figure 3.9 (A) Final UV-visible spectra for **6** with 25, 72 and 176 µM of $(dA)_{24}$ (dT) **(B)** The absorbance of **6** at 338 nm as a function of time for $(dA)_{24}$ $(dT)_{24}$, 25 µM (▲), 176 µM (●), 72 µM (♦), and buffer (■).

Figure 3.9A shows the change in absorbance at λ_{max} 338 nm of **6** in the presence of DNA. Figure 3.9B shows that the equilibrium has not been achieved. The absorbance at λ_{max} 338 nm of **6** is higher for the hole filled with 25 µM $(dA)_{24}$ $(dT)_{24}$ (▲). This problem was later

attributed to the middle hole in the device. The lid of the device had a hole in the middle as a result of the fabrication technique used. This hole allowed evaporating of the solution.

The final test for our method and our device involves a compound that shows no binding to DNA, viz. anionic **3**, with different concentrations of FS-DNA (24 μM, 68 μM, and 169 μM) in buffer (25 mM MOPS, pH 7.0, 50 mM NaCl, 1 mM EDTA) at 25 °C. The absorbance of **3** at 563 nm was plotted it as a function of time (Figure 3.10).

(A) (B)

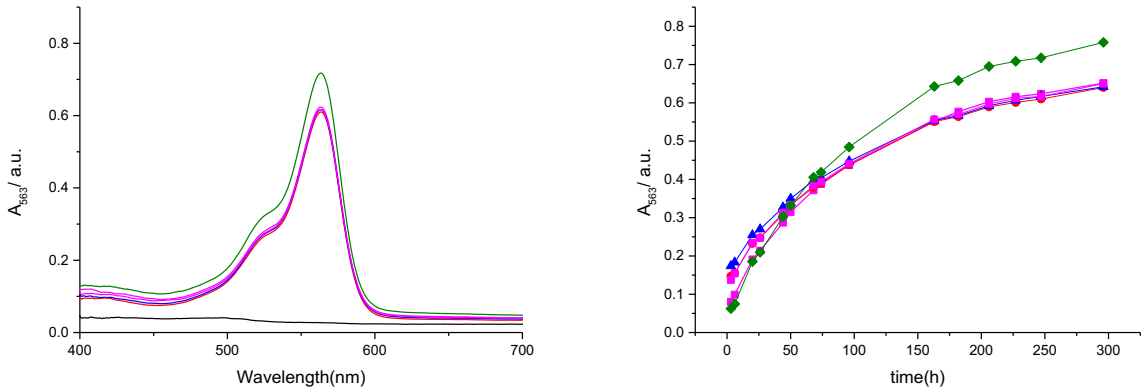

Figure 3.10 (A) Final UV-visible spectra for **3** with different concentrations of FS-DNA in buffer (25 mM MOPS, pH 7.0, 50 mM NaCl, 1 mM EDTA) at 25 °C. **(B)** The absorbance of **3** at 563 nm as a function of time for FS-DNA at 24 μM (♦), 68 μM (▲), 169 μM (■) and buffer (●), in buffer (25 mM MOPS, pH 7.0, 50 mM NaCl, 1 mM EDTA), at 25 °C.

Figure 3.10A shows the final spectra of **3** at the λ_{max} of **3** in the presence of DNA. Figure 3.10B shows that the absorbance of **3** for all holes of the device is close to the absorbance for the buffer, except for the hole where the DNA concentration is (24 μM) (♦). This problem was later attributed to the middle hole in the device where the lid for the device had a hole. The Figure shows equilibrium has been achieved after around 269 hours.

The concentrations and apparent affinities of the ligand for DNA were determined from the absorbance data at 563 nm (Table 3.13).

Table 3.13: Equilibrium constants *K* for 3 [a] interacting with FS-DNA[b]

DNA	FS-DNA	FS-DNA	FS-DNA	FS-DNA	buffer
$[DNA]_{total}$ / M	1.69×10^{-4}	6.8×10^{-5}	1.69×10^{-4}	2.4×10^{-5}	0
unit conc.	bp	bp	bp	Bp	/
bind. sites / unit conc. / M [d]	3.33×10^{-1}	3.33×10^{-1}	3.33×10^{-1}	3.33×10^{-1}	/
$[binding\ sites]_{total}$ / M	5.63×10^{-5}	2.27×10^{-5}	5.63×10^{-5}	8.00×10^{-6}	/
$A563_{nm}$	0.6517	0.642	0.6501	0.7579	0.6401
$A563,_{bound}$ [c]	0.0072	-0.0025	0.0056	0.1134	-0.0044
C_{bound} / M[c]	7.45×10^{-8}	/	5.79×10^{-8}	1.17×10^{-6}	/
$[ligand]_{free}$ / M	7.34×10^{-6}	/	7.34×10^{-6}	7.34×10^{-6}	7.34×10^{-6}
$[binding\ sites]_{free}$ / M	5.63×10^{-5}	/	5.63×10^{-5}	6.83×10^{-6}	/
K / M^{-1}	1.80×10^{2}	/	1.40×10^{2}	2.34×10^{4}	/

a) Concentration of **3** was 8.9 µM.

b) In buffer (25 mM MOPS, pH 7.0, 50 mM NaCl, and 1 mM EDTA), at 25 °C.

c) A_{bg}, 0.0244, A_{free}, 0.6201, $A563_{reservoir}$ was 0.6445, ε_{free} = 8683 M^{-1} cm^{-1} and ε_{bound} = 10285 M^{-1} cm^{-1}.

d) We assume the binding site size in base pairs is 3.0.

Table 3.13 shows that the absorbance of **3** at 563 nm with the concentration of DNA of 2.40×10^{-5} M is higher than the absorbance for the other holes. Accordingly, our calculations result in relatively high apparent affinity of **3** for FS-DN. We know that **3** has no affinity for DNA. This means that something else increases the concentration of **3** in this hole. The cause is probably evaporation because the lid of the device has a small hole above the center hole of the top part of the device.

One more alteration was therefore done to develop the top of this device, which is to close the hole in the lid of the device.

Part B

3.3 validation of dialysis and quantification.

The results of our validation of our dialysis methods for the quantification of affinities of **3**, **9**, **5** and **6** for different DNA sequences, viz. FS-DNA, $(dA)_{24}$ $(dT)_{24}$, $(dAdT)_{12}$●$(dAdT)_{12}$ and $(dGdC)_{12}$●$(dGdC)_{12}$ are given below.

3.3.1 Non-binding DNA

We wanted to confirm that the device works properly with the hole closed and that we can get quantitative data from our device.

We determined the affinity of anionic **3** in buffer (25 mM MOPS, pH 7.0, 50 mM NaCl, and 1 mM EDTA) for FS-DNA at different concentrations of FS-DNA (23 µM, 69 µM, and 167 µM). The spectra of **3** after equilibration with different concentrations of DNA are shown in Figure 3.11.

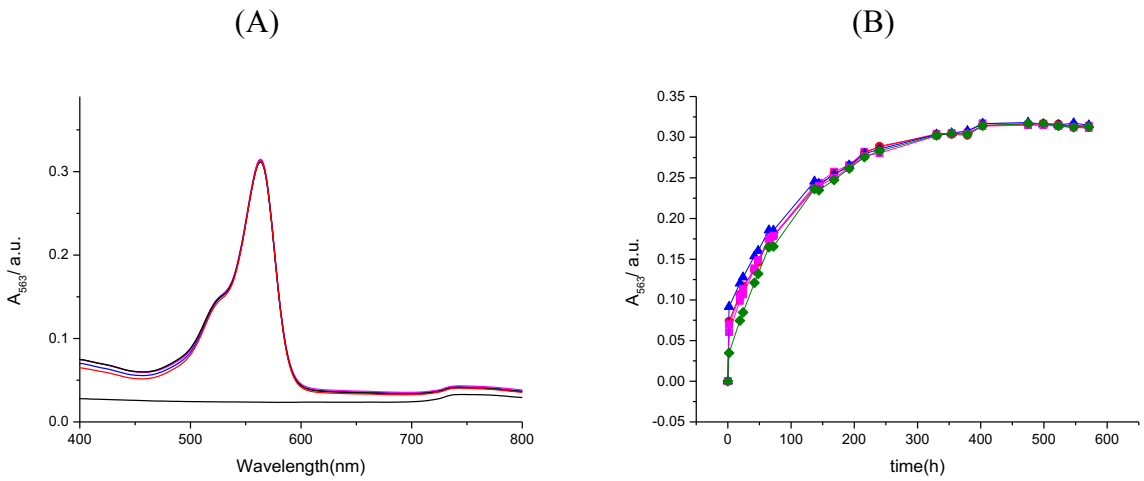

Figure 3.11 (A) UV-visible spectra after the equilibration for **3** with different concentrations of FS-DNA in buffer (25 mM MOPS, pH 7.0, 50 mM NaCl, 1 mM EDTA), at 25 °C. **(B)** The absorbance of **3** at 563 nm as a function of time for FS-DNA 23 µM (♦), 69 µM (▲), 167 µM (■) and buffer (●), in buffer (25 mM MOPS, pH 7.0, 50 mM NaCl, 1 mM EDTA), at 25 °C.

Figure 3.11A and Figure 3.11B show that the different concentrations of FS-DNA give spectra that are close to the buffer. Consequently, there is no affinity between **3** and FS-DNA

the result is in agreement with the results from the UV-visible titrations as shown in Chapter 2. Equilibrium has been achieved after around 500 hours.

The concentrations and apparent affinities of the ligand for FS-DNA after equilibration were determined (Table 3.14).

Table 3.14: Equilibrium constants *K* for 3 [a] interacting with FS-DNA[b]

DNA	FS-DNA	FS-DNA	FS-DNA	FS-DNA	buffer
$[DNA]_{total}$ / M	1.67×10^{-4}	6.9×10^{-5}	1.67×10^{-4}	2.3×10^{-5}	/
unit conc.	bp	bp	bp	bp	/
bind. sites / unit conc. [d]	3.33×10^{-1}	3.33×10^{-1}	3.33×10^{-1}	3.33×10^{-1}	/
$[binding\ sites]_{total}$ / M	5.57×10^{-5}	2.30×10^{-5}	5.57×10^{-5}	7.67×10^{-6}	/
$A563_{nm}$	0.3142	0.3148	0.3113	0.3127	0.3131
$A563,_{bound}$ [c]	0.0060	0.0066	0.0031	0.0045	0.0049
C_{bound} / M [c]	5.83×10^{-7}	6.42×10^{-7}	3.01×10^{-7}	4.37×10^{-7}	
$[ligand]_{free}$ / M	3.27×10^{-5}	3.28×10^{-5}	3.28×10^{-5}	3.27×10^{-5}	3.28×10^{-5}
$[binding\ sites]_{free}$ / M	5.51×10^{-5}	2.24×10^{-5}	5.54×10^{-5}	7.23×10^{-6}	/
K / M^{-1}	3.23×10^{2}	8.76×10^{2}	1.66×10^{2}	1.85×10^{3}	/

a) Concentration of **3** was 4.4 μM.

b) In buffer (25 mM MOPS, pH 7.0, 50 mM NaCl, and 1 mM EDTA), at 25 °C.

c) A_{bg}, 0.0238, A_{free}, 0.2844, $A563_{reservoir}$ was 0.3082, , ε_{free} = 8683 M^{-1} cm^{-1} and ε_{bound} = 10285 M^{-1} cm^{-1}.

d) We assume the binding site size in base pairs is 3.0.

It is apparent from the Table that the absorbance of **3** at 563 nm with the different concentrations of DNA are almost the same as the absorbance of buffer only. The low apparent equilibrium constant ($K_{binding}$) of (8.3 ± 7.6) $\times10^2$ M^{-1} suggests that no binding is taking place. Accordingly, the result is in agreement with the results from the UV-visible titrations as shown in chapter 2, which yielded an affinity of (0.66 ± 2.34) $\times10^2$ M^{-1}. These data also demonstrate what is expected from a non-binding ligand: absorbance as a function of time simply mirrors that of the buffer, reaching the same final absorbance. Our control

($A_{reservoir}$ = 0.3082and $A_{buffer\ hole}$ = 0.3131 i.e. 98 %) shows us that the device works well for this compound.

3.3.2 DNA binding

We decided to further study the validity of affinities determined using our approach to dialysis. We used three different concentrations of FS-DNA (24 µM, 69 µM, and 227 µM) together with 1.4 × 10^{-6} M (methylene blue) **9** in buffer (25 mM MOPS, pH 7.0, 50 mM NaCl, and 1 mM EDTA), at 25 °C. The spectra of **9** after equilibration for 168 hours are shown in Figure 3.12.

(A) (B)

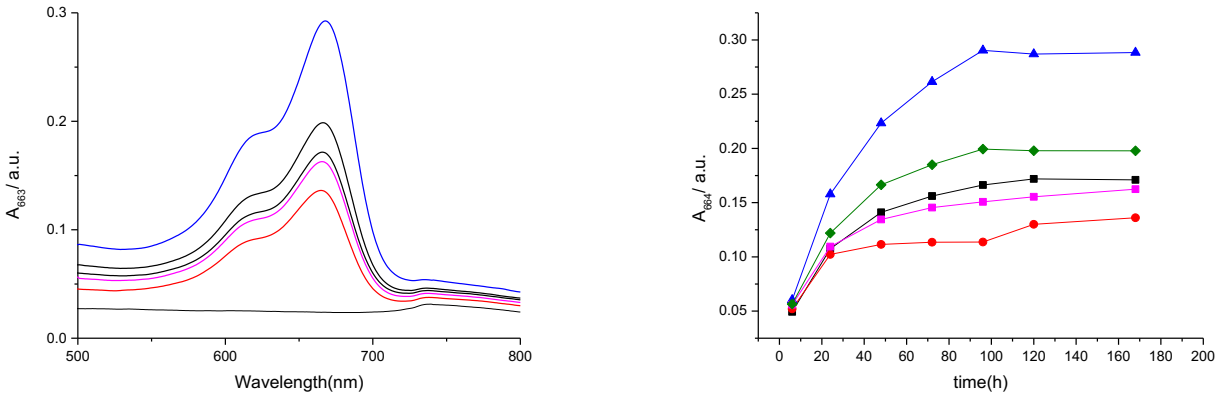

Figure 3.12 (A) Final UV-visible spectra for **9** with different concentrations of FS-DNA in buffer (25 mM MOPS, pH 7.0, 50 mM NaCl, 1 mM EDTA), at 25 °C. **(B)** The absorbance of **9** at 663 nm a function of time for the FS-DNA concentrations 24 µM (■), 69 µM (■) and (♦), for 227 µM (▲) and buffer (●).

Figure 3.12A shows the spectra following equilibration of **9** in the presence of the different concentrations of DNA. Figure 3.12B shows the highest absorbance of **9** with the highest DNA concentration of 227 µM. The Figure also shows that equilibrium has been achieved after around 150 hours.

The concentrations and apparent affinities of the ligand at equilibrium were determined (Table 3.15).

Table 3.15: Equilibrium constants *K* for 9 [a] interacting with FS-DNA[b]

DNA	FS-DNA	FS-DNA	FS-DNA	FS-DNA	Buffer
$[DNA]_{total}$ / M	6.9×10^{-5}	2.27×10^{-4}	2.4×10^{-5}	6.9×10^{-5}	0
unit conc.	bp	bp	bp	Bp	/
bind. sites / unit conc.[d]	3.33×10^{-1}	3.33×10^{-1}	3.33×10^{-1}	3.33×10^{-1}	/
$[binding\ sites]_{total}$ / M	2.30×10^{-5}	7.57×10^{-5}	8.00×10^{-6}	2.30×10^{-5}	0
$A663_{nm}$	0.171	0.2884	0.1624	0.1978	0.1361
$A663_{bound}$ [c]	0.0638	0.1812	0.0552	0.0906	0.0289
C_{bound} / M [c]	1.16×10^{-6}	3.32×10^{-6}	1.01×10^{-6}	1.66×10^{-6}	0
$[ligand]_{free}$ / M	8.166×10^{-7}	8.17×10^{-7}	8.17×10^{-7}	8.17×10^{-7}	8.17×10^{-7}
$[binding\ sites]_{free}$ / M	2.18×10^{-5}	7.23×10^{-5}	6.99×10^{-6}	2.13×10^{-5}	/
K / M^{-1}	6.55×10^{4}	5.61×10^{4}	1.77×10^{5}	9.52×10^{4}	/
K average / M^{-1}	$(9.85 \pm 5.50)\times10^{4}$				

a) Concentration of **9** was 1.4 µM.

b) In buffer (25 mM MOPS, 50 mM NaCl, 1 mM EDTA and pH=7), at 25 °C.

c) A_{bg}, 0.0435, A_{free}, 0.0637, $A663_{reservoir}$ was 0.1072, $\varepsilon_{free} = 78000\ M^{-1}\ cm^{-1}$ and $\varepsilon_{bound} = 54618\ M^{-1}\ cm^{-1}$.

d) Weassume the binding site size in base pairs is 3.0.

Table 3.15 presents a higher absorbance of **9** with a higher concentration of DNA. The equilibrium constant ($K_{binding}$) is $(9.8 \pm 5.5) \times10^4\ M^{-1}$, in reasonable agreement with the result of $(3.83 \pm 0.78) \times10^5\ M^{-1}$ from UV-visible titrations (Chapter 2). Unfortunately, our control ($A_{reservoir}$ = 0.1072 and $A_{buffer\ hole}$ = 0.1361 i.e. 78 %) shows us and that there is a problem with **9**. This problem was later attributed to fading of **9**.

3.3.2.a Competition dialysis methods for the quantification of affinities and selectivities for FS-DNA and specific sequences.

We wanted to study the selectivity of **5** for duplex DNA of different sequences. We therefore exposed 1.5×10^{-5} M of **5** to different DNA sequences, viz., FS-DNA (151 µM), $(dGdC)_{12}$●$(dGdC)_{12}$ (24 µM) and of $(dAdT)_{12}$●$(dAdT)_{12}$ (55 µM). The spectra of **5** after equilibration with different DNA sequences are shown in Figure 3.13.

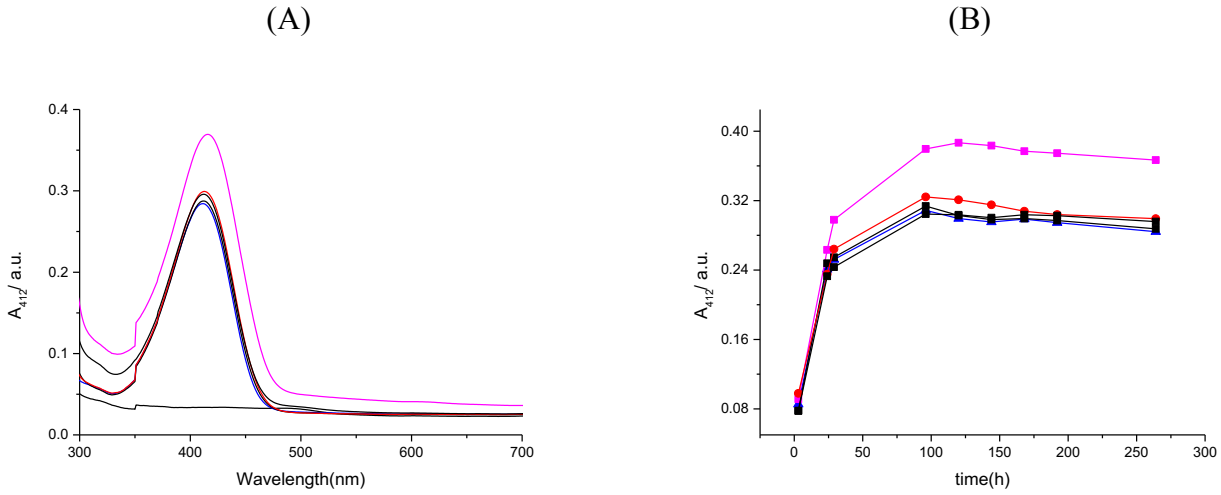

Figure 3.13 (A) post-equilibration UV-visible spectra for **5** with different DNA sequences in buffer (25 mM MOPS, pH 7.0, 50 mM NaCl, 1 mM EDTA), at 25 °C. **(B)** The absorbance of **5** at 412 nm as a function of time, 151 µM FS-DNA (■), 24 µM $(dGdC)_{12}$●$(dGdC)_{12}$ (■), 55 µM $(dAdT)_{12}$●$(dAdT)_{12}$ (●), and buffer (▲).

Figure 3.13A shows a higher absorbance of **5** with FS-DNA. This suggests that **5** has the highest affinity for FS-DNA. There is negligible affinity between **5** and $(dGdC)_{12}$●$(dGdC)_{12}$ and $(dAdT)_{12}$●$(dAdT)_{12}$. Figure 3.13 also shows that equilibrium has been achieved after around 150 hours.

The concentrations and apparent affinities of the ligand after equilibration were determined (Table 3.16).

Table 3.16: Equilibrium constants *K* for 5 [a] interacting with FS-DNA, $(dGdC)_{12}$●$(dGdC)_{12}$ and $(dAdT)_{12}$●$(dAdT)_{12}$ [b]

DNA	FS-DNA	$(dGdC)_{12}$● $(dGdC)_{12}$	$(dAdT)_{12}$● $(dAdT)_{12}$	$(dGdC)_{12}$● $(dGdC)_{12}$	Buffer
$[DNA]_{total}$ / M	1.51×10^{-4}	2.4×10^{-5}	5.5×10^{-5}	2.4×10^{-5}	0
unit conc.	Bp	bp	bp	Bp	/
bind. sites / unit conc. [d]	3.33×10^{-1}	3.33×10^{-1}	3.33×10^{-1}	3.33×10^{-1}	/
$[binding\ sites]_{total}$ / M	5.03×10^{-5}	8.00×10^{-6}	1.83×10^{-5}	8.00×10^{-6}	/
$A_{412\ nm}$	0.3667	0.2875	0.2992	0.2958	0.2842
$A_{412\ nm,bound}$ [c]	0.0905	0.0113	0.023	0.0196	0.008
C_{bound} / M [c]	5.00×10^{-6}	6.25×10^{-7}	1.27×10^{-6}	1.08×10^{-6}	/
$[ligand]_{free}$ / M	1.01×10^{-5}	1.01×10^{-5}	1.01×10^{-5}	1.01×10^{-5}	1.01×10^{-5}
$[binding\ sites]_{free}$ / M	4.53×10^{-5}	7.37×10^{-6}	1.71×10^{-5}	6.92×10^{-6}	/
K / M^{-1}	1.09×10^{4}	8.40×10^{3}	7.39×10^{3}	1.55×10^{4}	/

a) Concentartion of **5** was 15 μM.

b) in buffer (25 mM MOPS, 50 mM NaCl, 1 mM EDTA and pH=7), at 25 °C.

c) A_{bg}, 0.0333, A_{free}, 0.2429, $A412_{reservoir}$ was 0.2762, ε_{free} = 24073 M^{-1} cm^{-1} and ε_{bound} = 18073 M^{-1} cm^{-1}.

d) We assume the binding site size in base pairs is 3.0.

Table 3.16 shows that there is no significant difference between the absorbance of the buffer as control and the absorbance of ligand in the reservoir at λ_{max} 412 nm (the ligand absorbance of reservoir is 0.2762). This means that our device is working well in this experiment. The affinity for FS-DNA 1.09×10^{4} M is in agreement with the results of $(1.18 \pm 0.21) \times 10^{4}$ M from the UV-visible titrations as shown in chapter 2.

3.3.2.b Competition dialysis methods for the quantification of affinities and selectivities for FS-DNA and $(dA)_{24}$ ● $(dT)_{24}$, $(dAdT)_{12}$●$(dAdT)_{12}$ and $(dGdC)_{12}$●$(dGdC)_{12}$.

We repeat the previous experiment above, but this time using similar concentrations of the different DNA sequences in order to find out whether **5** has a high affinity for FS-DNA or for specific sequences such as $(dA)_{24}$ $(dT)_{24}$, $(dAdT)_{12}$●$(dAdT)_{12}$ and $(dGdC)_{12}$●$(dGdC)_{12}$.

A solution of 1.0×10^{-5} M of **5** was exposed to FS-DNA (70 µM), $(dGdC)_{12}$●$(dGdC)_{12}$ (74 µM), $(dA)_{24}$ $(dT)_{24}$ (79 µM) and $(dAdT)_{12}$●$(dAdT)_{12}$ (68 µM). The spectra of **5** after equilibration are shown in Figure 3.14.

(A) (B)

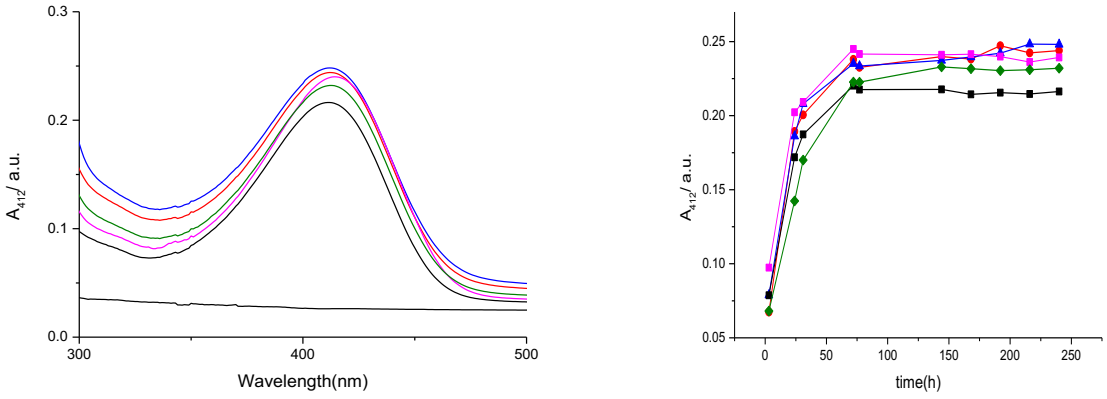

Figure 3.14 (A) UV-visible spectra for **5** exposed to different DNA sequences in buffer (25 mM MOPS, pH 7.0, 50 mM NaCl, 1 mM EDTA), at 25 °C. (B) The absorbance of **5** at 412 nm as a function of time, 70 µM FS-DNA (●), 74 µM $(dGdC)_{12}$●$(dGdC)_{12}$ (▲), 79 µM $(dA)_{24}$ $(dT)_{24}$ (■), buffer (■) and 68 µM $(dAdT)_{12}$●$(dAdT)_{12}$ (♦).

Figure 3.14A shows the absorbance at 412 nm after equilibration in the presence of the various DNA sequences. Figure 3.14B shows that **e**quilibrium has been achieved after around 150 hours.

The concentrations and apparent affinities of the ligand for the different sequences were determined (Table 3.17).

Table 3.17: Equilibrium constants *K* for 5 interacting with FS-DNA, $(dGdC)_{12}$●$(dGdC)_{12}$, $(dA)_{24}$ $(dT)_{24}$ and $(dAdT)_{12}$●$(dAdT)_{12}$ [a]

		$(dGdC)_{12}$●		$(dAdT)_{12}$●	
DNA	**FS-DNA**	**$(dGdC)_{12}$**	**$(dA)_{24}$ $(dT)_{24}$**	**$(dAdT)_{12}$**	**Buffer**
$[DNA]_{total}$ / M	7.0×10^{-5}	7.4×10^{-5}	7.9×10^{-5}	6.8×10^{-5}	0
unit conc.	bp	bp	bp	Bp	/
bind. sites / unit conc. [d]	3.33×10^{-1}	3.33×10^{-1}	3.33×10^{-1}	3.33×10^{-1}	/
$[binding\ sites]_{total}$ / M	2.33×10^{-5}	2.47×10^{-5}	2.63×10^{-5}	2.27×10^{-5}	/
A412, end	0.2409	0.2409	0.2387	0.2322	0.2161
error	0.0018	0.003	0.0039	0.0032	0.0028
$A412_{,\ bound}$ / M [c]	0.0371	0.0371	0.0349	0.0284	0.0123
C_{bound} / M [c]	2.07×10^{-6}	2.08×10^{-6}	1.95×10^{-6}	1.59×10^{-6}	/
$[ligand]_{free}$ / M	7.39×10^{-6}	7.39×10^{-6}	7.39×10^{-6}	7.39×10^{-6}	7.39×10^{-6}
$[binding\ sites]_{free}$ / M	2.13×10^{-5}	2.26×10^{-5}	2.44×10^{-5}	2.11×10^{-5}	/
***K* / M^{-1}**	1.32×10^{4}	1.24×10^{4}	1.08×10^{4}	1.02×10^{4}	/

a) Concentration of **5** was 10 µM.

b) In buffer (25 mM MOPS, 50 mM NaCl, 1 mM EDTA and pH=7), at 25 °C.

c) A_{bg}, 0.0258, A_{free}, 0.178, $A412_{\ reservoir}$ was 0.2038, ε_{free} = 24073 M^{-1} cm^{-1} and ε_{bound} = 17852 M^{-1} cm^{-1}.

d) We assume the binding site size in base pairs is 3.0.

Table 3.17 presents the same affinity of **5** for the sequences FS-DNA, $(dGdC)_{12}$●$(dGdC)_{12}$, $(dA)_{24}$ $(dT)_{24}$ and **(**$(dAdT)_{12}$●$(dAdT)_{12}$. The equilibrium constants are almost the same. The affinity for FS-DNA 1.32×10^{4} M, is in agreement with the results of $(1.18 \pm 0.21) \times 10^{4}$ M from the UV-visible titrations. Our control ($A_{reservoir}$ = 0.2038 and $A_{buffer\ hole}$ = 0.2161, i.e. 94 %) shows that the device works well.

We desired to know whether H33258 (**6**) has affinity for FS-DNA and for specific sequences $(dA)_{24}$ $(dT)_{24}$, $(dAdT)_{12}$●$(dAdT)_{12}$ and $(dGdC)_{12}$●$(dGdC)_{12}$.[172 193]

A solution of 2.4×10^{-6} M of **6** was exposed to FS-DNA (70 µM), $(dGdC)_{12}$●$(dGdC)_{12}$ (74 µM), $(dA)_{24}$ $(dT)_{24}$ (79 µM) and $(dAdT)_{12}$●$(dAdT)_{12}$ (68 µM). The spectra of **6** after equilibration are shown in Figure 3.15.

(A) (B)

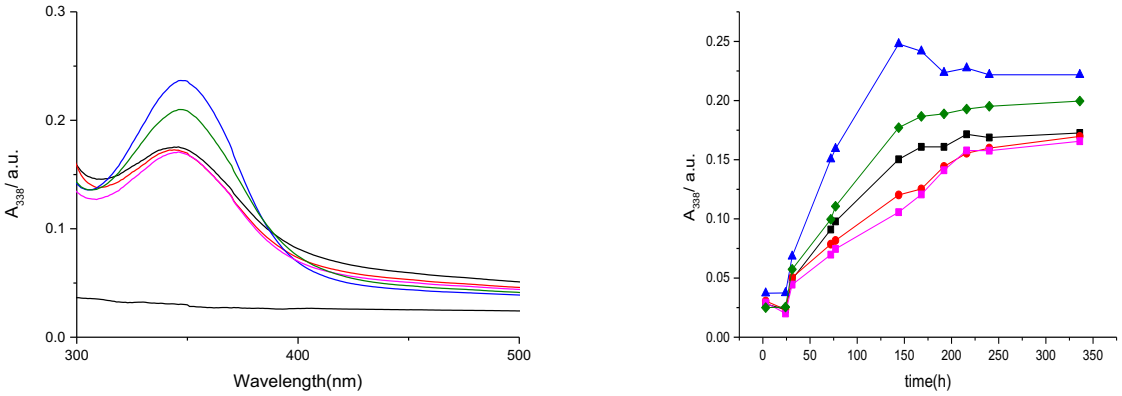

Figure 3.15 **(A)** UV-visible spectra for **6** exposed to different DNA sequences in buffer (25 mM MOPS, pH 7.0, 50 mM NaCl, 1 mM EDTA), at 25 °C. **(B)** The absorbance of **6** at 338 nm as a function of time, 70 µM FS-DNA (■), 74 µM $(dGdC)_{12}$●$(dGdC)_{12}$ (●), 79 µM $(dA)_{24}$ $(dT)_{24}$(▲), 68 µM $(dAdT)_{12}$●$(dAdT)_{12}$ (♦) and buffer (■).

Figure 3.15A and Figure 3.15B suggest that **6** has the highest affinity for $(dA)_{24}$ $(dT)_{24}$(▲). Furthermore, the equilibrium was reached after 300 hours. We cannot offer an explanation as to why $(dA)_{24}$ $(dT)_{24}$(▲) increases and subsequently decreases, but we noted that this behavior was typically only observed for $(dA)_{24}$ $(dT)_{24}$ sequences. We do not know why this is the case.

The concentrations and apparent affinities of the ligand after equilibration were determined (Table 3.18).

Table 3.18: Equilibrium constants *K* for 6 [a] interacting with FS-DNA, $(dGdC)_{12}$●$(dGdC)_{12}$, $(dA)_{24}$ $(dT)_{24}$ and $(dAdT)_{12}$●$(dAdT)_{12}$ [b]

		$(dGdC)_{12}$●		$(dAdT)_{12}$●	
DNA	**FS-DNA**	**$(dGdC)_{12}$**	**$(dA)_{24}$ $(dT)_{24}$**	**$(dAdT)_{12}$**	**buffer**
$[DNA]_{total}$ / M	7.0×10^{-5}	7.4×10^{-5}	7.9×10^{-5}	6.8×10^{-5}	0
unit conc.	bp	bp	bp	bp	/
bind. sites / unit conc. [d]	3.33×10^{-1}	3.33×10^{-1}	3.33×10^{-1}	3.33×10^{-1}	/
$[binding\ sites]_{total}$ / M	2.33×10^{-5}	2.47×10^{-5}	2.63×10^{-5}	2.27×10^{-5}	/
$A_{338,\ end}$	0.2072	0.2345	0.2494	0.2378	0.2738
Error	0.0261	0.0414	0.0211	0.0284	0.091
$A_{338\ bound}$ [c]	0.1646	0.1919	0.2068	0.1952	/
C_{bound} / M [c]	6.32×10^{-6}	7.37×10^{-6}	7.94×10^{-6}	7.50×10^{-6}	/
$[ligand]_{free}$ / M	1.21×10^{-7}	1.21×10^{-7}	1.21×10^{-7}	1.21×10^{-7}	1.21×10^{-7}
$[binding\ sites]_{free}$ / M	1.70×10^{-5}	1.73×10^{-5}	1.84×10^{-5}	1.52×10^{-5}	/
***K* / M^{-1}**	3.06×10^{6}	3.51×10^{6}	3.56×10^{6}	4.07×10^{6}	/

a) Concentration of **6** was 2.4 μM.

b) In buffer (25 mM MOPS, 50 mM NaCl, 1 mM EDTA and pH=7), at 25 °C.

c) A_{bg}, 0.0375, A_{free}, 0.0051, $A338_{\ reservoir}$ was 0.0426, $\varepsilon_{\ free}$ = 42000 M^{-1} cm^{-1} and $\varepsilon_{\ bound}$ = 26030 M^{-1} cm^{-1}.

d) We assume the binding site size in base pairs is 3.0

e) A_{bg} and A_{free} in the beginning were 0.0209 and 0.1013, respectively.

From Table 3.18, there is the same affinity of **6** for different DNA sequences. Unfortunately, our control ($A_{reservoir}$ = 0.0426 and $A_{buffer\ hole}$ = 0.2738, i.e. 61 %) revealed that there was a problem with **6**, which was later attributed to the fading of **6**.

Part C

3.4 Selection of promising ligands for double competition dialysis.

3.4.1 Competition dialysis methods for the quantification of affinities for quadruplex DNA, c-myc and 22AG and specific sequences $(dAdT)_{12}$●$(dAdT)_{12}$ and $(dGdC)_{12}$●$(dGdC)_{12}$.

We wanted to select which ligands have the required selectivity for different DNA structures. We determine the affinity and selectivity of ethidium bromide (**10)** for different sequences of quadruplex and duplex DNA in buffer (25 mM MOPS, pH 7.0, 50 mM NaCl, and 1 mM EDTA), at 25 °C. The spectra of **10** after equilibration with different DNA structures are reported in Figure 3.16.

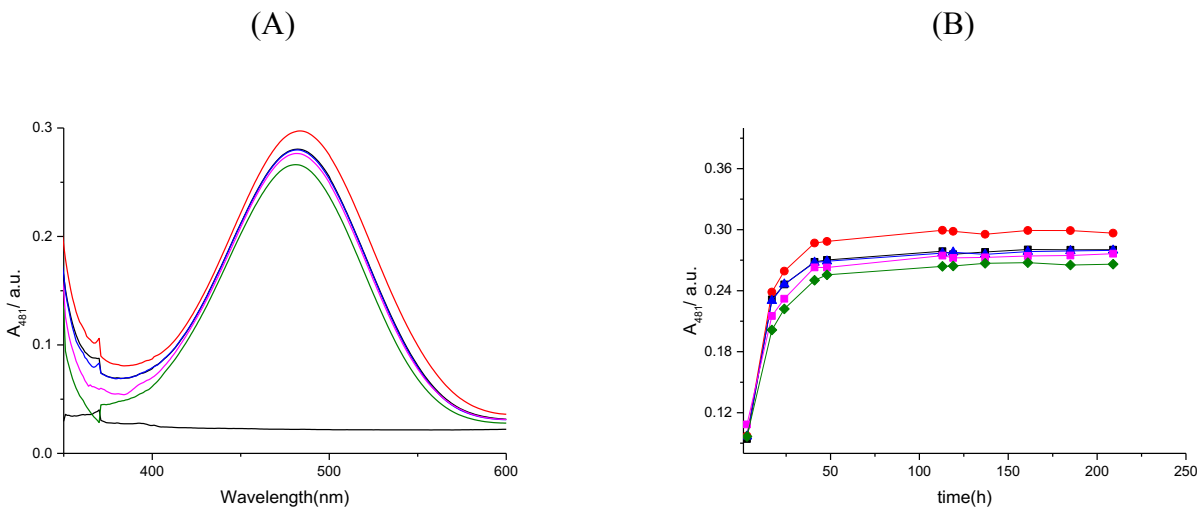

Figure 3.16 (A) UV-visible spectra for **10** after equilibration with 8.7 µM c-myc, 8.6 µM 22AG, and specific duplex forming sequences 33 µM $(dAdT)_{12}$●$(dAdT)_{12}$ and 34 µM $(dGdC)_{12}$●$(dGdC)_{12}$. **(B)** The absorbance of **10** at 481nm as a function of time for DNA, 8.7 µM c-myc (●), 8.6 µM 22AG (■), 33 µM $(dAdT)_{12}$●$(dAdT)_{12}$ (■), 34 µM of $(dGdC)_{12}$●$(dGdC)_{12}$ (▲) and buffer (♦).

Figure 3.16A shows the absorbance of **10** in the presence of the different nucleic acid structures. Compound **10** has a slightly higher absorbance with c-myc. Similarly, Figure 5.16B shows that the absorbance at λ_{max} 481 nm of **10** is slightly higher with c-myc and no

increase in absorbance is seem with 22AG. Moreover, the equilibrium has been achieved after around 100 hours.

The concentrations and apparent affinities of the ligand at equilibrium were determined (Table 3.19).

Table 3.19: Equilibrium constant *K* for 10 [a] interacting with $(dAdT)_{12}$•$(dAdT)_{12}$, c-myc, $(dGdC)_{12}$•$(dGdC)_{12}$, and 22AG [b]

	$(dAdT)_{12}$•		$(dGdC)_{12}$•		
DNA	$(dAdT)_{12}$	c-myc	$(dGdC)_{12}$	22AG	buffer
$[DNA]_{total}$ / M	3.3×10^{-5}	8.7×10^{-6}	3.4×10^{-5}	8.6×10^{-6}	0
unit conc.	bp	quadruplex	bp	quadruplex	/
bind. sites / unit conc. [d,e]	3.33×10^{-1}	3	3.33×10^{-1}	2	/
$[binding\ sites]_{total}$ / M	1.10×10^{-5}	2.61×10^{-5}	1.13×10^{-5}	1.72×10^{-5}	/
A481, end	0.27697	0.2963	0.27583	0.27107	0.26349
Error	0.00161	0.00168	0.00169	0.00374	0.00308
$A481_{,bound}$	0.03347	0.0528	0.03233	0.02757	0.01999
C_{bound} / M	7.52×10^{-6}	1.19×10^{-5}	7.27×10^{-6}	6.2×10^{-6}	/
$[ligand]_{free}$ / M	3.32×10^{-5}	3.32×10^{-5}	3.32×10^{-5}	3.32×10^{-5}	3.32×10^{-5}
$[binding\ sites]_{free}$/ M	3.48×10^{-6}	1.42×10^{-5}	4.07×10^{-6}	1.10×10^{-5}	/
***K* / M^{-1}**	6.52×10^{4}	2.51×10^{4}	5.38×10^{4}	1.70×10^{4}	/

a) Concentration of **10** was 41 µM.

b) In buffer (25 mM MOPS, pH 7.0, 50 mM NaCl, and 1 mM EDTA), at 25 °C.

c) A_{bg}, 0.0213, A_{free}, 0.2222, $A481_{reservoir}$ was 0.2435, $\varepsilon_{free} = 6696\ M^{-1}\ cm^{-1}$ and $\varepsilon_{bound} = 4450\ M^{-1}\ cm^{-1}$.

d) We assume the binding site size in base pairs is 3.0, which means 1 ligand binds to 3 base pairs.

e) We have assumed the binding sites per quadruplex of 22AG is two and we know that the binding sites per quadruplex of c-myc is three.

Table 3.19 shows that **10** has the same affinities for duplex and quadruplex forming sequences. Our control ($A_{reservoir}$ = 0.2435 and $A_{buffer\ hole}$ = 0.2634, i.e. 92 %) shows us that the device works well.

Next, we studied the affinity of **5** for c-myc and 22AG and specific duplex-forming sequences $(dAdT)_{12}$●$(dAdT)_{12}$ and $(dGdC)_{12}$●$(dGdC)_{12}$, in buffer (25 mM MOPS, pH 7.0, 50 mM NaCl, and 1 mM EDTA) at 25 °C. Figure 3.17 shows the spectra for **5** after equilibration.

(A) (B)

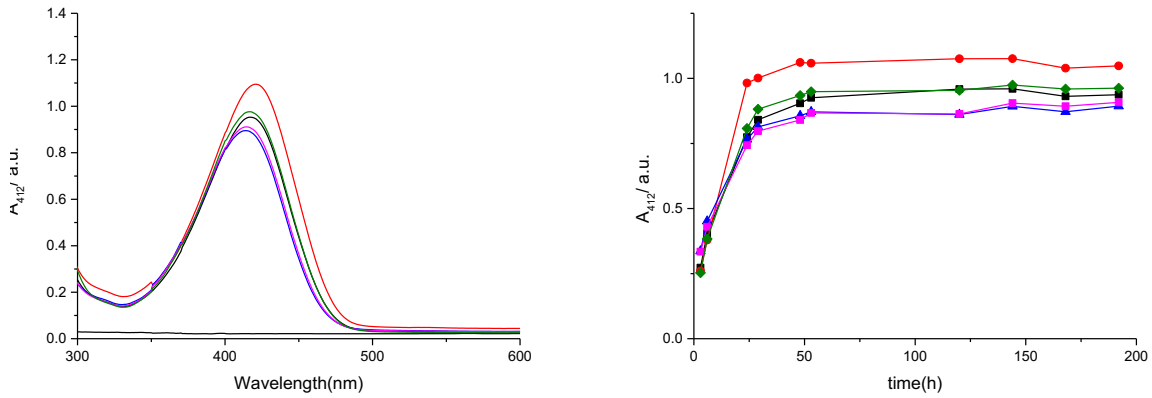

Figure 3.17 (A) UV-visible spectra for **5** with 8.9 µM c-myc, 8.7 µM 22AG, 34 µM $(dAdT)_{12}$●$(dAdT)_{12}$ and 34 µM $(dGdC)_{12}$●$(dGdC)_{12}$. **(B)** The absorbance of **5** at 412 nm as a function of time for 8.9 µM c-myc (●), 8.7 µM 22AG (♦), 34 µM $(dAdT)_{12}$●$(dAdT)_{12}$ (▲), 34 µM $(dGdC)_{12}$●$(dGdC)_{12}$ (■) and buffer (■).

Figure 3.17A shows the absorbance of **5** in the presence of the different DNA structures. It is evident from Figure 3.17B that **5** has a higher affinity for c-myc. The equilibrium has been achieved after around 100 hours.

The concentrations and apparent affinities of the ligand were determined (Table 3.20).

Table 3.20: Equilibrium constants *K* for 5 [a] interacting with c-myc, $(dAdT)_{12}\bullet(dAdT)_{12}$, $(dGdC)_{12}\bullet(dGdC)_{12}$, and 22AG [b]

DNA	c-myc	$(dAdT)_{12}\bullet$ $(dAdT)_{12}$	$(dGdC)_{12}\bullet$ $(dGdC)_{12}$	22AG	buffer
$[DNA]_{total}$ / M	8.9×10^{-6}	3.4×10^{-5}	3.4×10^{-5}	8.7×10^{-6}	0
unit conc.	quadruplex	bp	bp	quadruplex	/
bind. sites / unit conc. [d,e]	2	3.33×10^{-1}	3.33×10^{-1}	2	/
$[binding\ sites]_{total}$ / M	1.78×10^{-5}	1.13×10^{-5}	1.13×10^{-5}	1.74×10^{-5}	/
A412, end	1.0709	0.8643	0.8682	0.9598	0.9353
Error	0.0132	0.01245	0.0169	0.0058	0.0113
$A412_{bound}$	0.283	0.0764	0.0803	0.1719	/
C bound / M	1.58×10^{-5}	4.27×10^{-6}	4.49×10^{-6}	9.62×10^{-6}	/
$[ligand]_{free}$ / M	3.17×10^{-5}	3.17×10^{-5}	3.17×10^{-5}	3.17×10^{-5}	3.17×10^{-5}
$[binding\ sites]_{free}$ / M	1.95×10^{-6}	7.05×10^{-6}	6.84×10^{-6}	7.77×10^{-6}	/
K / M^{-1}	2.57×10^{5}	1.91×10^{4}	2.07×10^{4}	3.91×10^{4}	/

a) Concentration of **5** was 40 μM.

b) in buffer (25 mM MOPS, 50 mM NaCl, 1 mM EDTA and pH=7), at 25 °C.

c) A_{bg}, 0.0241, A_{free}, 0.7638, $A412_{reservoir}$ was 0.7879, $\varepsilon_{free} = 24073\ M^{-1}\ cm^{-1}$ and $\varepsilon_{bound} = 17852\ M^{-1}\ cm^{-1}$.

d) We assume the binding site size in base pairs is 3.0, which means 1 ligand binds to 3 base pairs.

e) We have assumed the binding sites per quadruplex of c-myc and 22AG are two.

Table 3.20 provides the affinities of **5** for quadruplex-forming c-myc and 22AG and for duplex-forming $(dAdT)_{12}\bullet(dAdT)_{12}$ and $(dGdC)_{12}\bullet(dGdC)_{12}$. There is a significant difference between the affinities. For example, **5** has a higher affinity for c-myc than for 22AG. On the other hand, there is no affinity for $(dAdT)_{12}\bullet(dAdT)_{12}$. The control hole suggests that the experiment did not work well; ($A_{reservoir}$ at the end of the experiment was 0.7879 while $A_{buffer\ hole}$ was 0.9353, (i.e. 84 %).

3.4.1.a Competition dialysis methods for the quantification of affinities of 9 for different nucleic acid structures. [194] [195] [194]

The present experiment was designed to determine the affinity of methylene blue (**9**) for quadruplex sequences c-myc and 22AG, and duplex sequences $(dAdT)_{12}$●$(dAdT)_{12}$ and $(dGdC)_{12}$●$(dGdC)_{12}$ in buffer (25 mM MOPS, pH 7.0, 50 mM NaCl, and 1 mM EDTA), at 25 °C. The spectra of **9** after equilibration with different DNA structures are shown in Figure 3.18.

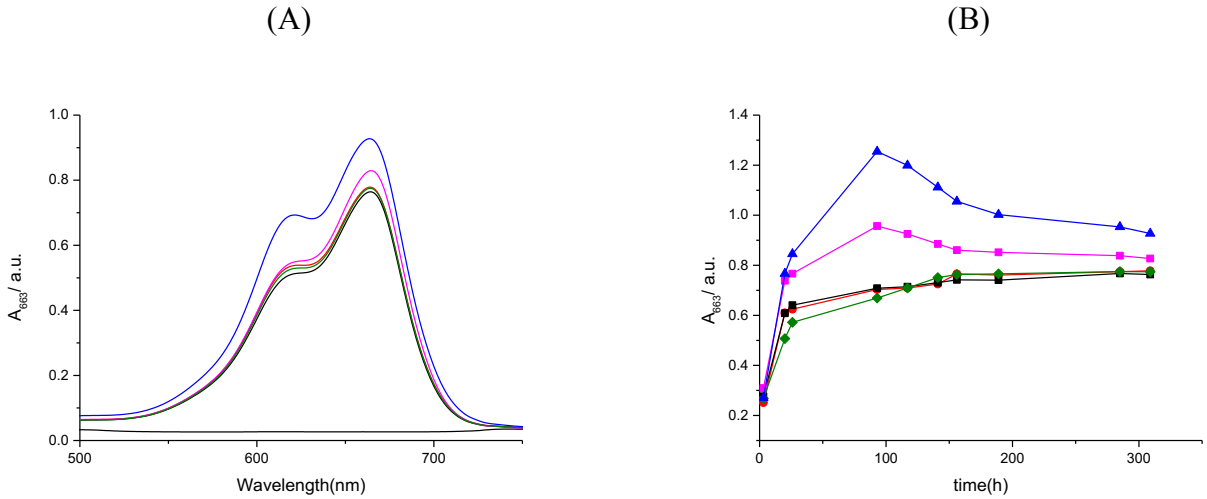

Figure 3.18 (A) UV-visible spectra for **9** with 4.5 µM c-myc, 4.9 µM 22AG, 24 µM $(dAdT)_{12}$●$(dAdT)_{12}$ and 39 µM $(dGdC)_{12}$●$(dGdC)_{12}$. **(B)** The absorbance of **9** at 663nm as a function of time for 4.5 µM c-myc (▲), 4.9 µM 22AG (■), 24 µM $(dAdT)_{12}$●$(dAdT)_{12}$ (■), 39 µM $(dGdC)_{12}$●$(dGdC)_{12}$ (●) and buffer (♦).

Figure 3.18A shows the spectra of **9** after equilibration, the highest absorbance, in the presence of c-myc. Figure 3.18B shows the absorbance at λ_{max} 663 nm of **9** is highest with c-myc. The equilibrium has been achieved after around 300 hours. Surprisingly, the absorbance goes through a maximum after 100 hours, before decreasing again. Again, we cannot explain this, but we noted that this behavior is typically observed only for quadruplex-forming sequences.

The concentrations and apparent affinities of the ligand after equilibrium were determined (Table 3.21).

Table 3.21: Equilibrium constant *K* for 9 [a] interacting with $(dGdC)_{12}$●$(dGdC)_{12}$, $(dAdT)_{12}$●$(dAdT)_{12}$, 22AG and, c-myc [b]

DNA	$(dGdC)_{12}$● $(dGdC)_{12}$	$(dAdT)_{12}$● $(dAdT)_{12}$	22AG	c-myc	buffer
$[DNA]_{total}$ / M	3.9×10^{-5}	2.4×10^{-5}	4.9×10^{-6}	4.5×10^{-6}	0
unit conc.	bp	bp	quadruplex	quadruplex	/
bind. sites / unit conc. [d,e]	3.33×10^{-1}	3.33×10^{-1}	7	6	/
$[binding\ sites]_{total}$ / M	1.30×10^{-5}	8.00×10^{-6}	3.43×10^{-5}	2.70×10^{-5}	/
$A_{663,\ end}$	0.7409	0.732	0.8718	1.0693	0.7418
Error	0.014	0.0131	0.0185	0.0417	0.0213
$A_{663\ bound}$	0.281	0.2721	0.4119	0.6094	0.2819
C_{bound} / M	5.14×10^{-6}	4.98×10^{-6}	7.54×10^{-6}	1.11×10^{-5}	/
$[ligand]_{free}$ / M	5.56×10^{-6}	5.56×10^{-6}	5.56×10^{-6}	5.56×10^{-6}	5.5×10^{-6}
$[binding\ sites]_{free}$ / M	7.86×10^{-6}	3.02×10^{-6}	2.68×10^{-5}	1.58×10^{-5}	/
K / M^{-1}	1.18×10^{5}	2.96×10^{5}	5.06×10^{4}	1.26×10^{5}	/

a) Concentration of **9** was 8.1 µM.

b) In buffer (25 mM MOPS, 50 mM NaCl, 1 mM EDTA and pH 7), at 25 °C.

c) A_{bg}, 0.0255, A_{free}, 0.4344, $A663_{\ reservoir}$ was 0.4599, $\varepsilon_{\ free} = 78000\ M^{-1}\ cm^{-1}$ and $\varepsilon_{\ bound} = 54618\ M^{-1}\ cm^{-1}$.

d) We assume the binding site size in base pairs is 3.0.

e) We know the binding sites per quadruplex of 22AG is seven and six for c-myc.

Table 3.21 shows that the affinity of **9** is for $(dAdT)_{12}$●$(dAdT)_{12}$ with a binding constant of $2.96\times10^{5}\ M^{-1}$. The lowest affinity of **9** is for 22AG. Unfortunately, our control ($A_{reservoir}$ = 0.4599 and $A_{buffer\ hole}$ = 0.7418, i.e. 61 %) shows us that there is a problem with **9**. This problem was later attributed to the fading of **9**.

We repeated the experiment and recorded the spectra of **9** after equilibration with different DNA sequences are shown in Figure 3.19.

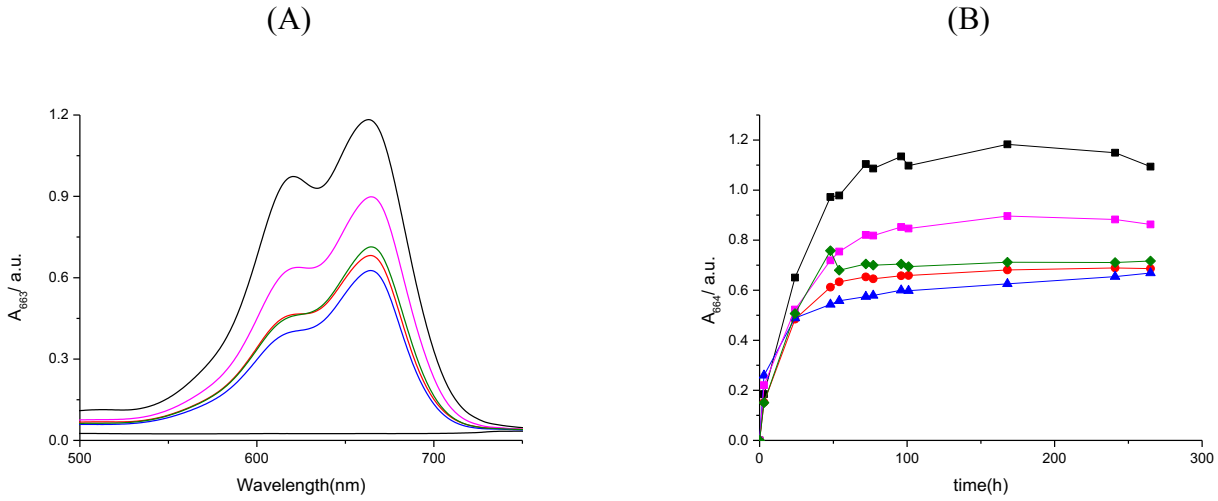

Figure 3.19 (A) UV-visible spectra for **9** with c-myc 5.6 µM, 22AG 6 µM, and specific sequences such as, $(dAdT)_{12}$●$(dAdT)_{12}$ 40 µM and 40 µM $(dGdC)_{12}$●$(dGdC)_{12}$. **(B)** The absorbance of **9** at 663 nm as a function of time for 5.6 µM (■) c-myc, 6 µM 22AG (■), 40 µM $(dAdT)_{12}$●$(dAdT)_{12}$ (●), 40 µM $(dGdC)_{12}$●$(dGdC)_{12}$ (♦) and buffer (▲).

Figure 3.19A shows the spectra of **9** at λ_{max} 663 nm with the highest absorbance for the hole containing c-myc. It is apparent from B that the equilibrium has been achieved after around 200 hours. We also note that the maximum in absorbance observed in the previous experiment has now disappeared. The absorbance at λ_{max} 663 nm suggests that **9** has the highest affinity for c-myc, but this needs to be confirmed taking nucleic acid concentrations into account in the determination of the apparent affinities. The concentrations and apparent affinities of the ligand were determined (Table 3.22).

Table 3.22: Equilibrium constants *K* for 9 [a] interacting with c-myc, $(dAdT)_{12}\bullet(dAdT)_{12}$, (22AG) and $(dGdC)_{12}\bullet(dGdC)_{12}$ [b]

DNA	c-myc	$(dAdT)_{12}\bullet$ $(dAdT)_{12}$	22AG	$(dGdC)_{12}\bullet$ $(dGdC)_{12}$	buffer
$[DNA]_{total}$ / M	5.6×10^{-6}	4.0×10^{-5}	6.0×10^{-6}	4.0×10^{-5}	0
unit conc.	quadruplex	bp	quadruplex	bp	/
bind. sites / unit conc. [d,e]	6	3.33×10^{-1}	7	3.33×10^{-1}	/
$[binding\ sites]_{total}$ / M	3.36×10^{-5}	1.33×10^{-5}	4.20×10^{-5}	1.33×10^{-5}	/
A663, end	1.1483	0.6717	0.8729	0.7153	0.5922
Error	0.0156	0.0062	0.0172	0.0124	0.0165
$A663_{bound}$	0.7529	0.2763	0.4775	0.3199	0.1968
C_{bound} / M	1.37×10^{-5}	5.06×10^{-6}	8.74×10^{-6}	5.86×10^{-6}	/
$[ligand]_{free}$ / M	4.73×10^{-6}	4.74×10^{-6}	4.74×10^{-6}	4.74×10^{-6}	4.74×10^{-6}
$[binding\ sites]_{free}$ / M	1.98×10^{-5}	8.27×10^{-6}	3.33×10^{-5}	7.48×10^{-6}	/
K / M^{-1}	1.47×10^{5}	1.29×10^{5}	5.55×10^{4}	1.65×10^{5}	/

a) Concentration of **9** was 7.7 µM.

b) In buffer (25 mM MOPS, 50 mM NaCl, 1 mM EDTA and pH=7), at 25 °C.

c) A_{bg}, 0.0258, A_{free}, 0.3696, $A663_{reservoir}$ was 0.3954, ε_{free} = 78000 M^{-1} cm^{-1} and ε_{bound} = 54618 M^{-1} cm^{-1}.

d) We assume the binding site size in base pairs is 3.0.

e) We know the binding sites per quadruplex of 22AG is seven and six for c-myc.

Table 3.22 presents the affinities of **9** for different nucleic acid sequences and confirms Table 20. Compound **9** has the highest affinity toward $(dGdC)_{12}\bullet(dGdC)_{12}$. The results are in agreement with the results from the UV-visible titrations as shown in Chapter 2 which gave $K_{binding}$ of (5.25 ± 7.79) $\times10^{6}$ M^{-1} with c-myc and $K_{binding}$ of (5.95 ± 7.64) $\times10^{4}$ M^{-1} with 22AG. Similarly, the result of Table 5.22 is also in reasonable agreement with Table 5.21. However, the control hole clearly shows a problem again; our control ($A_{reservoir}$ = 0.3954 and $A_{buffer\ hole}$ = 0.5922, i.e. 66 %). This problem was later attributed to the fading of **9** as discussed in Chapter 2.

A recent study suggested that **9** interacts with quadruplex EAD2. We therefore repeated the competition dialysis of **9** in buffer (25 mM MOPS, pH 7.0, 100 mM KCl, and 1 mM EDTA) but using EAD2 instead of c-myc and in a buffer containing KCl instead of NaCl buffer because potassium chloride is widely accepted to stabilise G-quadruplex structures. [196, 197, 198] The spectra of **9** after equilibration with the different DNA structures are shown in Figure 3.20.

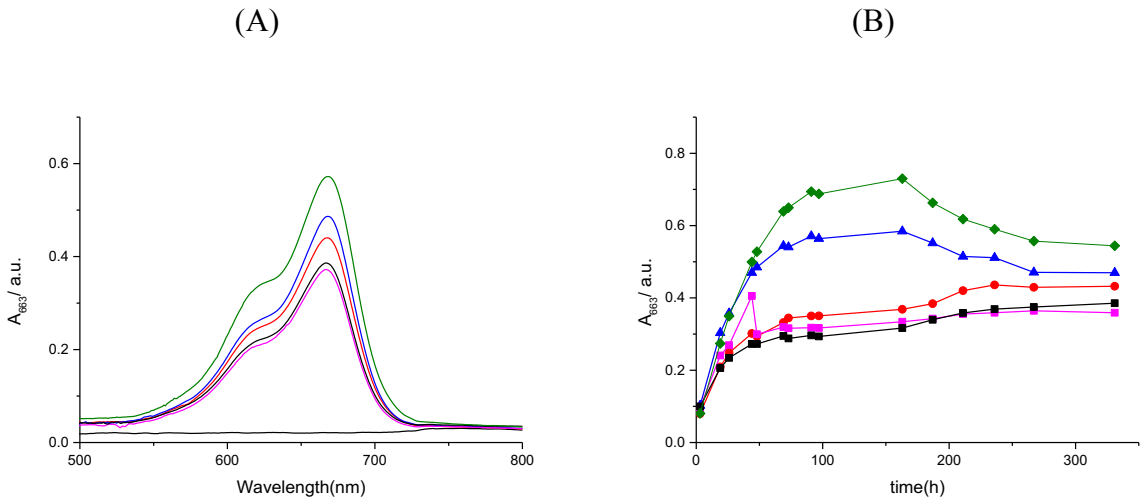

Figure 3.20 (A) UV-visible spectra for **9** after equilibration with 10 µM EAD2, 10 µM 22AG, 39 µM $(dAdT)_{12}$●$(dAdT)_{12}$ and 32 µM $(dGdC)_{12}$●$(dGdC)_{12}$. **(B)** The absorbance of **9** at 663 nm as a function of time for 10 µM (♦) EAD2, 10 µM 22AG (▲), 39 µM $(dAdT)_{12}$●$(dAdT)_{12}$ (●), 32 µM of $(dGdC)_{12}$●$(dGdC)_{12}$ (■) and buffer (■).

Figure 3.20A shows the spectra of **9** and the highest absorbance is observed with EAD2. It is apparent from B that the equilibrium has been achieved after around 355 hours, but surprisingly the absorbance has gone through a maximum again.

The concentrations and apparent affinities of **9** for the different nucleic acid structures were determined (Table 3.23).

Table 3.23: Equilibrium constants *K* for 9 [a] interacting with $(dAdT)_{12}$●$(dAdT)_{12}$, 22AG, $(dGdC)_{12}$●$(dGdC)_{12}$, and EAD2 [b]

	$(dAdT)_{12}$●		$(dGdC)_{12}$●		
DNA	**$(dAdT)_{12}$**	**22AG**	**$(dGdC)_{12}$**	**EAD2**	**buffer**
$[DNA]_{total}$ / M	3.9×10^{-5}	1.0×10^{-5}	3.2×10^{-5}	1.0×10^{-5}	0
unit conc.	bp	quadruplex	bp	quadruplex	/
bind. sites / unit conc. [d,e]	3.33×10^{-1}	7	3.33×10^{-1}	3	/
$[binding\ sites]_{total}$ / M	1.30×10^{-5}	7.00×10^{-5}	1.07×10^{-5}	3.00×10^{-5}	0
A663, end	0.3985	0.5438	0.3402	0.6593	0.3344
Error	0.0107	0.0121	0.01	0.0227	0.011
$A663_{bound}$	0.2067	0.352	0.1484	0.4675	0.1426
C_{bound} / M	3.78×10^{-6}	6.44×10^{-6}	2.72×10^{-6}	8.56×10^{-6}	/
$[ligand]_{free}$ / M	2.24×10^{-6}	2.24×10^{-6}	2.24×10^{-6}	2.24×10^{-6}	2.24×10^{-6}
$[binding\ sites]_{free}$ / M	9.22×10^{-6}	6.36×10^{-5}	7.95×10^{-6}	2.14×10^{-5}	/
K / M^{-1}	1.83×10^{5}	4.52×10^{4}	1.52×10^{5}	1.78×10^{5}	/

a) Concentration of **9** was 3.2 μM.

b) In buffer (25 mM MOPS, pH 7.0, 100 mM KCl, and 1 mM EDTA), at 25 °C.

c) A_{bg}, 0.0167, A_{free}, 0.1751, $A663_{reservoir}$ was 0.1918, $\varepsilon_{free} = 78000\ M^{-1}\ cm^{-1}$ and $\varepsilon_{bound} = 54618\ M^{-1}\ cm^{-1}$.

d) We assume the binding site size in base pairs is 3.0.

e) We know the binding sites per quadruplex of 22AG is seven and three for EAD2.

Table 3.23 shows that **9** has very high affinity for $(dAdT)_{12}$●$(dAdT)_{12}$ with binding constant of $1.83\times10^{5}\ M^{-1}$, in agreement with the previous two experiments. Affinity for EAD2 was also high, albeit not as high as expected. However, the absorbance of the control does not match with the absorbance of **9** in the reservoir (57% recovery). This problem was later attributed to the fading.

To find out whether the results are reproducible, we repeated the experiment, replacing $(dGdC)_{12}$●$(dGdC)_{12}$ with c-myc. The spectra of **9** after equilibration with different DNA sequences are shown in Figure 3.21.

(A) (B)

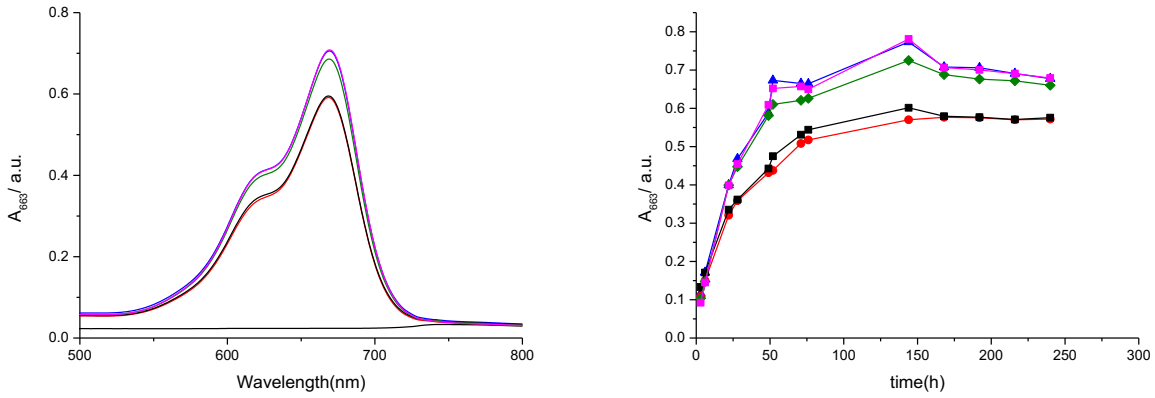

Figure 3.21 (A) UV-visible spectra for **9** after equilibration with EAD2, 22AG, c-myc and $(dAdT)_{12}$●$(dAdT)_{12}$ **(B)** The absorbance of **5.9** at 663nm as a function of time for 10 µM EAD2 (♦), 10 µM 22AG (▲), 10 µM c-myc (■), 39 µM $(dAdT)_{12}$●$(dAdT)_{12}$ (●), and buffer (■).

Figure 3.21A shows the spectra of **9** following equilibration. A higher absorbance is observed with c-myc and 22AG. It is apparent from B that the equilibrium has been achieved after around 240 hours. The absorbance at λ_{max} 663 nm of **9** suggests affinity toward quadruplexes sequences c-myc, 22AG and EAD2. The concentrations and apparent affinities of **9** were determined (Table 3.24).

Table 3.24: Equilibrium constants *K* for 9 [a] interacting with 22AG, $(dAdT)_{12}$●$(dAdT)_{12}$, EAD2 and c-myc[b]

DNA	22AG	$(dAdT)_{12}$● $(dAdT)_{12}$	EAD2	c-myc	buffer
$[DNA]_{total}$ / M	1.0×10^{-5}	3.9×10^{-5}	1.0×10^{-5}	1.0×10^{-5}	0
unit conc.	Quadruplex	bp	quadruplex	quadruplex	/
bind. sites / unit conc. [d,e]	7	3.33×10^{-1}	3	6	/
$[binding\ sites]_{total}$ / M	7.00×10^{-5}	1.30×10^{-5}	3.00×10^{-5}	6.00×10^{-5}	0
A663, end	0.7107	0.5692	0.6810	0.7114	0.5773
Error	0.0105	0.0088	0.0794	0.0113	0.011
$A663_{bound}$	0.498	0.3565	0.4683	0.4987	0.3646
C bound / M	9.11×10^{-6}	6.53×10^{-6}	8.57×10^{-6}	9.13×10^{-6}	/
$[ligand]_{free}$ / M	2.44×10^{-6}	2.44×10^{-6}	2.44×10^{-6}	2.44×10^{-6}	2.44×10^{-6}
$[binding\ sites]_{free}$ / M	6.09×10^{-5}	6.47×10^{-6}	2.14×10^{-5}	5.09×10^{-5}	/
K / M^{-1}	6.13×10^{4}	4.13×10^{5}	1.64×10^{5}	7.35×10^{4}	/

a) Concentration of **9** was 4.3 μM.

b) In buffer (25 mM MOPS, pH 7.0, 100 mM KCl, and 1 mM EDTA), at 25 °C.

c) A_{bg}, 0.0221, A_{free}, 0.1906, $A663_{reservoir}$ was 0.2127, ε_{free} = 78000 M^{-1} cm^{-1} and ε_{bound} = 54618 M^{-1} cm^{-1}.

d) We assume the binding site size in base pairs is 3.0.

e) We know the binding sites per quadruplex of 22AG is seven and three for EAD2 and six for c-myc.

From Table 3.24, it is still clear that **9** has high affinity for $(dAdT)_{12}$●$(dAdT)_{12}$. However, compound **9** also has high affinity for EAD2. However, our control ($A_{reservoir}$ = 0.2127 and $A_{buffer\ hole}$ = 0.5773 i.e. 36 %) shows us there is once more a problem with **9**. This problem was later attributed to the fading of **9**.

3.5 Conclusion

The result of the traditional approach to dialysis methods for the quantification of affinities for FS-DNA produces results that are similar to those from UV-visible titrations. The average value for the equilibrium constant of **9** without co-solvent ($K_{binding}$) is (8.5 ± 2.22) × 10^4 M^{-1}. The result is in reasonable agreement with the results from the UV-visible titrations, as shown in Chapter 2, which gave $K_{binding}$ of (3.83 ± 0.78) ×10^5 M^{-1}. The average equilibrium constant of **9** in the presence of 9 vol-% DMSO ($K_{binding}$) is (4.42 ± 0.80) × 10^4 M^{-1}. The result is in reasonable agreement with the results from the UV-visible titrations, as shown in Chapter 2, which gave $K_{binding}$ of (8.5 ± 1.35) ×10^4 M^{-1}. It clearly shows that DMSO can affect the binding of hydrophobic compounds to DNA. However, use of 9 vol-% DMSO is sufficient to reduce any ligand precipitation as we have shown in Chapter 2. Therefore, we preferred more diluted solutions of compounds to avoid precipitation of the ligand.

We have successfully developed a device that allows us to study affinities using dialysis in an easy way. The final test for our method and our device involves a compound that shows no binding to DNA, viz. anionic **3**, with different concentrations of FS-DNA. The result is in agreement with the results from the UV-visible titrations as shown in chapter 4, which was (0.66 ± 2.34) ×10^2 M^{-1}. The competition dialysis assay has been successfully used.

We found optimal experimental conditions for the competition dialysis for promising ligands such as **5** and **10** for the quantification of affinities for quadruplex DNA c-myc and 22AG and specific sequences $(dAdT)_{12}$●$(dAdT)_{12}$ and $(dGdC)_{12}$●$(dGdC)_{12}$. Compound **5** has a high affinity toward c-myc 2.57×10^5 M^{-1}. Moreover, **10** has the same affinities to duplex and quadruplex forming sequences which is ~ 10^4 M^{-1}. On the other hand, problems with unpromising ligands such as **9** were later attributed to the fading. Compound **9** shows a higher affinity for $(dAdT)_{12}$●$(dAdT)_{12}$ gives a binding constant of 2.96×10^5 M^{-1} and binding to $(dGdC)_{12}$●$(dGdC)_{12}$ is accompanied by a binding constant of 1.65×10^5 M^{-1}. The results are in agreement with the results from the UV-visible titrations as shown in Chapter 4 which gives $K_{binding}$ of (5.25 ± 7.79) ×10^6 M^{-1} with c-myc and $K_{binding}$ of (5.95 ± 7.64) ×10^4 M^{-1} with 22AG. Moreover, our control shows that this device works well with promising compounds such as **5** and **10**. However, our control shows us there is a problem related to the stability of the ligand of **9** as we mentioned that before.

3.6 Materials and Methods

3.6.1 Buffer preparation

All experiments were carried out in one of 3 buffers. Buffer A contained 25 mM MOPS, 50 mM NaCl and 1 mM EDTA, pH 7.0; buffer B contained 25 mM MOPS, 50 mM NaCl, 1 mM EDTA and 9 vol-% of DMSO, pH 7.0; buffer C contained 25 mM MOPS, 100 mM KCl and 1 mM EDTA, pH 7.0. The buffer components were purchased from Melford (CAS 1132-61-2), NaCl was purchased from Fisher Scientific (CAS 7647-14-5), KCl was purchased from Sigma Aldrich (CAS 7447-40-7), EDTA was purchased from VWR (CAS 60-00-4) and DMSO from Fisher Scientific (CAS 67-68-5). Buffers were titrated with aqueous NaOH and KOH to the required pH. The pH of aqueous solutions was determined using a Hanna microprocessor pH 113 pH-meter equipped with a VWR 662-1382 glass electrode. Materials were weighed out on a Fisherbrand 4-decimal balance. De-ionised water was produced using an ELGA water purifier for all solutions.

Buffer A, containing 25 mM MOPS (3-(N-morpholino) propanesulfonic acid) and 50 mM sodium chloride (NaCl) was prepared by dissolving MOPS and sodium chloride (NaCl) in distilled water and stirring at room temperature until the solid dissolved. The solution of sodium hydroxide (NaOH) was used for adjusting the pH to 7.0 and the buffer was made up to 2 liters.

Buffer B containing 25 mM MOPS (3-(N-morpholino) propanesulfonic acid), 50 mM sodium chloride (NaCl) and 1 mM EDTA was prepared by dissolving MOPS, sodium chloride (NaCl) and EDTA in distilled water and stirring at room temperature until the solid dissolved. 9 vol-% of DMSO was add to the buffer solution. Sodium hydroxide (NaOH) was used for adjusting the pH to 7.0 and the buffer was made up to 2 liters.

Buffer C, containing 25 mM MOPS (3-(N-morpholino) propanesulfonic acid) and 100 mM potassium chloride (KCl) was prepared by dissolving MOPS and potassium chloride (KCl) in distilled water and stirring at room temperature until the solid dissolved. Potassium hydroxide (KOH) was used for adjusting the pH to 7.0 and the buffer was made up to 2 liters.

3.6.2 DNA preparation

Fish sperm DNA was purchased from Acros Organics (CAS 68938-01-2). The stock solution of fish sperm DNA was prepared by dissolving the DNA in buffer and then sonicating the suspension of FS-DNA for about 10 minutes to get a homogeneous solution. All DNA

solutions were dialysed against buffer. The dialysis process for the DNA solution was carried out by taking the DNA solution and placing it into the dialysis tube of appropriate pore size (3.5 kDa MWCO).[189] The dialysis tube was suspended for 24 hours inside a beaker that contains the MOPS buffer until the impurities were completely diffused out. The DNA concentrations were determined from the absorbance using the extinction coefficient of FS-DNA of 12800 M^{-1} cm^{-1} in terms of base pair molarity as recorded using UV-visible spectroscopy at 260 nm.[190]

The concentration of c-myc (dTdGdA dGdGdG dTdGdG dGdTdT dGdGdG dTdGdG dGdTdAdA) was determined using UV-visible spectroscopy in terms of quadruplex molarity by using the extinction coefficient of 228700 M^{-1} cm^{-1} at 260 nm. The concentration of 22AG (dAdGdG dGdTdT dAdGdG dGdTdT dAdGdG dGdTdT dAdGdGdG) was determined using UV-visible spectroscopy in terms of quadruplex molarity using the extinction coefficient of 228500 M^{-1} cm^{-1} at 260 nm.[76] The concentration of EAD2 (CTG-GGA-GGG-AGG-GAG-GGA) was determined using UV-visible spectroscopy in terms of quadruplex molarity by using the extinction coefficient of 189900 M^{-1} cm^{-1} at 260 nm.[181]

For the double-stranded synthetic DNA, i.e. poly (dAdT) and poly (dGdC), we dissolve each sequence in 1 ml of buffer. Then, the dialysis process for the DNA solution was carried out by taking the DNA solution and placing it into dialysis tubing of sufficient pore size (3.5 kDa MWCO). The dialysis tube was suspended for 24 hours inside a beaker that contains the MOPS buffer until the impurities were completely diffused out. The DNA concentration was determined using UV-visible spectroscopy in terms of base pair molarity using the extinction coefficient of 14800 M^{-1} cm^{-1} at 254 nm for poly (dGdC) and of 12000 M^{-1} cm^{-1} at 260 nm for poly (dAdT).[127] Then the DNA solutions were annealed placing each DNA solution into an Eppendorf and placing the Eppendorf in a beaker that contains water at 95 °C, allowing to cool down and finally determine the concentration of each solution.

For single-stranded DNA such as poly (dA) and poly (dT), we dissolve each sequence in 1 ml of buffer in (25 mM MOPS, 50 mM NaCl, 1 mM EDTA and 9 vol-% of DMSO, pH 7.0, at 25 °C). The dialysis process for the DNA solution was carried out by taking the DNA solution and placing it into the dialysis tube of sufficient pore size (3.5 kDa MWCO). The dialysis tube was suspended for 24 hours inside a beaker that contains the MOPS buffer until the impurities were completely diffused out. The DNA concentration was determined using UV-visible spectroscopy and using the extinction coefficient of 8600 M^{-1} cm^{-1} at 257 nm for

single-stranded $(dA)_{24}$ and 8520 M^{-1} cm^{-1} at 264 nm for single stranded of $(dT)_{24}$. We then mixed both sequences to have a 1:1 mixture of strands in an Eppendorf. The duplex was annealed by placing the Eppendorf in a beaker that contains water at 95 °C and allowing to cool down. Finally, the concentration of each solution was determined using UV-visible spectroscopy in terms of base pair molarity using the extinction coefficient of 12000 M^{-1} cm^{-1} at 260 nm for poly (dA) ●poly (dT).[127]

3.6.3 Dialysis units

Dialysis using dialysis tubing was carried out by taking the DNA solution and placing it into the dialysis tube of sufficient pore size (3.5 kDa MWCO). The dialysis tube was suspended for 24 hours inside a beaker that contains the MOPS buffer until the impurities were completely diffused out. The dialysis tubing was purchased from Medicell Membranes Ltd, MWCO 12-14000 Daltons. Dialysis membrane was also purchased from Medicell Membranes Ltd, (MWCO 3500 Daltons) and was used for the dialysis device, in the middle part of the device.[124]

3.6.4 Competition dialysis data analysis.

For duplex DNA, $[DNA]_{total}$ is the DNA concentration of FS-DNA, $(dAdT)_{24}$ and $(dGdC)_{24}$ in terms of base pairs. For quadruplex DNA, $[DNA]_{total}$ equals the concentration of quadruplex structures such as c-myc, 22AG and EAD2 (i.e. not in terms of quartets). Depending on the unit of DNA concentrations, we use a binding site size (if the concentrations are in units of bp for duplex DNA) or a stoichiometry in units of $quadruplex^{-1}$ for the different quadruplexes.

We expressed the binding site size in term of base pairs and this was typically set to 3.0, which means 1 ligand binds to 3 base pairs. For the quadruplexes we have typically assumed two binding sites per quadruplex structure. For **9**, we knew the number of binding sites per quadruplex for c-myc, 22AG and EAD2 (Chapter 4). The stoichiometries are 6 ligands per quadruplex of c-myc, 7 ligands per quadruplex of 22AG and 3 ligands per quadruplex of EAD2.

The total concentration of binding sites in solution is given as follows;

$[binding\ sites]_{total}$ is defined as "binding sites per unit concentration" × the total concentration of DNA in the selected unit of concentration.

A is the ligand absorbance observed at a specific wavelength (λ_{max})

A_{bound} is given by:

$A_{bound} = A_{obs}-(A_{bg}+A_{free})$

$A_{obs} = A_{bg}+A_{free}+A_{bound}$

$A_{obs}= A_{bg}+ \varepsilon_{free} \times c_{free} \times l + \varepsilon_{bound} \times c_{bound} \times l$

$A_{obs}-(A_{bg}+A_{free}) = \varepsilon_{bound} \times c_{bound} \times l$

Subsequently:

$A_{obs}-(A_{bg}+A_{free})$

A_{obs} is the observed signal for the ligand

A_{bg} is the background signal or the buffer absorbance

A_{free} is the difference (A_{obs} - A_{bg})

We can determine $[ligand]_{bound}$ from A_{bound} / $epsilon_{bound} \times$ pathlength

$ligand_{free} = A_{free}$ / $epsilon_{free} \times$ pathlength

$[binding\ site]_{free}$ is given by:

$[binding\ site\ size]_{free} = [binding\ site\ size]_{total} - [ligand]_{bound}$

To calculate *K* value:

$K = [ligand]_{bound} / [ligand]_{free} \times [binding\ sites]_{free}$

The absorption is plotted against time to obtain the optimal approximation for $signal_{end}$ and k_{obs} from the best fit of a pseudo-first-order kinetic rate model to the data [199] (Equation 1).

$(signal_{start} - signal_{end}) \times \exp(-1 \times k_{obs} \times time) + signal_{end}$

$(\Delta A)\ e^{-kobst \times t} + signal_{end}$ Equation 1

The terms in the equation are defined as follows.

ΔA is the difference between the ligand absorbance and the buffer absorbance, k_{obs} is the observed pseudo-first-order rate constant, *t* is defined as the time in hours.

3.7 Equipment

3.7.1 Spectroscopic studies

UV-visible spectra were recorded using a Jasco V-630BIO spectrophotometer with a Peltier temperature controller at 25 °C. All UV-visible absorbances were determined using a 1.0 cm path length cuvette at 25 °C, except for experiments involving **9** (in tables 5.1 and 5.2) where experiments were carried out in a 1 mm path length cuvette. The ligand concentrations were determined using the extinction coefficient.

Chapter 4

Double competition dialysis studies

Abstract

In this Chapter, we explore how double competition dialysis allows simultaneous screening of two potentially competing ligands against an array of nucleic acids structures. We describe how couples of ligands are selected for screening based on selectivity, optical emission, absorption and stability. The use of a control buffer allows facile identification of problematic experiments. Several of the tested compounds [TF1 ***(8)****, methylene blue (****9****), thiazole orange (****12****) and DODC (****13****)] fade upon exposure to light and we show that our assay deals with this reasonably well unless fading progresses to the extent that absorbances become too low to measure reliably. Although we have identified individual compounds with interesting affinity profiles, even in the presence of a second binder, we have not yet identified a couple of binders with the orthogonal selectivity profile required for construction of a self-assembled nanostructure.*

4.1 Introduction

The G-Quadruplex structures are able to protect the internal sequences of the chromosomes.[200] Research of functions and structure of G-quadruplexes intensified since discovery of G-quadruplexes and G-tetraplexes telomeric DNA.[201] This is due to the fact that these structures are substrates for telomerase, therefore stabilizers of quadruplex can antitumor action as shown in Chapter 1.[202, 203]

Scientists have explored the use of small ligands which target the nucleic acids for example as future therapeutic agents. In a sequence-specific manner, duplex groove binding molecules can recognize DNA during the binding process. On the side of quadruplex-binding ligands, some molecules show a degree of selectivity between G-quadruplex and duplex DNA.[204, 205,206]

4.1.1 Competition dialysis

Competition dialysis is a powerful tool for studying ligand binding selectivity.[125] We explore how double competition dialysis allows screening of two ligands against an array of nucleic acids structures.

4.1.2 Double competition dialysis as a high throughput tool for identifying orthogonal host-guest pairs.

Double competition dialysis is very similar to competition dialysis but we will use multiple ligands simultaneously. A few examples of simultaneous binding to nucleic acid structures have been reported in the literature. These will be discussed briefly.

4.1.2a Simultaneous binding of a groove binder and an intercalator to a duplex DNA.

Hoechst 33258 (H33258) and ethidium bromide (EtBr) are widely used fluorescent cytological stains.[207] The literature suggests that resonance energy transfer (FRET) could occur between H33258 (donor) and EtBr (acceptor). H33258 and ethidum bromide area minor groove binder and an intercalator, respectively. H33258 and EtBr bind to DNA.[205, 208, 209] the application of X-ray crystallography, NMR analysis, Raman and spectroscopy in combination with theoretical calculations have shown that the specific binding of the molecules are very much sensitive to the polarity environment.[210] Simultaneous binding ligands to DNA may find application in drug design because it provides an opportunity to maintain molecular weights low (thus fitting with Lipinski's rules). FRET has been used to study the distance between the bound ligand, H33258 (donor) and EtBr (acceptor) in genomic

DNA. To explain more, the minor groove binding of the H33258 and the intercalation by the EtBr have the capability to take place independently in a particular site of the dodecamer. When bound to DNA H33258 and ethidum bromide have their transition dipoles oriented at an angle of about 66 degrees. The majority of the acceptor molecules are placed at a distance of around 0.92nm from the donor in the central position of the DNA. A smaller number of acceptors are intercalated in the end of the dodecamer at a distance of 1.92nm. Different types of DNA offer binding sites of binding nature. The two types of genomic DNA are separated with the help of the base pair with a persistence length or a formation of a loop at a distance of 3.3nm. The calculated value of the orientation parameter of 0.04 is very important for the estimation of the distance between the donor and the acceptor which are bound to the dodecamer. [211] The application of the value of the orientation parameter allows for the random distribution of an acceptor. At the same time it can be concluded that DNA partially restricts the effective distribution of the acceptors and these restrictions can lead to different kinds of errors in the final analyses.[211]

4.1.2b System combining a groove binder and a quadruplex binder.

To provide more direct evidence for the existence of quadruplex structures, fluorescent signal detection with potential G-quadruplex targeting fluorophores can be used to make the structures visible under fluorescence microscopy. The fluorescent image detection method is popular because of its convenience and visibility. For this method, it is important to have a good G-quadruplex stabilizer or recognizer with fluorescent emission in the visible region.

Researchers have found that the G-quadruplex structure of the human telomere (TTAGGG)4 can be stabilized with the help of the organic small molecule BMVC .[212] In addition, fluorescence yield and the distinct fluorescence properties of BMVC bound to various DNA structures has been increased as a result of binding. This has been allowing the mapping of the G-quadruplex structure within the choromosomes of human metaphase. The distinguishable properties have also allowed observing the bright fluorescence spots from BMVC in the cancer cell nucleus in comparison to the weak fluorescence as observed within the normal cell BMVC. Furthermore, a simple handheld device incorporating the BMVC molecule was designed for low cost point-of-care screening of cancer cells (a). Athough BMVC is a potent quadruplex recognizing fluorophore, its fluorescent signal cannot be detected by microscopy due to interference with duplex structures, which are in excess in chromosomes. Additionally, the emission wavelength comes to a difference in nature when

BMVC binds with duplex and, as a result, the quadruplex is observed to be less than 20 nm shift in fluorescence wavelength. It means that the fluorescent color assortment sandwiched between quadruplex and duplex is imperceptible when BMVC stains the chromosome. Therefore, a strategy has been developed to increase the color contrast of the image using FRET to resolve this challenge in the molecular imaging of quadruplexes. This is why researchers have chosen Hoechst and propidium iodide (PI) as duplex-binding fluorophores and present the predictable results with suitable staining procedure.

To summarize, based on FRET studies, it can be said that the binding modes of duplex-binding molecules are intercalation or groove binding, while the binding modes of quadruplex-binding molecules are stacking or groove binding. Furthermore, the number of quadruplex structures is very low with respect to the duplexes in the chromosome. Hence, research has shown that the duplex structures spread everywhere around the quadruplex structure unit in chromosome. Based on the results it has been proposed that the FRET of quadruplex binding molecule might occur with Hoechst, which binds to the same quadruplex structure unit with different binding modes and the free Hoeschst that binds to duplex structures around the quadruplex structures. Thus, the research proves that the experiment results in increasing the contrast of the fluorescent colors.

4.1.3 Summary and objectives

Our self-selection approach uses different types of nucleic acid structures such as single-stranded and double–stranded DNA; quadruplex and triplex, each of those structures have its own functionalities associated with them. The other types of hybrid duplexes involve PNA and RNA. A specific type of technique such as the orthogonal recognition are applied so that the multiple nucleic acid structures are differentiated and evaluated.

The importance of different in structures of the types of nucleic acids and the selectivity of the structure is very much different for each properties such as the optoelectronic properties. Some examples for the different types of opto-electronic properties are tetra substituted phenanthrolines, and berberine have a selectivity for the quadruplex. Another example, neomycin has selectivity for triplex structures.

Glenn Burley's optical gradient was the photonic waveguide described in Chapter 1.[123] In this waveguide, the routing of FRET is unidirectional and lateral to a track of a double-stranded DNA. It is very important that the duplex-binding fluorophore recognizes specific sequence

in this approach. Hence, PAs were the minor groove binding molecular ligands that provided control. The PAs bind within the minor groove of the duplex DNA, and enable targeting of sequences of 6 to 10 base pairs. Binding for these systems has high affinity and effectively modulates the efficiency of FRET by fluorophores which have been supramolecularly organised laterally to the double-stranded DNA. The enhancement of the FRET that is uni-directional evidences the whole association of all the integral parts, leading to the discerning routing of light along DNA duplexes that are simple as the three-way junction. As they mentioned in their report the designing of the experiments for the testing of the PAs was done to check the programmable nature of the PAs for programming FRET processes that are uni-directional along DNA duplex and a 3-way junction. The base stacking of the Cy3.5 dye is possible. There may be unfavourable orientations but the observed FRET results from the average orientations and is relatively efficient, even though this may not be applicable to the other dyes.[122]

4.1.4 Aims

Our aim is to identify couples of compounds displaying orthogonal selectivity for nucleic acids structures such as duplex, triplex and quadruplex DNA. The mutually orthogonal interaction pairs are required for the construction of self-assembled functional nanostructures. We will, for example, use common redox indicators and fluorescent molecules such as **6** and **8** (orange and blue dots) as illustrated in Figure 4.1.

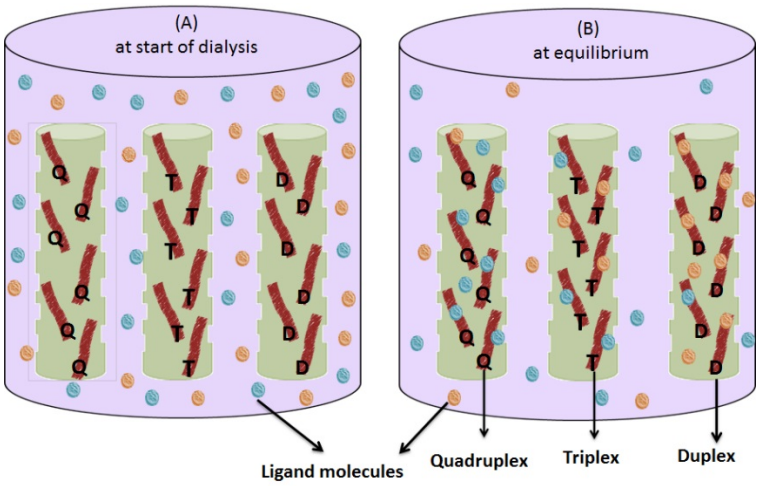

Figure 4.1. Schematic illustration of the double competition dialysis process involving three nucleic acid structures, viz. quadruplex (Q), triplex (T) and duplex (D) and two ligands (orange and blue dots).

The reason to use these compounds in this process is that they have been reported to have selectivity[127] toward nucleic acid structures while their optoelectronic properties will allow us to confirm assembly formation by FRET. In this case, we will see if **6** and **8** selectively bind with different nucleic acid structures. To explain further, in the hypothetical example shown in Figure 4.1, **8** (blue dots) has a high affinity and selectivity for the quadruplex DNA, **6** (orange dots) has a high affinity and selectivity for the duplex DNA, while **6** and **8** both bind to the triplex. Therefore, the quadruplex[192] and the duplex will provide high affinity and selectivity binding sites for **6** and **8**, respectively. However, the triplex DNA has affinity for both ligands and binds with both ligands **6** and **8**. Therefore, in this hypothetical example we would select the quadruplex and duplex DNA based on the dialysis results because each nucleic acid structure uniquely binds with one binder only. We would then use the duplex DNA and the quadruplex DNA as building blocks for a template (or scaffold) for self-assembly. The template will place **6** and **8** in a pre-determined arrangement. We will then use FRET to measure the energy which is transferred from **6** on the duplex DNA to **8** on the

quadruplex DNA.[196] The observation of energy transfer would therefore provide the evidence that the self-assembled nanostructure has been formed successfully. In order to select pairs of binders for testing, we require an overview of spectroscopic properties and binding selectivities for optoelectronically active nucleic acid binders (Table 4.1).

Table 4.1: Optical emission, absorption and nucleic acid targets for optoelectronically active nucleic acid binders.

ligand	*Solubility*	*Nucleic acid target*	λ_{ex} */nm*	λ_{em} */nm*	*Ref.*
basic yellow (thioflavin)	Soluble	Quadruplex 22AG	330	450	191
H33258	Soluble	Duplex A·T	338	454	62
methylene blue	Soluble	Telomere G-quadruplex DNA	663	/	124
ethidium bromide	Soluble	polyA • polyT Triplex	481	616	125,126
DAPI	Soluble	AT- rich duplex c-myc quadruplex	342	470	125
thiazole orange	Soluble	Duplex DNA	500	527	213
DODC	Soluble	Quadruplex and Triplex DNA	576	603	127
coralyne	Slightly soluble	Poly(A) Quadruplex Triplex DNA	423	565	158

Table 4.1 shows properties like optical emission, absorption and selectivity for nucleic acids for the chosen ligands. We chose basic yellow and methylene blue because it has been shown that methylene blue can bind by several modes to nucleic acids. Optical emission and absorption for the basic yellow and methylene blue are highly important in the selection of the competition because the emission of the donor needs to overlap with the absorption of the acceptor.

The primary aim of this system is to direct the opto-electronically active compound into a judicious sequence alongside a chain of nucleic acid structures. The feasibility of the transportation of the electrons and/or excitation energy are focused in this system. Our system is applied only forunidirection transport of excitation energy. Other potential uses involve

self-assembled catalytic systems which involves the redirection of the reactivity with the help of the nucleic acid structures. The main determinants of this step is the positioning of the reactants. Careful reaction design will be used in this system in order to prevent multivalency. The application of our systems will help in the having a perception about the self-selection approach considering the different structures of the nucleic acids. The self-selection criteria of the orthogonal and modified completion dialysis approach can be implemented to yield more accurate results.

Our system shows how orthogonal pairs of recognition elements can be made to self-select using a modified competition dialysis approach. We have targeted nucleic acid structures to take advantage of the relative ease of identifying selective binders, that means that different nucleic acids can have very different shapes so that a duplex binder does not necessarily bind to quadruplex DNA. Identification of the selective binders is an important ability of our device as the selection of the nucleic acid structures is vital for this research.

A modified competition dialysis approach can be implemented. The prime purpose of this device is to compare the current use of the different structures of the nucleic acid in the competition and double competition dialysis. Measuring the affinities of nucleic acid binders individually and in combination is challenging. This is because some binders have two types of binding i.e. stronger and weaker binding and this can have a significant impact on the apparent affinity.

Glenn Burley's gradient focus on only one shape of nucleic acid structure which is duplex DNA. The application Glenn Burley's gradient was just to transfer the energy from one place to another place. On the other hand, our gradient can make a big difference due to different nucleic acid structures e.g. single-stranded, duplex, triplex, quadruplex DNA, DNA•PNA and DNA•RNA hybrid duplexes. In addition, our gradient can be applicable to the other dyes (see chapter 2).

4.2 Results and discussion

This section is divided into two parts. Sections 4.2.1a – 4.2.1b deal with compounds which lack stability and in particular with fading compounds. Sections 4.2.2a and 4.2.2b report on studies on stable compounds. At the time of carrying out these experiments, we had not yet established the fact that these compounds fade on exposure to light.

4.2.1a Validation of the double competition dialysis method for the simultaneous quantification of affinities of basic yellow (5) and methylene blue (9) for different sequences of duplex DNA.

It is essential that the ligands used in the proposed assay are carefully chosen, based on their optoelectronic properties, such as optical emission and absorption. The first experiment was a test run performed to investigate the affinity and selectivity of two ligands, basic yellow (**5**) and methylene blue (**9**), against an array of nucleic acids structures.[166] Compouds **5** and **9** have a high selectivety to different nucleic acid structures.

Ligands **5** and **9** were exposed to FS-DNA and different sequences of duplex DNA, viz. $(dGdC)_{12}$●$(dGdC)_{12}$, $(dAdT)_{12}$●$(dAdT)_{12}$ and $(dA)_{24}$ $(dT)_{24}$ in buffer (25 mM MOPS, pH 7.0, 50 mM NaCl, and 1 mM EDTA), at 25 °C. The equilibration kinetics and the spectra of **5** and **9** after equilibration with the different DNA structures are reported in Figure 4.2.

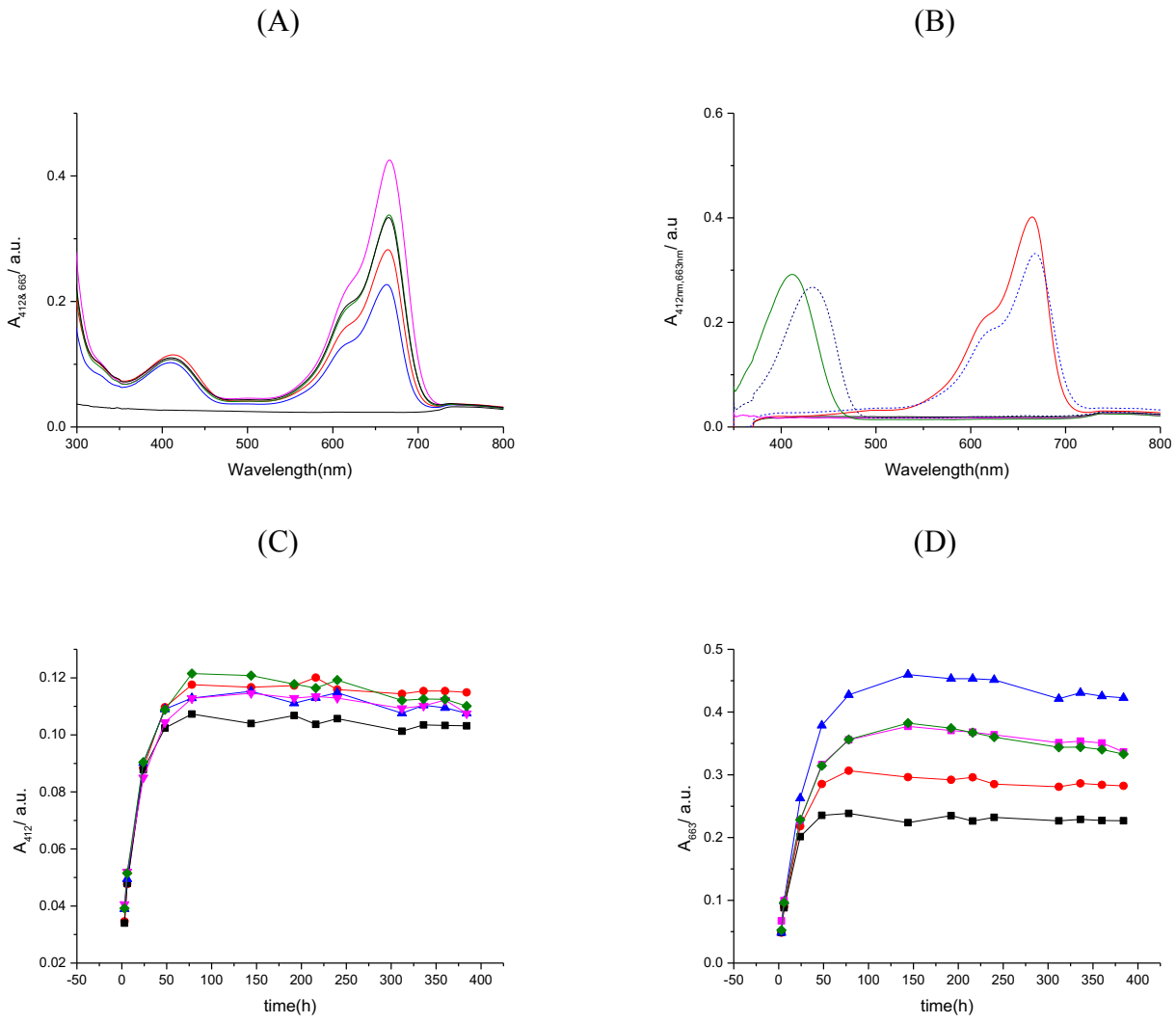

Figure 4.2 (A) UV-visible spectra for basic yellow (**5**) and methylene blue (**9**) following equilibration in the presence of FS-DNA, $(dA)_{24}$ $(dT)_{24}$, $(dGdC)_{12}$●$(dGdC)_{12}$ and $(dAdT)_{12}$●$(dAdT)_{12}$ **(B)** free and bound ligands at 412 nm and 663 nm (also see Section 4.2.1e and 4.2.1i in Chapter 2 **(C)** the absorbance at 663 nm (mainly **9**) as a function of equilibration time and **(D)** the absorbance at 412 nm (mainly **5**) as a function of equilibration time for 75 µM FS-DNA (♦), 70 µM $(dA)_{24}$ $(dT)_{24}$ (●), 72µM $(dGdC)_{12}$●$(dGdC)_{12}$ (▲), 77 µM $(dAdT)_{12}$●$(dAdT)_{12}$ (■) and buffer (■).

Figure 4.2A presents the final spectra for the solutions in the 5 holes of the device after equilibration. For reference, Figure 4.2B shows the spectra for the free and bound forms of both, both in the free and bound forms. Figures 4.2C and D show the changes in absorbance at 412 nm and 663 nm as a function of time. Figure 4.2 shows that the absorbances at 412 nm

and 663 nm remain constant after approximately 100 hours. Therefore, Figures 4.2C and D show that equilibrium has been achieved after around 100 hours. Figure 4.2C shows that the absorbance at 663 nm, which is mainly caused by **9**, is highest with $(dGdC)_{12}$●$(dGdC)_{12}$ (▲). On the other hand, Figure 4.2D shows that the absorbance at 412 nm, which is mainly caused by **5**, is similar for all sequences and for the buffer, suggesting that **5** has low affinity and selectivity for the different DNA sequences. The concentrations and apparent affinities of the ligands at equilibrium were determined (Table 4.2).

Table 4.2: Apparent equilibrium constants *K* for 5 and 9 [a] interacting with FS-DNA, $(dGdC)_{12}$●$(dGdC)_{12}$, $(dAdT)_{12}$●$(dAdT)_{12}$ and $(dA)_{24}$ $(dT)_{24}$ [b]

DNA	$(dA)_{24}$ $(dT)_{24}$		$(dGdC)_{12}$● $(dGdC)_{12}$		$(dAdT)_{12}$● $(dAdT)_{12}$		FS-DNA		buffer	
$[DNA]_{total}$ / µM	70		72		77		75		/	
unit conc.	bp								/	
bind. sites / unit conc. [i]	3.33×10^{-1}								/	
$[binding\ sites]_{total}$ / M	2.33×10^{-5}		2.40×10^{-5}		2.57×10^{-5}		2.50×10^{-5}		/	
Ligand	9	5	9	5	9	5	9	5	9	5
$A_{663nm,end(9)}$; $A_{412nm,end(5)}$	0.291	0.116	0.441	0.111	0.359	0.111	0.357	0.115	0.231	0.104
Error	0.003	0.001	0.005	0.001	0.003	0.001	0.003	0.001	0.002	0.001
$A_{663nm,bound}$; $A_{412nm,bound}$	0.083	0.023	0.233	0.018	0.152	0.018	0.149	0.022	0.023	0.011
C_{bound} / µM	1.52	1.32	4.28	1.04	2.79	1.04	2.73	1.27	/	/
$[ligand]_{free}$ / µM	33	28	33	28	33	28	33	28	33	28
$[binding\ sites]_{free}$ / µM	21	22	19	23	22	24	22	23	/	/
K / M^{-1}	2.07×10^{4}	2.14×10^{4}	6.40×10^{4}	1.61×10^{4}	3.59×10^{4}	1.51×10^{4}	3.62×10^{4}	1.91×10^{4}	/	/

e) Concentrations of **5** = 8.5 µM and **9** = 8.1 µM.

f) In buffer (25 mM MOPS, pH 7.0, 50 mM NaCl, and 1 mM EDTA), at 25 °C.

g) $A_{412nm,bg}$= 0.0256, $A_{412nm,free}$ = 0.0676 and $A_{412nm,reservoir}$ was 0.0932, ε_{free} = 24073 M^{-1} cm^{-1} and ε_{bound} = 18073 M^{-1} cm^{-1}.

h) $A_{663nm,bg}$= 0.0227, $A_{663nm,free}$ = 0.1851 and $A_{663nm,reservoir}$ was 0.2078, ε_{free} = 78000 M^{-1} cm^{-1} and ε_{bound} = 54618 M^{-1} cm^{-1}.

i) We assume the number of binding site size in base pairs is 3.0.

j) The absorbances of the solution in the reservoir at the beginning of the experiment were 0.2312 ($A_{412\ nm}$) and 0.6565 ($A_{663\ nm}$).

As shown in Table 4.2, **9** has the highest affinity for $(dGdC)_{12}\bullet(dGdC)_{12}$, giving a binding constant of 6.40×10^4 M^{-1}. Nevertheless, there was no significant difference between the calculated affinities for DNA and equilibrium constants of **5** and **9** for all sequences are almost equal. Moreover, the fact that the absorbance in the hole containing the buffer is also slightly higher than in the reservoir indicates that some of the increases observed for the nucleic acid solutions may be within the error of the experiment.

At the end of the experiment, the absorbances in the reservoir and in the buffer control hole for **5** and **9** are similar, suggesting good equilibration. However, comparison with the absorbances at the beginning of the experiments show that both compounds faded a lot. Overall, the experiment is working well if fading is ignored.

To explore the reproducibility of the data, we repeated the experiment involving **5** and **9** and the same DNA sequences. The spectra of **5** and **9** after equilibration with different DNA seuences and the absorbances at 412 and 663 nm are shown in Figure 4.3.

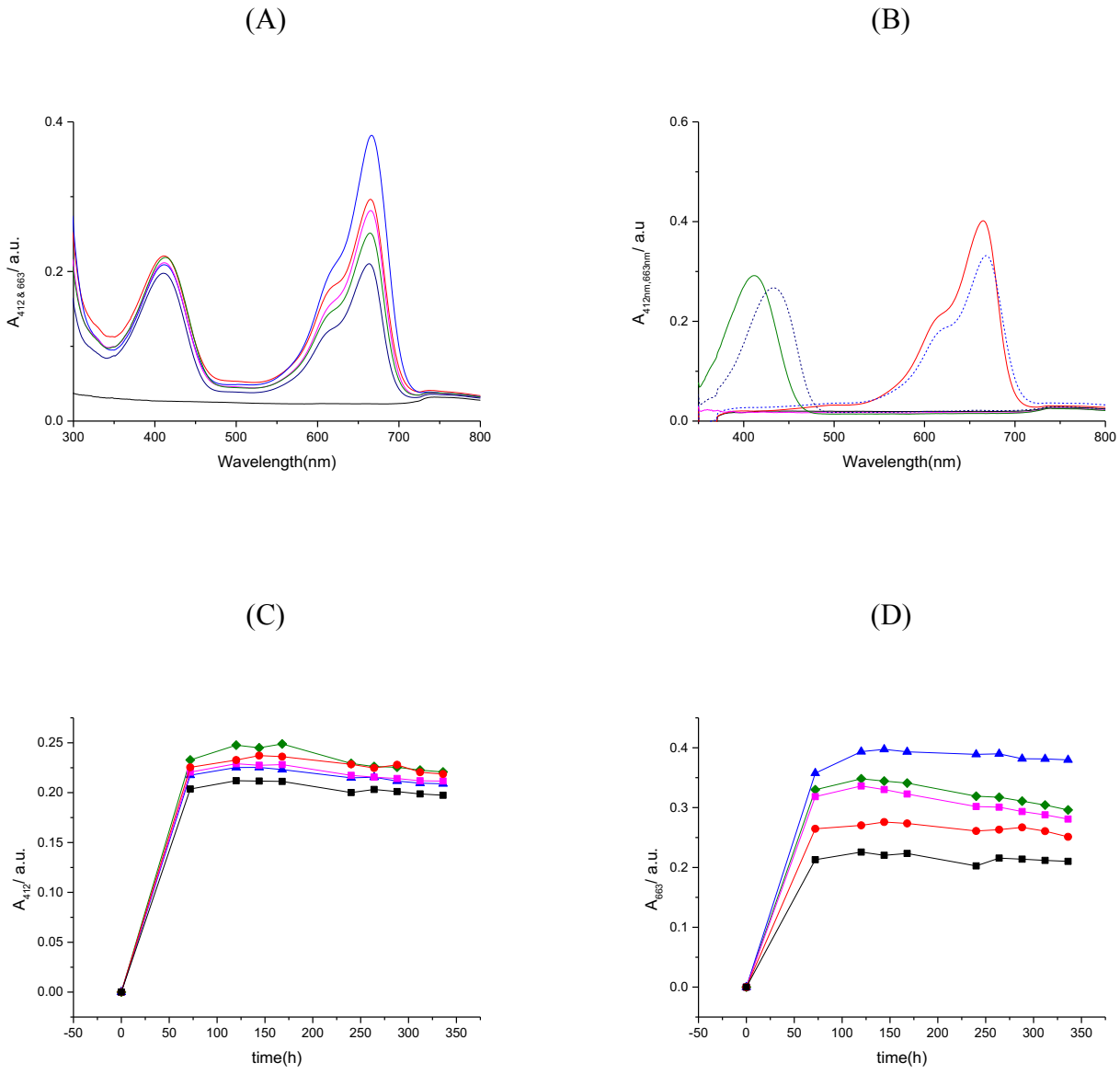

Figure 4.3 (A) UV-visible spectra for **5** (basic yellow) and **9** (methylene blue) following equilibration in the presence of DNA **(B)** free and bound ligands at 412 nm and 663 nm also see Section 4.2.1e and 4.2.1i in Chapter 2. **(C)** the absorbance at 412 nm (mainly **5**) as a function of equilibration time and **(D)** the absorbance at 663 nm (mainly **9**) as a function of equilibration time for 75 µM FS-DNA (♦), 70 µM $(dA)_{24}$ $(dT)_{24}$ (●), 72µM $(dGdC)_{12}$●$(dGdC)_{12}$ (▲), 77 µM $(dAdT)_{12}$●$(dAdT)_{12}$ (■) and buffer (■).

Figure 4.3A presents the final spectra for the solutions in the 5 holes of the device after equilibrium. For reference, Figure 4.3B shows the spectrafor the free and bound forms of both ligands. Figures 4.3C and D show that the changes in absorbance at 412 nm and 663 nm as a function of time. Figure 4.3 shows that the absorbance at 412 nm and 663 nm remain constant after approximately 150 hours. Therefore, Figures 4.3B and C show that equilibrium

has been achieved after around 150 hours. Figure 4.3B shows the absorbance at 412 nm of **5**, this suggests that **5** has the same affinity for all different DNA sequences. Figure 6.3D the absorbance at 663 nm, which is mainly caused by **9**, which is highest with $(dGdC)_{12}$●$(dGdC)_{12}$ (▲).

The concentrations and apparent affinities of the ligands at equilibrium were determined (Table 4.3).

Table 4.3: Apparent equilibrium constants *K* for 5 and 9 [a] interacting with FS-DNA, $(dGdC)_{12}\bullet(dGdC)_{12}$, $(dAdT)_{12}\bullet(dAdT)_{12}$ and $(dA)_{24}\,(dT)_{24}$ [b]

DNA	FS-DNA		$(dGdC)_{12}\bullet$ $(dGdC)_{12}$		$(dAdT)_{12}\bullet$ $(dAdT)_{12}$		$(dA)_{24}\,(dT)_{24}$		buffer	
$[DNA]_{total}$ / µM	75		72		77		70		/	
unit conc.	bp								/	
bind. sites / unit conc. [e]	3.33×10^{-1}								/	
$[binding\ sites]_{total}$ /M	2.50×10^{-5}		2.40×10^{-5}		2.57×10^{-5}		2.33×10^{-5}		/	
Ligand	9	5	9	5	9	5	9	5	9	5
$A_{663nm,end(9)}$; $A_{412nm,end(5)}$	0.323	0.233	0.388	0.216	0.308	0.219	0.265	0.228	0.215	0.204
Error	0.006	5.15×10^{-3}	0.004	3.8×10^{-3}	0.007	3.9×10^{-3}	0.003	0.004	0.003	3.9×10^{-3}
$A_{663nm,bound}$; $A_{412nm,bound}$	0.137	0.053	0.202	0.036	0.122	0.039	0.079	0.048	0.029	0.024
C_{bound} /µM	2.52	2.9	3.7	2.06	2.24	2.21	1.46	2.69	/	/
$[ligand]_{free}$ /µM	2.98	6.3	2.98	6.3	2.98	6.3	2.98	6.3	2.98	6.3
$[binding\ sites]_{free}$ /µM	22.	22	20.	21	23.	23	21.	20	/	/
K / M^{-1}	3.77×10^{4}	2.12×10^{4}	6.15×10^{4}	1.48×10^{4}	3.21×10^{4}	1.48×10^{4}	2.24×10^{4}	2.05×10^{4}	/	/

a) Concentrations of **5** = 25 µM and **9** = 7.1 µM.

b) In buffer (25 mM MOPS, pH 7.0, 50 mM NaCl, and 1 mM EDTA), at 25 °C.

c) $A_{412nm,bg}$= 0.0271 $A_{412nm,\ free}$ = 0.153 and $A_{412nm,\ reservoir}$ was 0.1801, ε_{free} = 24073 M^{-1} cm^{-1} and ε_{bound} = 18073 M^{-1} cm^{-1}.

d) $A_{663nm,bg}$= 0.0232 $A_{663nm,\ free}$ = 0.1625 and $A_{663nm,\ reservoir}$ was 0.1857, ε_{free} = 78000 M^{-1} cm^{-1} and ε_{bound} = 54618 M^{-1} cm^{-1}.

e) We assume the number of binding site size in base pairs is 3.0.

f) The absorbances of the solution in the reservoir at the beginning of the experiment were 0.6431 ($A_{412\ nm}$) and 0.5817 ($A_{663\ nm}$).

Table 4.3 is in good agreement with Table 4.2 and confirms that **9** has a higher affinity for $(dGdC)_{12}$●$(dGdC)_{12}$ than for other types of DNA. However, these data also confirm that **5** has no selectivity for one of the four different types of duplex DNA because affinities are very similar. Finally, comparison of the absorbances of the solution in the reservoir at the beginning and the end of the experiment and the buffer in the control hole still show us that fading of both **5** and **9** occurred during this experiment.

4.2.1b Double competition dialysis methods for the quantification of affinities of 9 and 11 for duplex and quadruplex DNA.

In Chapter 3 we have seen that **11** binds to quadruplex structures such as c-myc and 22AG. As mentioned before, **9** has already shown fading in competition dialysis.

In order to estimate the affinities of methylene blue (**9**) and DAPI (**11**) for duplex-forming sequences $(dGdC)_{12}$●$(dGdC)_{12}$, $(dAdT)_{12}$●$(dAdT)_{12}$, and quadruplex-forming sequences[214] 22AG and c-myc, the two compounds were dialysed against these structures in our device in buffer (25 mM MOPS, pH 7.0, 50 mM NaCl, and 1 mM EDTA), at 25 °C. The spectra for **11** and **9** after equilibration with different types of DNA are reported in Figure 4.4.

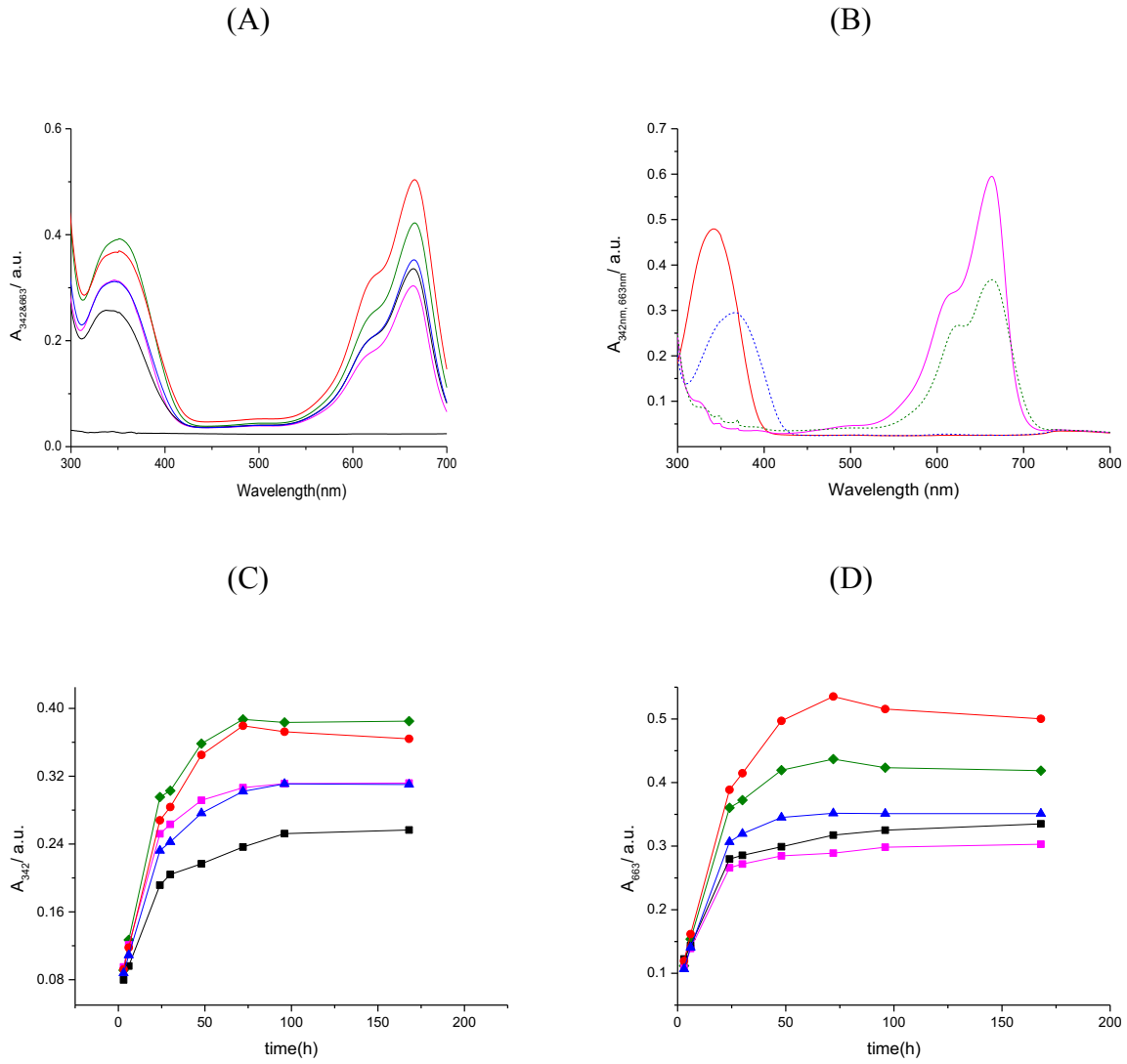

Figure 4.4 (A) UV-visible spectra for **9** and **11** following equilibration in the presence of DNA **(B)** free and bound ligands at 342 nm and 663 nm also see Section 4.2.4e and 4.2.1i in Chapter 2. **(C)** the absorbance (mainly **9**) at 663 nm as a function of equilibration time and **(D)** the absorbance at 342 nm (mainly **11**) as a function of equilibration time for 9.7 µM 22AG (♦), 9.3 µM c-myc (●), 38 µM $(dGdC)_{12}$●$(dGdC)_{12}$ (▲), 37 µM $(dAdT)_{12}$●$(dAdT)_{12}$ (■) and buffer (■).

Figure 4.4A shows the final spectra for the solutions in the 5 holes of the device after equilibration. For reference, Figure 4.4B shows the spectra for the free and bound forms of both ligands. Figure 4.4C show that changes in absorbance at 342 nm and 663 nm as a function of time. Figure 4.4 shows that the absorbances at 342 nm and 663 nm remain constant after approximately 100 hours. Therefore, Figures 4.4 C and D show the equilibrium has been achieved after around 100 hours. Figure 4.4C shows the absorbance at 342 nm, which is dominated by **11** which shows **11** has affinity toward 22AG (♦).

The concentrations and apparent affinities of the ligands at equilibrium were determined (Table 4.4).

Table 4.4: Apparent equilibrium constants *K* for 9 and 11[a] simultaneously interacting with 22AG, $(dAdT)_{12}\bullet(dAdT)_{12}$, (c-myc) and $(dGdC)_{12}\bullet(dGdC)_{12}$ [b]

DNA	22AG		$(dAdT)_{12}\bullet(dAdT)_{12}$		c-myc		$(dGdC)_{12}\bullet(dGdC)_{12}$		buffer	
$[DNA]_{total}$ / µM	9.7		37		9.3		38		/	
unit conc.	quadruplex		bp		quadruplex		bp		/	
Ligand	9	11	9	11	9	11	9	11	9	11
bind. sites / unit conc.	7	11	3.33×10^{-1}		6	4	3.33×10^{-1}		/	
$[binding\ sites]_{total}$ /M	6.7×10^{-5}	1.07×10^{-4}	1.1×10^{-5}	1.23×10^{-5}	5.5×10^{-5}	3.7×10^{-5}	1.2×10^{-5}	1.27×10^{-5}	/	
$A_{663nm,end(9)}$; $A_{342nm,end(11)}$	0.4280	0.3865	0.2927	0.3078	0.5200	0.3745	0.3516	0.3070	0.31716	0.2458
Error	0.0051	0.0046	0.0043	0.0042	0.0096	0.0069	0.0032	0.0057	0.0079	0.0065
$A_{663nm,bound}$ $A_{342nm,\ bound}$	0.1669	0.2084	0.0316	0.1297	0.2589	0.1964	0.0905	0.1289	0.0560	0.0677
C_{bound} /µM	3.05	17	0.57	10	4.74	16	1.66	10	/	/
$[ligand]_{free}$ /µM	4.32	7.1	4.32	7.1	4.32	7.1	4.32	7.1	4.32	7.1
$[binding\ sites]_{free}$ /µM	64.8	89	11.8	1.68	51.1	21.1	11	2.08	/	/
K / M^{-1}	1.09×10^{4}	2.6×10^{4}	1.14×10^{4}	8.9×10^{5}	2.15×10^{4}	1.08×10^{5}	3.48×10^{4}	7.1×10^{5}	/	/

a) Concentrations of **11** = 22 µM and **9** = 8.0 µM.
b) In buffer (25 mM MOPS, pH 7.0, 50 mM NaCl, and 1 mM EDTA)), at 25 °C.
c) $A_{663nm,bg}$= 0.0249 $A_{663nm,free}$ = 0.2113 and $A_{663nm,\ reservoir}$ was 0.2362, ε_{free} = 78000 M^{-1} cm^{-1} and ε_{bound} = 54618 M^{-1} cm^{-1}.
d) $A_{342nm,bg}$= 0.0107 $A_{342nm,free}$ = 0.1567 and $A_{342nm,\ reservoir}$ was 0.1674, ε_{free} = 23570 M^{-1} cm^{-1} and ε_{bound} = 12180 M^{-1} cm^{-1}.
e) We assume the number of binding site size in base pairs is 3.0, which means 1 ligand binds to 3 base pairs.
f) For **9** and **11**, we know the number of binding sites per quadruplex of c-myc are six, four and for 22AG are seven and eleven, respectively.
g) The absorbances of the solution in the reservoir at the beginning of the experiment were 0.578($A_{342\ nm}$) and 0.6568 ($A_{663\ nm}$).

Table 4.4 presents the affinities of **9** and **11** for different types of nucleic acid structures. The affinity of **9** toward $(dGdC)_{12}$●$(dGdC)_{12}$ was confirmed. DAPI (**11)** has affinity toward $(dAdT)_{12}$●$(dAdT)_{12}$. Unfortunately, our control shows us and there is a problem related to the fading of both **9** and **11**. Table 6.4 shows useful affinity differences for **11**, but for this couple to become an applicable system in a self-assembled nanostructure, **9** should have a higher affinity for one of the structures as well.

4.2.1C Double competition dialysis methods for the quantification of affinities of 11 and 12 for duplex and quadruplex DNA.

We became interested in testing other ligands like **12** and to compare it with previous competition experiments. we decided to find out whether **DAPI** (**11**) and thiazole orange (**12**) **have** the required relative affinities toward duplex-forming sequences, $(dGdC)_{12}$●$(dGdC)_{12}$, $(dAdT)_{12}$●$(dAdT)_{12}$, and quadruplex-forming sequences 22AG and c-myc, in buffer (25 mM MOPS, pH 7.0, 50 mM NaCl, and 1 mM EDTA), at 25 °C. The spectra of **11** and **12** at equilibrium, as well as the changes in absorbance as a function of time during equilibration for the different types DNA are shown in Figure 4.5.

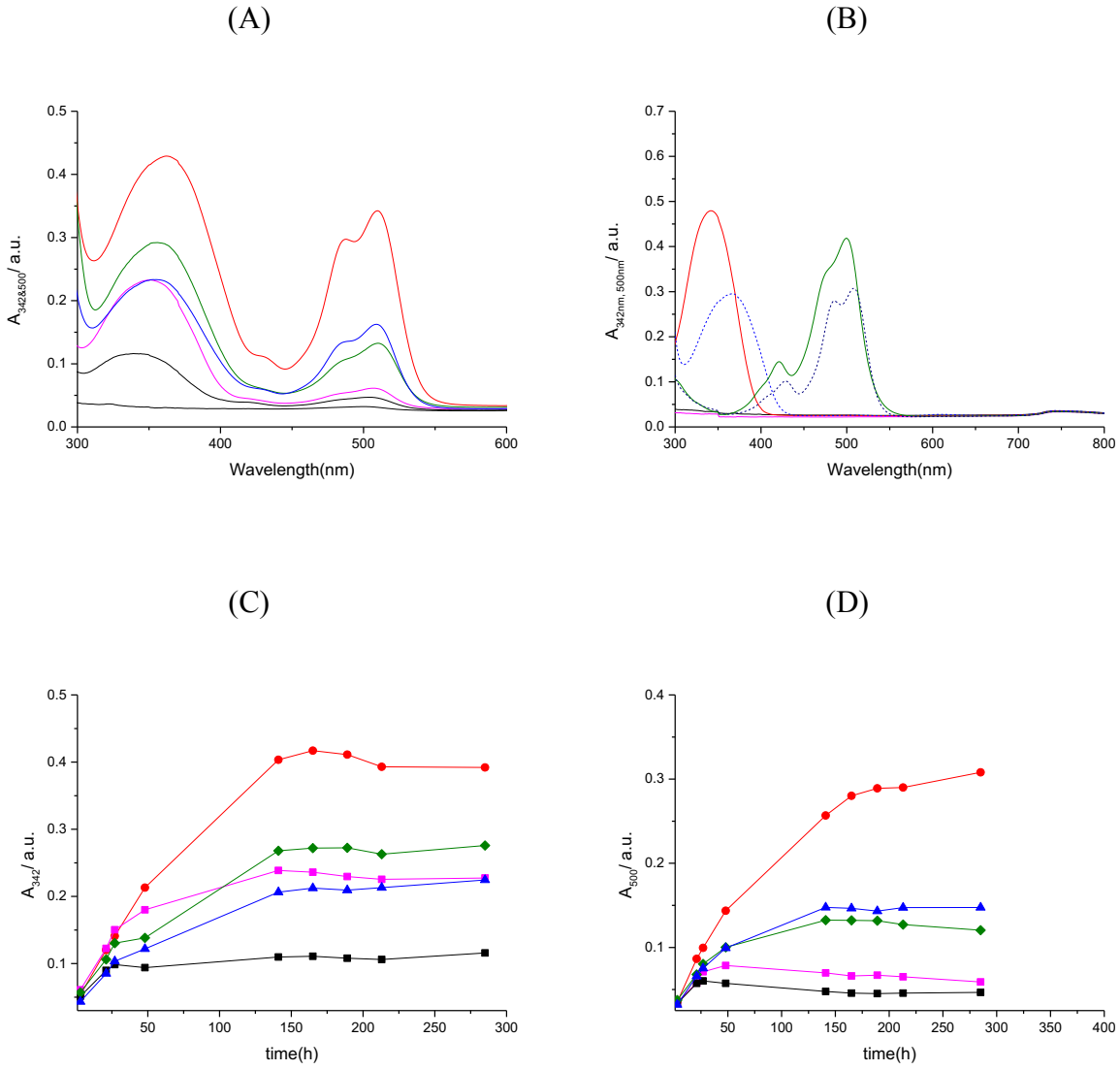

Figure 4.5 (A) UV-visible spectra for **11** and **12** exposed to DNA sequences **(B)** free and bound ligands at 342 nm and 500 nm also see Section 4.2.1e and 4.2.4g in Chapter 2. (**C**) the absorbance at 342 nm (primarily **11**) as a function of equilibration time and **(D)** the absorbance at 500 nm (primarily **12**) as a function of equilibration time for 12 µM 22AG (♦), 11 µM c-myc (●), 40 µM $(dGdC)_{12}$●$(dGdC)_{12}$ (▲), 40 µM $(dAdT)_{12}$●$(dAdT)_{12}$ (■) and buffer (■).

Figure 4.5 presents the final spectra for the solutions in the 5 holes of the device after equilibration. For reference, Figure 4.5B shows the spectra for the free and bound forms of both ligands. Figures 4.5C and D show the changes in absorbance at 342 nm and 500 nm as a function of time. Figure 4.5 shows that the absorbances at 342 nm and 500 nm remain constant after approximately 200 hours. Therefore, Figures 4.5C and D show that equilibrium

has been achieved after around 200 hours. Figure 4.5C shows that the absorbance at 342 nm, which is mainly caused by **11**, is highest with c-myc (●). Figure 4.5D shows that the absorbance at 500 nm, which is mainly caused by 12, is also highest c-myc (●). Therefore, **11** and **12** both have their highest affinity for c-myc (●). The concentrations and apparent affinities of the ligands at equilibration were determined (Table 4.5).

Table 4.5: Apparent equilibrium constants *K* for 11 and 12 [a] interacting with c-myc, $(dAdT)_{12}$●$(dAdT)_{12}$, (22AG) and $(dGdC)_{12}$●$(dGdC)_{12}$ [b]

DNA	c-myc		$(dAdT)_{12}$● $(dAdT)_{12}$		22AG		$(dGdC)_{12}$● $(dGdC)_{12}$		buffer	
$[DNA]_{total}$ / μM	11		40		12		40		/	
unit conc.	quadruplex		bp		quadruplex		bp		/	
Ligand	11	12	11	12	11	12	11	12	11	6.12
bind. sites / unit conc.	4	12	3.33×10^{-1}		11	10	3.33×10^{-1}		/	
$[binding\ sites]_{total}$ / M	4.4×10^{-5}	1.3×10^{-4}	1.3×10^{-5}	1.3×10^{-5}	1.3×10^{-4}	1.2×10^{-4}	1.3×10^{-5}	1.3×10^{-5}	/	
$A_{342nm,end(11)};A_{500,end(12)}$	0.4289	0.3289	0.2318	0.0679	0.2832	0.1297	0.2249	0.1512	0.1084	0.0505
Error	0.0173	0.0059	0.0035	0.0027	0.0098	0.0024	0.0040	0.0025	0.0024	0.1038
$A_{342nm,boud}$; $A_{500nm,bound}$	0.3184	0.2932	0.1213	0.0322	0.1727	0.0940	0.1144	0.1155	/	/
C_{bound} / μM	6.9	6.7	2.6	0.74	3.7	2.1	2.5	2.6	/	/
$[ligand]_{free}$ / μM	1.05	0.034	1.05	0.034	1.05	0.034	1.05	0.034	1.05	0.034
$[binding\ sites]_{free}$ / μM	37	120	10	12	128	118	10	10	/	/
K / M^{-1}	1.7×10^{5}	1.5×10^{6}	2.3×10^{5}	1.7×10^{6}	2.7×10^{4}	5.3×10^{5}	2.1×10^{5}	7.3×10^{6}	/	/

a) Concentrations of **11** = 13 μM and **12** = 1.8 μM.
b) In buffer (25 mM MOPS, pH 7.0, 50 mM NaCl, and 1 mM EDTA), at 25 °C.
c) $A_{342nm,\ bg}$= 0.0430 $A_{342nm,\ free}$ = 0.0675 and $A_{342nm,\ reservoir}$ was 0.1105, ε_{free} = 64095 M^{-1} cm^{-1} and ε_{bound} = 45826 M^{-1} cm^{-1}.
d) $A_{500nm,\ bg}$= 0.0335 $A_{500nm,\ free}$ = 0.0022 and $A_{500nm,\ reservoir}$ was 0.0357, ε_{free} = 46095 M^{-1} cm^{-1} and ε_{bound} = 43185 M^{-1} cm^{-1}.
e) We assume the number of binding site size in base pairs is 3.0, which means 1 ligand binds to 3 base pairs.
f) For **11** and **12**, we know the number of binding sites per quadruplex of c-myc are four, twelve and for 22AG are eleven and ten, respectively.
g) The absorbances of the solution in the reservoir at the beginning of the experiment were 0.3633($A_{342\ nm}$) and 0.1386 ($A_{500\ nm}$).

Our control shows us that **12** has faded almost entirely during the experiment, meaning that concentrations of remaining **12** are very low. This makes our data difficult to interpret because error margins on affinities are high. This observation suggests that **11** and **12** are not a useful couple for a nanostructure, because of fading.

4.2.2 Double competition dialysis with stable ligands.

In this section, we present examples of compounds that are stable when exposed to light. We chose the compounds in this section based on properties such as emission and absorption and known affinities for nucleic acid structures.

4.2.2a Double competition dialysis for the quantification of affinities of 5 and 10 for duplex- and quadruplex-forming DNA

Compounds **5** and **10** are promising based on their know affinities, stability as well as optical emission and absorption. Both of them are soluble in water and stable. Compounds **5** and **10** can bind to different nucleic acid structures. Compound **5** has a high affinity to binds to quadruplex-forming sequences 22AG. However, Compound **10** binds to poly A●polyT and triplex.

We employed basic yellow (**5**) and ethidium bromide (**10**) in combination with duplexes $(dGdC)_{12}$●$(dGdC)_{12}$, $(dAdT)_{12}$●$(dAdT)_{12}$, and quadruplexes 22AG and c-myc, in buffer (25 mM MOPS, pH 7.0, 50 mM NaCl, and 1 mM EDTA), at 25 °C. The spectra of **5** and **10** after equilibration were determined and are shown in Figure 4.6. Similarly, the evolution of the absorbance at 412 nm and 481 nm is shown in Figure 4.6.

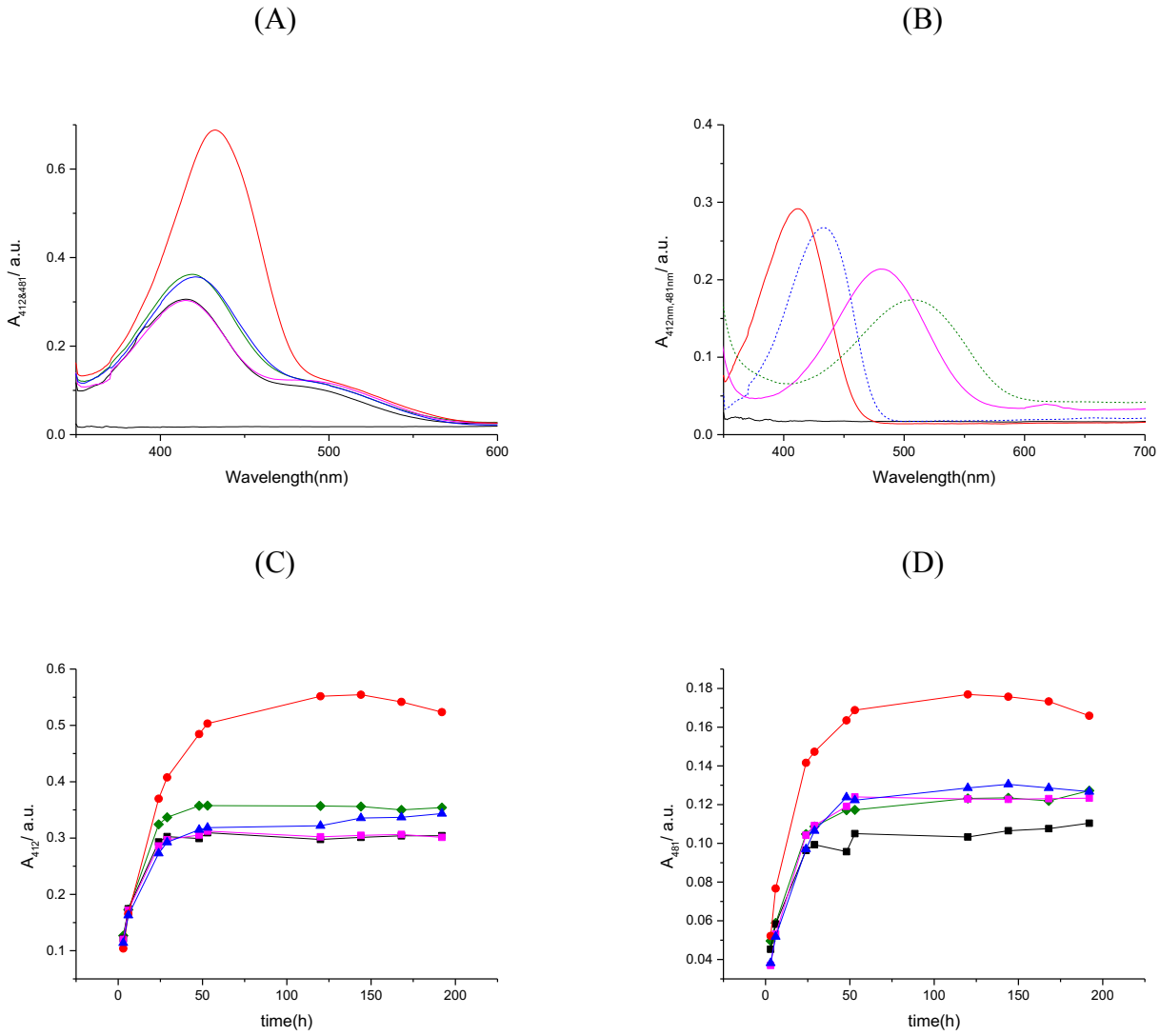

Figure 4.6 (A) UV-visible spectra for **5** and **10** following equilibration in the presence of DNA **(B)** spectra for free and bound ligands also see Section 4.2.1e and 4.2.4d in Chapter 2. **(C)**the absorbance at 412 nm (mainly **5**) as a function of equilibration time and **(D)** the absorbance at 481 nm (mainly **10**) as a function of equilibration time for 8.7 μM 22AG (♦), 8.9 μM c-myc (●), 34 μM $(dGdC)_{12}$●$(dGdC)_{12}$ (▲), 34 μM $(dAdT)_{12}$●$(dAdT)_{12}$ (■) and buffer (■).

Figure 4.6A presents the final spectra for the solutions in the 5 holes of the device after equilibration. For reference, Figure 4.6B shows the spectra for the free and bound forms of both ligands. Figures 4.6C and D show the changes in absorbance at 412 nm and 481 nm as a function of time. Figure 4.6 shows that the absorbances at 412 nm and 481 nm remain constant after approximately 100 hours. Therefore, Figures 4.6C and D show that equilibrium

has been achieved after around 100 hours. Figure 4.6C shows that the absorbance at 412 nm, which is mainly caused by **5**, is highest with c-myc (●). Figure 4.6D shows that the absorbance at 481 nm, which is mainly caused by **10**, suggests that **10** has a high affinity for c-myc (●). The concentrations and apparent affinities of the ligands after equilibration were determined (Table 4.6).

Table 4.6: Apparent equilibrium constants *K* for 5 and 10 [a] interacting with 22AG, $(dAdT)_{12}$•$(dAdT)_{12}$, c-myc and $(dGdC)_{12}$•$(dGdC)_{12}$ [b]

DNA	22AG		(dAdT)$_{12}$• (dAdT)$_{12}$		c-myc		(dGdC)$_{12}$• (dGdC)$_{12}$		buffer	
$[DNA]_{total}$ / µM	8.7		34		8.9		34		/	
unit conc.	quadruplex		bp		quadruplex		bp		/	
Ligand	5	10	5	10	5	6.10	5	10	5	10
bind. sites / unit conc. [e,f,g]	2		3.33×10^{-1}		2	3	3.33×10^{-1}		/	
$[binding\ sites]_{total}$ / M	1.7×10^{-5}	1.7×10^{-5}	1.1×10^{-5}	1.1×10^{-5}	1.7×10^{-5}	2.6×10^{-5}	1.1×10^{-5}	1.1×10^{-5}	/	
$A_{412nm,end(5)}$; $A_{481nm,end(10)}$	0.3544	0.1217	0.3043	0.1235	0.5416	0.1715	0.3256	0.1286	0.3031	0.1046
Error	0.0027	0.00181	0.0001	0.0005	0.0006	0.002	0.0060	0.0009	0.0017	0.00162
$A_{412nm,\ bound}$;$A_{481nm,bound}$	0.067	0.0244	0.0169	0.0262	0.2542	0.07424	0.0382	0.0313	0.01577	0.00731
C_{bound} / µM	3.76	5.48	0.949	5.91	14.2	1.67	2.14	7.04	/	/
$[ligand]_{free}$ / µM	11.1	11.7	11.1	11.7	11.1	11.7	11.1	11.7	11.1	11.7
$[binding\ sites]_{free}$ / µM	13.6	11.9	10.4	5.43	3.56	10	9.19	4.29	/	/
K / M^{-1}	2.4×10^{4}	3.9×10^{4}	8.2×10^{3}	9.3×10^{4}	3.5×10^{5}	1.4×10^{5}	2.09×10^{4}	1.4×10^{5}	/	/

a) Concentrations of **5** = 28 µM and **10** = 28 µM.
b) In buffer (25 mM MOPS, pH 7.0, 50 mM NaCl, and 1 mM EDTA), at 25 °C.
c) $A_{412nm,\ bg}$= 0.0191 $A_{412nm,\ free}$ = 0.2683 and $A_{412nm,\ reservoir}$ was 0.2874, ε_{free} = 24073 M^{-1} cm^{-1} and ε_{bound} = 17850 M^{-1} cm^{-1}.
d) $A_{481nm,\ bg}$= 0.0191 $A_{481nm,\ free}$ = 0.0782 and $A_{481nm,\ reservoir}$ was 0.0973, ε_{free} = 6696 M^{-1} cm^{-1} and ε_{bound} = 4450 M^{-1} cm^{-1}.
e) We assume the binding site size in base pairs is 3.0.
f) For **5** and **10**, we assume the number of binding sites per quadruplex of 22AG are two and for **5** of c-myc is two.
g) For **10**, we know the number of binding sites per quadruplex of c-myc is three.
h) The absorbances of the solution in the reservoir at the beginning of the experiment were 0.7081($A_{412\ nm}$) and 0.2131 ($A_{481\ nm}$).

Table 4.6 shows that both **5** has the highest affinity toward c-myc while **10** has the highest affinities for c-myc and $(dGdC)_{12}$●$(dGdC)_{12}$. Equilibration has been successful considering the similar absorbance in the reservoir and in the control hole containing the buffer. However, there is a big different between the absorbance in the reservoir at the beginning and the end of the experiment. Because these compounds should be stable upon exposure to light, the decrease is not attributed to fading but may represent either precipitation of these compounds or the compounds stick to the materials used in the device. The affinity for **5** is in reasonable agreement with the results from the UV-visible titrations as shown in Chapter 2 which gave ($K_{binding}$) of of $(1.18 \pm 0.21) \times 10^4$ M^{-1}. The affinity for **10** is in reasonable agreement with the results from the UV-visible titrations as shown in Chapter 2 which gave ($K_{binding}$) of $(4.01 \pm 2.60) \times 10^5$ M^{-1}.

We wanted to evaluate the affinities and selectivities of H33258 (**6**) and ethidium bromide (**10**) for duplex-forming $(dAdT)_{12}$●$(dAdT)_{12}$ and $(dGdC)_{12}$●$(dGdC)_{12}$ and quadruplex-forming 22AG and c-myc in buffer (25 mM MOPS, pH 7.0, 100 mM KCl, and 1 mM EDTA), at 25 °C using double competition dialysis. The spectra of **6** and **10** after equilibration with the different DNA sequences are shown in Figure 4.7. Figure 4.7 also shows the evolution of the absorbance at 338 nm and at 481 nm.

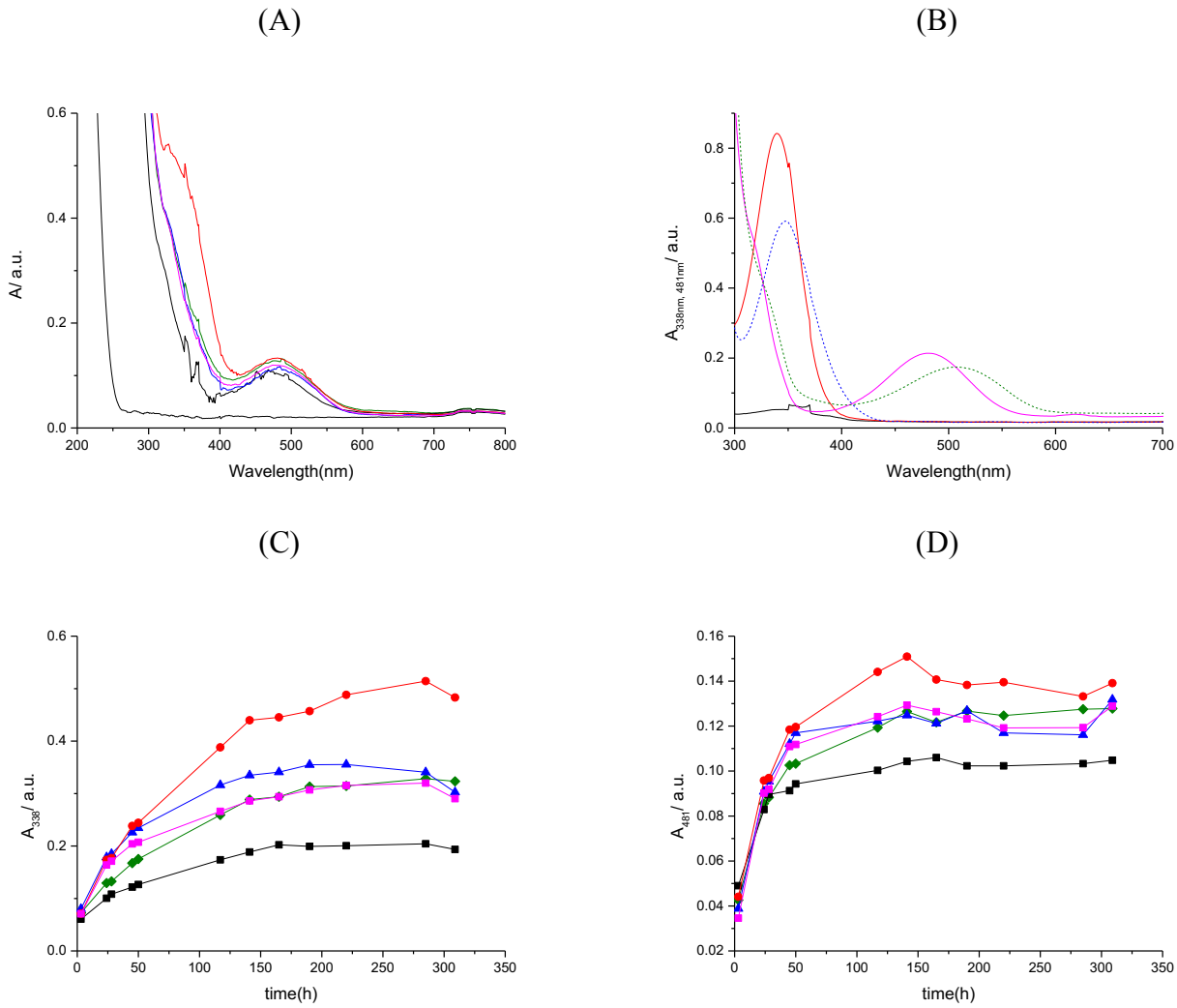

Figure 4.7 (A) UV-visible spectra for **6** and **10** following equilibration in the presence of DNA **(B)** spectra for the free and bound forms of both ligands (also see Section 4.2.1f and 4.2.4d in Chapter 2). **(C)** the absorbance at 338 nm (mainly **6**) as a function of equilibration time and **(D)** the absorbance at 481 nm (mainly **10**) as a function of equilibration time for 10 µM 22AG (♦), 10 µM c-myc (●), 32 µM $(dGdC)_{12}$●$(dGdC)_{12}$ (▲), 39 µM $(dAdT)_{12}$●$(dAdT)_{12}$ (■) and buffer (■).

Figure 4.7A presents the final spectra for the solutions in the 5 holes of the device after equilibration. For reference, Figure 4.7B shows the spectra the free and bound forms of both ligands. Figures 4.7C and D show the changes in absorbance at 338 nm and 481 nm as a function of time. Figure 4.7 shows that the absorbances at 338 nm and 481 nm remain constant after approximately 300 hours. Therefore, Figures 4.7C and D show that equilibrium has been achieved after around 300 hours. Figure 4.2C shows that the absorbance at 338 nm, which is mainly caused by **6**, is highest with c-myc (●). Figure 4.7D shows that the absorbance at 481 nm, which is mainly caused by **10**, also suggests the highest for c-myc (●). The concentrations and apparent affinities of the ligands at equilibrium were determined (Table 4.7).

Table 4.7: Apparent equilibrium constants *K* for 6 and 10 [a] interacting with 22AG, $(dGdC)_{12}$•$(dGdC)_{12}$, c-myc and $(dAdT)_{12}$•$(dAdT)_{12}$ [b]

DNA	22AG		$(dGdC)_{12}$• $(dGdC)_{12}$		c-myc		$(dAdT)_{12}$• $(dAdT)_{12}$		buffer	
$[DNA]_{total}$ / µM	10		32		10		39		/	
unit conc.	quadruplex		bp		quadruplex		bp		/	
Ligand	6	10	6	10	6	10	6	10	6	10
bind. sites / unit conc. [e,f]	2	2	3.33×10^{-1}		3	3	3.33×10^{-1}		/	
$[binding\ sites]_{total}$ / µM	20		10.7		30		13		/	
$A_{338nm,end(6)}$; $A_{481nm,end(10)}$	0.3278	0.1248	0.3397	0.123	0.5083	0.1406	0.3027	0.1244	0.2012	0.10207
Error	0.0073	0.0016	0.0078	0.0016	0.0097	0.0021	0.0063	0.0012	0.0046	0.0018
$A_{338nm,bound}$; $A_{481nm,bound}$	0.15	0.0209	0.17	0.0191	0.34	0.0367	0.13	0.0205	0.0331	0.00183
C_{bound} / µM	6.14	4.7	6.5	4.2	13	8.2	5.17	4.6	/	/
$[ligand]_{free}$ / µM	2.99	11.1	2.99	11.1	2.99	11.1	2.99	11.1	2.99	11.1
$[binding\ sites]_{free}$ / µM	13.9	15	4.07	6.3	16.9	21	7.83	8.3	/	/
K / M^{-1}	1.4×10^{5}	2.77×10^{4}	5.4×10^{5}	6.07×10^{4}	2.5×10^{5}	3.4×10^{4}	2.2×10^{5}	4.9×10^{4}	/	/

a) Concentrations of **6** = 9.2 µM and **10** = 27 µM.

b) In buffer (25 mM MOPS, pH 7.0, 100 mM KCl, and 1 mM EDTA), at 25 °C.

c) $A_{338nm,\ bg}$= 0.0427 $A_{338nm,\ free}$ = 0.1254 and $A_{338nm,\ reservoir}$ was 0.1681, ε_{free} = 42000 M^{-1} cm^{-1} and ε_{bound} = 26030 M^{-1} cm^{-1}.

d) $A_{481nm,\ bg}$= 0.0296 $A_{481nm,\ free}$ = 0.0743 and $A_{481nm,\ reservoir}$ was 0.1039, ε_{free} = 6696 M^{-1} cm^{-1} and ε_{bound} = 4450 M^{-1} cm^{-1}.

e) we assume the binding site size in base pairs is 3.0.

f) For **10**, we know the number of binding sites per quadruplex of c-myc is three and for **6** and **10** we assume the number of binding sites per quadruplex of 22AG are two.

g) The absorbances of the solution in the reservoir at the beginning of the experiment were 0.4209($A_{338\ nm}$) and 0.2006 ($A_{481\ nm}$).

Table 4.7 indicates that **6** and **10** have similar affinities toward all nucleic acids with **6** consistently binding a bit more strongly than **9**. On other hand, Table 4.7 shows that the absorbance of the buffer as a control and the absorbance of ligands in the reservoir at the end are relatively similar, but both differ significantly from the absorbances of the ligands in the reservoir at the start of the experiment. Therefore, **6** and **10** faded a lot. That might be related to fading or to precipitation, because we keep the solutions inside the device for long time. The result of **10** is in agreement with the results from the UV-visible titrations as shown in Chapter 3 which gave $K_{binding}$ of $(4.01 \pm 2.60) \times 10^5$ M^{-1}.

4.2.2b Double competition dialysis for the quantification of affinities of 6 and 14 for duplex and quadruplex.

Compounds H33258 (**6**) and coralyne (**14**) might form a useful couple of compounds that have different affinity to different sequences and also display the required stability. Consequently, to explore whether **6** and **14** have the required relative affinities toward nucleic acids structures, this experiment involved **6** and **14** in combination with duplex-forming and quadruplex-forming sequences c-myc, $(dAdT)_{12}\bullet(dAdT)_{12}$, 22AG, and $(dGdC)_{12}\bullet(dGdC)_{12}$ in buffer (25 mM MOPS, pH 7.0, 100 mM KCl, and 1 mM EDTA), at 25 °C. The spectra of **6** and **14** after equilibration are shown in Figure 4.8. Figure 4.8 also shows the evolution of the absorbance at 338 nm and 423 nm.

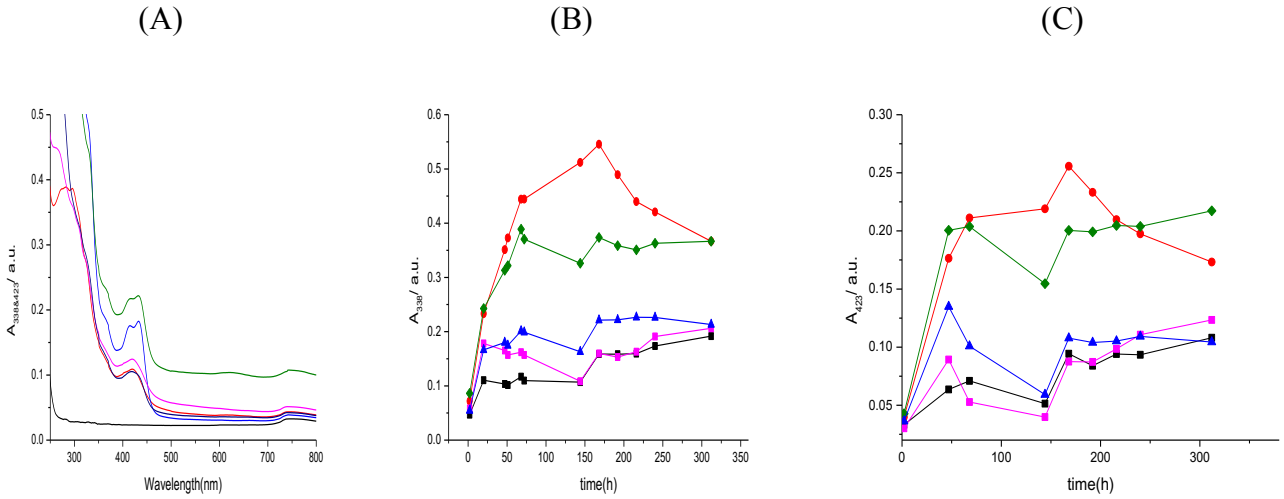

Figure 4.8 (A) UV-visible spectra for **6** and **14** following equilibration in the presence of DNA. **(C)** the absorbance at 338 nm as a function of equilibration time and **(D)** the

absorbance at 423 nm as a function of equilibration time for 10 μM 22AG (♦), 10 μM c-myc (●), 32 μM $(dGdC)_{12}$●$(dGdC)_{12}$ (▲), 39 μM $(dAdT)_{12}$●$(dAdT)_{12}$ (■) and buffer (■).

Figure 4.8A presents the final spectra for the solutions in the 5 holes of the device after equilibration. For reference, Figure 4.8B and C show the changes in absorbance at 338 nm and 423 nm as a function of time. Figure 4.8B shows that the absorbance at 338 nm is highest with c-myc, suggesting that **6** has highest affinity toward c-myc (●) while Figure 4.8C shows the higest final absorbance with 22AG, suggesting that **14** has the highest affinity toward 22AG. Figures 4.8B and C also show that the absorbance as a function of time shows a lot of scatter. We are unsure what caused this scatter. Unfortunately, we cannot analyse this data to find the apparent affinities of the ligands after equilibration. We cannot recorded the UV-visible titration because the poor solubility of coralyne (**14**) in buffer. [58, 59, 188]

4.2.2c Double competition dialysis methods for the quantification of affinities of 10 and 11 for duplex and quadruplex DNA.

We select **10** (ethidium bromide) and **11** (DAPI) because of the stability of these compounds. To know whether **10** and **11** have different affinities toward duplexes $(dAdT)_{12}$●$(dAdT)_{12}$, $(dGdC)_{12}$●$(dGdC)_{12}$ and quadruplex DNA c-myc and 22AG in buffer (25 mM MOPS, pH 7.0, 100 mM KCl, and 1 mM EDTA), at 25 °C we carried out a double competition dialysis experiment. The spectra of **10** and **11** after equilibration with different DNA structures are shown in Figure 4.9. Figure 4.9 also shows the evolution of the absorbance at 342 nm and 481 nm.

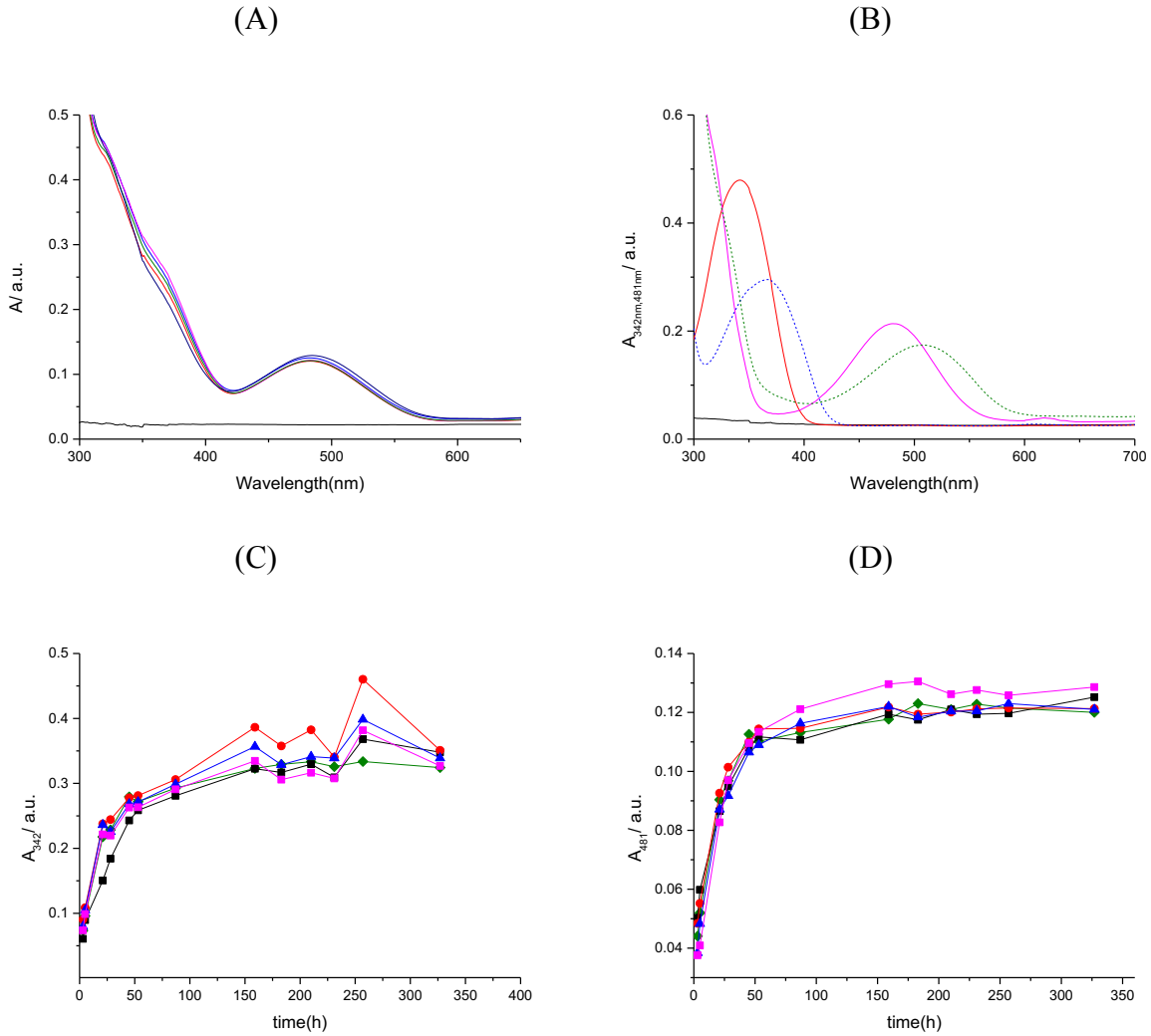

Figure 4.9 (A) UV-visible spectra for **10** and **11** following equilibration in the presence of DNA **(B)** spectra for the free and bound forms of both ligands (also see Section 4.2.4d and

4.2.4e in Chapter 2). **(C)** the absorbance at 342 nm (mainly **11**) as a function of time and **(D)** the absorbance at 481 nm (mainly **10**) as a function of equilibration time for 10 μM 22AG (♦), 10 μM c-myc (●), 32 $(dGdC)_{12}$●$(dGdC)_{12}$ (▲), 39 μM $(dAdT)_{12}$●$(dAdT)_{12}$ (■) and buffer (■).

Figure 4.9A presents the final spectra for the solutions in the 5 holes of the device after equilibration. Figures 4.9C and D show that equilibrium has been achieved after around 300 hours. Figure 4.9C shows the absorbance at 342 nm is also similar to the hole containing buffer only, this suggests that **11** has negligible affinity for the different DNA sequences. Figure 4.9D shows that the absorbance at 481 nm is more or less the same for all sequences and for buffer only. This suggests no affinity of **10** for these sequences. The concentrations and apparent affinities of the ligands after equilibration were nevertheless determined (Table 4.8).

Table 4.8: Apparent equilibrium constants *K* for 10 and 6.11[a] interacting with 22AG, c-myc, $(dGdC)_{12}$•$(dGdC)_{12}$ and $(dAdT)_{12}$•$(dAdT)_{12}$ [b]

DNA	22AG		c-myc		$(dGdC)_{12}$• $(dGdC)_{12}$		$(dAdT)_{12}$• $(dAdT)_{12}$		buffer	
$[DNA]_{total}$ / µM	10		10		32		39		/	
unit conc.	quadruplex		quadruplex		bp		bp		/	
Ligand	10	11	10	11	10	11	10	11	10	11
bind. sites / unit conc. [e,f,g]	2	11	3	4	3.33×10^{-1}		3.33×10^{-1}		/	
$[binding\ sites]_{total}$ / M	2.0×10^{-5}	1.1×10^{-4}	3.0×10^{-5}	4.0×10^{-5}	1.07×10^{-5}		1.30×10^{-5}		/	
$A_{481nm,end(10)}$; $A_{342nm,end(11)}$	0.1192	0.3223	0.1189	0.3703	0.1198	0.34255	0.1274	0.32221	0.1177	0.33198
Error	0.0014	0.0052	0.0014	0.0157	0.0010	0.01084	0.00088	0.00978	0.0024	0.0070
$A_{481nm,bound}$;$A_{342nm,bound}$	0.0157	0.13585	0.0154	0.1838	0.0163	0.1560	0.0239	0.1357	0.0142	0.1454
C_{bound} / µM	3.54	11	3.47	15	3.68	12	5.37	11	/	/
$[ligand]_{free}$ / µM	12	6.87	12	6.87	12	6.87	12	6.87	12	6.87
$[binding\ sites]_{free}$ / µM	16	98.8	26	24	6.99	2.15	7.63	1.86	/	/
K / M^{-1}	1.7×10^{4}	1.6×10^{4}	1.09×10^{4}	8.8×10^{4}	4.3×10^{4}	8.6×10^{5}	5.8×10^{4}	8.7×10^{5}	/	/

a) Concentrations of **10** = 29 µM and **11** = 14 µM.
b) In buffer (25 mM MOPS, pH 7.0, 100 mM KCl, and 1 mM EDTA), at 25 °C.
c) $A_{481nm,\ bg}$= 0.0228 $A_{481nm,\ free}$ = 0.0807 and $A_{481nm,\ reservoir}$ was 0.1035, ε_{free} = 6696 M^{-1} cm^{-1} and ε_{bound} = 4450 M^{-1} cm^{-1}.
d) $A_{342nm,\ bg}$= 0.0245 $A_{342nm,\ free}$ = 0.162 and $A_{342nm,\ reservoir}$ was 0.1865, ε_{free} = 64095 M^{-1} cm^{-1} and ε_{bound} = 45826 M^{-1} cm^{-1}.
e) We assume the binding site size in base pairs is 3.0.
f) For **10** and **11**, we know that the number of binding sites per quadruplex of c-myc is three and four, respectively.
g) for **11** we also know the number of binding sites per quadruplex of 22AG is eleven, but we assume the number of binding sites per quadruplex of 22AG is two for **10**.
h) Absorbances of the solution in the reservoir at the beginning of the experiment were 0.3683($A_{342\ nm}$) and 0.2191 ($A_{481\ nm}$).

It appears from Table 4.8 that the **10** has a high affinity toward to $(dAdT)_{12}$●$(dAdT)_{12}$ and $(dGdC)_{12}$●$(dGdC)_{12}$. However, **11** has no affinity toward DNA. There is a big difference between the absorbance of the reservoir and the absorbance in the control hole for ligand **11**. The control therefore shows us that there is a problem with **11**. Therefore, these two ligands are not useful for the double competition dialysis.

4.3 Conclusion

We show data for a series of nucleic acid binders, comparing selectivity and affinity obtained using double competition dialysis. We show that the assay works well and the results are in agreement with the results from the UV-visible titrations (Chapter 2). The quantification of affinities of **5** and **10** for duplex- and quadruplex-forming DNA shows that **5** has affinity toward c-myc and **10** has affinity to c-myc and $(dGdC)_{12}\bullet(dGdC)_{12}$. Equilibration has been successful considering the similar absorbance in the reservoir and in the control hole containing the buffer. The result for **5** is in reasonable agreement with the results from the UV-visible titrations as shown in Chapter 2 which gave ($K_{binding}$) of of $(1.18 \pm 0.21) \times 10^4$ M^{-1}. The result for **10** is in reasonable agreement with the results from the UV-visible titrations as shown in Chapter 2 which gave ($K_{binding}$) of $(4.01 \pm 2.60) \times 10^5$ M^{-1}. However, the affinities of **10** and **11** for duplex and quadruplex DNA are not a successful example for the double competition dialysis. This is because a big difference between the absorbance of the reservoir and the absorbance in the control hole for ligand **11**. On the other hand, the control buffer can identify problems in this experiment. The typical problem in these experiments is the fading of compounds such as methylene blue, thiazole orange and coralyne upon the exposure of light. Therefore, stability for the compounds is a very important selection criterion when selecting compounds for the competition.

4.4 Materials and Methods

4.4.1 Buffer preparation

All experiments were carried out in one of 2 buffers, viz. (25 mM MOPS, 50 mM NaCl and 1 mM EDTA, pH 7.0) or (25 mM MOPS, 100 mM KCl and 1 mM EDTA, pH 7.0). The buffer components were purchased from Melford (CAS 1132-61-2), NaCl was purchased from Fisher Scientific (CAS 7647-14-5), KCl was purchased from Sigma Aldrich (CAS 7447-40-7), EDTA was purchased from VWR (CAS 60-00-4). Buffers were titrated with aqueous NaOH and KOH. The pH of aqueous solutions was determined using a Hanna microprocessor pH 113 pH-meter equipped with a VWR 662-1382 glass electrode. Materials were weighed out on a Fisherbrand 4-decimal balance. De-ionised water was produced using an ELGA water purifier for all solutions.

A buffer containing 25 mM MOPS (3-(N-morpholino) propanesulfonic acid) and 50 mM sodium chloride (NaCl) was prepared by dissolving MOPS and sodium chloride (NaCl) in distilled water and stirring at room temperature until the solid dissolved. A solution of sodium hydroxide (NaOH) is used for adjusting the pH to 7.0 and the buffer was made up to 2 liters in a volumetric flask.

A buffer containing 25 mM MOPS (3-(N-morpholino) propanesulfonic acid) and 100 mM potassium chloride (KCl) was prepared by dissolving MOPS and potassium chloride (KCl) in distilled water and stirring at room temperature until the solid dissolved. Potassium hydroxide (KOH) was used for adjusting the pH to 7.0 and the buffer was made up to 2 liters in a volumetric flask.

4.4.2 DNA preparation

Fish sperm DNA was purchased from Acros Organics (CAS 68938-01-2). The stock solution of fish sperm DNA was prepared by placing the DNA in buffer and then sonicating the suspension of FS-DNA for about 10 minutes to get a homogeneous solution. All DNA solutions were dialysed against buffer. The dialysis process for the DNA solution was carried out by taking the DNA solution and placing it into dialysis tubing of appropriate pore size (3.5 kDa MWCO).[189] The dialysis tube was suspended for 24 hours inside a beaker that contains the MOPS buffer until the impurities were completely diffused out. The DNA concentrations were determined from the absorbance using the extinction coefficient of FS-DNA of 12800 M^{-1} cm^{-1} in terms of base pair molarity as recorded using UV-visible spectroscopy at 260 nm.[190]

The concentration of quadruplex DNA c-myc (dTdGdA dGdGdG dTdGdG dGdTdT dGdGdG dTdGdG dGdTdAdA) was determined using UV-visible spectroscopy in terms of quadruplex molarity by using the extinction coefficient of 228700 M^{-1} cm^{-1} at 260 nm. The concentration of 22AG (dAdGdG dGdTdT dAdGdG dGdTdT dAdGdG dGdTdT dAdGdGdG) was determined using UV-visible spectroscopy in terms of quadruplex molarity by using the extinction coefficient of 228500 M^{-1} cm^{-1} at 260 nm.[76] The concentration of EAD2 (CTG-GGA-GGG-AGG-GAG-GGA) was determined using UV-visible spectroscopy in terms of quadruplex molarity by using the extinction coefficient of 189900 M^{-1} cm^{-1} at 260 nm.[181]

For the preparation of double-stranded DNA solutions of poly (dAdT) and poly (dGdC), we dissolve each sequence in 1 ml of buffer. Then the dialysis process for the DNA solution was carried out by taking the DNA solution and placing it into dialysis tubing of sufficient pore size (3.5 kDa MWCO). The dialysis tube was suspended for 24 hours inside a beaker that contains the MOPS buffer until the impurities were completely diffused out. The DNA concentration was determined using UV-visible spectroscopy in terms of base pair molarity using the extinction coefficient of 14800 M^{-1} cm^{-1} at 254 nm for poly (dGdC) and 12000 M^{-1} cm^{-1} at 260 nm for poly (dAdT).[127] Duplexes were then annealed by placing the each DNA solution into an eppendorf and placing the eppendorf in a beaker that contains water at 95°C allowing to cool down. Finally, we determine the concentration of each solution.

For single stranded DNA such as poly (dA) and poly (dT), we dissolve each sequence in 1ml of buffer in (25 mM MOPS, 50 mM NaCl and 1 mM EDTA, pH 7.0). The dialysis process for the DNA solution was carried out by taking the DNA solution and placing it into the dialysis tubing of sufficient pore size (3.5 kDa MWCO). The dialysis tube was suspended for 24 hours inside a beaker that contains the MOPS buffer until the impurities were completely diffused out. The DNA concentration was determined using UV-visible spectroscopy and using the extinction coefficient of 8600 M^{-1} cm^{-1} at 257 nm for single-stranded $(dA)_{24}$ and 8520 M^{-1} cm^{-1} at 264 nm for single stranded of $(dT)_{24}$. We then mixed both sequences to form one solution in an eppendorf that was then placed in a beaker that contains water at 95°C allowing to cool down to room temperature. Finally, the concentration of each solution was determined using UV-visible spectroscopy in terms of base pair molarity using the extinction coefficient of 12000 M^{-1} cm^{-1} at 260 nm for poly (dA) ●poly (dT).[127]

4.4.3 Dialysis units

Dialysis using dialysis tubing was carried out by taking the DNA solution and placing it into the dialysis tube of sufficient pore size (3.5 kDa MWCO). The dialysis tube was suspended for 24 hours inside a beaker that contains the MOPS buffer until the impurities were completely diffused out. The dialysis tubing was purchased from Medicell Membranes Ltd, MWCO 12-14000 Daltons. Dialysis membrane was also purchased from Medicell Membranes Ltd, (MWCO 3500 Daltons) and was used for the dialysis device (double competition dialysis), in the middle part of the device.[124]

4.4.4 Competition dialysis data analysis.

For duplex DNA, $[DNA]_{total}$ is the DNA concentration of FS-DNA, $(dAdT)_{12}$●$(dAdT)_{12}$ and $(dGdC)_{12}$●$(dGdC)_{12}$ in terms of base pairs. For quadruplex DNA, $[DNA]_{total}$ equals the concentration of quadruplex structures such as c-myc, 22AG and EAD2 (i.e. not in terms of quartets). Depending on the unit of DNA concentrations, we use a binding site size (if the concentrations are in units of bp for duplex DNA) or a stoichiometry in units of quadruplex^{-1} for the different quadruplexes.

We expressed the binding site size in term of base pairs and this was typically set to 3.0, which means 1 ligand binds to 3 base pairs. For the quadruplexes we have typically assumed two binding sites per quadruplex structure. For **9**, we knew the number of binding sites per quadruplex for c-myc, 22AG and EAD2 (Chapter 2). The stoichiometries are 6 ligands per quadruplex of c-myc, 7 ligands per quadruplex of 22AG and 3 ligands per quadruplex of EAD2.

The total concentration of binding sites in solution is given by $[\text{binding sites}]_{total}$.

$[\text{binding sites}]_{total}$ is defined as "binding sites per unit concentration" × the total concentration of DNA in the selected unit of concentration.

A is the ligand absorbance observed at a specific wavelength (λ_{max})

A_{bound} is given by:

$$A_{bound} = A_{obs}-(A_{bg}+A_{free})$$

$$A_{obs} = A_{bg}+A_{free}+A_{bound}$$

$$A_{obs} = A_{bg}+ \varepsilon_{free} \times c_{free} \times l + \varepsilon_{bound} \times c_{bound} \times l$$

$A_{obs}-(A_{bg}+A_{free}) = \varepsilon_{bound} \times c_{bound} \times l$

Subsequently:

$A_{obs}-(A_{bg}+A_{free})$

A_{obs} is the observed signal for the ligand

A_{bg} is the background signal or the buffer absorbance

A_{free} is the difference (A_{obs} - A_{bg})

We can determine $[ligand]_{bound}$ from A_{bound} / $epsilon_{bound} \times$ pathlength

$ligand_{free} = A_{free}$ / $epsilon_{free} \times$ pathlength

$[binding\ site]_{free}$ is given by:

$[binding\ site\ size]_{free} = [binding\ site\ size]_{total} - [ligand]_{bound}$

To calculate *K* value:

$K = [ligand]_{bound} / [ligand]_{free} \times [binding\ sites]_{free}$

The absorption is plotted against time to obtain the optimal approximation for $signal_{end}$ and k_{obs} from the best fit of a pseudo-first-order kinetic rate model to the data [199] (Equation 1).

$(signal_{start} - signal_{end}) \times \exp(-1 \times k_{obs} \times time) + signal_{end}$

$(\Delta A)\ e^{-kobst \times t} + signal_{end}$ Equation 1

The terms in the equation are defined as follows.

ΔA is the difference between the ligand absorbance and the buffer absorbance, k_{obs} is the observed pseudo-first-order rate constant and *t* is defined as the time in hours.

4.5 Equipment

4.5.1 Spectroscopic studies

UV-visible spectra were recorded using a Jasco V-630BIO spectrophotometer with a Peltier temperature controller. All concentrations were determined in a 1.0 cm cuvette path length at 25 °C. Ligands concentrations were determined using the extinction coefficient. The stock solutions of different ligands were added into 2500 µl of buffer in a 1.0 cm cuvette path length at 25 °C. UV-visible spectra in the range 200 - 600 nm were recorded. The absorption was kept in the range of 0.1-0.8 a.u. to avoid any non-linearity of signals and precipitation or self-aggregation of ligand. The absorptions at selected wavelength λ_{max} were plotted against time. The evolution of absorbances as a function of time were analysed in terms of a first-order kinetics model using Origin 9.

Chapter 5

Epilogue

Abstract

This chapter presents an overview and general conclusions of the work described in this thesis and an outlook for future work.

5.1 General conclusions

The main objective of this project was the development of a custom competition dialysis device that allows us to carry out double competition dialysis assays conveniently.

Chapter 2 of this thesis describes our work to determine the extinction coefficients for selected optolectronically active π-conjugated molecules in our aqueous buffer solutions. These studies also established that eosin b, ponceau s, sulforhodamine, basic fuchsin, basic yellow (thioflavin T), ethidium bromide and DAPI are sufficiently stable and soluble in aqueous solutions. The extinction coefficients were determined successfully are summarised in Table 5.1.

Compound	Extinction coefficients / M^{-1} cm^{-1}
eosin b	(57063 ± 457)
ponceau s	(36355 ± 581)
Sulforhodamine	(84469 ± 563)
basic fuchsin	(79644 ± 192)
basic yellow (thioflavin T)	(24073 ± 135)
ethidium bromide	(6645 ± 65.27)
DAPI	(23570 ± 786)
H33258	42000
GB01	33000
Coralyne	14500

TF1, methylene blue, thiazole orange and DODC were found to fade significantly upon exposure to light. We found that different buffers do not affect significantly the sensitivity to light, indicating that the buffer does not affect the fading. Because of limited solubility, we also determined the extinction coefficient of TF1 (**8**) in pure DMSO and pure acetonitrile and in aqueous mixtures containing these cosolvents. The extinction coefficients for TF1 (**8**) in aqueous acetonitrile and aqueous DMSO are similar.

In addition, we describe the binding studies of a series of potential nucleic acid binders from a library of available (commercial and in-house synthesised) ligands to double-stranded FS-DNA and to different quadruplex-forming sequences (c-myc, 22AG and EAD2). According to UV-visible spectroscopy titrations, eosin b, ponceau s and sulforhodamine

show no binding affinity for duplex FS-DNA. For these compounds, the lack of binding is because the negative charge of the sulphonate group leads to increase in electrostatic repulsion between ligand and DNA. On the contrary, compounds methylene blue (**9**) with a high affinity of **9** duplex FS-DNA with a binding constant of ~ 10^5 M^{-1} and TF1 (**8**) shows a moderate affinity for duplex FS-DNA with a binding constant of ~ 10^3 M^{-1}. At the same time, basic fuchsin (**4**) and basic yellow (thioflavin T) (**5**) have a high affinity (~ 10^4 M^{-1}) for DNA.

We also investigated the effect of added cosolvents on affinities and we show decreasing binding affinity of methylene blue (**9**) for DNA in the presence of DMSO comparing with only buffer. Moreover, the DNA-binding affinity of compound **8** in the presence of DMSO is higher (~ 10^5 M^{-1}) than in the presence of acetonitrile (~ 10^3 M^{-1}).

Moreover, compounds **9-11** bind to a specific quadruplex-forming sequences such as c-myc, 22AG and EAD2. Compound **9** has a higher affinity for c-myc than for 22AG and EAD2. The binding stoichiometry for **9** with c-myc was found to be 6 ligands per quadruplex. Compound **11** also binds more strongly to c-myc than to 22AG. The binding stoichiometry for **11** with c-myc was found to be 4 ligands bind per quadruplex.

To investigate the binding mode of **3**, **4** and **7** with FS-DNA, we used circular dichroism spectroscopy. The interaction of **3** with FS-DNA does not result in an important induced circular dichroism signal, which suggests that **3** does not interact strongly with DNA. However, we found that the binding modes for **4** and **7** with FS-DNA are intercalation and groove binding, respectively. Finally, ITC shows the affinity of **7** for FS-DNA and suggests the presence of at least one binding event.

In Chapter 3, we describe the creation of a dialysis device that works very well and gives good affinity data for ligands interacting with nucleic acid structures as evidenced by agreement with affinities from UV-visible spectroscopy. Furthermore, we used competition dialysis as a test for affinity and selectivity of ligands for nucleic acid structures such as quadruplex, c-myc, 22AG and specific duplex-forming sequences such as, $(dAdT)_{12}$●$(dAdT)_{12}$ and $(dGdC)_{12}$●$(dGdC)_{12}$. We compare the results with the results from UV-vis titration (as shown in Chapter 2) and conclude that the results are in reasonable agreement.

Finally, in Chapter 4, we show data for couples of nucleic acid binders, comparing selectivity and affinity obtained using double competition dialysis. We show that the assay works well and the results are in agreement with the results from the UV-visible titrations (Chapter 2).

On the other hand, the control buffer identifies problems in this experiment. The typical problem in these experiments is the fading of compounds such as methylene blue, thiazole orange and DODC upon the exposure to light for the long duration of these experiments. Therefore, stability for the compounds is very important in order to select compounds for the competition.

5.2 Suggestion and future work

Important future goals include modifications to the competition dialysis device, such as keeping the device inside a closed box during the experiment to reduce exposure of the binders to light. Alternatively, we could explore using a less transparent material to construct the device. It is also a good idea to test individual dyes and pairs of dyes in the device with just buffer in all holes. This experiment will allow us to identify problematic dyes, but will also give us a quantitative understanding of intrinsic variability in post equilibration absorbances. Moreover, we should understand the fading more. This can be achieved by studying fading kinetics and determining the reaction mechanisms of fading of these compounds (such as TF1, methylene blue and DODC)

In addition, other important future goals include the double competition dialysis. We should try more compounds with selectivity for different sequences of quadruplex, duplex and DNA● PNA hybrid duplexes. We should identify more candidate compounds and potential target sequences to enhance the chances of identifying orthogonal recognition couples. A further way by which this may be achieved is through further development of the dialysis device to hold more different solutions of nucleic acid solutions than the current four (with the fifth hole used for the buffer control solution).

In addition, we have to repeat experiments more than one time to determine the affinity of H33258 for quadruplex sequences such as c-myc and 22AG and duplex sequences, such as $(dAdT)_{12}$●$(dAdT)_{12}$ and $(dGdC)_{12}$●$(dGdC)_{12}$.

Once orthogonal recognition elements have been identified, the self-assembled nanostructure can be created.

APPENDIX

This Appendix to Chapter 2

A1 UV-visible titration of compound of 1

Table A1 UV-visible titration of 0.015 mM 1 upon addition of 0 – 4.17 mM FS-DNA in buffer (25 mM MOPS, pH 7.0, 50 mM NaCl, 1 mM EDTA), at 25 °C. $[DNA]_{stock}$ = 16.1 mM, $[Ligand]_{stock}$ = 1.2 mM

Cumulative added volume DNA (µL)	Added volume ligand (µL)	Total volume (µL)	[DNA] (M)	[ligand] ($x10^{-5}$ M)	A520 nm
0	0	0	0	0	0.024963
0	30	2405	0	1.51	0.860931
10	30	2415	6.67E-05	1.5	0.854969
20	30	2425	0.000133	1.49	0.851524
35	30	2440	0.000231	1.49	0.847892
55	30	2460	0.00036	1.47	0.841878
85	30	2490	0.00055	1.46	0.833937
125	30	2530	0.000796	1.43	0.8212
175	30	2580	0.001093	1.4	0.807157
240	30	2645	0.001462	1.37	0.790369
315	30	2720	0.001866	1.33	0.770511
400	30	2805	0.002298	1.29	0.747155
495	30	2900	0.00275	1.25	0.725424
600	30	3005	0.003217	1.21	0.702668
715	30	3120	0.003692	1.16	0.67644
840	30	3245	0.004171	1.12	0.651607

A2UV-visible titration of compound of 2

Table A2UV-visible titration of 0.016 mM. 2 upon addition of 0 – 4.26 mM FS-DNA in buffer (25 mM MOPS, pH 7.0, 50 mM NaCl, 1 mM EDTA), at 25 °C. $[DNA]_{stock}$ = 16.1 mM, $[Ligand]_{stock}$ = 0.9 mM.

Cumulative added volume DNA (µL)	Added volume ligand (µL)	Total volume (µL)	[DNA] (M)	[ligand] ($x10^{-5}$ M)	A520 nm
0	0	0	0	0	0.0295219
0	40	2415	0	1.639	0.608532
10	40	2425	6.64412E-05	1.632	0.607947
15	40	2430	9.94568E-05	1.628	0.607103
30	40	2445	0.000197693	1.618	0.606371
45	40	2460	0.000294732	1.609	0.601195
65	40	2480	0.00042229	1.596	0.598383
90	40	2505	0.000578874	1.580	0.593598
120	40	2535	0.000762698	1.561	0.591259
155	40	2570	0.000971735	1.540	0.582787
195	40	2610	0.00120377	1.516	0.575538
240	40	2655	0.001456452	1.490	0.56534
290	40	2705	0.001727349	1.463	0.555694
345	40	2760	0.002014	1.434	0.546512
405	40	2820	0.002313957	1.403	0.53702
470	40	2885	0.002624832	1.372	0.527928
540	40	2955	0.002944325	1.339	0.51264
615	40	3030	0.003270257	1.306	0.504382
695	40	3110	0.003600592	1.272	0.490638
780	40	3195	0.003933446	1.238	0.481089
870	40	3285	0.004267105	1.204	0.46755

A3 UV-visible titration of compound of 3

Table A3 UV-visible titration of 0.0097 mM 3 upon addition of 0 – 3.70 mM FS-DNA in buffer (25 mM MOPS, pH 7.0, 50 mM NaCl, 1 mM EDTA), at 25 °C. [DNA]stock = 16.1 mM, [Ligand]stock = 0.58 mM.

Cumulative added volume DNA (µL)	Added volume ligand (µL)	Total volume (µL)	[DNA] (M)	[ligand] ($x10^{-6}$ M)	A563 nm
0	0	0	0	0	0.0230762
0	40	2415	0	9.74	0.845436
5	40	2420	3.33E-05	9.72	0.844315
20	40	2435	0.000132	9.66	0.839522
50	40	2465	0.000327	9.54	0.82932
95	40	2510	0.00061	9.37	0.817463
150	40	2565	0.000942	9.17	0.799077
225	40	2640	0.001373	8.91	0.779044
320	40	2735	0.001885	8.6	0.753538
435	40	2850	0.002459	8.25	0.725201
570	40	2985	0.003077	7.88	0.694903
720	40	3135	0.0037	7.5	0.663657

A4 UV-visible titration of compound of 4

Table A4 UV-visible titration of 0.0080 mM 4 upon addition of 0 – 4.25 mM FS-DNA in buffer (25 mM MOPS, pH 7.0, 50 mM NaCl, 1 mM EDTA), at 25 °C. [DNA]stock = 16.1 mM, [Ligand]stock = 0.9 mM.

Cumulative added volume DNA (µL)	Added volume ligand (µL)	Total volume (µL)	[DNA]	[ligand] ($x10^{-6}$ M)	A539 nm
0	0	0	0	0	0.027419
0	20	2395	0	8.021	0.957865
5	20	2400	3.35667E-05	8.004	0.922753
10	20	2405	6.69938E-05	7.987	0.898413
15	20	2410	0.000100282	7.971	0.884886
25	20	2420	0.000166446	7.938	0.85869
35	20	2430	0.000232066	7.905	0.848627
45	20	2440	0.000297148	7.873	0.842011
60	20	2455	0.000393776	7.825	0.831079
95	20	2490	0.000614715	7.715	0.807193
160	20	2555	0.001008971	7.518	0.78183
310	20	2705	0.001846477	7.101	0.739657
460	20	2855	0.002595979	6.728	0.70928
610	20	3005	0.003270656	6.392	0.680763
860	20	3255	0.004256934	5.901	0.636237

A5 UV-visible titration of compound of 5

Table A5 UV-visible titration of 0.011 mM 5 upon addition of 0 – 0.74 mM FS-DNA in buffer (25 mM MOPS, pH 7.0, 50 mM NaCl, 1 mM EDTA), at 25 °C. [DNA]stock = 11 mM, [Ligand]stock = 0.070 mM.

Cumulative added volume DNA (µL)	Added volume ligand (µL)	Total volume (µL)	[DNA]	[ligand] ($x10^{-5}$ M)	A412 nm
0	0	0	0	0	0.017465
0	400	2400	0	1.1709	0.29165
1	400	2401	4.58E-06	1.170	0.28866
2	400	2402	9.16E-06	1.170	0.297099
3	400	2403	1.37E-05	1.169	0.286899
4	400	2404	1.83E-05	1.169	0.284639
5	400	2405	2.29E-05	1.168	0.286469
7	400	2407	3.2E-05	1.167	0.280367
10	400	2410	4.56E-05	1.166	0.27812
14	400	2414	6.38E-05	1.164	0.273843
19	400	2419	8.64E-05	1.161	0.268764
29	400	2429	0.000131	1.157	0.262926
39	400	2439	0.000176	1.152	0.252965
54	400	2454	0.000242	1.145	0.245867
74	400	2474	0.000329	1.135	0.23909
124	400	2524	0.00054	1.113	0.222239
174	400	2574	0.000744	1.091	0.212333

A6 UV-visible titrations of compound of 6

Table A6 UV-visible titration of 0.018 mM 6 upon addition of 0 – 0.17 mM FS-DNA in buffer (25 mM MOPS, pH 7.0, 50 mM NaCl, 1 mM EDTA), at 25 °C. [DNA]stock = 16 mM, [Ligand]stock = 0.44 mM.

Cumulative added volume DNA (µL)	Added volume ligand (µL)	Total volume (µL)	[DNA]	[ligand] ($x10^{-5}$ M)	A338 nm
0	0	0	0	0	0.052425
0	100	2400	0	1.87	0.839554
1	100	2401	6.66E-06	1.87	0.707175
2	100	2402	1.33E-05	1.87	0.657087
3	100	2403	2E-05	1.87	0.606835
4	100	2404	2.66E-05	1.87	0.585521
5	100	2405	3.33E-05	1.87	0.570176
6	100	2406	3.99E-05	1.87	0.558692
8	100	2408	5.32E-05	1.86	0.546678
11	100	2411	7.3E-05	1.86	0.551399
16	100	2416	0.000106	1.86	0.548176
26	100	2426	0.000171	1.85	0.548244

Table A6.1 UV-visible titration of 0.017 mM 6 upon addition of 0 – 0.65 mM FS-DNA in buffer (25 mM MOPS, pH 7.0, 50 mM NaCl, 1 mM EDTA), at 25 °C. [DNA]stock = 10 mM, [Ligand]stock = 0.43 mM.

Cumulative added volume DNA (µL)	Added volume ligand (µL)	Total volume (µL)	[DNA]	[ligand] ($x10^{-5}$ M)	A338 nm
0	0	0	0	0	0.038435
0	100	2400	0	1.8	0.794067
1	100	2401	4.1649E-06	1.8	0.730034
2	100	2402	8.3264E-06	1.79	0.665407
3	100	2403	1.2484E-05	1.79	0.616172
4	100	2404	1.6639E-05	1.79	0.580509
5	100	2405	2.079E-05	1.79	0.556638
7	100	2407	2.9082E-05	1.79	0.533729
9	100	2409	3.736E-05	1.79	0.519196
12	100	2412	4.9751E-05	1.79	0.512089
17	100	2417	7.0335E-05	1.78	0.508502
27	100	2427	0.00011125	1.78	0.510529
42	100	2442	0.00017199	1.76	0.520502
62	100	2462	0.00025183	1.75	0.519449
87	100	2487	0.00034982	1.73	0.516946
122	100	2522	0.00048374	1.71	0.518197
167	100	2567	0.00065056	1.68	0.514737

A7 UV-visible titration of compound of 7

Table A7 UV-visible titration of 0.028 mM 7 upon addition of 0 – 2.90 mM FS-DNA in buffer (25 mM MOPS, pH 7.0, 50 mM NaCl, 1 mM EDTA), at 25 °C. [DNA]stock = 17 mM, [Ligand]stock = 0.98 mM.

Cumulative added volume DNA (µL)	Added volume ligand (µL)	Total volume (µL)	[DNA]	[ligand] ($x10^{-5}$ M)	A331 nm
0	0	0	0	0	0.033005
0	70	2445	0	2.83	0.966682
5	70	2450	3.61E-05	2.82	0.7262
10	70	2455	7.21E-05	2.82	0.725121
15	70	2460	0.000108	2.81	0.735498
20	70	2465	0.000144	2.81	0.749349
30	70	2475	0.000215	2.8	0.763345
40	70	2485	0.000285	2.78	0.772927
50	70	2495	0.000355	2.77	0.780035
65	70	2510	0.000458	2.76	0.785839
80	70	2525	0.000561	2.74	0.792399
105	70	2550	0.000729	2.71	0.796304
130	70	2575	0.000894	2.69	0.798039
165	70	2610	0.001119	2.65	0.799567
200	70	2645	0.001339	2.62	0.799893
245	70	2690	0.001612	2.57	0.793153
290	70	2735	0.001877	2.53	0.789441
340	70	2785	0.002161	2.48	0.781579
405	70	2850	0.002516	2.43	0.769321
480	70	2925	0.002905	2.37	0.757858

A7.1 ITC of compound of 7

Table A7.1 Thermodynamic parameters for diluting of 7 into MOPS buffer, pH 7.0, at 25 °C

variable	initial	change?	avoid 0?	fit value	att. changes
DHdil	-1.00E+03	1	y	-9.39E+02	196696
offset	0.00E+00	0	n	0.00E+00	0
Kdim	0.00E+00	0	n	0.00E+00	0
DHdim	0.00E+00	0	n	0.00E+00	0
Kagg	1.00E+04	1	y	1.48E+03	196922
DHagg	-6.00E+03	1	y	-9.02E+03	196382
KA1	0.00E+00	0	y	0.00E+00	0
DHA1	0.00E+00	0	y	0.00E+00	0
nA1	0.00E+00	0	y	0.00E+00	0
KA2	0.00E+00	0	n	0.00E+00	0
DHA2	0.00E+00	0	n	0.00E+00	0
nA2	0.00E+00	0	n	0.00E+00	0
KB1	0.00E+00	0	n.d.	0.00E+00	0
DHB1	0.00E+00	0	n.d.	0.00E+00	0
nB1	0.00E+00	0	n.d.	0.00E+00	0

Table A7.2 Thermodynamic parameters for binding of 7 to DNA in MOPS buffer, pH 7.0, at 25 °C

variable	initial	change?	avoid 0?	fit value	att. changes
DHdil	-9.39E+02	0	n	-9.39E+02	0
offset	0.00E+00	0	n	0.00E+00	0
Kdim	0.00E+00	0	n	0.00E+00	0
DHdim	0.00E+00	0	n	0.00E+00	0
Kagg	1.48E+03	0	n	1.48E+03	0
DHagg	-9.02E+03	0	n	-9.02E+03	0
KA1	5.00E+04	1	y	4.48E+05	196696
DHA1	2.00E+03	1	y	-6.45E+03	196922
nA1	3.00E-01	1	y	8.48E-01	196382
KA2	0.00E+00	0	n	0.00E+00	0
DHA2	0.00E+00	0	n	0.00E+00	0
nA2	0.00E+00	0	n	0.00E+00	0
KB1	0.00E+00	0	n.d.	0.00E+00	0
DHB1	0.00E+00	0	n.d.	0.00E+00	0
nB1	0.00E+00	0	n.d.	0.00E+00	0

Figure 1 normalised $\Sigma dev^2/dof$ for a stepwise self-aggregation model fitted to ITC data for dilution of a 0.95 mM solution of **7** into a 25 mM MOPS, 50 mM NaCl, pH 7, 1 mM EDTA at 25 °C as a function of ΔH_{agg}.

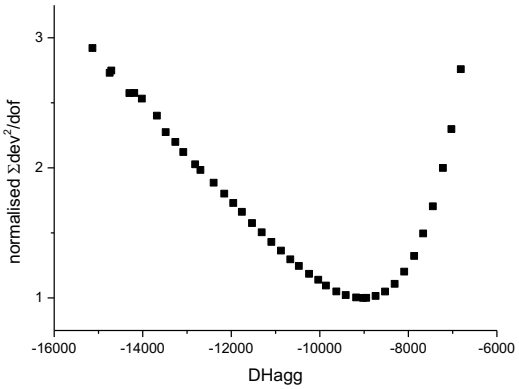

Figure 2 normalised $\Sigma dev^2/dof$ for a stepwise self-aggregation model fitted to ITC data for dilution of a 0.95 mM solution of **7** into a 25 mM MOPS, 50 mM NaCl, pH 7, 1mM EDTA at 25 °C as a function of ΔH_{dil}.

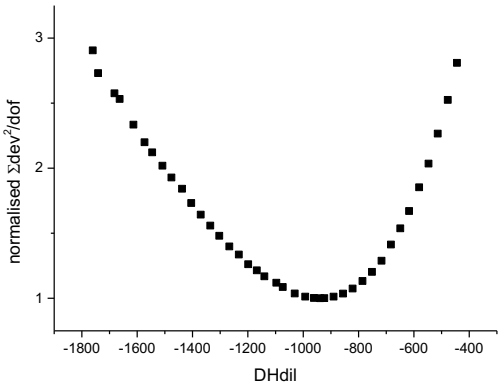

Figure 3 normalised $\Sigma dev^2/dof$ for a stepwise self-aggregation model fitted to ITC data for dilution of a 0.95 mM solution of **7** into a 25 mM MOPS, 50 mM NaCl, pH 7, 1 mM EDTA at 25 °C as a function of K_{gg}.

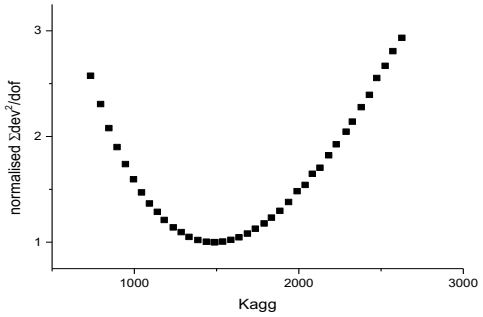

Figure 4 normalised $\Sigma dev^2/dof$ for a stepwise self-aggregation model fitted to ITC data for dilution of a 0.95 mM solution of **7** into a 25 mM MOPS, 50 mM NaCl, pH 7, 1 mM EDTA at 25 °C as a function of ΔG_{agg}.

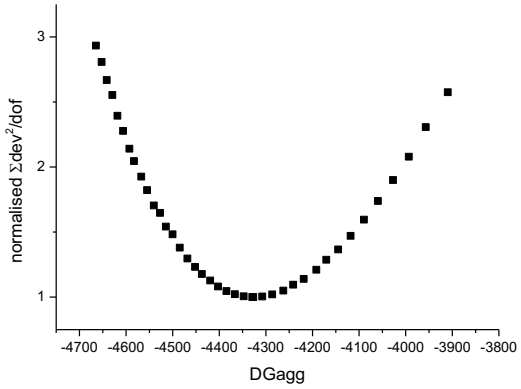

A8 UV-visible titration of compound of 8

Table A8UV-visible titration of 0.0029 mM 8 in presence of 1.04 % of acetonitrile upon addition of 0 – 1.04 mM FS-DNA in buffer (25 mM MOPS, pH 7.0, 50 mM NaCl, 1 mM EDTA), at 25 °C. [DNA]stock$_1$ = 17 mM and [DNA]stock$_2$ = 1.7 mM, [Ligand]stock = 0.28 mM.

Cumulative added volume DNA (µL)	Added volume ligand (µL)	Total volume (µL)	[DNA]	[ligand] (x10^{-6} M)	A476 nm
0	0	2375	0	0	0.027701
0	25	2400	0	2.93	0.178401
1	25	2401	7.08E-07	2.93	0.163616
2	25	2402	1.42E-06	2.93	0.157205
3	25	2403	2.12E-06	2.93	0.148839
5	25	2405	3.53E-06	2.93	0.143132
8	25	2408	5.65E-06	2.92	0.134969
12	25	2412	8.46E-06	2.92	0.125868
17	25	2417	1.2E-05	2.91	0.120721
22	25	2422	1.54E-05	2.91	0.122923
27	25	2427	1.89E-05	2.9	0.118094
7.7	25	2432	5.61E-05	2.89	0.109457
12.7	25	2437	9.23E-05	2.89	0.120128
22.7	25	2447	0.000164	2.88	0.128531
32.7	25	2457	0.000236	2.86	0.136591
47.7	25	2472	0.000342	2.85	0.143664
72.7	25	2497	0.000515	2.82	0.153688
107.7	25	2532	0.000753	2.78	0.160581
152.7	25	2577	0.001049	2.73	0.162239

Table A8.1 UV-visible titration of 0.0008 mM 8 upon addition of 0 – 0.44 mM FS-DNA in buffer (25 mM MOPS, pH 7.0, 100 mM KCl, 9 vol-% DMSO and 1 Mm EDTA), at 25 °C. [DNA]stock = 15 mM, [Ligand]stock = 0.0031 mM

Cumulative added volume DNA (µL)	Added volume ligand (µL)	Total volume (µL)	[DNA]	[ligand] ($x10^{-7}$ M)	A476 nm
0	0	0	0	0	0.026018
0	800	2800	0	8.897	0.071762
1	800	2801	5.36594E-06	8.893	0.070785
2	800	2802	1.07281E-05	8.890	0.067611
3	800	2803	1.60863E-05	8.887	0.066927
5	800	2805	2.67914E-05	8.881	0.066881
8	800	2808	4.28205E-05	8.871	0.064229
11	800	2811	5.88154E-05	8.862	0.063979
15	800	2815	8.00888E-05	8.849	0.063239
20	800	2820	0.000106596	8.834	0.062852
25	800	2825	0.000133009	8.818	0.062423
35	800	2835	0.000185556	8.787	0.06248
45	800	2845	0.000237733	8.756	0.06083
55	800	2855	0.000289545	8.725	0.062236
70	800	2870	0.000366585	8.680	0.060135
85	800	2885	0.000442825	8.635	0.059629

Table A8.2 UV-visible titration of 0.0015 mM 8 upon addition of 0 – 0.45 mM FS-DNA in buffer (25 mM MOPS, pH 7.0, 100 mM KCl, 9 vol-% DMSO and 1 mM EDTA), at 25 °C. [DNA]stock = 15 mM, [Ligand]stock = 0.0060 mM

Cumulative added volume DNA (µL)	Added volume ligand (µL)	Total volume (µL)	[DNA]	[ligand] ($x10^{-6}$ M)	A476 nm
0	0	0	0	0	0.02038
0	700	2700	0	1.57	0.10083
1	700	2701	5.56E-06	1.56	0.09741
2	700	2702	1.11E-05	1.56	0.09466
3	700	2703	1.67E-05	1.56	0.09417
5	700	2705	2.78E-05	1.56	0.09334
8	700	2708	4.44E-05	1.56	0.08948
11	700	2711	6.1E-05	1.56	0.08936
15	700	2715	8.3E-05	1.56	0.08796
20	700	2720	0.000111	1.55	0.08722
25	700	2725	0.000138	1.55	0.08718
35	700	2735	0.000192	1.55	0.08565
45	700	2745	0.000246	1.54	0.08345
55	700	2755	0.0003	1.53	0.08337
70	700	2770	0.00038	1.53	0.08255
85	700	2785	0.000459	1.52	0.08213

A9 UV-visible titrations of compound of 9

Table A9UV-visible titration of 0.0035 mM 9 upon addition of 0 – 4.6 mM FS-DNA in buffer (25 mM MOPS, pH 7.0, 50 mM NaCl, 1 mM EDTA), at 25 °C. [DNA]stock = 14 mM, [Ligand]stock = 1.4 mM

Cumulative added volume DNA (µL)	Added volume ligand (µL)	Total volume (µL)	[DNA]	[ligand] ($x10^{-6}$ M)	A663 nm
0	0	2000	0	0	0.02248
0	5	2005	0	3.57	0.30085
1	5	2006	7.33E-06	3.57	0.269774
3	5	2008	2.2E-05	3.56	0.252462
5	5	2010	3.66E-05	3.56	0.240762
7	5	2012	5.12E-05	3.56	0.232359
9	5	2014	6.57E-05	3.55	0.228138
11	5	2016	8.03E-05	3.55	0.22493
16	5	2021	0.000116	3.54	0.222443
21	5	2026	0.000152	3.53	0.220084
26	5	2031	0.000188	3.52	0.218901
31	5	2036	0.000224	3.51	0.215157
36	5	2041	0.000259	3.51	0.21633
46	5	2051	0.00033	3.49	0.214286
66	5	2071	0.000469	3.46	0.212827
116	5	2121	0.000805	3.37	0.211435
166	5	2171	0.001125	3.3	0.208606
316	5	2321	0.002003	3.08	0.198093
516	5	2521	0.003011	2.84	0.184381
716	5	2721	0.003871	2.63	0.174674
916	5	2921	0.004613	2.45	0.165187

Table A9.1UV-visible titration of 0.004 mM 9 upon addition of 0 – 0.19 mM FS-DNA in buffer (25 mM MOPS, pH 7.0, 100 mM KCl, 9 vol-% DMSO and 1 mM EDTA), at 25 °C. [DNA]stock = 19 mM, [Ligand]stock = 0.14 mM

Cumulative added volume DNA (µL)	Added volume ligand (µL)	Total volume (µL)	[DNA]	[ligand] ($x10^{-6}$ M)	A663 nm
0	0	2000	0	0	0.019418
0	70	2070	0	4.88	0.400304
1	70	2071	9.24E-06	4.88	0.385613
3	70	2073	2.77E-05	4.88	0.365823
5	70	2075	4.61E-05	4.87	0.351676
7	70	2077	6.45E-05	4.87	0.342728
9	70	2079	8.29E-05	4.86	0.343271
11	70	2081	0.000101	4.86	0.336805
16	70	2086	0.000147	4.85	0.327029
21	70	2091	0.000192	4.83	0.322373

Table A9.2 UV-visible titration of 0.0037 mM 9 upon addition of 0 – 0.006 mM c-myc in buffer (25 mM MOPS, pH 7.0, 50 mM NaCl, and 1 mM EDTA), at 25 °C. [c-myc]stock = 0.43 mM, [Ligand]stock = 0.37 mM

Cumulative added volume DNA (µL)	Added volume ligand (µL)	Total volume (µL)	[DNA]	[ligand] ($x10^{-6}$ M)	A663 nm
0	0	0	0	0	0.025621
0	50	2550	0	7.3	0.595289
1	50	2551	1.69E-07	7.3	0.547168
2	50	2552	3.37E-07	7.3	0.514325
3	50	2553	5.05E-07	7.29	0.482571
5	50	2555	8.41E-07	7.29	0.434554
7	50	2557	1.18E-06	7.28	0.397027
10	50	2560	1.68E-06	7.27	0.357836
13	50	2563	2.18E-06	7.27	0.338535
17	50	2567	2.85E-06	7.26	0.3342
22	50	2572	3.68E-06	7.24	0.340724
27	50	2577	4.51E-06	7.23	0.350041
37	50	2587	6.15E-06	7.2	0.367759

Table A9.3 UV-visible titration of 0.0038 mM 9 upon addition of 0 – 0.035 mM 22AG in buffer (25 mM MOPS, pH 7.0, 50 mM NaCl, and 1 mM EDTA), at 25 °C. [22AG]stock = 0.37 mM, [Ligand]stock = 0.38 mM

Cumulative added volume DNA (μL)	Added volume ligand (μL)	Total volume (μL)	[DNA]	[ligand] ($x10^{-6}$ M)	A663 nm
0	0	0	0	0	0.024336
0	25	2525	0	3.81	0.321684
1	25	2526	1.46E-07	3.81	0.317579
3	25	2528	4.39E-07	3.81	0.311755
6	25	2531	8.77E-07	3.8	0.298048
10	25	2535	1.46E-06	3.8	0.2904
15	25	2540	2.19E-06	3.79	0.283499
25	25	2550	3.63E-06	3.77	0.271128
35	25	2560	5.06E-06	3.76	0.262249
50	25	2575	7.18E-06	3.74	0.255163
70	25	2595	9.98E-06	3.71	0.248022
120	25	2645	1.68E-05	3.64	0.2391
170	25	2695	2.33E-05	3.57	0.233499
270	25	2795	3.57E-05	3.44	0.223599

Table A9.4 UV-visible titration of 0.0051 mM 9 upon addition of 0 – 0.0069 mM EAD2 in buffer (25 mM MOPS, pH 7.0, 100 mM KCl, and 1 mM EDTA), at 25 °C. [EAD2]stock = 0.089 mM, [Ligand]stock = 0.26 mM

Cumulative added volume DNA (µL)	Added volume ligand (µL)	Total volume (µL)	[DNA]	[ligand] ($x10^{-6}$ M)	A663 nm
0	0	0	0	0	0.02317
0	50	2550	0	5.17	0.426721
5	50	2555	1.74E-07	5.16	0.415568
10	50	2560	3.48E-07	5.15	0.405448
15	50	2565	5.2E-07	5.14	0.393989
20	50	2570	6.93E-07	5.13	0.383441
25	50	2575	8.64E-07	5.12	0.374234
30	50	2580	1.03E-06	5.11	0.367119
40	50	2590	1.37E-06	5.09	0.351191
50	50	2600	1.71E-06	5.07	0.337987
60	50	2610	2.05E-06	5.05	0.328734
70	50	2620	2.38E-06	5.04	0.320336
80	50	2630	2.71E-06	5.02	0.313191
90	50	2640	3.03E-06	5	0.307767
105	50	2655	3.52E-06	4.97	0.300127
120	50	2670	0.000004	4.94	0.294553
135	50	2685	4.47E-06	4.91	0.291214
150	50	2700	4.94E-06	4.89	0.287755
170	50	2720	5.56E-06	4.85	0.284336
190	50	2740	6.17E-06	4.81	0.278467
215	50	2765	6.92E-06	4.77	0.274208

A10 UV-visible titration of compound of 10

Table A10 UV-visible titration of 0.027 mM 10 upon addition of 0 – 0.023 mM c-myc in buffer (25 mM MOPS, pH 7.0, 100 mM KCl, and 1 mM EDTA), at 25 °C. [c-myc]stock = 0.34 mM, [Ligand]stock = 0.37 mM

Cumulative added volume DNA (µL)	Added volume ligand (µL)	Total volume (µL)	[DNA]	[ligand] ($x10^{-5}$ M)	A481 nm
0	0	0	0	0	0.037602
0	200	2700	0	2.76	0.221167
2	200	2702	2.52E-07	2.75	0.213641
7	200	2707	8.79E-07	2.75	0.21181
12	200	2712	1.5E-06	2.74	0.207669
17	200	2717	2.13E-06	2.74	0.204787
27	200	2727	3.37E-06	2.73	0.197448
37	200	2737	4.6E-06	2.72	0.191412
47	200	2747	5.82E-06	2.71	0.185026
57	200	2757	7.03E-06	2.7	0.179755
72	200	2772	8.83E-06	2.68	0.172849
87	200	2787	1.06E-05	2.67	0.166421
102	200	2802	1.24E-05	2.66	0.162605
122	200	2822	1.47E-05	2.64	0.156249
142	200	2842	1.7E-05	2.62	0.15702
162	200	2862	1.92E-05	2.6	0.154009
182	200	2882	2.15E-05	2.58	0.149465
202	200	2902	2.37E-05	2.56	0.153578

A11 UV-visible titrations of compound of 11

Table A11 UV-visible titration of 0.019 mM 11 upon addition of 0 – 0.007mM 22AG in buffer (25 mM MOPS, pH 7.0, 50 mM NaCl, and 1 mM EDTA), at 25 °C. [22AG]stock = 0.37 mM, [Ligand]stock = 0.7 mM

Cumulative added volume DNA (µL)	Added volume ligand (µL)	Total volume (µL)	[DNA]	[ligand] ($x10^{-5}$ M)	A342 nm
0	0	0	0	0	0.028171
0	70	2570	0	1.95	0.488855
1	70	2571	1.44E-07	1.95	0.477623
3	70	2573	4.31E-07	1.95	0.461553
5	70	2575	7.18E-07	1.95	0.445539
7	70	2577	1.01E-06	1.95	0.432206
9	70	2579	1.29E-06	1.95	0.419181
11	70	2581	1.58E-06	1.95	0.406492
13	70	2583	1.86E-06	1.94	0.395623
15	70	2585	2.15E-06	1.94	0.389088
18	70	2588	2.57E-06	1.94	0.376518
21	70	2591	3E-06	1.94	0.369977
26	70	2596	3.71E-06	1.93	0.358677
36	70	2606	5.11E-06	1.93	0.338019
46	70	2616	6.51E-06	1.92	0.330084
56	70	2626	7.89E-06	1.91	0.327357

Table A11.1 UV-visible titration of 0.019 mM 11 upon addition of 0 – 0.025mM c-myc in buffer (25 mM MOPS, pH 7.0, 100 mM KCl, and 1 mM EDTA), at 25 °C. [c-myc]stock = 0.34 mM, [Ligand]stock = 2.4 mM

Cumulative added volume DNA (µL)	Added volume ligand (µL)	Total volume (µL)	[DNA]	[ligand] ($x10^{-5}$ M)	A342 nm
0	0	0	0	0	0.047873
0	20	2520	0	1.96	0.510126
2	20	2522	2.69627E-07	1.96	0.497406
4	20	2524	5.38827E-07	1.96	0.481601
6	20	2526	8.07601E-07	1.96	0.47021
8	20	2528	1.07595E-06	1.95	0.457545
13	20	2533	1.74497E-06	1.95	0.433789
18	20	2538	2.41135E-06	1.95	0.411758
23	20	2543	3.07511E-06	1.94	0.390788
33	20	2553	4.39483E-06	1.94	0.355235
43	20	2563	5.70425E-06	1.93	0.324969
53	20	2573	7.0035E-06	1.92	0.304024
68	20	2588	8.93354E-06	1.91	0.289233
83	20	2603	1.08413E-05	1.9	0.282941
98	20	2618	1.27273E-05	1.89	0.281062
118	20	2638	1.52085E-05	1.87	0.282079
138	20	2658	1.76524E-05	1.86	0.276557
158	20	2678	2.00597E-05	1.85	0.272735
183	20	2703	2.30189E-05	1.83	0.270489
208	20	2728	2.59238E-05	1.81	0.26825

A12UV-visible titrations of compound of 12

Table A12 UV-visible titration of 0.0061 mM 12 upon addition of 0 – 0.0027mM c-myc in buffer (25 mM MOPS, pH 7.0, 50 mM NaCl, and 1 mM EDTA), at 25 °C. [c-myc]stock = 0.24 mM, [Ligand]stock = 0.7 mM

Cumulative added volume DNA (µL)	Added volume ligand (µL)	Total volume (µL)	[DNA]	[ligand] (x10^{-6} M)	A500 nm
0	0	0	0	0	0.022018
0	20	2520	0	6	0.418617
1	20	2521	9.52E-08	6.1	0.392908
2	20	2522	1.9E-07	6.1	0.363493
3	20	2523	2.85E-07	6.09	0.343658
4	20	2524	3.8E-07	6.09	0.319716
5	20	2525	4.75E-07	6.09	0.303139
7	20	2527	6.65E-07	6.08	0.280882
9	20	2529	8.54E-07	6.08	0.271141
14	20	2534	1.33E-06	6.07	0.263451
19	20	2539	1.8E-06	6.06	0.268503
24	20	2544	2.26E-06	6.04	0.277617
29	20	2549	2.73E-06	6.03	0.284707

Table A12.1 UV-visible titration of 0.0083 mM 12 upon addition of 0 – 0.0066 mM c-myc in buffer (25 mM MOPS, pH 7.0, 50 mM NaCl, and 1 mM EDTA), at 25 °C. [c-myc]stock = 0.4 mM, [Ligand]stock = 0.42 mM

Cumulative added volume DNA (µL)	Added volume ligand (µL)	Total volume (µL)	[DNA]	[ligand] (x10^{-6} M)	A500 nm
0	0	0	0	0	0.022866
0	50	2550	0	8.33	0.564345
1	50	2551	1.57E-07	8.33	0.509113
2	50	2552	3.13E-07	8.32	0.463323
3	50	2553	4.7E-07	8.32	0.43757
4	50	2554	6.26E-07	8.32	0.423453
6	50	2556	9.39E-07	8.31	0.391805
8	50	2558	1.25E-06	8.3	0.374462
10	50	2560	1.56E-06	8.3	0.374582
13	50	2563	2.03E-06	8.29	0.385841
18	50	2568	2.8E-06	8.27	0.391768
33	50	2583	5.11E-06	8.22	0.398861
43	50	2593	6.63E-06	8.19	0.396215

Table A12.2 UV-visible titration of 0.0048 mM 12 upon addition of 0 – 0.003 mM 22AG in buffer (25 mM MOPS, pH 7.0, 50 mM NaCl, and 1 mM EDTA), at 25 °C. [22AG]stock = 0.28 mM, [Ligand]stock = 0.61 mM

Cumulative added volume DNA (µL)	Added volume ligand (µL)	Total volume (µL)	[DNA]	[ligand] ($x10^{-6}$ M)	A500 nm
0	0	0	0	0	0.021377
0	20	2520	0	4.88	0.338487
1	20	2521	1.11E-07	4.88	0.310966
2	20	2522	2.22E-07	4.87	0.285808
3	20	2523	3.33E-07	4.87	0.285808
4	20	2524	4.44E-07	4.87	0.252222
5	20	2525	5.54E-07	4.87	0.244721
7	20	2527	7.76E-07	4.87	0.239943
9	20	2529	9.96E-07	4.86	0.240551
14	20	2534	1.55E-06	4.85	0.24065
19	20	2539	2.1E-06	4.84	0.242608
24	20	2544	2.64E-06	4.83	0.245497
29	20	2549	3.19E-06	4.82	0.249563

Table A13 the absorbance of 13 and the time exposed to light and oxygen in buffer (25 mM MOPS, pH 7.0, 50 mM NaCl, 1 mM EDTA), at 25 °C.

Time (min)	Absorbance
0	0.1355
2	0.1343
5	0.1261
10	0.1127
15	0.0936
20	0.0790
60	0.0598

References

1. Larson, H.W., *PHYSIOLOGY AND BIOCHEMISTRY IN MODERN MEDICINE, 5th edition.* American Journal of Nursing, 1928. **28**(7): p. 748-748.
2. Dahm, R., *Discovering DNA: Friedrich Miescher and the early years of nucleic acid research.* Human Genetics, 2008. **122**(6): p. 565-581.
3. Klug, A., *The discovery of the DNA double helix (vol 335, pg 3, 2004).* Journal of Molecular Biology, 2004. **336**(1): p. 303-303.
4. Stent, G.S., *Double Helix - Personal Account of the Discovery of the Structure of DNA - Watson,Jd.* Human Nature, 1978. **1**(8): p. 92-&.
5. Pederson, T., *Molecular Biology of the Gene.* Faseb Journal, 2015. **29**(11): p. 4399-4401.
6. Arnott, S., *Principles of Nucleic-Acid Structure - Saenger,W.* Nature, 1984. **312**(5990): p. 174-174.
7. Gannon, F., J. Neilan, and R. Powell, *Basic Methods in Molecular-Biology - Davis,Lg, Dibner,M, Battey,Jf.* Nature, 1988. **333**(6171): p. 309-310.
8. Kimura, M., *A Simple Method for Estimating Evolutionary Rates of Base Substitutions through Comparative Studies of Nucleotide-Sequences.* Journal of Molecular Evolution, 1980. **16**(2): p. 111-120.
9. Alt, K.W., *Fundamentals of molecular evolution, 2nd edition.* Homo, 2001. **52**(1): p. 81-81.
10. *Biochemistry for Medical Students 5th Edition.* Journal of Medical Education, 1952. **27**(5): p. 366-366.
11. Ledvina, M., *What Should Be Included in a Textbook of Biochemistry for Medical-Students.* Biochemical Education, 1991. **19**(3): p. 128-128.
12. Lim, V.I. and G.V. Aglyamova, *The principles of formation of spatial structures of proteins and nucleic acids. Stereochemical modeling.* Molecular Biology, 1999. **33**(6): p. 908-913.
13. Travers, A. and G. Muskhelishvili, *DNA structure and function.* Febs Journal, 2015. **282**(12): p. 2279-2295.
14. McCarthy, N., *DNA structure - Form and function.* Nature Reviews Cancer, 2005. **5**(9): p. 669-669.
15. Belmont, P., J.F. Constant, and M. Demeunynck, *Nucleic acid conformation diversity: from structure to function and regulation.* Chemical Society Reviews, 2001. **30**(1): p. 70-81.
16. Smith, J.O., D.A. Olson, and B.A. Armitage, *Molecular recognition of PNA-containing hybrids: Spontaneous assembly of helical cyanine dye aggregates on PNA templates.* Journal of the American Chemical Society, 1999. **121**(12): p. 2686-2695.
17. Shakked, Z. and D. Rabinovich, *The Effect of the Base Sequence on the Fine-Structure of the DNA Double Helix.* Progress in Biophysics & Molecular Biology, 1986. **47**(3): p. 159-195.
18. Watson, J.D. and F.H. Crick, *Molecular structure of nucleic acids: a structure for deoxyribose nucleic acid. J.D. Watson and F.H.C. Crick. Published in Nature, number 4356 April 25, 1953.* Nature, 1974. **248**(5451): p. 765-765.
19. Stella, S., D. Cascio, and R.C. Johnson, *The shape of the DNA minor groove directs binding by the DNA-bending protein Fis.* Genes & Development, 2010. **24**(8): p. 814-826.
20. Barawkar, D.A. and K.N. Ganesh, *Fluorescent D(Cgcgaattcgcg) - Characterization of Major Groove Polarity and Study of Minor-Groove Interactions through a Major Groove Semantophore Conjugate.* Nucleic Acids Research, 1995. **23**(1): p. 159-164.
21. Wang, A.H.J., et al., *Molecular-Structure of a Left-Handed Double Helical DNA Fragment at Atomic Resolution.* Nature, 1979. **282**(5740): p. 680-686.
22. Dickerson, R.E., et al., *The Anatomy of a-DNA, B-DNA, and Z-DNA.* Science, 1982. **216**(4545): p. 475-485.
23. Rich, A. and S.G. Zhang, *Z-DNA: the long road to biological function.* Nature Reviews Genetics, 2003. **4**(7): p. 566-572.

24. Geis, I., *Visualizing the Anatomy of a-DNA,B-DNA and Z-DNA.* Journal of Biomolecular Structure & Dynamics, 1983. **1**(3): p. 581-&.
25. Maher, L.J., B. Wold, and P.B. Dervan, *Inhibition of DNA-Binding Proteins by Oligonucleotide-Directed Triple Helix Formation.* Science, 1989. **245**(4919): p. 725-730.
26. Asensio, J.L., et al., *The contribution of cytosine protonation to the stability of parallel DNA triple helices.* Journal of Molecular Biology, 1998. **275**(5): p. 811-822.
27. Sathyamoorthy, B., et al., *Insights into Watson-Crick/Hoogsteen breathing dynamics and damage repair from the solution structure and dynamic ensemble of DNA duplexes containing m(1)A.* Nucleic Acids Research, 2017. **45**(9): p. 5586-5601.
28. Osborne, S.D., et al., *Selectivity and affinity of triplex-forming oligonucleotides containing 2 '-aminoethoxy-5-(3-aminoprop-1-ynyl)uridine for recognizing AT base pairs in duplex DNA.* Nucleic Acids Research, 2004. **32**(15): p. 4439-4447.
29. Biffi, G., et al., *Quantitative visualization of DNA G-quadruplex structures in human cells.* Nature Chemistry, 2013. **5**(3): p. 182-186.
30. Arola, A. and R. Vilar, *Stabilisation of G-Quadruplex DNA by Small Molecules.* Current Topics in Medicinal Chemistry, 2008. **8**(15): p. 1405-1415.
31. Jantos, K., et al., *Oxazole-based peptide macrocycles: A new class of G-quadruplex binding ligands.* Journal of the American Chemical Society, 2006. **128**(42): p. 13662-13663.
32. Bhasikuttan, A.C. and J. Mohanty, *Targeting G-quadruplex structures with extrinsic fluorogenic dyes: promising fluorescence sensors.* Chemical Communications, 2015. **51**(36): p. 7581-7597.
33. Rhodes, D. and H.J. Lipps, *G-quadruplexes and their regulatory roles in biology.* Nucleic Acids Research, 2015. **43**(18): p. 8627-8637.
34. Nakano, S., D. Miyoshi, and N. Sugimoto, *Effects of Molecular Crowding on the Structures, Interactions, and Functions of Nucleic Acids.* Chemical Reviews, 2014. **114**(5): p. 2733-2758.
35. Lemaitre, B., *The genome sequence of Drosophila melanogaster.* M S-Medecine Sciences, 2000. **16**(5): p. 693-695.
36. Venter, J.C., H.O. Smith, and M.D. Adams, *The Sequence of the Human Genome.* Clinical Chemistry, 2015. **61**(9): p. 1207-1208.
37. Birney, E., et al., *Identification and analysis of functional elements in 1% of the human genome by the ENCODE pilot project.* Nature, 2007. **447**(7146): p. 799-816.
38. Gilley, D., H. Tanaka, and B.S. Herbert, *Telomere dysfunction in aging and cancer.* International Journal of Biochemistry & Cell Biology, 2005. **37**(5): p. 1000-1013.
39. Siderakis, M. and M. Tarsounas, *Telomere regulation and function during meiosis.* Chromosome Research, 2007. **15**(5): p. 667-679.
40. Shore, D., *Telomere length regulation: Getting the measure of chromosome ends.* Biological Chemistry, 1997. **378**(7): p. 591-597.
41. Makarov, V.L., Y. Hirose, and J.P. Langmore, *Long G tails at both ends of human chromosomes suggest a C strand degradation mechanism for telomere shortening.* Cell, 1997. **88**(5): p. 657-666.
42. Barabasi, A.L. and Z.N. Oltvai, *Network biology: Understanding the cell's functional organization.* Nature Reviews Genetics, 2004. **5**(2): p. 101-U15.
43. Harris, L.M. and C.J. Merrick, *G-Quadruplexes in Pathogens: A Common Route to Virulence Control?* Plos Pathogens, 2015. **11**(2).
44. Huppert, J.L. and S. Balasubramanian, *G-quadruplexes in promoters throughout the human genome (vol 35, pg 406, 2006).* Nucleic Acids Research, 2007. **35**(6): p. 2105-2105.
45. Lam, E.Y.N., et al., *G-quadruplex structures are stable and detectable in human genomic DNA.* Nature Communications, 2013. **4**.
46. Shi, X.C. and J.B. Chaires, *Sequence- and structural-selective nucleic acid binding revealed by the melting of mixtures.* Nucleic Acids Research, 2006. **34**(2).

47. Piras, V., M. Tomita, and K. Selvarajoo, *Is central dogma a global property of cellular information flow?* Frontiers in Physiology, 2012. **3**.
48. Crick, F., *Central Dogma of Molecular Biology.* Nature, 1970. **227**(5258): p. 561-&.
49. Sponer, J., et al., *Hydrogen-bonded trimers of DNA bases and their interaction with metal cations: Ab initio quantum-chemical and empirical potential study.* Journal of Biomolecular Structure & Dynamics, 1997. **14**(5): p. 613-628.
50. Neto, B.A.D. and A.A.M. Lapis, *Recent Developments in the Chemistry of Deoxyribonucleic Acid (DNA) Intercalators: Principles, Design, Synthesis, Applications and Trends.* Molecules, 2009. **14**(5): p. 1725-1746.
51. Djuric, S.W. and N.A. Meanwell, *Journal of Medicinal Chemistry, Technological Advances: Highlights 2015-2016.* Journal of Medicinal Chemistry, 2017. **60**(1): p. 1-3.
52. Kaulage, M.H., et al., *Targeting G-quadruplex DNA structures in the telomere and oncogene Promoter regions by benzimidazole-carbazole ligands.* European Journal of Medicinal Chemistry, 2018. **148**: p. 178-194.
53. Nafisi, S., et al., *Stability and structural features of DNA intercalation with ethidium bromide, acridine orange and methylene blue.* Journal of Molecular Structure, 2007. **827**(1-3): p. 35-43.
54. Mergny, J.L., et al., *Intercalation of Ethidium-Bromide into a Triple-Stranded Oligonucleotide.* Nucleic Acids Research, 1991. **19**(7): p. 1521-1526.
55. Eckel, R., et al., *Identification of binding mechanisms in single molecule-DNA complexes.* Biophysical Journal, 2003. **85**(3): p. 1968-1973.
56. Bhadra, K. and G.S. Kumar, *Interaction of berberine, palmatine, coralyne, and sanguinarine to quadruplex DNA: A comparative spectroscopic and calorimetric study.* Biochimica Et Biophysica Acta-General Subjects, 2011. **1810**(4): p. 485-496.
57. Wilson, W.D., et al., *Coralyne - Intercalation with DNA as a Possible Mechanism of Antileukemic Action.* Journal of Medicinal Chemistry, 1976. **19**(10): p. 1261-1263.
58. Xing, F.F., et al., *Molecular recognition of nucleic acids: Coralyne binds strongly to poly(A).* Febs Letters, 2005. **579**(22): p. 5035-5039.
59. Giri, P. and G.S. Kumar, *Self-structure induction in single stranded poly(A) by small molecules: Studies on DNA intercalators, partial intercalators and groove binding molecules.* Archives of Biochemistry and Biophysics, 2008. **474**(1): p. 183-192.
60. Wemmer, D.E. and P.B. Dervan, *Targeting the minor groove of DNA.* Current Opinion in Structural Biology, 1997. **7**(3): p. 355-361.
61. Hud, N.V. and M. Polak, *DNA-cation interactions: the major and minor grooves are flexible ionophores.* Current Opinion in Structural Biology, 2001. **11**(3): p. 293-301.
62. Buurma, N.J. and I. Haq, *Calorimetric and spectroscopic studies of Hoechst 33258: Self-association and binding to non-cognate DNA.* Journal of Molecular Biology, 2008. **381**(3): p. 607-621.
63. Wartell, R.M., J.E. Larson, and R.D. Wells, *Netropsin - Specific Probe for a-T Regions of Duplex Deoxyribonucleic-Acid.* Journal of Biological Chemistry, 1974. **249**(21): p. 6719-6731.
64. Kopka, M.L., et al., *Binding of an Antitumor Drug to DNA Netropsin and C-G-C-G-a-a-T-T-Brc-G-C-G.* Journal of Molecular Biology, 1985. **183**(4): p. 553-563.
65. Mrksich, M., *Antiparallel side-by-side dimeric motif for sequence-specific recognition in the minor groove of DNA by the designed peptide 1-methylimidazole-2-carboxamidenetropsin.* Proc. Natl Acad. Sci. USA, 1992. **89**: p. 7586-7590.
66. Du, D.X., et al., *Graphene-modified electrode for DNA detection via PNA-DNA hybridization.* Sensors and Actuators B-Chemical, 2013. **186**: p. 563-570.
67. Jarikote, D.V., et al., *Exploring base-pair-specific optical properties of the DNA stain thiazole orange.* Chemistry-a European Journal, 2007. **13**(1): p. 300-310.
68. de la Faverie, A.R., et al., *Thioflavin T as a fluorescence light-up probe for G4 formation.* Nucleic Acids Research, 2014. **42**(8).

69. Perkampus, H.-H., *UV-VIS spectroscopy and its applications*. Springer laboratory. 1992, Berlin ; New York: Springer-Verlag. ix, 244 p.
70. Kanjanawarut, R., B. Yuan, and X.D. Su, *UV-Vis Spectroscopy and Dynamic Light Scattering Study of Gold Nanorods Aggregation.* Nucleic Acid Therapeutics, 2013. **23**(4): p. 273-280.
71. Mayer, R.G. and R.S. Drago, *Interpretation of Isosbestic Points.* Inorganic Chemistry, 1976. **15**(8): p. 2010-2011.
72. Giacometti, G., *Introduction to spectroscopy.* Spectroscopic Techniques in Biophysics, 2001. **4**: p. 1-10.
73. Arshad, N., et al., *Synthesis, photochemical and electrochemical studies on triphenyltin(IV) derivative of (Z)-4-(4-cyanophenylamino)-4-oxobut-2-enoic acid for its binding with DNA: Biological interpretation.* Arabian Journal of Chemistry, 2016. **9**(3): p. 451-462.
74. Vardevanyan, P.O., et al., *Determination of the Isosbestic Point in the Absorption Spectra of DNA-Ethidium Bromide Complexes.* Journal of Applied Spectroscopy, 2015. **81**(6): p. 1060-1063.
75. Sirajuddin, M., S. Ali, and A. Badshah, *Drug-DNA interactions and their study by UV-Visible, fluorescence spectroscopies and cyclic voltametry.* Journal of Photochemistry and Photobiology B-Biology, 2013. **124**: p. 1-19.
76. Hahn, L., N.J. Buurma, and L.H. Gade, *A Water-Soluble Tetraazaperopyrene Dye as Strong G-Quadruplex DNA Binder.* Chemistry - A European Journal, 2016. **22**(18): p. 6314-6322.
77. Wallace, B.A., *Using Circular Dichroism (CD) and Synchrotron Radiation Circular Dichroism (SRCD) Spectroscopy to Study Membrane Proteins.* Biophysical Journal, 2010. **98**(3): p. 209a-210a.
78. Chang, Y.M., C.K.M. Chen, and M.H. Hou, *Conformational Changes in DNA upon Ligand Binding Monitored by Circular Dichroism.* International Journal of Molecular Sciences, 2012. **13**(3): p. 3394-3413.
79. Eriksson, M. and B. Norden, *Linear and circular dichroism of drug-nucleic acid complexes.* Drug-Nucleic Acid Interactions, 2001. **340**: p. 68-98.
80. Lyng, R., A. Rodger, and B. Norden, *The Cd of Ligand-DNA Systems .2. Poly(Da-Dt) B-DNA.* Biopolymers, 1992. **32**(9): p. 1201-1214.
81. Lyng, R., A. Rodger, and B. Norden, *The Cd of Ligand-DNA Systems .1. Poly(Dg-Dc) B-DNA.* Biopolymers, 1991. **31**(14): p. 1709-1720.
82. Kelly, S.M. and N.C. Price, *The Use of Circular Dichroism in the Investigation of Protein Structure and Function.* Current Protein & Peptide Science, 2000. **1**(4): p. 349-384.
83. Whitmore, L. and B.A. Wallace, *Protein secondary structure analyses from circular dichroism spectroscopy: Methods and reference databases.* Biopolymers, 2008. **89**(5): p. 392-400.
84. Garbett, N.C., P.A. Ragazzon, and J.B. Chaires, *Circular dichroism to determine binding mode and affinity of ligand-DNA interactions.* Nature Protocols, 2007. **2**(12): p. 3166-3172.
85. Joshi, H., et al., *Isothermal titration calorimetry studies on the binding of amino acids to gold nanoparticles.* Journal of Physical Chemistry B, 2004. **108**(31): p. 11535-11540.
86. Grossoehme, N.E., A.M. Spuches, and D.E. Wilcox, *Application of isothermal titration calorimetry in bioinorganic chemistry.* Journal of Biological Inorganic Chemistry, 2010. **15**(8): p. 1183-1191.
87. Saboury, A.A., *A review on the ligand binding studies by isothermal titration calorimetry.* Journal of the Iranian Chemical Society, 2006. **3**(1): p. 1-21.
88. Perspicace, S., et al., *Isothermal titration calorimetry with micelles: Thermodynamics of inhibitor binding to carnitine palmitoyltransferase 2 membrane protein.* Febs Open Bio, 2013. **3**: p. 204-211.
89. Buurma, N.J. and I. Haq, *Advances in the analysis of isothermal titration calorimetry data for ligand-DNA interactions.* Methods, 2007. **42**(2): p. 162-172.
90. Althagafi, I., *Structural variation in π-conjugated DNA binders through click chemistry: synthesis and interaction studies*. 2012, Cardiff University. p. 292.

91. Birchenhall, C., *Numerical Recipes in C - the Art of Scientific Computing.* Economic Journal, 1994. **104**(424): p. 725-726.
92. Didenko, V.V., *DNA probes using fluorescence resonance energy transfer (FRET): designs and applications (vol 31, pg 1106, 2001).* Biotechniques, 2002. **32**(5): p. 1012-1012.
93. Weiss, S., *Fluorescence spectroscopy of single biomolecules.* Science, 1999. **283**(5408): p. 1676-1683.
94. Clegg, R.M., *[18] Fluorescence resonance energy transfer and nucleic acids.* Methods in Enzymology, 1992. **211**: p. 353-388.
95. Gust, D., T.A. Moore, and A.L. Moore, *Molecular Mimicry of Photosynthetic Energy and Electron-Transfer.* Accounts of Chemical Research, 1993. **26**(4): p. 198-205.
96. Ma, L.L., F. Yang, and J. Zheng, *Application of fluorescence resonance energy transfer in protein studies.* Journal of Molecular Structure, 2014. **1077**: p. 87-100.
97. Ying, L.M., et al., *Studies on the structure and dynamics of the human telomeric G quadruplex by single-molecule fluorescence resonance energy transfer.* Proceedings of the National Academy of Sciences of the United States of America, 2003. **100**(25): p. 14629-14634.
98. Schweitzer, B. and S. Kingsmore, *Combining nucleic acid amplification and detection.* Current Opinion in Biotechnology, 2001. **12**(1): p. 21-27.
99. Howell, W.M., M. Jobs, and A.J. Brookes, *iFRET: an improved fluorescence system for DNA-melting analysis.* Genome Research, 2002. **12**(9): p. 1401-1407.
100. Neidle, S., *Nucleic acid structure and recognition*. 2002, Oxford: Oxford University Press. xi, 188 p.
101. Sohrabi, N., et al., *Basics of DNA biosensors and cancer diagnosis.* Artificial Cells Nanomedicine and Biotechnology, 2016. **44**(2): p. 654-663.
102. Teles, F.R.R. and L.R. Fonseca, *Trends in DNA biosensors.* Talanta, 2008. **77**(2): p. 606-623.
103. Turner, A.P.F., *Biosensors: Fundamentals and applications - Historic book now open access.* Biosensors & Bioelectronics, 2015. **65**: p. A1-A1.
104. Medyantseva, E.P., E.V. Khaldeeva, and G.K. Budnikov, *Immunosensors in biology and medicine: Analytical capabilities, problems, and prospects.* Journal of Analytical Chemistry, 2001. **56**(10): p. 886-900.
105. Zhao, W.W., J.J. Xu, and H.Y. Chen, *Photoelectrochemical DNA Biosensors.* Chemical Reviews, 2014. **114**(15): p. 7421-7441.
106. Zhang, L.Y., et al., *A Conjugated Polymer-Based Electrochemical DNA Sensor: Design and Application of a Multi-Functional and Water-Soluble Conjugated Polymer (vol 29, pg 1489, 2008).* Macromolecular Rapid Communications, 2008. **29**(19): p. 1626-1626.
107. Palchetti, I. and M. Mascini, *Nucleic acid biosensors for environmental pollution monitoring.* Analyst, 2008. **133**(7): p. 846-854.
108. Lee, T.Y. and Y.B. Shim, *Direct DNA hybridization detection based on the oligonucleotide-functionalized conductive polymer.* Analytical Chemistry, 2001. **73**(22): p. 5629-5632.
109. Peng, H., et al., *Label-free electrochemical DNA sensor based on functionalised conducting copolymer.* Biosensors & Bioelectronics, 2005. **20**(9): p. 1821-1828.
110. Baker, B.A. and V.T. Milam, *Hybridization kinetics between immobilized double-stranded DNA probes and targets containing embedded recognition segments.* Nucleic Acids Research, 2011. **39**(15).
111. Papadopoulou, E., et al., *Specifically horizontally tethered DNA probes on Au surfaces allow labelled and label-free DNA detection using SERS and electrochemically driven melting.* Chemical Science, 2016. **7**(1): p. 386-393.
112. Lee, T.Y., Y.B. Shim, and S.C. Shin, *Simple preparation of terthiophene-3'-carboxylic acid and characterization of its polymer.* Synthetic Metals, 2002. **126**(1): p. 105-110.
113. Choi, Y., et al., *Oligonucleotide-templated reactions based on Peptide Nucleic Acid (PNA) probes: Concept and biomedical applications.* Bioorganic & Medicinal Chemistry, 2014. **22**(16): p. 4395-4398.

114. Nielsen, P.E. and G. Haaima, *Peptide nucleic acid (PNA). A DNA mimic with a pseudopeptide backbone.* Chemical Society Reviews, 1997. **26**(2): p. 73-78.
115. Porcheddu, A. and G. Giacomelli, *Peptide nucleic acids (PNAs), a chemical overview.* Current Medicinal Chemistry, 2005. **12**(22): p. 2561-2599.
116. Wang, J., et al., *Peptide nucleic acid probes for sequence-specific DNA biosensors.* Journal of the American Chemical Society, 1996. **118**(33): p. 7667-7670.
117. De, A., et al., *Peptide Nucleic Acid (PNA)-DNA Duplexes: Comparison of Hybridization Affinity between Vertically and Horizontally Tethered PNA Probes (vol 5, pg 4607, 2013).* Acs Applied Materials & Interfaces, 2013. **5**(15): p. 7659-7659.
118. Tilani, N., S. De Costa, and J.M. Heemstra, *Evaluating the Effect of Ionic Strength on Duplex Stability for PNA Having Negatively or Positively Charged Side Chains.* Plos One, 2013. **8**(3).
119. Liu, X.G., et al., *Electrochemical detection of DNA hybridization using a water-soluble branched polyethyleneimine-cobalt(III)-phenanthroline indicator and PNA probe on Au electrodes.* Electrochimica Acta, 2010. **55**(22): p. 6491-6495.
120. Le Floch, F., et al., *Ferrocene-functionalized cationic polythiophene for the label-free electrochemical detection of DNA.* Advanced Materials, 2005. **17**(10): p. 1251-+.
121. Bandy, T.J., et al., *DNA as supramolecular scaffold for functional molecules: progress in DNA nanotechnology.* Chemical Society Reviews, 2011. **40**(1): p. 138-148.
122. Su, W., et al., *Site-Specific Assembly of DNA-Based Photonic Wires by Using Programmable Polyamides.* Angewandte Chemie-International Edition, 2011. **50**(12): p. 2712-2715.
123. Su, W., C.R. Bagshaw, and G.A. Burley, *Addressable and unidirectional energy transfer along a DNA three-way junction programmed by pyrrole-imidazole polyamides.* Scientific Reports, 2013. **3**.
124. Ragazzon, P. and J.B. Chaires, *Use of competition dialysis in the discovery of G-quadruplex selective ligands.* Methods, 2007. **43**(4): p. 313-23.
125. Ragazzon, P.A., N.C. Garbett, and J.B. Chaires, *Competition dialysis: a method for the study of structural selective nucleic acid binding.* Methods, 2007. **42**(2): p. 173-82.
126. Ren, J. and J.B. Chaires, *Sequence and structural selectivity of nucleic acid binding ligands.* Biochemistry, 1999. **38**(49): p. 16067-16075.
127. Chaires, J.B., *Structural selectivity of drug-nucleic acid interactions probed by competition dialysis.* DNA Binders and Related Subjects, 2005. **253**: p. 33-53.
128. Erickson, G.L. and J.V. Ebenezer, *Chemistry students' conceptions of solubility: A phenomenography - Response.* Science Education, 1997. **81**(5): p. 601-603.
129. Corezzi, S., D. Fioretto, and F. Sciortino, *Chemical and physical aggregation of small-functionality particles.* Soft Matter, 2012. **8**(44): p. 11207-11216.
130. Steiger, R. and P.A. Brugger, *Photochemical studies on the lightfastness of ink-jet systems.* Is&T's Nip14: International Conference on Digital Printing Technologies, Proceedings, 1998: p. 114-117.
131. Das, S. and P. Purkayastha, *Modulating Thiazole Orange Aggregation in Giant Lipid Vesicles: Photophysical Study Associated with FLIM and FCS.* Acs Omega, 2017. **2**(8): p. 5036-5043.
132. Cristea, D. and G. Vilarem, *Improving light fastness of natural dyes on cotton yarn.* Dyes and Pigments, 2006. **70**(3): p. 238-245.
133. Peters, A.T., *Organic-Chemistry in Color - Gordon,Pf, Gregory,P.* Chemistry in Britain, 1984. **20**(9): p. 822-822.
134. Terai, T. and T. Nagano, *Fluorescent probes for bioimaging applications.* Current Opinion in Chemical Biology, 2008. **12**(5): p. 515-521.
135. Grynkiewicz, G., M. Poenie, and R.Y. Tsien, *A New Generation of Ca-2+ Indicators with Greatly Improved Fluorescence Properties.* Journal of Biological Chemistry, 1985. **260**(6): p. 3440-3450.
136. Nagano, T., *Development of fluorescent probes for bioimaging applications.* Proceedings of the Japan Academy Series B-Physical and Biological Sciences, 2010. **86**(8): p. 837-847.

137. Carreon, J.R., et al., *Cyanine dye conjugates as probes for live cell imaging.* Bioorganic & Medicinal Chemistry Letters, 2007. **17**(18): p. 5182-5185.
138. Kanony, C., B. Akerman, and E. Tuite, *Photobleaching of asymmetric cyanines used for fluorescence imaging of single DNA molecules.* Journal of the American Chemical Society, 2001. **123**(33): p. 7985-7995.
139. Deligeorgiev, T., S. Kaloyanova, and A. Vasilev, *A novel general method for preparation of neutral monomethine cyanine dyes.* Dyes and Pigments, 2011. **90**(2): p. 170-176.
140. Lee, L.G., C.H. Chen, and L.A. Chiu, *Thiazole Orange - a New Dye for Reticulocyte Analysis.* Cytometry, 1986. **7**(6): p. 508-517.
141. Guan, L., et al., *Nonplanar Monocyanines: Meso-Substituted Thiazole Orange with High Photostability and Their Synthetic Strategy as well as a Cell Association Study.* Journal of Organic Chemistry, 2016. **81**(15): p. 6303-6313.
142. Mahmood, T., A. Paul, and S. Ladame, *Synthesis and Spectroscopic and DNA-Binding Properties of Fluorogenic Acridine-Containing Cyanine Dyes.* Journal of Organic Chemistry, 2010. **75**(1): p. 204-207.
143. Monchaud, D., C. Allain, and M.P. Teulade-Fichou, *Thiazole orange: A useful probe for fluorescence sensing of G-quadruplex-ligand interactions.* Nucleosides Nucleotides & Nucleic Acids, 2007. **26**(10-12): p. 1585-1588.
144. Nygren, J., N. Svanvik, and M. Kubista, *The interactions between the fluorescent dye thiazole orange and DNA.* Biopolymers, 1998. **46**(1): p. 39-51.
145. Lau, V. and B. Heyne, *Calix[4]arene sulfonate as a template for forming fluorescent thiazole orange H-aggregates.* Chemical Communications, 2010. **46**(20): p. 3595-3597.
146. Mowry, S. and P.J. Ogren, *Kinetics of methylene blue reduction by ascorbic acid.* Journal of Chemical Education, 1999. **76**(7): p. 970-974.
147. Colombini, M.P., et al., *Colour fading in textiles: A model study on the decomposition of natural dyes.* Microchemical Journal, 2007. **85**(1): p. 174-182.
148. Bilmes, G.M., J.O. Tocho, and S.E. Braslavsky, *Spectrum, Energy Content, and Relaxation Mechanism of the Photoisomer of the Laser-Dye 3,3'-Diethyloxadicarbocyanine Iodide - Laser-Induced Optoacoustic Studies.* Journal of Physical Chemistry, 1988. **92**(21): p. 5958-5962.
149. Tuite, E.M. and J.M. Kelly, *Photochemical Interactions of Methylene-Blue and Analogs with DNA and Other Biological Substrates.* Journal of Photochemistry and Photobiology B-Biology, 1993. **21**(2-3): p. 103-124.
150. Shank, N.I., et al., *Twisted Cyanines: A Non-Planar Fluorogenic Dye with Superior Photostability and its Use in a Protein-Based Fluoromodule.* Journal of the American Chemical Society, 2013. **135**(1): p. 242-251.
151. Prato, F.S., M. Kavaliers, and J.J.L. Carson, *Behavioural responses to magnetic fields by land snails are dependent on both magnetic field direction and light (vol 263, pg 1437, 1996).* Proceedings of the Royal Society B-Biological Sciences, 1997. **264**(1381): p. 623-623.
152. Griffiths, J. and C. Hawkins, *Oxidation by Singlet Oxygen of Arylazonaphthols Exhibiting Azo-Hydrazone Tautomerism.* Journal of the Chemical Society-Perkin Transactions 2, 1977(6): p. 747-752.
153. *Color Chemistry - Synthesis, Properties and Applications of Organic-Dyes and Pigments - Zollinger,H.* Leonardo, 1989. **22**(3-4): p. 456-456.
154. Baer, N.S., *Accelerated aging: Photochemical and thermal aspects - Feller,RL.* Journal of the American Institute for Conservation, 1996. **35**(2): p. 163-165.
155. Zhang, F.T., et al., *Methylene Blue as a G-Quadruplex Binding Probe for Label-Free Homogeneous Electrochemical Biosensing.* Analytical Chemistry, 2014. **86**(19): p. 9489-9495.
156. Garbett, N.C., N.B. Hammond, and D.E. Graves, *Influence of the amino substituents in the interaction of ethidium bromide with DNA.* Biophysical Journal, 2004. **87**(6): p. 3974-3981.

157. Guo, Q., et al., *Interaction of the Dye Ethidium-Bromide with DNA Containing Guanine Repeats.* Biochemistry, 1992. **31**(9): p. 2451-2455.
158. Lee, J.S., L.J.P. Latimer, and K.J. Hampel, *Coralyne Binds Tightly to Both T.A.T-Containing and C.G.C+-Containing DNA Triplexes.* Biochemistry, 1993. **32**(21): p. 5591-5597.
159. Vardevanyan, P.O., et al., *Mechanisms for Binding between Methylene Blue and DNA.* Journal of Applied Spectroscopy, 2013. **80**(4): p. 595-599.
160. Chaudhury, N.K. and R. Bhardwaj, *Structural stabilization by Hoechst 33258 in gamma-irradiated DNA: Evidenced by spectroscopic studies.* Current Science, 2004. **87**(9): p. 1256-1262.
161. Eriksson, S., et al., *Binding of 4',6-Diamidino-2-Phenylindole (Dapi) to at Regions of DNA - Evidence for an Allosteric Conformational Change.* Biochemistry, 1993. **32**(12): p. 2987-2998.
162. Breusegem, S.Y., R.M. Clegg, and F.G. Loontiens, *Base-sequence specificity of Hoechst 33258 and DAPI binding to five (A/T)(4) DNA sites with kinetic evidence for more than one high-affinity Hoechst 33258-AATT complex.* Journal of Molecular Biology, 2002. **315**(5): p. 1049-1061.
163. Xie, X., et al., *Asymmetric Distyrylpyridinium Dyes as Red-Emitting Fluorescent Probes for Quadruplex DNA.* Chemistry-a European Journal, 2013. **19**(4): p. 1214-1226.
164. White, E.W., et al., *Structure-specific recognition of quadruplex DNA by organic cations: Influence of shape, substituents and charge.* Biophysical Chemistry, 2007. **126**(1-3): p. 140-153.
165. Cundall, R.B., et al., *Factors Influencing the Photosensitizing Properties and Photo-Luminescence of Thioflavin-T.* Journal of Photochemistry, 1981. **17**(3-4): p. 369-376.
166. Ilanchelian, M. and R. Ramaraj, *Emission of thioflavin T and its control in the presence of DNA.* Journal of Photochemistry and Photobiology a-Chemistry, 2004. **162**(1): p. 129-137.
167. Sun, N., et al., *The interaction of a structural flexible small molecule with nucleic acid structures: Investigation of the origin of fluorescence signal discrimination in sensing and the utilization in live cell imaging.* Sensors and Actuators B-Chemical, 2017. **250**: p. 543-551.
168. Lubitz, I., D. Zikich, and A. Kotlyar, *Specific High-Affinity Binding of Thiazole Orange to Triplex and G-Quadruplex DNA.* Biochemistry, 2010. **49**(17): p. 3567-3574.
169. Atherton, S.J. and A. Harriman, *Photochemistry of Intercalated Methylene-Blue - Photoinduced Hydrogen-Atom Abstraction from Guanine and Adenine.* Journal of the American Chemical Society, 1993. **115**(5): p. 1816-1822.
170. Jang, M.S., et al., *Triphenylmethane reductase from Citrobacter sp strain KCTC 18061P: Purification, characterization, gene cloning, and overexpression of a functional protein in Escherichia coli.* Applied and Environmental Microbiology, 2005. **71**(12): p. 7955-7960.
171. Biancardi, A., et al., *Mechanistic aspects of thioflavin-T self-aggregation and DNA binding: evidence for dimer attack on DNA grooves.* Physical Chemistry Chemical Physics, 2014. **16**(37): p. 20061-20072.
172. Amirbekyan, K.Y., et al., *Molecular interactions between benzimide trichloride (Hoechst 33258) and DNA in dimethyl sulfoxide aqueous solutions, according to spectroscopy data.* Russian Journal of Physical Chemistry A, 2013. **87**(12): p. 2027-2029.
173. Behrens, C., N. Harrit, and P.E. Nielsen, *Synthesis of a hoechst 32258 analogue amino acid building block for direct incorporation of a fluorescent, high-affinity DNA binding motif into peptides.* Bioconjugate Chemistry, 2001. **12**(6): p. 1021-1027.
174. Varma, Y.T., et al., *Solvent effects on the absorption and emission spectra of novel (E)-4-((4-(heptyloxy)phenyl)diazenyl)benzyl (((9H-fluoren-9-yl) methoxy)carbonyl)-D-alaninate (Fmoc-al-az): Determination of dipole moment by experimental and theoretical study.* Journal of Molecular Structure, 2017. **1129**: p. 248-255.
175. Horobin, R.W. and Kevillda.Im, *Basic Fuchsin in Acid Alcohol - Simplified Alternative to Schiff Reagent.* Stain Technology, 1971. **46**(2): p. 53-&.

176. Fornili, S.L., G. Sgroi, and V. Izzo, *Effects of Solvent on Stacking Interactions - a Spectrophotometric Study of Methylene-Blue Dimerization in Aqueous-Solutions of Some Monohydric Alcohols.* Journal of the Chemical Society-Faraday Transactions I, 1983. **79**: p. 1085-1090.
177. Kryakan, A.V. and A.N. Terenin, *Photosensitization of the Fading of Adsorbed Methylene Blue.* Zhurnal Fizicheskoi Khimii, 1962. **36**(10): p. 2286-2287.
178. Stenstrom, W. and C.E. Nurnberger, *Fading of methylene blue-acetone solutions by ultra-violet light.* Proceedings of the Society for Experimental Biology and Medicine, 1934. **31**(9): p. 1073-1078.
179. Diaz, M.S., M.L. Freile, and M.I. Gutierrez, *Solvent effect on the UV/Vis absorption and fluorescence spectroscopic properties of berberine.* Photochemical & Photobiological Sciences, 2009. **8**(7): p. 970-974.
180. Chan, D.S.-H., et al., *Structure-based optimization of FDA-approved drug methylene blue as a c-myc G-quadruplex DNA stabilizer.* Biochimie, 2011. **93**(6): p. 1055-1064.
181. Cao, T., et al., *Investigation of the interactions between methylene blue and intramolecular G-quadruplexes: an explicit distinction in electrochemical behavior.* Analyst, 2017. **142**(6): p. 987-993.
182. Higuchi, R., et al., *Simultaneous Amplification and Detection of Specific DNA-Sequences.* Bio-Technology, 1992. **10**(4): p. 413-417.
183. Jansen, K., B. Norden, and M. Kubista, *Sequence Dependence of 4',6-Diamidino-2-Phenylindole (Dapi) DNA Interactions.* Journal of the American Chemical Society, 1993. **115**(23): p. 10527-10530.
184. Pei, R., et al., *Light-up properties of complexes between thiazole orange-small molecule conjugates and aptamers.* Nucleic Acids Research, 2009. **37**(8).
185. Rye, H.S., et al., *Stable Fluorescent Complexes of Double-Stranded DNA with Bis-Intercalating Asymmetric Cyanine Dyes - Properties and Applications.* Nucleic Acids Research, 1992. **20**(11): p. 2803-2812.
186. Ohashi, M., et al., *Molecular Mechanics Studies on Inclusion-Compounds of Cyanine Dye Monomers and Dimers in Cyclodextrin Cavities.* Journal of the American Chemical Society, 1990. **112**(15): p. 5824-5830.
187. Abbott, L.C., et al., *Ultrafast time-resolved UV-visible and infrared absorption spectroscopy of binuclear rhenium(I) polypyridyl complexes in solution.* Journal of Physical Chemistry A, 1998. **102**(8): p. 1252-1260.
188. Giri, P. and G.S. Kumar, *Binding of protoberberine alkaloid coralyne with double stranded poly(A): a biophysical study.* Molecular Biosystems, 2008. **4**(4): p. 341-348.
189. Regan, E.M., et al., *A novel cobalt complex for enhancing amperometric and impedimetric DNA detection.* Electrochimica Acta, 2014. **128**: p. 10-15.
190. Mullice, L.A., et al., *Rhenium complexes of chromophore-appended dipicolylamine ligands: Syntheses, spectroscopic properties, DNA binding and X-ray crystal structure.* New Journal of Chemistry, 2008. **32**(12): p. 2140-2149.
191. Mohanty, J., et al., *Thioflavin T as an Efficient Inducer and Selective Fluorescent Sensor for the Human Telomeric G-Quadruplex DNA.* Journal of the American Chemical Society, 2013. **135**(1): p. 367-376.
192. Murat, P. and S. Balasubramanian, *Existence and consequences of G-quadruplex structures in DNA.* Current Opinion in Genetics & Development, 2014. **25**: p. 22-29.
193. Stokke, T. and H.B. Steen, *Multiple Binding Modes for Hoechst 33258 to DNA.* Journal of Histochemistry & Cytochemistry, 1985. **33**(4): p. 333-338.
194. Garner, T.P., et al., *Selectivity of small molecule ligands for parallel and anti-parallel DNA G-quadruplex structures.* Organic & Biomolecular Chemistry, 2009. **7**(20): p. 4194-4200.
195. Chan, D.S.H., et al., *Structure-based optimization of FDA-approved drug methylene blue as a c-myc G-quadruplex DNA stabilizer.* Biochimie, 2011. **93**(6): p. 1055-1064.

196. Gao, J., et al., *Yeast transcription co-activator Sub1 and its human homolog PC4 preferentially bind to G-quadruplex DNA.* Chemical Communications, 2015. **51**(33): p. 7242-7244.
197. Zhou, C.Q., et al., *Dinickel-Salphen Complexes as Binders of Human Telomeric Dimeric G-Quadruplexes.* Chemistry-a European Journal, 2017. **23**(19): p. 4713-4722.
198. Scaria, P.V., S.J. Shire, and R.H. Shafer, *Quadruplex Structure of D(G3t4g3) Stabilized by K+ or Na+ Is an Asymmetric Hairpin Dimer.* Proceedings of the National Academy of Sciences of the United States of America, 1992. **89**(21): p. 10336-10340.
199. Onel, L. and N.J. Buurma, *The Nature of the Sodium Dodecylsulfate Micellar Pseudophase as Studied by Reaction Kinetics.* Journal of Physical Chemistry B, 2011. **115**(45): p. 13199-13211.
200. Lipps, H.J. and D. Rhodes, *G-quadruplex structures: in vivo evidence and function.* Trends in Cell Biology, 2009. **19**(8): p. 414-422.
201. Cech, T.R., *Life at the end of the chromosome: Telomeres and telomerase.* Angewandte Chemie-International Edition, 2000. **39**(1): p. 34-43.
202. Phatak, P. and A.M. Burger, *Telomerase and its potential for therapeutic intervention.* British Journal of Pharmacology, 2007. **152**(7): p. 1003-1011.
203. Balasubramanian, S. and S. Neidle, *G-quadruplex nucleic acids as therapeutic targets.* Current Opinion in Chemical Biology, 2009. **13**(3): p. 345-353.
204. Panich, S., et al., *Real-Time Monitoring of Ligand Binding to G-Quadruplex and Duplex DNA by Whispering Gallery Mode Sensing.* Acs Sensors, 2016. **1**(9): p. 1097-1102.
205. Jain, A.K. and S. Bhattacharya, *Interaction of G-Quadruplexes with Nonintercalating Duplex-DNA Minor Groove Binding Ligands.* Bioconjugate Chemistry, 2011. **22**(12): p. 2355-2368.
206. Nanjunda, R., et al., *Selective G-Quadruplex DNA Recognition by a New Class of Designed Cyanines.* Molecules, 2013. **18**(11): p. 13588-13607.
207. Gromyko, A.V., et al., *DNA sequence-specific ligands: XII. Synthesis and cytological studies of dimeric Hoechst 33258 molecules.* Russian Journal of Bioorganic Chemistry, 2005. **31**(4): p. 344-351.
208. Maiti, S., N.K. Chaudhury, and S. Chowdhury, *Hoechst 33258 binds to G-quadruplex in the promoter region of human c-myc.* Biochemical and Biophysical Research Communications, 2003. **310**(2): p. 505-512.
209. Kelley, S.O., et al., *Photoinduced electron transfer in ethidium-modified DNA duplexes: Dependence on distance and base stacking.* Journal of the American Chemical Society, 1997. **119**(41): p. 9861-9870.
210. Lane, A.N., T.C. Jenkins, and T.A. Frenkiel, *Hydration and solution structure of d(CGCAAATTTGCG)(2) and its complex with propamidine from NMR and molecular modelling.* Biochimica Et Biophysica Acta-Gene Structure and Expression, 1997. **1350**(2): p. 205-220.
211. Banerjee, D. and S.K. Pal, *Simultaneous binding of minor groove binder and intercalator to dodecamer DNA: Importance of relative orientation of donor and acceptor in FRET.* Journal of Physical Chemistry B, 2007. **111**(19): p. 5047-5052.
212. Chan, Y.C., et al., *Direct visualization of the quadruplex structures in human chromosome using FRET: Application of quadruplex stabilizer and duplex-binding fluorophore.* Biosensors & Bioelectronics, 2013. **47**: p. 566-573.
213. Ghasemi, J., et al., *Spectroscopic characterization of thiazole orange-3 DNA interaction.* Applied Biochemistry and Biotechnology, 2008. **149**(1): p. 9-22.
214. Tuite, E. and B. Norden, *Sequence-Specific Interactions of Methylene-Blue with Polynucleotides and DNA - a Spectroscopic Study.* Journal of the American Chemical Society, 1994. **116**(17): p. 7548-7556.